ENZYME-RESPONSIVE DOTA-BASED OPTICAL PROBES

Inaugural-Dissertation

to obtain the academic degree

Doctor rerum naturalium (Dr. rer. nat.)

submitted to the Department of Biology, Chemistry, Pharmacy

of Freie Universität Berlin

by

BENJAMIN JAKOB BRENNECKE

Berlin, 2021

I hereby declare that the submitted thesis is my own work and was prepared autonomously without the aid of other sources than the ones cited and acknowledged. This work was not submitted to any prior doctoral procedure.

The following work has been carried out in the research group of Dr. Marc Nazaré at the Leibniz-Institut für Molekulare Pharmakologie Berlin (FMP) from March 2016 to January 2021.

1st Reviewer: Dr. Marc Nazaré
(Leibniz-Institut für Molekulare Pharmakologie Berlin)
2nd Reviewer: Prof. Dr. Rainer Haag
(Institute of Chemistry and Biochemistry, Freie Universität Berlin)

Date of defense: 30.06.2021

ACKNOWLEDGEMENTS

First and foremost, I would like to thank Dr. Marc Nazaré for the opportunity to carry out my doctorate in his group and to supervise this work, as well as for providing the possibility to conduct a research stay at Hoffmann-La Roche and to spend ten highly interesting days in Beijing.

I also thank Prof. Rainer Haag for complying to be the second supervisor of this work.

I want to thank our collaboration partners: Prof. Hai-Yu Hu, Qinghua Wang, and Dr. Qingyang Zhang for a fruitful scientific cooperation in handling most of the biology part of the projects, and the whole Hu group for welcoming and hosting us so warmly in Beijing.

I also want to thank Uwe Grether for hosting me in his lab at Roche for three truly amazing months in Basel and for involving me in a really interesting project.

I thank Lisa Teichmann, Beate Nachtigall and Cedric Scholz for their contributions to the projects during their internships. I furthermore thank Carola and Andreas from the Screening Unit for their help with enzyme kinetic measurements and support with the plate reader.

I am very grateful to all my fellow and former group members: Liudmila for treating me with chocolate and food in the evenings, Sandra and Peter for repairing the LCMS countless times and for always being supportive with all kinds of maintenance issues, Keven for helping me with all the form sheets required to send probes to China, Thais for being member in crime with respect to the DOTAM projects, Leo, Yelena and Murat for simply being very enjoyable company, and Rana, Jens, Phani, Edgar, Marie, Jessi, Upendra and Vera. And, of course, Jérôme.

A special thanks goes to all my friends, the Bajackis, my former LeoWG, the woodwind quartet. Friends are just important. I am truly grateful for my family: my mother Dorin who is also a very good grandmother, my little daughter Eleah who gave and gives life entirely new perspectives, Feja for having been the best cuddly dog and a loved companion, and, most of all, Rebekka, for standing by my side and taking me as I am. Thank you!

ABSTRACT

Small-molecule optical probes have proven to be valuable tools for research and preclinical applications and are successively being incorporated into clinical practice as indispensable sensitive imaging diagnostics that allow for the non-invasive real-time monitoring of pathological alterations on a molecular level. The present work deals with the development, characterization, and application of novel enzyme-activatable optical probes based on the DOTA (1,4,7,10-tetraazacyclododecane-1,4,7,10-tetraacetic acid) scaffold as central, multifunctionalizable and highly flexible template.

Within the first project of this work, the development of a sophisticated dual functional DOTAM-based fluorescent probe for cancer imaging is presented, combining favorable features of a targeted probe and a substrate-based probe. The probe comprises the DOTAM-scaffold as inherent structural motif of a cathepsin S activatable internally quenched fluorescent (IQF) substrate, as well as cRGDfK peptidic ligands that preferentially bind to $\alpha_v\beta_3$ integrins, thus combining recognition motifs for two highly relevant and specific cancer targets. Biochemical profiling revealed that the probe and a non-targeted control analogue feature excellent *in vitro* activation kinetics towards cathepsin S exhibiting site-specific cleavage of the sequence, and that they are stable in presence of a series of common intracellular bioanalytes. Comparison to the non-targeted control probe revealed significantly better staining intensity of cancer cells for the dual functional probe, which correlated with the extent of $\alpha_v\beta_3$ receptors on the different cell lines. Moreover, staining was significantly impaired upon preincubation with cRGDfK peptide or the cysteine protease inhibitor E64d, implying integrin-mediated uptake and cathepsin-mediated activation of the targeted cathepsin S probe in cancer cells. In contrast, application in a healthy cell line resulted in negligible fluorescence intensities, suggesting high overall selectivity of the probe for cancer cells and demonstrating the potential of the presented DOTAM-based dual functionality approach for future probe design.

The second part of this work describes the development of a DOTA-based lanthanide luminescent nitroreductase (NTR) activatable probe. NTR, an enzyme that is capable of reducing aromatic nitro groups to their corresponding amines, is almost exclusively found in bacteria and thus constitutes an attractive target for bacterial imaging applications. The probe is activated through NTR-mediated formation of a carbostyril sensitizing antenna proceeding from a conceptually novel silent caged carbostyril precursor, by which subsequently energy transfer to a DOTA-chelated terbium ion is facilitated. This results in a large signal increase through long-lived lanthanide-centered luminescence allowing for time-gated detection of NTR activity. We could demonstrate that the probe is selectively activated by NTR while remaining essentially non-emissive in presence of other reductive and oxidative bioanalytes. Additionally, the probe

not only enabled the detection of NTR in bacterial lysates but was also capable of tracing NTR activity in live bacteria of the ESKAPE family, a group of clinically highly relevant pathogens often developing multidrug resistance responsible for the majority of nosocomial infections. The probe system further features a favorable accumulation behavior: while the inactivated precursor is readily taken up by bacterial cells, the activated probe is not able to enter these, conversely suggesting intracellular entrapment. The presented work thus constitutes the first example to enable detection of bacterial NTR activity with lanthanide luminescent probes and, moreover, the first example to demonstrate fluorescence lifetime imaging of enzymatic activity in live cells with this type of probes.

KURZFASSUNG

Molekulare optische Sonden sind wertvolle Werkzeuge für Forschung und präklinische Anwendungen und werden zunehmend in die klinische Praxis als sensitive bildgebende Diagnostika integriert, um die nichtinvasive Echtzeitüberwachung pathologischer Abweichungen auf der molekularen Ebene ermöglichen. Die vorliegende Arbeit behandelt die Entwicklung, Charakterisierung und Anwendung neuartiger enzymaktivierbarer molekularer Sonden basierend auf dem DOTA-Gerüst (1,4,7,10-Tetraazacyclododecan-1,4,7,10-tetraessigsäureamid) als zentrales, multifunktionalisierbares und hochflexibles Templat.

Das erste Projekt der Arbeit befasst sich mit der Entwicklung komplexer doppelt funktionaler DOTAM-basierter fluoreszenter Sonden für die Erkennung von Krebs, welche vorteilhafte Eigenschaften von zielgerichteten und substratbasierten Sonden vereint. Die Sonde beinhaltet das DOTAM-Gerüst als inhärentes strukturelles Motiv einer Cathepsin S-aktivierbaren FRET-Sequenz sowie cRGDfK-Peptidliganden, welche bevorzugt an $\alpha_v\beta_3$-Integrine binden, und kombiniert hierdurch Erkennungsmotive für zwei hochrelevante und spezifische Krebstargets. Es konnte gezeigt werden, dass die Sonde und ein nicht-zielgerichtetes Kontrollanalog exzellente *in vitro* Aktivierungskinetiken aufweisen und regiospezifisch durch Cathepsin S gespalten werden, und dass sie unempfindlich gegenüber einer Reihe intrazellulärer Bioanalyten sind. Der Vergleich zur nicht-zielgerichteten Kontrolle ergab eine signifikant verbesserte Markierungseffizienz von Krebszellen für die doppelt funktionale Sonde, welche mit der Anzahl an $\alpha_v\beta_3$-Rezeptoren auf den verschiedenen Zelllinien korrelierte. Darüber hinaus wurde die Aktivierung der Sonde stark sowohl durch Präinkubation mit cRGDfK Peptid als auch dem Cysteinprotease-Inhibitor E64d abgeschwächt. Dies lässt auf Integrin-vermittelte Aufnahme und Cathepsin-vermittelte Aktivierung der Sonde in Krebszellen schließen. In einer gesunden Zelllinie wurden hingegen vernachlässigbare Fluoreszenzintensitäten beobachtet, was auf eine hohe übergreifende Selektivität der Sonde für Krebszellen hindeutet und das Potential des vorgestellten Ansatzes DOTAM-basierter doppelt funktionaler Sonden demonstriert.

Der zweite Teil der vorliegenden Arbeit beschreibt die Entwicklung einer aktivierbaren DOTAM-basierten Lanthanoid-lumineszenzsonde für Nitroreduktase (NTR). NTR ist ein Enzym, das in der Lage ist, aromatische Nitrogruppen zu den entsprechenden Aminen zu reduzieren. Da es fast ausschließlich in Bakterien vorkommt, stellt es ein attraktives Target für Anwendungen bakterieller Bildgebung dar. Ausgehend von einem neuartigen stillen Carbostyril-Vorläufer wird die Sonde durch die NTR-vermittelte Bildung einer sensibilisierenden Carbostyril-Antenne aktiviert. Dies ermöglicht Energietransfer zu einem

DOTA-komplexierten Terbiumion. Dies resultiert in einer starken Signalzunahme durch langlebige, Lanthanoid-zentrierte Lumineszenz, welche die zeitgesteuerte Detektion von NTR-Aktivität erlaubt. Es konnte gezeigt werden, dass die Sonde selektiv durch NTR aktiviert wird, während sie in Gegenwart anderer reduktiver und oxidativer Bioanalyten still bleibt. Weiterhin ermöglicht die Sonde nicht nur die Detektion von NTR in bakteriellen Lysaten, sondern ist ebenfalls in der Lage, das Enzym in lebenden Bakterien der ESKAPE-Familie nachzuweisen, eine Gruppe klinisch hochrelevanter Krankheitserreger welche oft Multiresistenzen ausbilden und für den Großteil der Krankenhausinfektionen verantwortlich sind. Das Sondensystem weist zusätzlich ein vorteilhaftes Akkumulationsverhalten auf: während der inaktive Vorläufer schnell von Bakterienzellen aufgenommen wird, ist die aktivierte Sonde nicht in der Lage in diese zu permeieren, was darauf hindeutet, dass sie intrazellulär eingeschlossen und angereichert wird. Die vorliegende Arbeit stellt das erste Beispiel von Lanthanoid-Lumineszenzsonden zum Nachweis bakterieller NTR-Aktivität dar und beinhaltet darüber hinaus die erste Anwendung von Fluoreszenzlebensdauer-Mikroskopie zur Bildgebung enzymatischer Aktivität in lebenden Zellen mit Lanthanoid-Lumineszenzsonden.

TABLE OF CONTENTS

ABBREVIATIONS

ABP	Activity-based probe
Acetyl CoA	Acetyl coenzyme A
AIE	Aggregation-induced emission
AMC	Aminomethylcoumarin
AMR	Antimicrobial resistance
AOMK	Acyloxymethyl ketone
CCKR	Cholecystokinin receptor
CEA	Carcinoembryonic antigen
CT	Computed tomography
CTSS	Cathepsin S
Cy	Cyanine
DELFIA	Dissociation-enhanced lanthanide fluorescence immunoassay
DNA	Deoxyribonucleic acid
DO3A	1,4,7,10-Tetraazacyclododecane-1,4,7-triacetic acid
DOTA	1,4,7,10-Tetraazacyclododecane-1,4,7,10-tetraacetic acid
DOTAM	1,4,7,10-tetraazacyclododecane-1,4,7,10-tetraacetic amide
ΔE_g	Energy gap (between lowest emissive and highest ground state of a lanthanide)
EALL	Enzyme-amplified lanthanide luminescence
ECM	Extracellular matrix
EDTA	Ethylenediaminetetraacetic acid
ET	Energy transfer
FA	Folic acid
FAP	Fluorogen activating protein
EGFR	Epidermal growth factor receptor
FDA	U.S. Food and Drug Administration
FDG	Fluorodeoxyglucose
FLIM	Fluorescence lifetime imaging
FRα	Folate receptor α
FRET	Förster-resonance energy transfer
GAG	Glycosaminoglycan

GDEPT	Gene-directed enzyme prodrug therapy
GH	Growth hormone
HCV	Hepatitis C virus
HER2	Human epidermal growth factor receptor 2
HIV	Human immunodeficiency virus
HTRF	Homogeneous Time Resolved Fluorescence
ICT	Intramolecular charge transfer
IQF	Internally quenched fluorescence
J	Total angular momentum
K_D	Dissociation constant
λ	Wavelength/[nm]
LAP	Leucine aminopeptidase
LC/MS	Liquid chromatography coupled mass spectrometry
LRET	Luminescence resonance energy transfer
MDR	Multidrug resistance
MG	Malachite green
MMP	Matrix metalloproteinase
MRI	Magnetic resonance imaging
NAT	*N*-acetyltransferase
NIR	Near-infrared
NOTA	1,4,7-Triazacyclononane-1,4,7-triacetic acid
NTR	Nitroreductase
OI	Optical imaging
PAI	Photoacoustic imaging
PCR	Polymerase chain reaction
PeT	Photoinduced electron transfer
PET	Positron emission tomography
PMK	Phenoxymethyl ketone
qABP	Quenched activity-based probe
RAFT	Regioselectively addressable functionalized template
RGD	Arginine-glycine-aspartic acid
SAR	Structure-activity relationship
SMVT	Sodium-dependent multivitamin transporter

SPECT	Single photon emission computed tomography
SSEA-1	Stage-specific embryonic antigen-1
SST_2	Somatostatin receptor type 2
STS	Soft-tissue sarcoma
TACN	Triazacyclononane
$\tilde{v}$	Wavenumber/[cm^{-1}]
VEGF	Vascular endothelial growth factor
YLL	Years of life lost

1 INTRODUCTION

Small-molecule chemical probes are powerful tools for the investigation of fundamental biological questions. Moreover, they constitute invaluable components for bioimaging and molecular imaging applications on a translational level and in clinical settings. Not only can they be precisely tailored and tuned by means of chemical modification to incorporate specific functions governing their interaction with a certain biological target of interest, including structural features for recognition, their mode of activation, and their localization behavior, but they also can be endowed with an analytical readout of choice. In particular the synergistic combination of rational probe design and sophisticated imaging instrumentation allows for the non-invasive real-time monitoring of biological processes in their native context at a molecular level.[1]

The main modalities employed for molecular imaging to date are positron emission tomography (PET), single photon emission computed tomography (SPECT), magnetic resonance imaging (MRI), optical imaging (OI) including fluorescence and bioluminescence imaging, and, more recently, photoacoustic imaging (PAI). These molecular imaging modalities are often used in conjunction with complementary structural imaging methods (CT, MRI) for an anatomic reference when it comes to whole-body imaging.[2-6] Each modality has particular advantages and resulting application areas owing to distinct sensitivities, resolution, and penetration depths. Optical imaging techniques may not yet have the capabilities of deep-tissue imaging due to light scattering and absorption; however, they stand out due to their very good resolution and sensitivities as well as their comparably low instrumentation costs and short acquisition times suited for real-time imaging.[4,7-8] Especially small-molecule fluorescent probes are powerful, widely utilized research tools for the imaging of biological systems on a cellular level, in particular because of the convenience of introducing a fluorescent label to a chemical scaffold.[9-13] Their applications include the investigation of the underlying mechanisms of gene expression, protein function and -interaction, signaling pathways, and the imaging of cellular compartments. Additionally, in recent years the translation of small-molecule fluorescent probes towards clinical implementation has made a big step forward with regard to biopsy, intraoperative imaging and endoscopy applications with some candidates being evaluated in clinical trials, demonstrating the high significance of this research area.[14-19] While the utilization of optical probes for *in vivo* whole-body imaging is still restricted to preclinical small-animal disease models due to optophysical constraints, their broader application in clinical diagnostics and pre-operative planning is only a matter of time considering the continuing development of probes with enhanced optical properties as well as rapid instrumental advancement.[14]

1.1 Small-Molecule Fluorescent Probes for Imaging Enzymatic Activity

Studying the activity of proteins and enzymes within their natural environment is crucial for the understanding of their mechanisms and biological functions. Enzymes and their catalyzed reactions are needed to maintain homeostasis in living organisms, and aberrant enzymatic activity often causes biological disorders and pathogenicity connected to various diseases.[20-22] However, probing enzyme activity is not only a central and essential approach for unraveling the complex networks of human health and disease, but also an important aspect in the development and profiling of biomarkers and new drugs.[23-24] Fluorescence microscopy and imaging with small-molecule fluorescent probes have proven to be powerful tools for the tracing of enzymatic activity; the molecular reporters allow precise modifications and fine-tuning of their properties up to the smallest detail resulting in good overall cellular permeability, low cytotoxicity and high brightness, and the whole approach enables real-time investigations of the biological system in its natural state without requiring genetic manipulation.[17,24-28]

In general, the design of fluorescent probes for the imaging of enzymatic activity can be divided into activity-based probes (ABPs) labeled with a fluorescent tag and activatable "smart" probes. Fluorescent ABPs will covalently label the active site of a protein with a fluorophore thus rendering the target enzyme inactive, while activatable probes usually rely on the modulation of the probe's fluorescent signal through the specific reactivity of the enzyme.[24] In addition, combinations of both principles have been reported.[29-30] More recently, a third class of "traceless" ligand-directed labeling probes has been developed. These probes reversibly interact with the binding site of a target protein and transfer their fluorescent moiety onto a neighboring amino-acid side chain, thus leaving the enzyme's activity intact.[31-33]

Numerous different design concepts for fluorescent small-molecule enzyme-activatable probes have been developed. The fundamental strategy relies on the type of physical quenching mechanism they exploit, including Förster-resonance energy transfer (FRET), photoinduced electron transfer (PeT), intramolecular charge-transfer (ICT), rotational quenching in the case of aggregation-induced emission probes (AIE), or otherwise alterations of the absorption or emission properties of a dye.[24,26-27] The activation of the fluorescent signal can hereby be induced by purely physical intermolecular interactions or through enzyme-induced chemical modifications of a fluorophore, a fluorogenic substrate, or the environment of a fluorophore, such as cleavage of a proximal quencher.

1.1.1 Cysteine Cathepsin Proteases

Proteases are a distinct class of enzymes that catalyze the degradation of proteins through the hydrolytic cleavage of amide bonds. However, their physiological significance lies far beyond the role of simple destructive enzymes, as they have been shown to be involved in a multitude of biological events. These range from regulating the localization and activity of other proteins and modulating protein-protein interactions, over contributing to cellular signal transduction, tissue homeostasis and immune response, to influencing DNA replication and transcription.[34-36] Likewise, deviations of the enzymes' activity from their native regulation is connected to various inflammatory diseases and cancer. Moreover, proteases are integral components of the invasive machinery of many infectious pathogens, such as HIV, HCV, and *Bacillus anthracis*.[37-38]

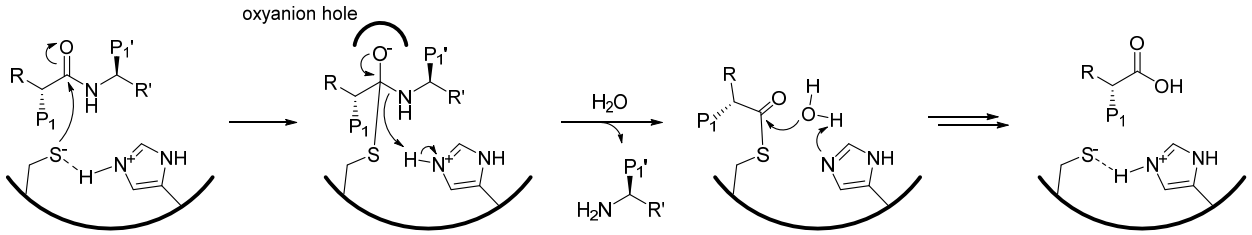

Scheme 1: Simplified mechanism for substrate hydrolysis by cysteine proteases.

Proteases can be divided into several subclasses depending on the amino acid or metal that is performing the nucleophilic attack on the peptide bond ultimately leading to scission of the substrate, including serine, aspartic, threonine, cysteine and metalloproteases.[23] Cysteine proteases, and in particular cysteine cathepsins, play a key role amongst the lysosomal proteases. The cathepsins B, L, C, X, F, O and V are ubiquitously expressed in human tissues, whereas the cathepsins K, W and S have a very limited expression range.[39] Cathepsin S (CTSS) is mainly confined to antigen-presenting cells such as dendritic cells and B-cells and is increasingly expressed by macrophages upon exposure to proinflammatory stimuli.[40] In contrast to its related family members, cathepsin S is not restricted to acidic pH domains but retains it activity still in neutral and slightly basic pH.

The mechanism of substrate hydrolysis for cysteine proteases is illustrated in Scheme 1; findings are mainly derived from papain as a well-studied model enzyme for cysteine proteases.[41] The substrate is bound through specific intermolecular interactions of its peptide backbone and amino acid side chains (designated P_1, P_2 and P_1', P_2' and so forth, counting from the cleavage site towards the *N*- or *C*-terminus, respectively) with well-defined corresponding subsites of the protease (designated S_1, S_2, S_1', S_2',…).[42] It is assumed that a thiolate-imidazolium ion pair constituted by proximal cysteine and histidine side chains (Cys-25 and

His-159 for papain) is present as catalytically active dyad within the enzyme active site, although the exact protonation state is still under debate.[43-44] The thiolate attacks the peptide substrate to form a transient tetrahedral intermediate. The resulting oxygen anion is stabilized by the oxyanion hole of the active site, which is defined by a glutamine side chain and a cysteine amide. Following release of the first amine cleavage product, the acyl-enzyme adduct is subsequently hydrolyzed by a water molecule, resulting in the formation of the second carboxylic acid fragment and regeneration of the free active site.

Cathepsins are tightly controlled under normal conditions, being expressed as preproenzymes and regulated by a number of endogenous inhibitors after their posttranslational activation to prevent any improper activity.[39] Equally, the dysregulation of cathepsin expression and activation has been linked to inflammatory diseases such as atherosclerosis[45] and rheumatoid arthritis[46], and cancer[47-48]. Especially in cancer, cathepsins have been found to be pivotally involved in processes such as tumor growth, invasion, metastasis, and degradation and remodeling of the extracellular matrix (ECM).[48-49] Elevated cathepsin levels are directly correlated with poor prognosis in cancers including breast, lung, and colorectal cancer, and are furthermore predictive markers for treatment response.[48,50-52] These aspects highlight the acute relevance of proteases and in particular cysteine cathepsins as central targets for the development of drugs and imaging tools exploiting them as diagnostic and prognostic biomarkers in cancer and inflammatory diseases.[53]

1.1.2 Fluorescent Probes for Cysteine Proteases

A series of different strategies have been developed for the design of fluorescent protease probes (see Figure 1). A basic approach is connecting a protease-specific sequence at the C-terminus to an amine-containing dye, such as aminomethyl coumarin[54], 7-amino-4-trifluoromethylcoumarin[55], or rhodamine110[56], *via* an amide bond. Hydrolytic cleavage of the bond leads to release of the parent fluorophore that exhibits shifted absorption and emission maxima likely due to modulation of the intramolecular charge transfer (ICT) through conversion from the electron-withdrawing amide to an electron-rich amine.[57] These probes have been mainly used *in vitro*, such as for detection of caspase activity in apoptotic cells[55], or of cathepsin B and L activity in rat microglia by flow cytometry[56].

A second class of fluorescent probes exploits a distance-dependent non-radiative energy transfer mechanism - termed Förster-resonance energy transfer - by placing a fluorescent donor in spatial proximity (<100 Å) to a suitable acceptor linked by a protease-specific substrate sequence. The donor/acceptor pair has to be selected such that a preferably high spectral overlap between donor emission and acceptor absorption is given.[11] The acceptor can be a fluorescent dye itself giving rise to FRET substrates, or a dark

quencher resulting in more narrowly defined 'internally quenched fluorescent' (IQF) probes.[58] Protease-mediated cleavage of the sequence eventually gives rise to the donor-centered fluorescence due to release of the acceptor.

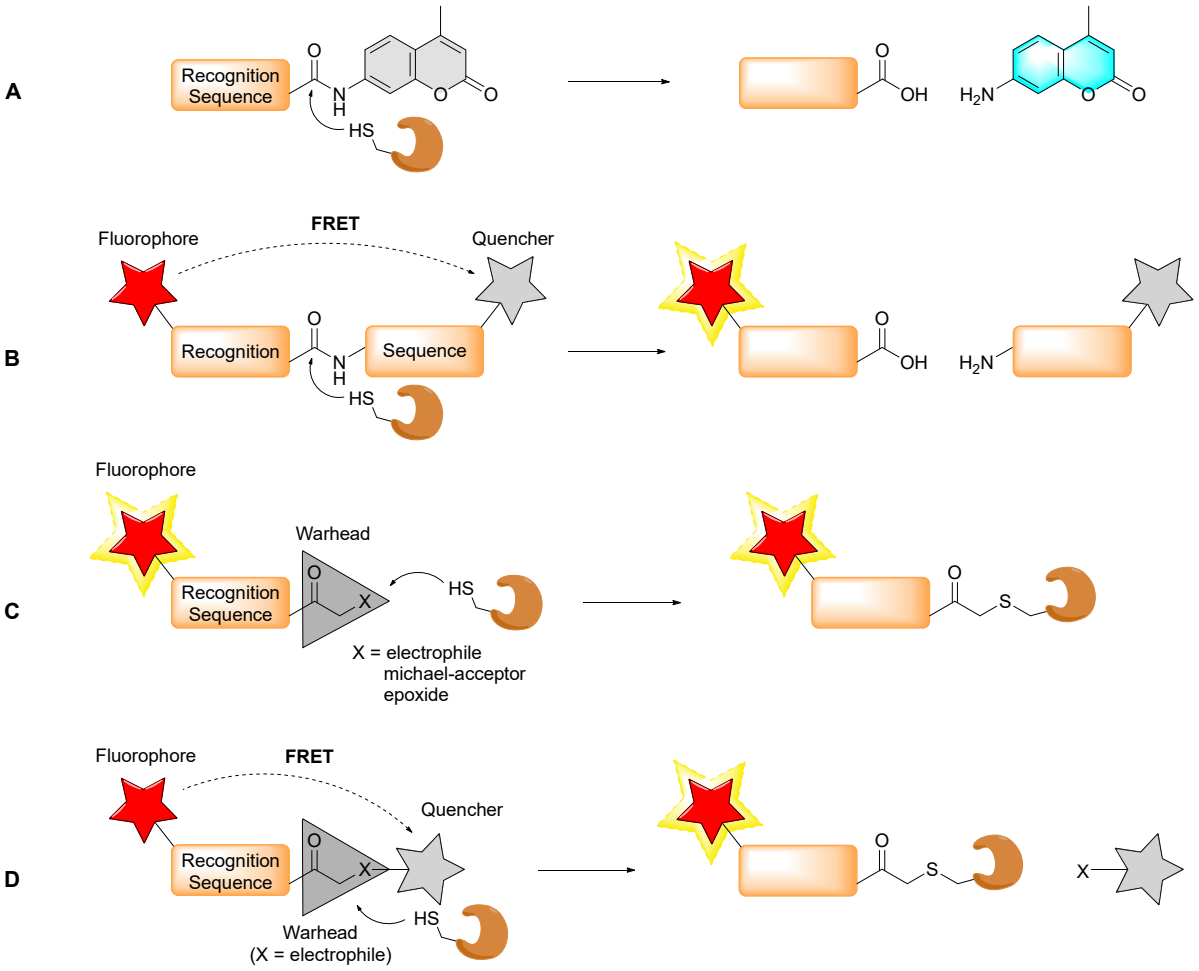

Figure 1: Strategies for the design of fluorescent protease probes. **A)** *Fluorogenic substrate*. A dye (depicted is aminomethylcoumarin, AMC) is linked to a protease substrate *via* amide bond. Scission at this bond results in liberation of the dye with shifted absorption and emission wavelengths and intensities. **B)** *FRET-quenched substrate*. A native or inhibitor-derived sequence connects fluorophore and quencher. Cleavage of the substrate by the target protease results in spatial separation of the dye from the quencher giving rise to excitable fluorescence. **C)** *Activity-based probe (ABP)*. A fluorophore is attached to a protease recognition feature equipped with a reactive moiety (warhead). Attack of the target protease at the warhead leads to formation of a covalent bond between protease and fluorescent ABP, thus labeling the protease. **D)** *Quenched activity-based probe (qABP)*. Essentially a combination of **B)** and **C)**. A fluorophore is attached to a protease recognition feature that is linked to a leaving group connected to a quencher. Attack of the target protease at the warhead leads to formation of a covalent bond between protease and probe with concomitant release of the quencher, thus giving rise to excitable fluorescence.

The latter strategy has been employed extensively for the design of activatable protease probes. One of the most prominent group of quenched probes used for preclinical fluorescence imaging of protease activity, in particular cathepsins, are the commercially available polymer-based ProSense NIR probes (Perkin Elmer, see Figure 2, A), which were initially developed and reported by the Weissleder group in 1999.[59-60] These

probes, consisting of a partially pegylated Cy5.5-labeled polylysine copolymer, have been thoroughly utilized for the *in vivo* imaging of tumor models in mice and for elucidating the contributions of cathepsins to asthma, focal inflammation, angiogenesis, and polyp growth in mouse models.[61-62] A current example for an IQF cathepsin probe that is being evaluated in clinical trials is LUM015, a pegylated GGRK peptide linked to Cy5 and the dark quencher QSY-21. The probe is activated by cathepsins S, K and L (Figure 2, B). LUM015 is the first of its kind that has successfully passed phase 1 clinical trials for the intraoperative optical imaging of soft-tissue sarcoma (STS) and breast cancer during surgical resection upon intravenous administration.[63] Further clinical studies are currently in progress for the intraoperative detection of residual cancer tissue in breast cancer patients (phase II and III) and for the feasibility of LUM015 for the *ex vivo* detection of adenocarcinomas (phase I/II).[64-66]

While natural substrates for proteases are peptides, structural features derived from non-natural protease inhibitors can also serve as cleavable substrates. This concept, which was termed 'reverse design', takes advantage of the use of drug-like and highly selective optimized irreversible inhibitor scaffolds that are converted into scissile substrates by replacing their reactive warhead with a cleavable amide bond.[67-69] Additionally, the availability of extensive structure-activity relationships (SARs) for such scaffolds further allows for the deliberate introduction of appropriate reporter groups to generate selective activatable fluorescent protease probes. This strategy was applied for the generation of cathepsin S-selective fluorescent activatable probes for the imaging of cancer cells based on a cathepsin S-specific irreversible inhibitor.[67,70] It was demonstrated that these inhibitor-derived probes can be used to visualize cathepsin S activity in a murine model of zymosan-induced paw inflammation with a much faster activation compared to the commercial substrate ProSense680.[68] However, one of the major drawbacks of substrate-based probes is insufficient tumor-accumulation when they are administered systemically. This disadvantage has been addressed by a lipidation approach to locate the probe to cell surfaces. By introducing a palmitic acid residue to the probe, highly favorable accumulation properties and higher retention in a mouse tumor model compared to its non-lipidated counterpart could be observed (Figure 2, C).[69]

A different approach as opposed to substrate-based probes constitute activity-based probes (ABPs). ABPs are constructed of a reactive group (warhead) and a reporter tag linked to it by a spacer that can contain a recognition sequence to induce selectivity for a certain protease.[71] ABPs will only react with active enzymes forming a covalent bond between the electrophilic warhead and the nucleophilic, catalytically active amino acid side chain, leading to the enzyme's irreversible inactivation. ABPs have been utilized for a series of applications in combination with biochemical techniques, including proteome profiling, inhibitor screening, and target identification, but can also be used as molecular tools for optical imaging applications *in vivo*.[72] As such, fluorescent ABPs have been used to verify cathepsin protease activity in different stages

of pancreatic tumorigenesis in mice[73] or non-invasively image caspase-induced apoptosis in mice[74]. However, this sort of ABPs has the drawback of being fluorescent regardless of target interaction.

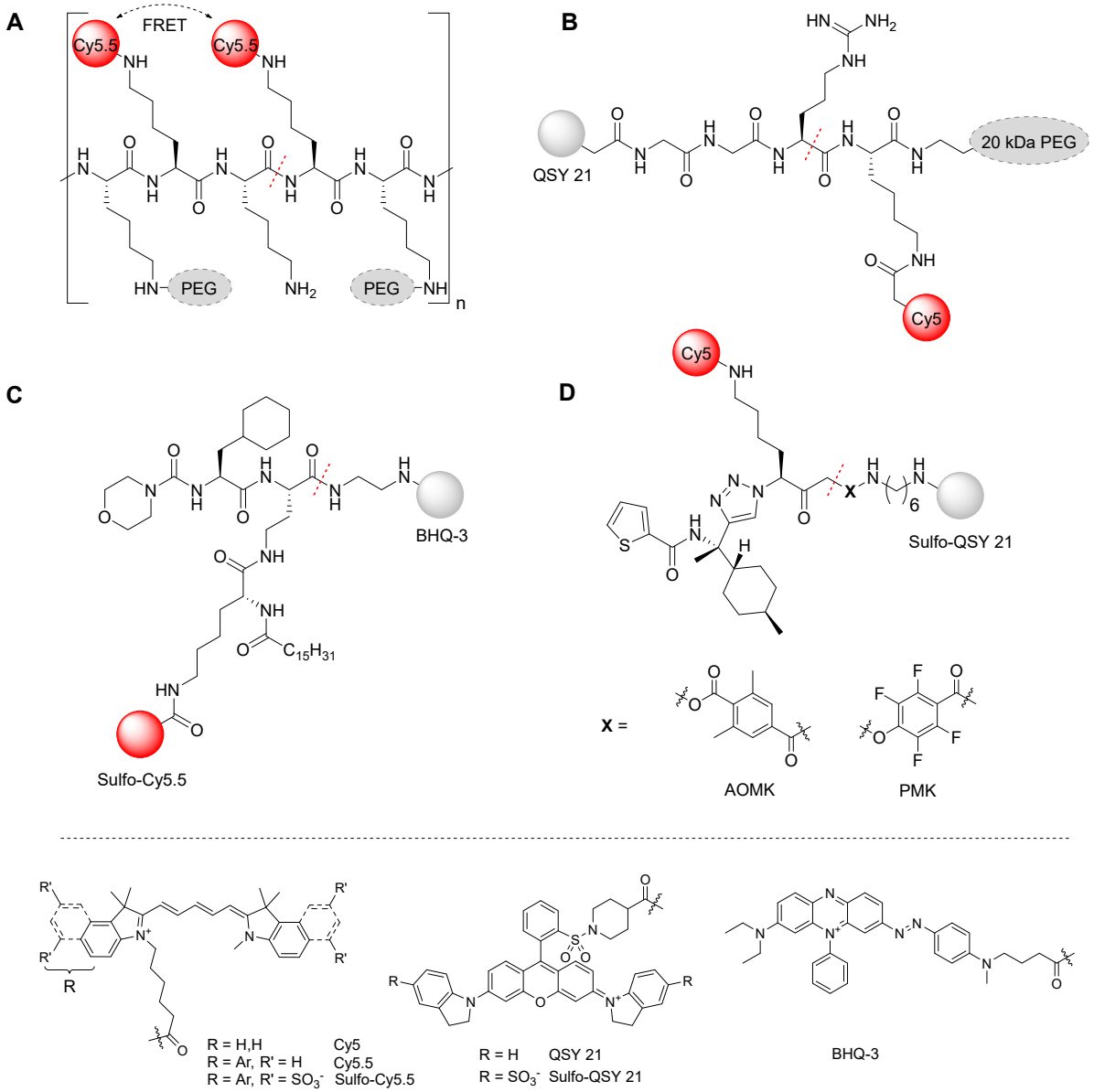

Figure 2: Fluorescent cysteine protease activatable probes. **A)** Schematic representation of Perkin Elmer's polylysine-based protease probe ProSense680 with indication of FRET-interaction between the dyes. **B)** Structure of CTS probe LUM015, currently in clinical phase II and III trials for intraoperative fluorescence-guided cancer resection. **C)** Structure of selective cathepsin S probe developed through 'reverse design' by Hu *et al.*[69] based on a CTSS inhibitor. **D)** Structure of CTSS selective qABPs containing AOMK or PMK warheads developed by Bender *et al.*[30] Red dotted lines indicate cleavage sites.

To overcome this limitation, quenched activity-based probes (qABPs) have been developed by Blum *et al.*, which are essentially non-emissive but become fluorescent upon labeling of the target protein, inducing associated cleavage of the quencher.[29] Acyloxymethyl ketone (AOMK) and phenoxymethyl ketone (PMK) linkers were explored serving as electrophilic leaving groups bearing the quencher, differing in their

intrinsic reactivity towards cathepsins. The probes were effective for *in vivo* fluorescence imaging of cysteine cathepsin activity in mouse tumors.[75] A highly selective cathepsin S probe was developed serving as imaging tool for cathepsin S activity in bone marrow-derived dendritic cells and mouse breast tumors (Figure 2, D).[30] Additionally, bifunctional pH-sensing cathepsin qABPs revealed increases in the endolysosomal pH of *salmonella typhimurium*-infected cells, which were understood as possible bacterial defense mechanism to attenuate cathepsin activity and dampen host immune response.[76]

Owing to their distinct mechanistic approaches, substrate-based probes and ABPs offer different advantages and disadvantages. While ABPs react with their target enzymes in a one-to-one fashion, substrate-based probes are in theory able to provide a huge signal amplification due to multiple probe molecules being activated by a single enzyme, thus being suitable for the detection of low-abundance enzymes with high sensitivity. On the other hand, the covalent labeling with ABPs enables the dynamic visualization of activation, localization, and distribution of the target enzyme within its natural compartments. However, it remains unclear to which extent the inactivation of the enzyme through covalent labeling alters the dynamics of the biological system. Collectively, the mentioned examples illustrate the high significance of developing fluorescent probes for cathepsin activity as highly sensitive tools for the imaging of diseases such as cancer and inflammation processes as well as for the elucidation of their underlying biological mechanisms.

1.1.3 Nitroreductases

Nitroreductases (NTRs) are members of an enzymatic flavin-containing superfamily that are able to catalyze a series of reductive reactions in the presence of NADH or NADPH, such as the reduction of aromatic nitro groups to their corresponding amines.[77-78] The majority of NTRs is of bacterial origin and can be classified based on the underlying reduction mechanism into oxygen-sensitive (type II) and –insensitive (type I) NTRs.[79-80] Reduction of nitroaromatics by type II NTRs proceeds *via* two consecutive one-electron transfers, initially yielding a nitro radical anion. This intermediate can subsequently be quenched by the presence of molecular oxygen, forming a superoxide anion which in turn regenerates the nitro functionality, hence the classification of the parent reductases (see Scheme 2). Reduction through type I NTRs proceeds through an initial single electron pair transfer to form a nitroso group as first intermediate of the reduction pathway. To date, a very limited number of nitroreductases has been characterized and surprisingly little is known about this enzyme class.[78] Most investigations in this context have been focused on the two type I *Escherichia coli* enzymes NfsA[81] and NfsB[82].

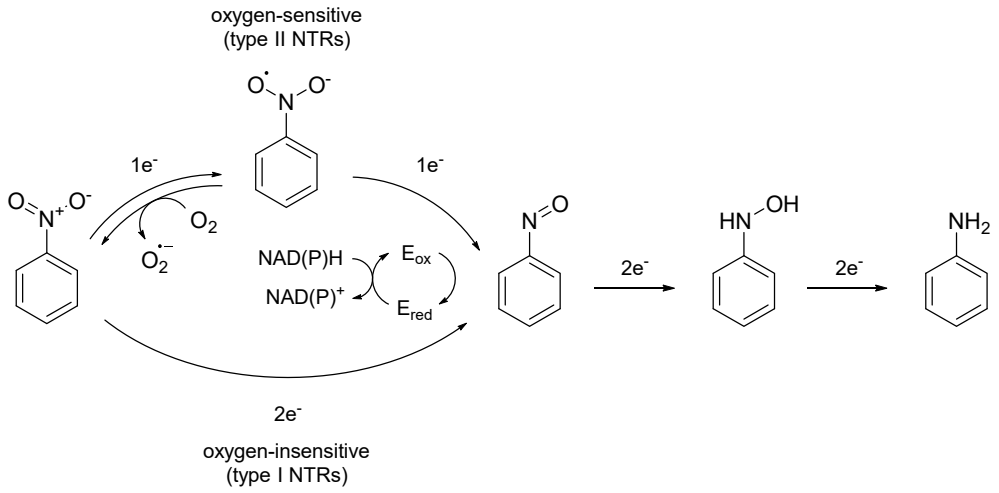

Scheme 2: Schematic representation of the reduction mechanisms of nitro substrates by type I (oxygen-insensitive) and type II nitroreductases; the coenzyme NAD(P)H is reduced to $NAD(P)^+$ in order to regenerate the reduced enzyme for each reduction step.

Nitroreductases have been explored as activating enzymes for gene-directed prodrug therapy (GDEPT) in cancer treatment.[83] GDEPT is a relatively new therapeutic approach that aims to reduce side-effects and improve efficiency of chemotherapy by delivering genetically encoded therapeutic enzymes specifically to cancer cells *via* a bacterial or viral vector that is selective for the cancer cells of choice.[83] The therapeutic enzyme, which consequently is exclusively expressed in cancer cells, will transform a systemically applied non-cytotoxic prodrug into its corresponding cytotoxic form at the cancer site. In this context the combination of nitroreductases, such as *E. coli* NfsB, with the chemotherapeutic prodrug CB1954 has been evaluated in multiple clinical trials and is still being actively pursued.[84-87] CB1954 is initially reduced by NfsB to the 2- and 4-hydroxylamine derivatives (Scheme 3). Reduction of the electron-withdrawing nitro groups generally increases the basicity of the aziridine-nitrogen, thus rendering it a more potent electrophile through facilitated protonation. The 2-hydroxylamine is converted in a disproportionation reaction to the 2-amine, which is a DNA monoalkylating agent because the basic aziridine functionality is protonated under physiological pH and thus highly electrophilic. It is assumed to be the CB1954 metabolite accountable for the strong "bystander effect" of the drug, exerting cytotoxic effects in local proximity to the NfsB-transfected tumor cells through diffusion to neighboring cells.[88] The 4-hydroxylamine is formed through 4-nitro reduction of CB1954 and can react with acetyl coenzyme A to form a 4-acetoxyamine. This metabolite undergoes elimination to a highly reactive nitrene, thereby acting as strong DNA-crosslinking chemotherapeutic through consecutive alkylation at the nitrene and the aziridine functionalities.[89]

Given the abundance of NTRs in the bacterial realm including *Mycobacterium tuberculosis*[90], those enzymes have recently become attractive targets as markers for bacterial imaging in the context of bacterial infections and bacterial gene delivery.[80,91] Infections caused over 8 million deaths in 2017 and are currently

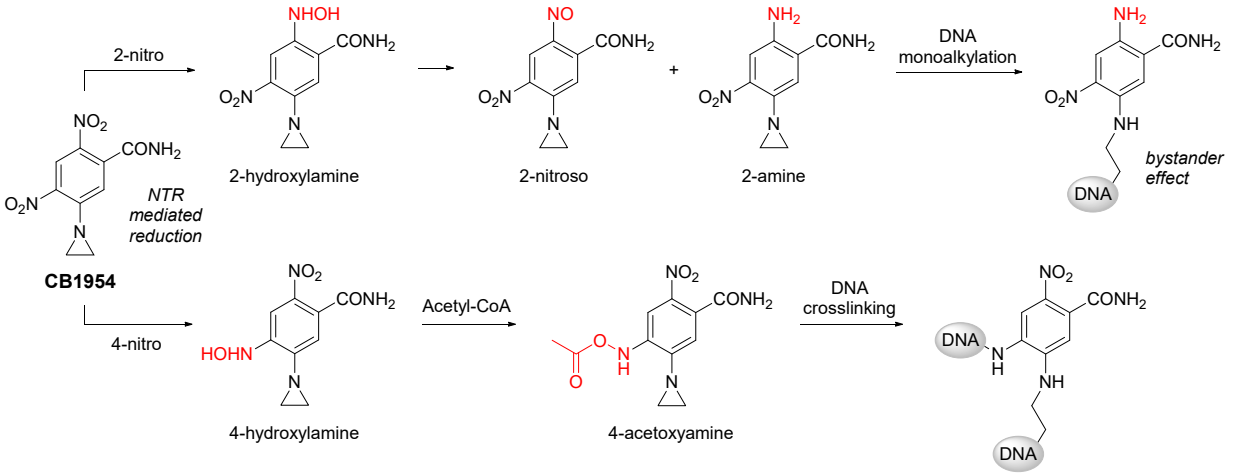

Scheme 3: Activation pathways of prodrug CB1954 by NTR-mediated reduction, leading to powerful genotoxic metabolites capable of DNA alkylation and crosslinking.

ranked the third highest amongst global mortality causes after cancer and cardiovascular diseases. Moreover, they are ranked the main global cause of morbidity with about 400 million years of live lost (YLL) in 2017.[92-93] In particular, antimicrobial resistance (AMR) is a major emerging health concern, with global deaths estimated to increase from 700,000 per year in 2016 to about 10 million in 2050 if no measures were taken.[94] For those reasons there is high incentive not only to develop new treatment options that tackle AMR, but also to provide novel diagnostic tools that allow for the rapid, non-invasive detection of multidrug resistant pathogens in real time.[95-98] Therefore, the development of functional and highly sensitive optical probes capable of tracking NTR activity in order to be able to directly visualize bacterial pathogens both *in vitro* and *in vivo* is subject of current research.

1.1.4 Fluorescent Probes for Nitroreductases

Although several reports have been published on the field of fluorescent NTR probes, in particular in the last 10 years, virtually all of these probes contain a nitro functionality as common motif that constitutes a reducible trigger for the activation of fluorescence. The nitro group is connected to a fluorogenic element either directly or by a (self-immolative) linker and often acts as quenching functionality through a PeT or ICT mechanism.[99-100] In this context, it should be noted that the present activation paradigm for fluorescent nitroreductase probes can also be transferred to probes for the imaging of hypoxia. This is the reason why many probes developed for NTR detection in the context of bacterial imaging were similarly applied for the imaging of hypoxic cancers or *vice versa*, thus both applications can hardly be separated.

Hypoxia describes a state of tissue regions with low oxygen partial pressure and is connected to diseases such as cardiovascular diseases, pulmonary diseases, and cancers associated with bad prognoses.[101-103] Cells in solid tumors proliferate in an uncontrolled fashion, leading to underdeveloped and chaotic vascularization. Hence, nutrient and oxygen supply quickly becomes non-sufficient. While nitroreductases are usually not found in mammals with the exception of iodotyrosine deiodinase, an enzyme that catalyzes the reductive dehalogenation of iodinated tyrosines to maintain the levels of thyroid hormones[104-105], other reductive enzymes are able to trigger similar overall reduction reactions to those observed with NTRs. These include cytochrome P450 reductase, NAD(P)H dehydrogenase and NADH cytochrome b_5 reductase, which can all act as one-electron donators.[106-107] Under normoxic conditions in healthy cells, one-electron reduction of the probe as the first activation step is reversed by subsequent reduction of molecular oxygen to the superoxide anion. However, in hypoxic tumor-associated cells this scavenging process does not occur. This allows for further reduction of the respective molecule to its active state, which enables the discrimination of healthy and solid tumor tissue. Likewise, hypoxia-activated prodrugs for cancer treatment such as evofosfamide are subjects of current research with promising results emerging from multiple clinical trials.[108-111]

Figure 3 shows the main design and activation principles for NTR probes. In general, they can be divided into probes with a static linkage connecting the reducible nitro functionality, or a self-immolative linkage that will be eliminated upon reduction of the nitro group *via* a fragmentation cascade. Early concepts of the static linkage class probes contained the nitro group as integral part of the fluorogenic substrate, rendering the probe fluorescent upon reduction of the nitro functionality to the corresponding amine.[112] However, this strategy has also been utilized in later probe designs, such as for a NTR probe developed by Lee *et al.* that was able to trace NTR localization on a sub-diffraction scale in *B. subtilis* bacteria.[113] This was achieved by a single-molecule fluorophore super-resolution imaging technique which was termed by the authors "Enzymatic Turnover Activated Localization Microscopy" (Figure 4, A).[113]

A common motif for the design of NTR and hypoxia sensing probes is the 2-nitroimidazole moiety attached *via* suitable linker to a chromophore. 2-Nitroimidazole was originally evaluated for its antibiotic capabilities against anaerobic bacteria in 1953[114] based on its bioreduction to reactive electrophilic species, and was later thoroughly investigated in the context of cancer as hypoxia selective drug and labeling agent[107,115-116]. However, the 2-nitroimidazole moiety also serves as potent PeT acceptor and can therefore be used to generate turn-on fluorescent probes for NTR or hypoxia imaging.[117] A recent example of such a probe was developed by the Hu group, linking the 2-nitroimidazole moiety to a Cy5.5 fluorophore to generate a turn-on NTR-sensitive probe (Figure 4, B). The probe was successfully applied for the imaging of live ESKAPE

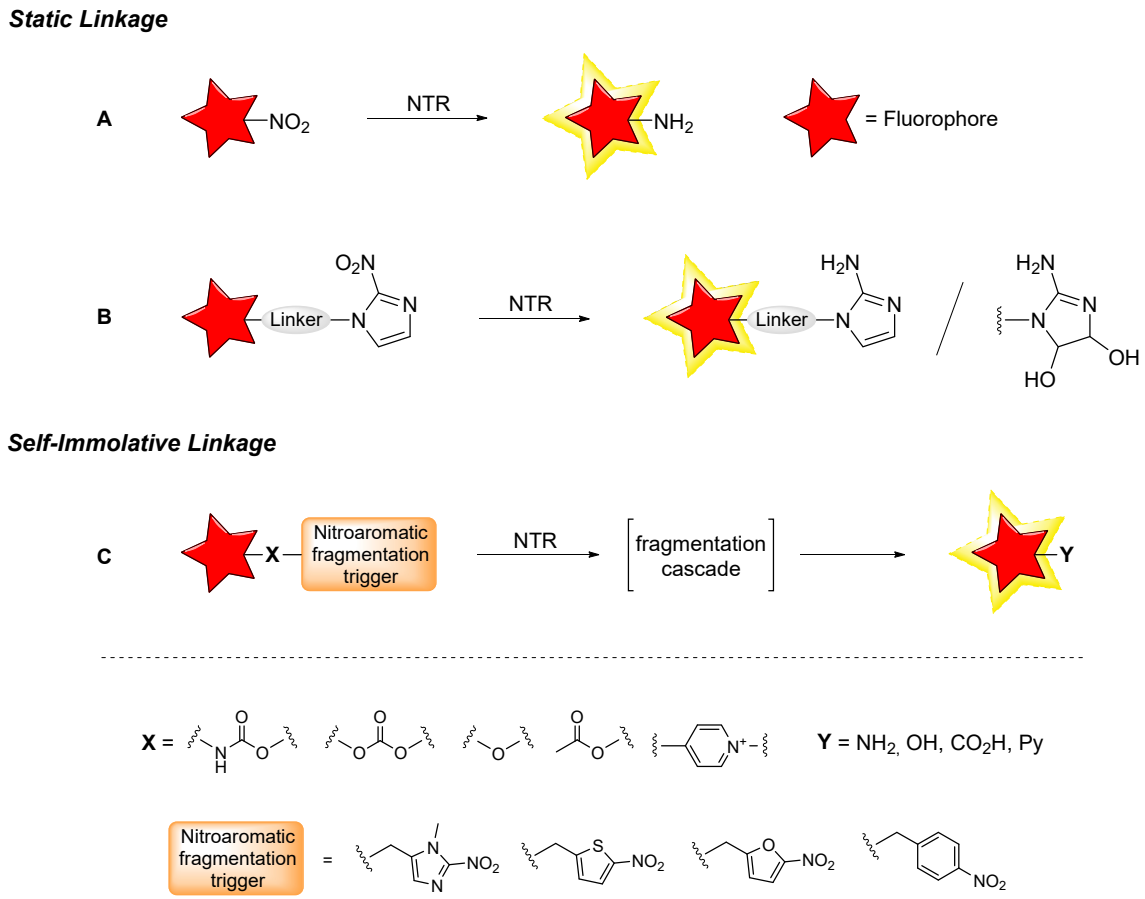

Figure 3: Major design principles for NTR-activatable probes based on static and self-immolative linkages. **A)** A nitro group is a direct part of a fluorogenic substrate acting as quencher through ICT. Reduction to the amine activates or shifts the fluorescence emission signal. **B)** 2-Nitroimidazole acts as quencher for the fluorophore it is connected to by a PeT mechanism. Reduction to the corresponding 2-aminoimidazole quenches PeT and enables fluorescence upon excitation. **C)** Strategies for NTR probes based on reduction-induced fragmentation: the fluorophore is connected to the nitroaromatic quenching moiety *via* a self-immolative linker. Commonly utilized nitroaromatic motifs include the 4-nitrobenzyl, 5-nitrofuran-2-yl, 5-nitrothiophen-2-yl and 2-nitro-*N*-methylimidazolyl residues. Those can be connected to the fluorophore *via* carbamate, carbonate, ether, ester, or pyridinium linkage.

pathogens (*Enterococcus faecium, Staphylococcus aureus, Klebsiella pneumoniae, Acinetobacter baumannii, Pseudomonas aeruginosa, and Enterobacter species*), a group of Gram-negative and –positive bacteria that are accountable for the majority of hospital infections through growing resistance against standard antibiotics treatments[118-120].

The overall concept of exploiting NTRs for the *in vivo* imaging of bacterial infections was greatly advanced by work of Stanton *et al.* in 2015, who developed the CytoCy5S probe consisting of a Cy5-derived squaraine dye connected to a 3,5-dinitrobenzyl quenching residue (Figure 4, C). The probe was initially studied for the non-invasive imaging of NTR expressing orthotopic tumor xenografts in mice in the context of GDEPT[121] and was later also applied for the *in vivo* bacterial imaging of *Salmonella* Typhimurium UK-1 and *E. coli* in mouse infection models[91].

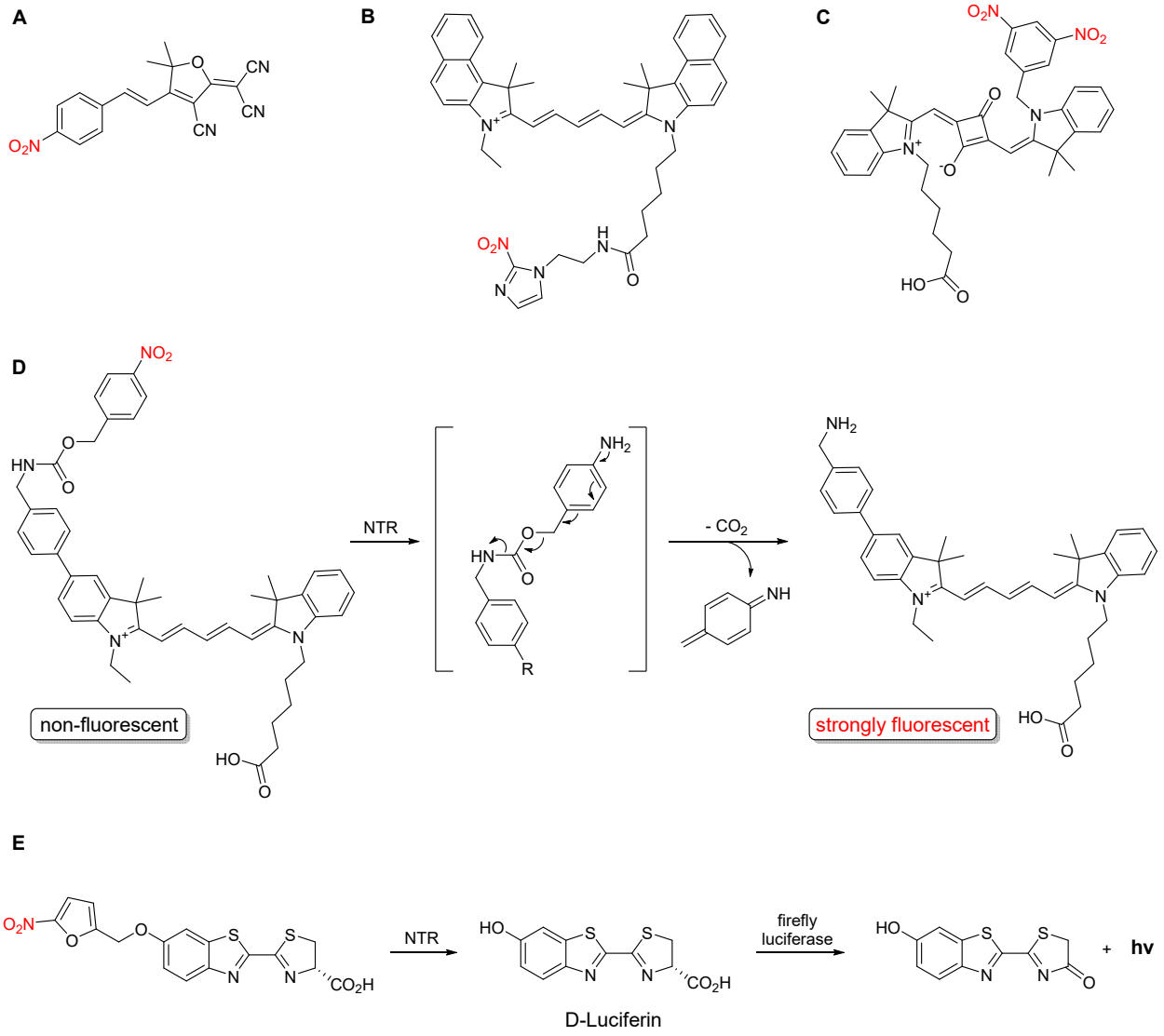

Figure 4: Probes for the detection of nitroreductase in the context of bacterial imaging or GDEPT tumor imaging. **A-C)** Fluorogenic probes based on static linkage of the nitro functionality. **D)** Fluorogenic Cy5-based probe with carbamate linked 4-nitrobenzyl residue that fragments upon exposure to NTR to release the parent benzylamine. **E)** Caged luciferin. Exposure to NTR leads to fragmentation of the 5-nitrofuranyl residue and release of D-luciferin which itself is the native substrate to firefly luciferase, generating bioluminescence upon oxidative decarboxylation by luciferase.

Regarding probes that employ a self-immolative linker strategy, nitroaromatic trigger motifs mainly include 4-nitrobenzyl, 5-nitrofuran-2-yl, 5-nitrothiophen-2-yl and 2-nitro-*N*-methylimidazolyl residues (see Figure 3 C), with the 4-nitrobenzyl residue representing the most commonly used.[25] These triggers can be linked to their corresponding parent fluorogenic substrate by different connecting functionalities, such as carbonate, carbamate, ether, ester, or pyridinium moieties. For instance, the Hu group further explored the concept of cyanine based NTR responsive substrates for bacterial imaging by attaching differently linked 4-nitrobenzyl residues either to the 5-position of the indolenine or to the methine backbone of the Cy5 parent dye. Here, a carbamate linked nitrobenzyl alcohol connected to a benzylamine bridge was found to be the most sensitive trigger with the best response towards NTR (see. Figure 4, D).[122]

Moreover, some bioluminescent NTR activatable substrates based on luciferin have been developed.[123-124] For instance, 5-nitrofuranyl caged D-luciferin (Figure 4, E) was successfully employed for the *in vivo* imaging of mouse models of bacterial infections with luciferase expressing *E. coli* bacteria as well as NTR and luciferase transfected breast cancer xenografts.[124]

Taken together, the development of probes for NTRs and NTR-like enzymes is a highly relevant field of current research, owing to widespread applications in cancer imaging and bacterial imaging. However, especially with regard to bacterial imaging, the capabilities and the potential for the development of more sensitive and better applicable probes are far from being exhaustively investigated.

1.2 Receptor Targeted Small-Molecule Probes for Cancer Imaging

Enzyme-targeted and -activatable probes constitute an effective design strategy for cancer imaging probes, which relies on elevated expression and activation levels of certain enzymes in cancer cells (see chapter 1.1). A complementary approach, intended to improve target-specific accumulation and cellular internalization of imaging probes or drugs, utilizes targeting ligands which are connected to a reporter modality or a cytotoxic payload. The ligands should bind with high affinity to receptors located on the surface of cancer cells, and their respective receptor targets have to be either very specific or they have to be overexpressed on cancer cells to allow for good contrast and discrimination from healthy tissue.[125] A broad spectrum of available targeting moieties can potentially be employed for this purpose, including antibodies and antibody fragments, proteins, peptides, and small molecules, provided that they exhibit an adequately high binding affinity for the relevant target receptor. The initial development of antibody-dye conjugates was fueled by the exploration of cancer-associated targets such as epidermal growth factor receptors (EGFRs) like HER2[126] and vascular endothelial growth factors (VEGFs), and the concomitant emergence of therapeutic antibodies for clinical use[127-128]. Monoclonal antibodies against carcinoembryonic antigen (CEA) and stage-specific embryonic antigen-1 (SSEA-1) conjugated to fluorescein and, shortly after, to cyanine dyes, have been the first targeting units explored for the *in vivo* fluorescence imaging of tumors in mouse models[129-131]. However, antibodies suffer from drawbacks such as potential immunogenicity, limited tissue penetration, high production costs and do not have the highly defined and controllable chemical architecture of small-molecule conjugates.[132]

As a consequence, endogenous and synthetic small molecules have been explored as homing ligands for cancer receptors.[15,133-134] One of the most extensively studied small-molecule ligands for cancer targeting is folic acid (FA, see Figure 5) which binds to the folate receptor α with high affinity (FRα, $K_d \approx 1$ nM).[135-136] Since folates are required for the biosynthesis of thymidine and purines, essential constituents of the DNA, FRα is upregulated on many cancer cells allowing them to maintain their high proliferation rates.[137-140] A series of folic acid conjugated imaging probes and drugs have been in clinical trials up to phase III, however, none of them could obtain clinical approval.[141-145] Examples for other receptors that have been addressed by means of small-molecule targeting are the cholecystokinin receptors (CCKRs) with the benzodiazepine-derived ligand Z-360[146-147] and biotin receptors such as SMVT with the native ligand biotin[148-149].

Similarly, small peptides have attracted considerable attention as targeting moieties for imaging purposes. They exhibit high affinity and specificity for their target and are relatively straightforward to synthesize, and they are readily modifiable as long as binding motif and mechanism are preserved.[133] An example for very successful, clinically approved peptide ligands used for both cancer imaging and treatment are the

somatostatin analogs like octreotide, lanreotide and pasireotide, which bind to the somatostatin receptor type 2 (SST_2).[150] These somatostatin receptor agonists are used in clinical practice for some time; octreotide was the first of its kind, approved by the FDA for the treatment of acromegaly and carcinoid neuroendocrine tumors already in 1988.[151-152] SST activation was shown to induce cell-cycle arrest, apoptosis, and ultimately tumor growth inhibition through multiple direct and indirect pathways, including suppression of growth hormone (GH) release and growth factor receptor inhibition.[153-154] Cyclic RGD peptides are another class of highly valuable peptidic ligands that were and still are thoroughly investigated for cancer imaging and treatment. Their protein targets – integrins – as well as their applications for cancer imaging will be discussed in the following chapter.

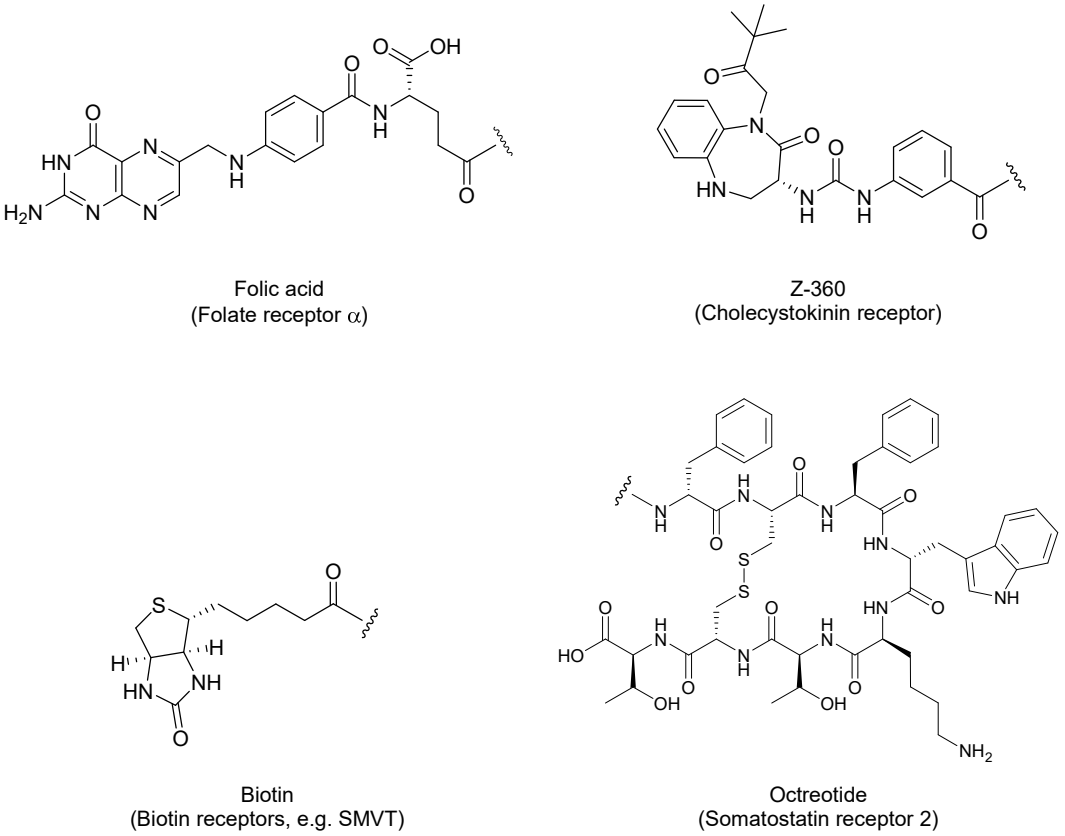

Figure 5: A selection of ligands and their respective binding receptors exploited for the generation of cancer imaging probes: the small-molecule ligands folic acid, Z-360, and biotin with indicated conjugation sites and the peptidic ligand octreotide as representative of the somatostatin analogs.

1.2.1 Integrin Receptors as Targets for Cancer Imaging Probes

Integrins, first described in 1986[155], belong to a family of 24 heterodimeric transmembrane receptors combining 18 different α subunits and eight different β subunits. They play fundamental roles in controlling cell adhesion to the extracellular matrix (ECM) and cell-cell adhesion. Integrin binding to the ECM triggers

the intracellular recruitment of a complex network of proteins and signaling factors, the so-called adhesome, regulating cellular migration, growth, differentiation and apoptosis.[156-157] Integrins thereby act as communicators between the cell and the ECM as well as mechanosensors and force-transducing modules.[158-160] They are unique among transmembrane receptors in that they are capable of bidirectional signaling, i.e., both inside-out and outside-in signaling. Along with their manifold functions, integrins have a multitude of physiological binding partners, including fibronectin, vitronectin and collagen, depending on the integrin subtype.[161] In addition, and as a consequence of their pivotal physiological functions, integrins play key roles in a number of pathologies such as bleeding disorders, cardiovascular diseases, and cancer.[162-163] Integrins have been shown to be strongly overexpressed in a variety of cancers. They have been found to be involved in virtually all stages of cancer progression, including tumor promotion, migration and invasion, metastasis and survival, and even drug resistance.[163] However, owing to their multiple subtypes, no general assignment can be made regarding the involvement and roles of integrins in cancer. The $\alpha_v\beta_3$ subtype, belonging to the RGD-binding (arginine-glycine-aspartic acid) subclass of integrins, has received close attention as target receptor for cancer treatment and imaging, since it is overexpressed on tumor endothelial cells and strongly associated with cancer angiogenesis and metastasis.[164-166] Early studies on the inhibition of $\alpha_v\beta_3$ signaling with specific antibodies and RGD-containing peptides demonstrated antiangiogenic and antitumorigenic effects, providing the basis for the development of highly potent peptidic RGD ligands.[165,167-170]

Extensive studies of the Kessler group on cyclic RGD peptides in the early 90's resulted in the discovery of cilengitide (c(RGDf-N(Me)V-), see Figure 6), a selective, subnanomolar (IC_{50} = 0.58 nM for inhibition of $\alpha_v\beta_3$ - fibrinogen interaction) integrin $\alpha_v\beta_3$ antagonist.[171-173] Cyclization of the RGD binding motif restricts the structural conformation of the peptide in particular through intramolecular hydrogen bonds, thus leading to higher binding affinities due to decreased entropic penalties as compared to their linear counterparts.[174] Scientists at Merck-Serono further developed cilengitide as an anti-cancer drug entering multiple clinical trials which, however, failed in phase III for the treatment of glioblastoma due to insufficient impact on overall survival.[175]

Apart from their development as drugs for cancer treatment, cyclic RGD peptides have proven valuable ligands for the generation of $\alpha_v\beta_3$ targeted cancer imaging probes. The two most frequently used derivatives are the cyclic peptides c(RDGfK) and c(RGDyK). Exchange and substitution of the amino acid before arginine does not significantly affect binding affinity and selectivity of the cyclopeptide, thus the lysine sidechain is readily available for further attachment of imaging functionalities.[172,176] Numerous radiolabeled SPECT and PET probes based on RGD peptides,[176-178] such as ^{99m}Tc-labeled NC100692 (maraciclatide by GE Healthcare, see Figure 6, shown without ^{99m}Tc label), have been developed. NC100692

is a cyclic RGD peptide derived from a phage display library conjugated to a diamine dioxime chelate, which was tested in a proof-of-concept study for the detection of breast cancer in humans by SPECT imaging.[179-181]

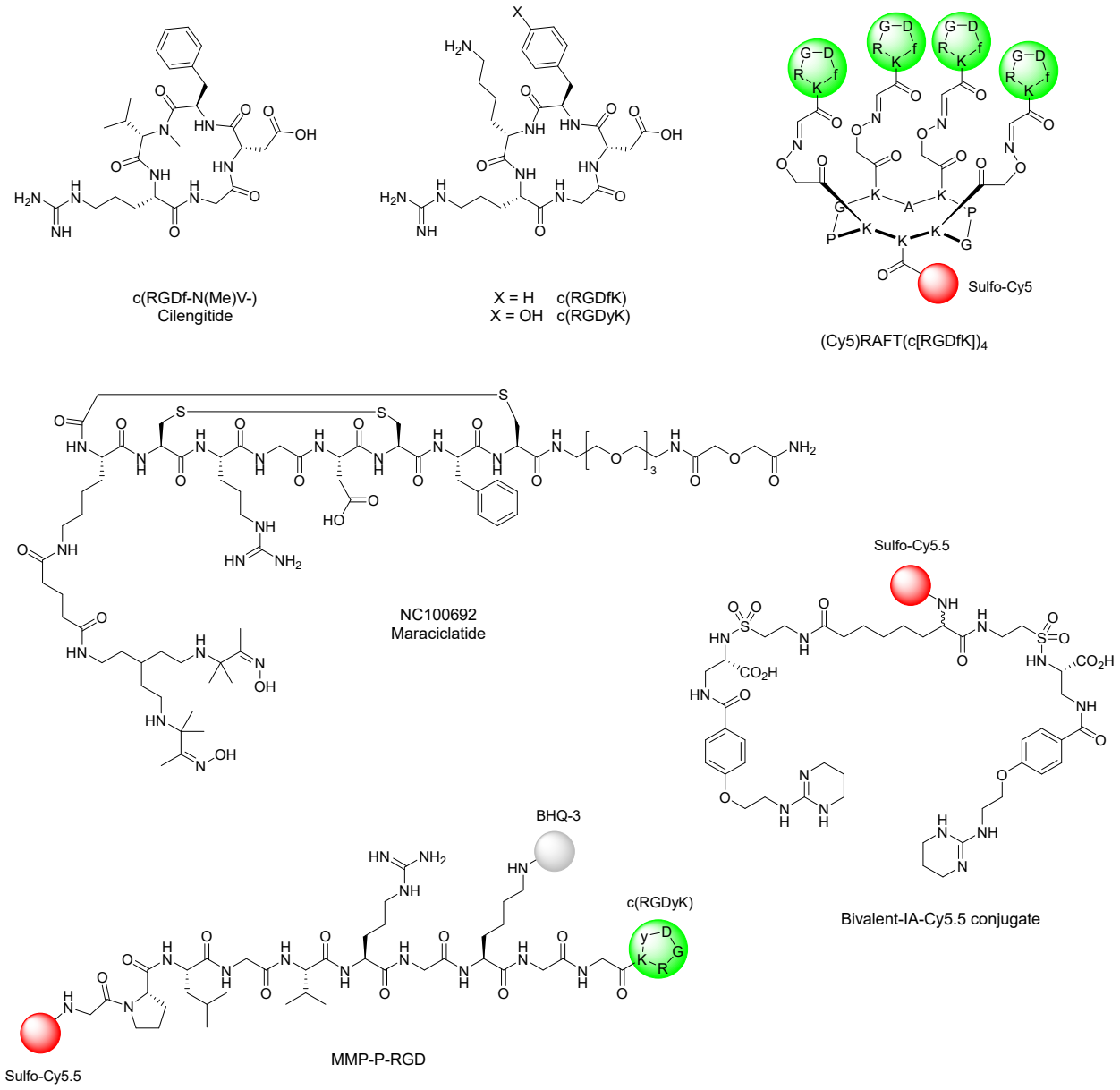

Figure 6: Selected ligands and probe conjugates for integrin $\alpha_v\beta_3$.

Besides radiolabeled probes, an array of fluorescently labeled RGD probes has been reported.[182-183] The first NIR fluorescently labeled c(RGDyK)/c(RGDfK) conjugates for the optical *in vivo* imaging of tumor xenografts in mice were published in 2004.[184-185] Subsequently, multivalently RGD-conjugated probes were explored, with the extent of peptide conjugation generally correlating with higher affinities towards integrin $\alpha_v\beta_3$.[186-189] For instance, a Cy5 labeled, tetrameric c(RGDfK) conjugated RAFT (regioselectively addressable

functionalized template) peptide (Figure 6), used for the imaging of metastatic tumors in mice, exhibited a K_D of 3.9 nM for $\alpha_v\beta_3$, while the monomeric Cy5 labeled peptide exhibited a K_D approximately ten times higher (41.7 nM).[190-191]

An advanced strategy was reported by Zhu *et al.* who developed a dual-functional probe containing an MMP-2 cleavable FRET-quenched peptide that was conjugated to a c(RGDyK) peptide (MMP-P-RGD, Figure 6).[192] The targeted probe displayed a significantly increased fluorescence signal and better contrast for the detection of U-87MG tumors in mouse tumor models *in vivo* compared to its non-targeted analog. Furthermore, multimodal RGD-targeted probes have been developed combining fluorescence imaging and nuclear imaging readouts.[193-194]

Besides RGD-containing peptides, some peptidomimetic nanomolar binders for integrin $\alpha_v\beta_3$ have been developed[195-197] and conjugated to fluorophores[198]. Interestingly, on a bivalent Cy5.5-conjugated probe for *in vivo* cancer imaging in mice, double functionalization with the non-peptidic integrin $\alpha_v\beta_3$ antagonist IA (bivalent-IA-Cy5.5 conjugate, Figure 6) also yielded additive effects on binding affinity as compared to the monovalent analog (IC_{50} = 0.4 *vs.* 22.3 nM, respectively, for $\alpha_v\beta_3$-vitronectin interaction).[199] The construct conceptualization was based on an *in silico* rational design approach.

So far, RGD peptides have not reached the stage of clinical applications. A major reason for that are the very complex roles and heterogeneous involvement of integrins in cancers. These factors do not only result in difficulties to design meaningful clinical trials, but also in overall complications to translate successes of integrin antagonists from preclinical cancer models to useful interventions in more complex clinical settings.[163] However, integrin ligands represent highly valuable tools for the generation of sensitive targeted probes for cancer imaging as well as for a deeper understanding of integrin expression, function and interaction.[182-183,200-201]

1.3 DOTA as Multipurpose Platform for Molecular Imaging Probes

The cyclen-derivative DOTA (1,4,7,10-tetraazacyclododecane-1,4,7,10-tetraacetic acid) is a member of a macrocyclic polyamine family, mainly known for its property to form exceptionally stable complexes with a series of metal ions and in particular with lanthanides due to its eightfold denticity.[202] While DOTA and its complexes with alkaline earth metals and some transition metals were first reported in 1976 by Stetter and Wolfram[203], the use of a DOTA-Gadolinium complex as $T_{1/2}$ (transversal/longitudinal) relaxation agent for MRI was introduced ten years later by Magerstadt *et al.*[204] Since its commercial launch in 1989, Gd-DOTA (gadoteric acid, gadoterate meglumine, Dotarem®, Clariscan®, see Figure 7) has become one of the most successful examples of inorganic drugs used in clinics and is still regarded the gold standard for contrast agents in MRI scans.[205] This is based on the invaluable diagnostic information the agent provides, combined with its superior safety profile. Gadobutrol (Gadovist®), a second-generation gadolinium-based contrast agent, is another example of a successful commercial DOTA-derived compound for the detection of pathological lesions by MRI (Figure 7).[206]

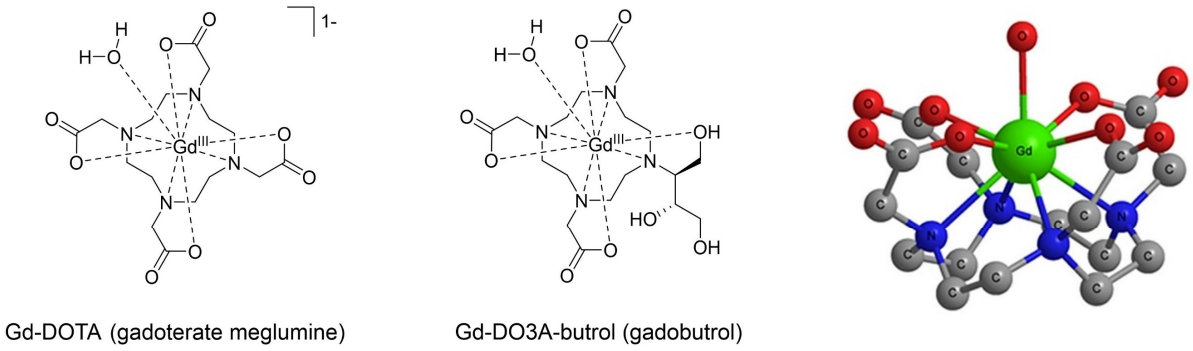

Figure 7: Chemical structures of FDA-approved DOTA-based imaging agents Gd-DOTA, Gd-DO3A-butrol and crystal structure of Gd-DOTA with apically bound water molecule[207] (CSD: JOPJIH01, adapted from Peters et al.[208]).

The metal complexation properties of the DOTA scaffold and its derivatives make this compounds highly useful as template for the development of gadolinium-based MR imaging agents and also more sophisticated MRI probes[205,209], including probes for the detection of small-molecule inorganic analytes[210], pH-responsive probes[211-212], redox-sensitive probes[213-214], or enzymatically activatable probes[215-216]. Additionally, the incorporation of radionuclides such as ^{64}Cu, ^{68}Ga, and ^{111}In, allows DOTA derivatives to be utilized for nuclear imaging applications like PET and SPECT as well as radionuclide therapy[209,217]. Furthermore, the use of other lanthanides like Tb and Eu enables the construction of luminescent probes (see chapter 1.3.3, below).[218-220] These multiple applications make the DOTA chelator particularly useful as a multifunctional imaging tag by applying a metal that determines the specific imaging readout of choice.

Besides that, the introduction of fluorescent dyes to the periphery of the DOTA scaffold further allows the design of fluorescent conjugates. The combination with a metal-based readout enables the generation of multimodal imaging probes, utilizing synergistically complementing modalities by combining fluorescence and MRI, PET, or SPECT imaging.[209,221]

1.3.1 Targeted DOTA Probes

The DOTA scaffold can be utilized for the generation of targeted imaging probes through conjugation to one or more ligands of choice. The most straightforward way for attaching the ligands to the DOTA scaffold is *via* connection through an amide bond to one of the carboxylate functionalities. The DOTA-amide still retains its eightfold denticity by using the amide oxygen lone pair for coordination. This concept has been thoroughly investigated in preclinical settings, and recent FDA approvals of the radiolabeled DOTA-peptide conjugate DOTA-TATE mirror the success of this strategy for cancer diagnosis and treatment (Figure 8). The DOTA chelate is hereby conjugated to Tyr^3-octreotate mainly targeting the somatostatin receptor type 2 (SST_2). In 2018, the beta-emitter ^{177}Lu-DOTA-TATE was approved by the FDA for peptide receptor radionuclide therapy of SST-expressing tumors and is considered by the FDA as first-in-class medication for gastroenteropancreatic neuroendocrine tumors.[222] In 2019, ^{68}Ga-DOTA-TATE was approved for PET-imaging of the same condition, being the first FDA-approved ^{68}Ga-radiopharmaceutical for PET-imaging.[223] DOTA-derived PET imaging probes conjugated to related SST agonists like DOTA-TOC and DOTA-NOC are not yet approved but have been extensively examined in several clinical trials, all surpassing the sensitivity of the 1994 approved SST targeted SPECT imaging agent ^{111}In-DTPA-octreotide.[224-226]

Similarly, a great variety of other ligands has been conjugated to the DOTA scaffold. It has been used as multivalent template for the generation of RGD-targeted SPECT and PET probes.[188-189,227] For instance, in a study conducted by Zhang *et al.* up to four c(RGDyK) peptides were coupled to the DOTA scaffold which was used as ^{64}Cu chelate for PET imaging of U-87MG tumors in mice (see DOTA-P2, Figure 8). However, more than two conjugated peptide ligands had very little effect on the binding affinity to $\alpha_v\beta_3$ integrin (IC_{50} = 380, 37, and 14 nM for binding of ^{125}I-echistatin to U-87MG cells).[189] Moreover, multimodal DOTA-RGD probes have been reported, combining fluorescence imaging and PET/SPECT.[194]

Another example of a targeted DOTA conjugate comprises the tetraamide-coupled DOTAM core (1,4,7,10-tetraazacyclododecane-1,4,7,10-tetraacetic amide) bound to iron-binding siderophores (catecholes) for bacterial targeting. Additional conjugation to malachite green (MG) as fluorophore activatable by the fluorogen activating protein (FAP) provided a turn-on response in FAP-expressing bacteria (Figure 8).

Copper chelation or conjugation to penicillin instead of MG additionally exhibited inhibitory effects on bacterial growth.[228]

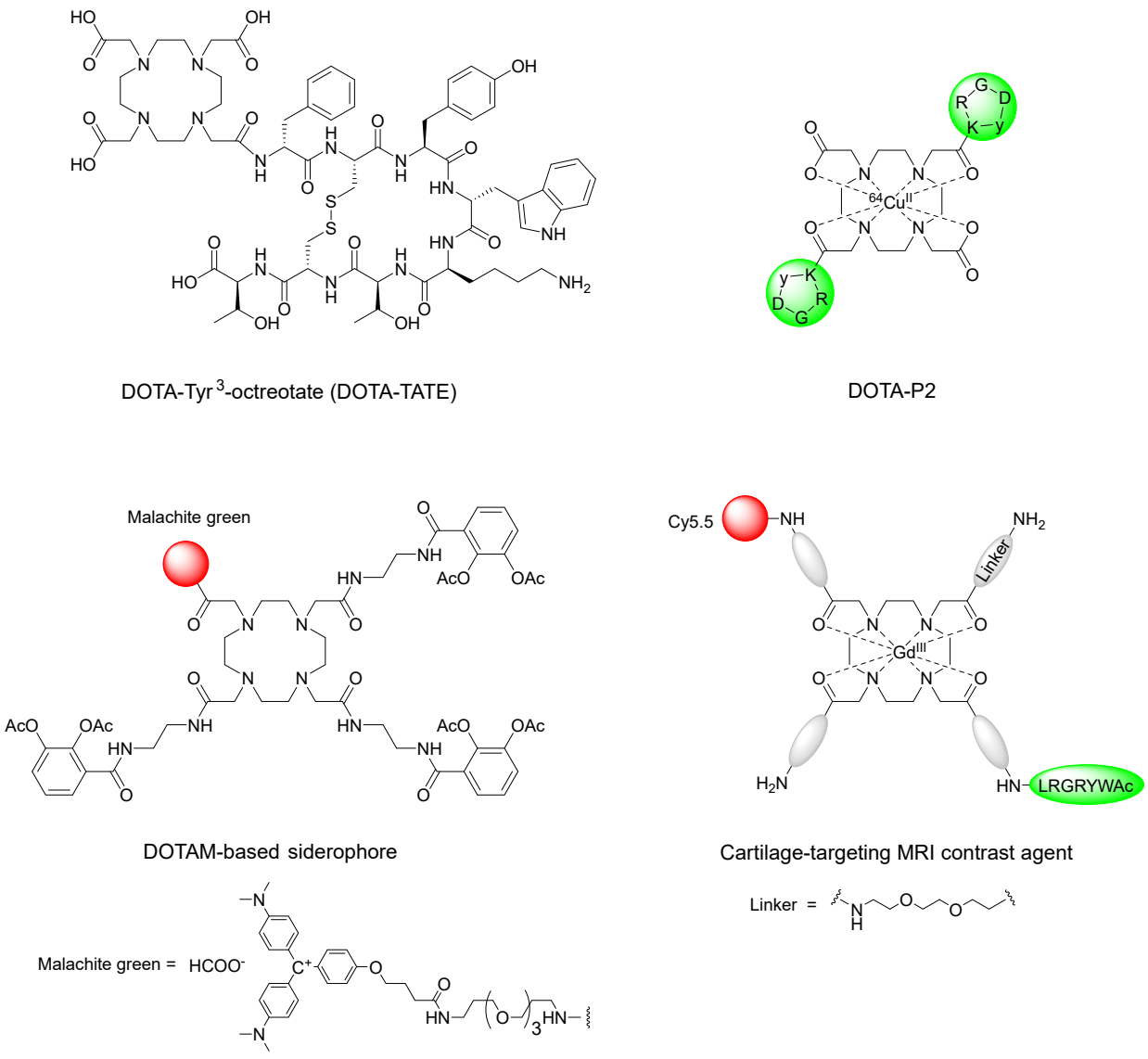

Figure 8: Selected examples of targeted DOTAM probes: DOTA-TATE (without complexed radionuclide), dimeric RGD-targeted DOTA-P2 with complexed ^{64}Cu for PET imaging, DOTAM-based siderophore for bacterial imaging and DOTAM-based cartilage-targeting contrast agent.

DOTAM has also been furnished with a collagen-targeting peptide (LRGRYWAc) in combination with a Cy5.5 fluorophore and Gd^{3+} for multimodal fluorescence/MRI imaging of osteoarthritis in rats. [229-230] The unsubstituted arms of the DOTAM scaffold were capped with terminal amines, positively charged at physiological pH, with the rationale of providing ionic interactions to negatively charged glycosaminoglycans (GAGs) located in the cartilage tissue (Figure 8). This work further demonstrated that the tetraamide-substituted DOTAM template is still able to form kinetically stable complexes with Gd^{3+}.

1.3.2 Fluorescent DOTA-Conjugates for Protease Imaging

Due to its facile attachment to other functionalities, the DOTA scaffold has been used as complementary nuclear imaging tag on fluorescence-based probes for the detection of protease activity, yielding dual modality enzymatic probes combining fluorescence and PET readout.

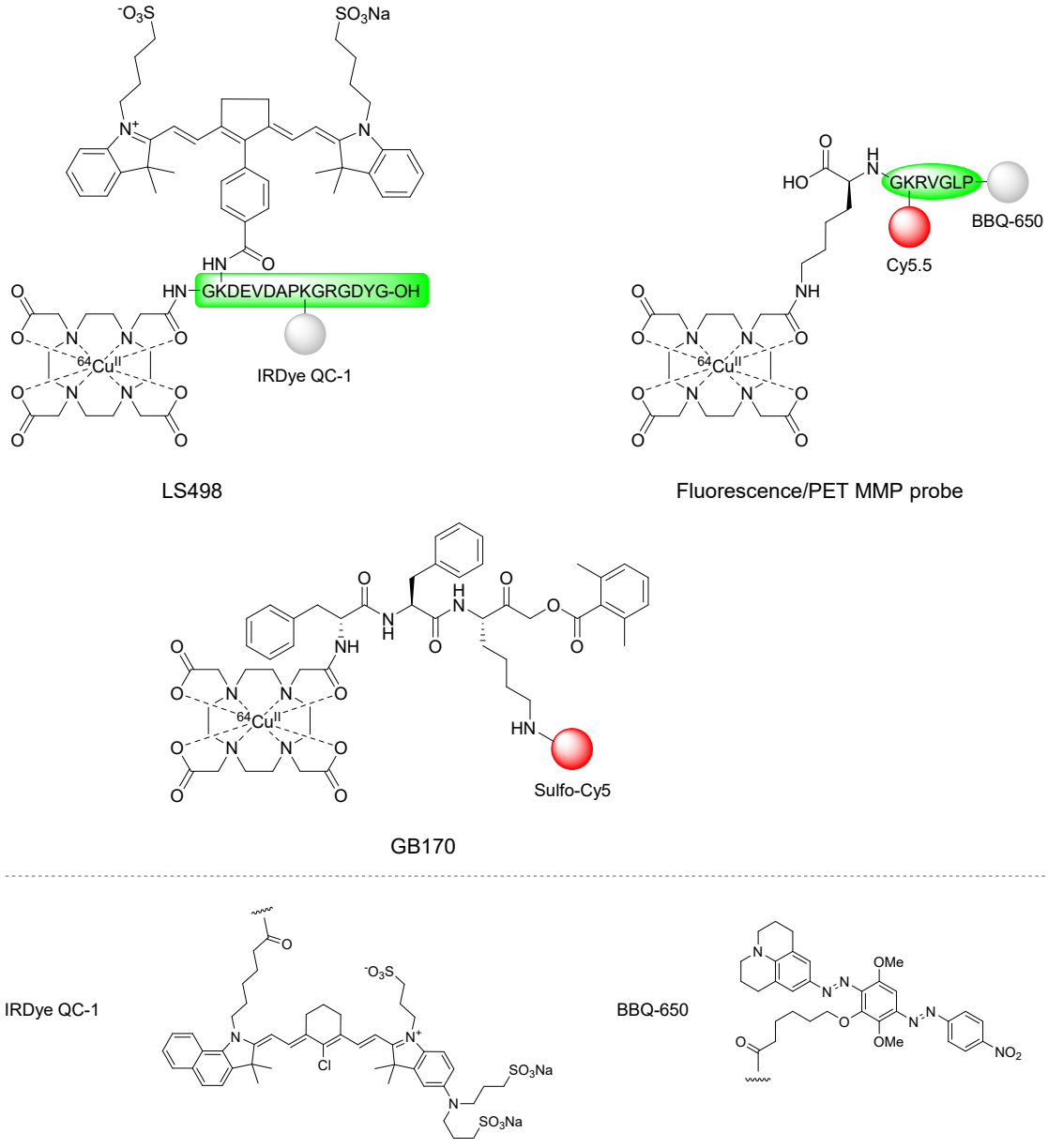

Figure 9: Selected ^{64}Cu-DOTA-tagged protease probes based on fluorescent FRET-sequences (LS498, MMP probe) or a fluorescently labeled ABP (GB170).

This strategy was utilized with FRET-quenched caspase-3 and MMP sequences for imaging of apoptotic cells and tumor xenografts in mice, respectively (LS498 and MMP probe, see Figure 9).[231-232] The sequences were conjugated *via* a glycine *N*-terminus or a lysine side chain to a ^{64}Cu-labeled DOTA tag for PET

imaging. This allowed for tracing of the respective probes both in their inactivated and their activated form, providing a reference tool to quantify and localize probe distribution.

A similar strategy was applied for the imaging of cysteine proteases in different tumor cell lines in the context of tumor imaging in preclinical animal models. In this case the ^{64}Cu-labeled DOTA chelate was conjugated to an ABP carrying an AOMK warhead (GB170, Figure 9).[233] However, the probe suffered from high background signal in the PET imaging experiments, which was attributed to release of free $^{64}Cu^{2+}$ from the complex as well as copper transchelation to other proteins.

1.3.3 The DOTA Scaffold as Template for Lanthanide Luminescent Probes

Luminescent lanthanide complexes have emerged as promising tools for potential applications in biosensing and bioimaging, receiving considerable attention due to their favorable photophysical properties as compared to conventional fluorescent probes, such as long-lived emission lifetimes, a large shift between absorption and emission and high photostability.[234-238] By virtue of these features, lanthanides are commonly applied in commercial ultrasensitive photometric assays like dissociation-enhanced lanthanide fluorescence immunoassays (DELFIA)[239-241] and luminescence resonance energy transfer (LRET) based assays, such as HTRF[242-243], Lance, or LanthaScreen.[236,244] Moreover, a plethora of lanthanide-based responsive probes for the detection of small inorganic analytes, enzymes, DNA/RNA, and for the imaging of cellular compartments have been reported to date, demonstrating the high utility of lanthanide luminescence for bioimaging applications.[218,220,237-238,245-246] While cyclen derivatives like DOTA are frequently utilized chelators for lanthanides, other ligands that are commonly applied for this purpose include triazacyclononane (TACN)-derived compounds such as NOTA (1,4,7-triazacyclononane-1,4,7-triacetic acid) and DTPA, but also ligands that are able to directly sensitize the lanthanide, such as dipicolinates and terpyridines.[220,237-238,245,247]

1.3.3.1 Basic Principles of Lanthanide Luminescence

Lanthanide luminescence is based on electronic 4f-4f transitions, which are formally parity-forbidden due to the Laporte and spin rule. However, in a ligand field the centrosymmetry of the lanthanide ion is disrupted, thus allowing for low-intensity transitions.[248-249] To sufficiently populate a lanthanide`s excited state by direct excitation, high-intensity lasers would be needed which do not comply with most biological applications.[218,248] To circumvent this issue, sensitizing moieties in form of organic light-harvesting ligands (“antennas”) can be utilized.[248,250]

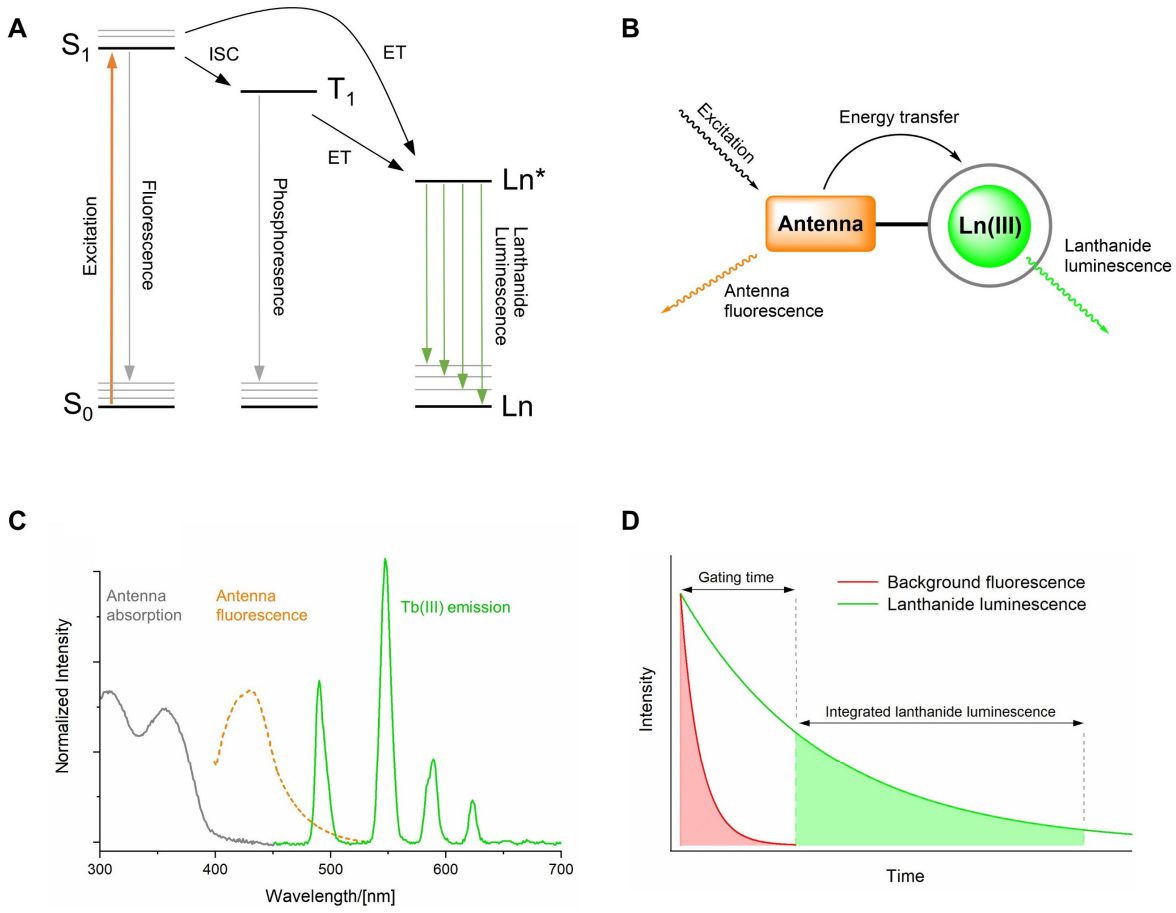

Figure 10: A) Simplified energy diagram illustrating the antenna effect. S – singlet state, T – triplet state, Ln*- lanthanide emitting level, Ln – lanthanide ground states, ISC – intersystem crossing, ET – energy transfer. **B)** Schematic simplified representation of the antenna effect. **C)** Representative absorption, ligand fluorescence, and lanthanide luminescence spectra of a luminescent terbium(III) complex with sensitizing antenna as depicted in **B)**, showing the huge shift between antenna-centered absorption and lanthanide emission (adapted from Brennecke et al.[251], emission intensities are adapted for better visibility). **D)** Principle of time-gated imaging: upon excitation of the lanthanide complex, short-lived background fluorescence arising through biological species, scattering, and antenna fluorescence is eliminated by recording the lanthanide luminescence after a certain time frame, the gating time.

The most common and generally accepted pathway for ligand-sensitized lanthanide luminescence is depicted in Figure 10 (A and B). Ligand-centered absorption from the ground state (S_0) leads to population of the first excited singlet state (S_1) which in turn can undergo intersystem crossing to the long-lived triplet state (T_1). Energy transfer (ET) from the antenna triplet state to the lanthanide's lowest excited state (Ln*) is assumed to be the main sensitizing process. However, excited singlet states can also contribute to a significant extent as energy donor states, in particular in Tb excitation and energetically low ligand triplet states.[252] Relaxation of the emitting lanthanide state Ln* to its ground levels (Ln) gives rise to a set of characteristic emission bands, depending on the lanthanide. Since relaxation from the lanthanide's excited state is still formally forbidden, radiative lifetimes reach values from micro- to milliseconds. This allows for time-gated and time-resolved imaging techniques, consequently improving signal-to-noise ratios in

bioimaging applications due to elimination of the background fluorescence arising from scattering and biological species (Figure 10, D).[235] Moreover, antenna-centered excitation gives rise to large pseudo-Stokes' shifts (i.e. the shift between absorption and emission wavelength), minimizing self-absorption (see Figure 10, C).

The 4f orbitals do not participate in binding interactions and are shielded by the larger expanded $5s^2 5p^6$ orbitals, thus the emission wavelengths are only minimally affected by the chemical environment of the lanthanide ion (i.e. chelator or ligand).[253] This results in fingerprint-like emission bands that are characteristic for each lanthanide, enabling ratiometric analyses by utilizing different lanthanides for the same chelate. The main emissive and final states and the resulting f-f emission bands exemplified for Eu^{3+} and Tb^{3+} are summarized in Table 1.[248]

Table 1: Spectral characteristics of Eu^{3+} and Tb^{3+}, including ground state (G), main emissive (I) and final states (F), commonly observed emission bands and energy gap ΔE_g between emissive state and highest final state.

Ln(III)	G	I	F	λ/nm	ΔE_g/cm^{-1}
Eu	$^7F_0$	$^5D_0$	^7F_J (J = 0-6)	580, 590, 615, 650, 720, 750, 820	12300
Tb	$^7F_6$	$^5D_4$	^7F_J (J = 6-0)	490, 540, 580, 620, 650, 660, 675	14800

Trivalent lanthanide complexes mostly feature Tb^{3+} and Eu^{3+} based on their lower propensity to vibrational quenching by O-H (water), N-H and C-H oscillators, which is the most common non-radiative deactivation pathway for lanthanide emission.[250,254] Vibrational quenching occurs less likely the larger the energy gap ΔE_g between emitting level and highest ground state level of the lanthanide is, because more vibrational modes are needed to bridge the gap. In case of Tb(III) and Eu(III) it corresponds to 14800 cm^{-1} and 12300 cm^{-1}, which constitutes the largest energy gap amongst visible to NIR emitting lanthanides. For comparison, ΔE_g for the NIR emitter Yb^{3+} is about 10300 cm^{-1}, being very susceptible to quenching by O-H oscillators ($\tilde{\nu}$ ≈ 3600 cm^{-1}) and even C-H oscillators.[246,250,254-255] A second quenching mechanism which is often observed with Tb(III) complexes is energy back transfer from the terbium excited state to the antenna triplet state, which is subsequently prone to quenching by molecular oxygen.[256-257]

1.3.3.2 Enzyme-Responsive Luminescent Lanthanide Complexes

As already stated, lanthanide labels are commonly applied in photometric assays, where they are attached to antibodies, and their excited luminescence is either directly or indirectly used as a readout for enzymatic activity. The introduction of lanthanide binding tags and labels into target proteins through biochemical recombinant protein techniques and the occurrence of natural lanthanide binding sites allow for the

visualization of protein structure, function, and localization. In these cases, sensitization of the bound lanthanide has to proceed by a neighboring amino acid residue such as tryptophan.[258-263] Moreover, responsive lanthanide probes for biomolecules such as nucleotides can be used to indirectly monitor the activity of enzymes that catalyze their conversion.[238,264-265] However, these approaches are often not suited for the selective detection of enzymatic activity in a complex biological environment but are limited to applications in biochemical assays. Moreover, engineered or labeled proteins cannot be used to detect enzyme activity in native systems and need to be prepared by rather sophisticated biochemical methods. Therefore, the following section will be restricted on the development and application of reaction-based lanthanide luminescent probes that rely on physicochemical alterations of the sensitizing antenna and consequently modulate the absorption or emission properties of the whole probe system through an enzyme-specific reaction.

Early work in the 1990's on lanthanide complexes for the detection of enzyme activity covered caged salicylic acid derivatives. This concept featured a caging group that is cleaved by a specific enzymatic reaction to generate the parent salicylic acid derivative, which is able to form highly luminescent complexes with a Tb^{3+}-EDTA chelate in basic pH (12-13).[266-267] Based on this principle, which was termed "enzyme-amplified lanthanide luminescence" (EALL), a number of systems were developed, such as for the detection of alkaline phosphatase, xanthine oxidase, and β-galactosidase that involved phosphoester hydrolysis, aldehyde oxidation, and glycosidic bond cleavage as ligand-forming step, respectively (Figure 11, A). The authors claimed that ideally a combination of the alteration of the absorption, the energy transfer, and the chelating properties of the ligand would take place upon cleavage of the caging group.[266]

Conversely, the coumarin derivative 4-methylumbelliferyl phosphate was found to serve as a good ligand for Eu(III) sensitization while the product 4-methylumbelliferone, generated by alkaline phosphatase-catalyzed cleavage of the phosphoester, did not form fluorescent complexes with the lanthanide.[268] While the EALL concept did not directly provide tools for the imaging of enzymatic activity and rather was used for the development of heterogeneous immunoassays[241], it laid the foundation for the generation of reactivity-based probes for enzymatic imaging.

PeT is a common underlying mechanism for the construction of luminescent lanthanide 'turn-on' or 'turn-off' probes. Terai *et al.* conducted a study on carbostyril antennas substituted at C-4 with differently decorated phenyl rings and examined the substituents' ability to serve as PeT donors for quenching of the antenna excited state and consequently quenching of terbium or europium luminescence. Based on their findings, a turn-on probe for leucine aminopeptidase (LAP) was developed that was capable of determining LAP activity in human serum.[269] The same mechanism was later utilized for the generation of a turn-on

probe for *N*-acetyltransferases (NAT) which catalyze the transfer of an acetyl residue from acetyl CoA onto aromatic amines.[270] The probe could be used for the detection of NAT activity in cell lysates (Figure 11, B).

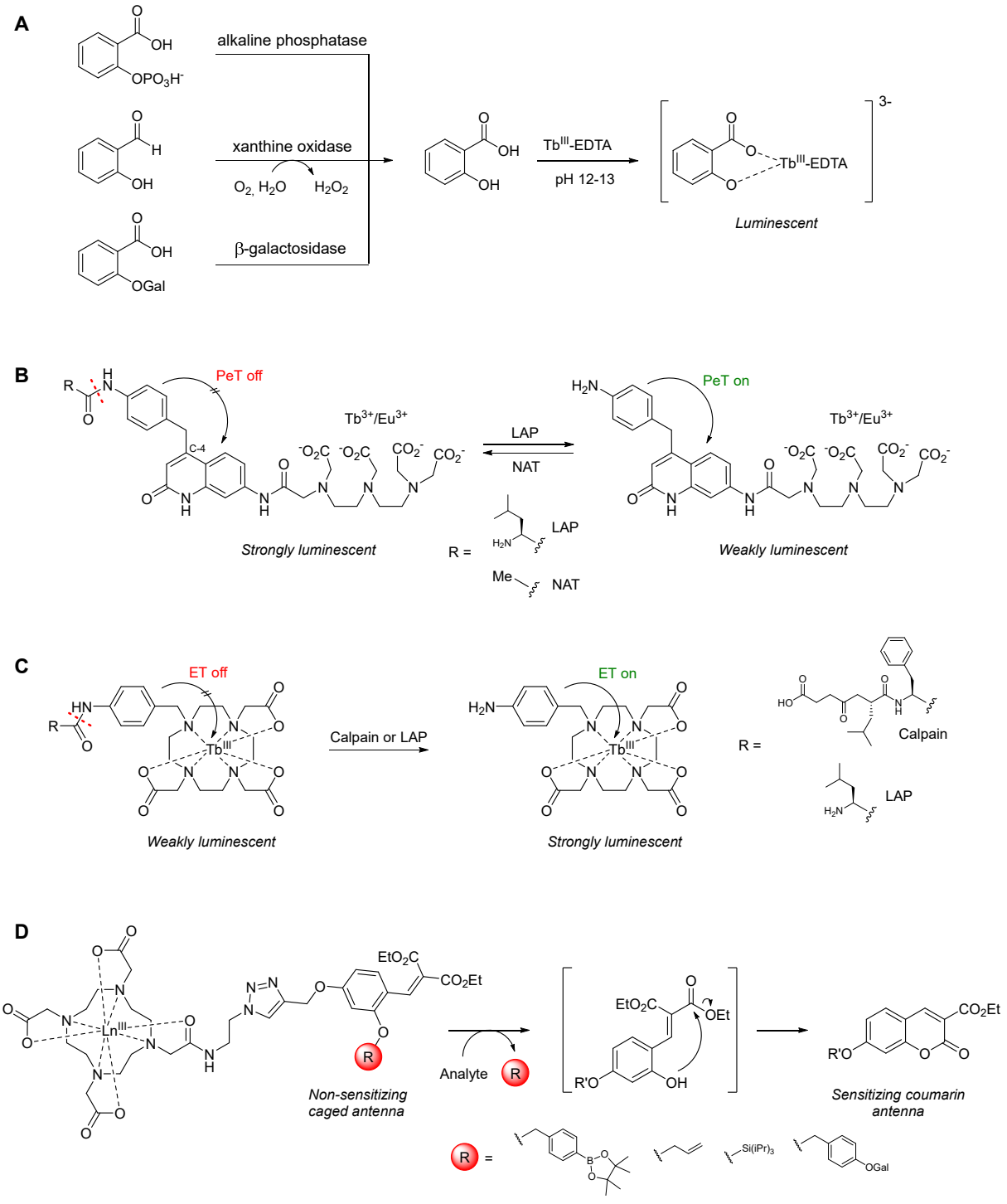

Figure 11: Lanthanide luminescent reactivity-based probes for monitoring enzyme activity. **A)** Caged salicylic acid ligands that form luminescent complexes with Tb-EDTA upon enzyme-mediated uncaging (enzyme-amplified lanthanide luminescence). **B)** Tb-DTPA complexes with PeT-quenched coumarin antenna for the detection of leucine aminopeptidase or *N*-acetyltransferase. **C)** Tb-DO3A complex with amide-substituted aniline-antenna that enables energy transfer upon proteolytic cleavage of the substrate. **D)** Eu/Tb-DOTA probes based on analyte-triggered antenna formation.

Another concept introduced by Mizukami *et al.* for the construction of protease probes involved amide substitution of an aminobenzyl antenna with the residue being cleaved by calpain or LAP.[271] Cleavage of the protease-specific residue facilitates energy transfer from the antenna to the DO3A-complexed (1,4,7,10-tetraazacyclodocecane-1,4,7-triacetic acid) terbium center, activating the probe's luminescence upon excitation (Figure 11, C). However, the concept was only investigated in an assay format, and excitation at a wavelength of 250 nm strongly limits the use of the probe for biological applications.

The Borbas group introduced an interesting design principle for analyte-responsive lanthanide probes that relies on the *in situ*-formation of a sensitizing coumarin antenna from a non-sensitizing precursor. The response is elicited by the cleavage of an analyte-specific substrate trigger. Different triggers, including a boronic acid ester, an allyl group, a silyl group, and galactose were introduced for uncaging by hydrogen peroxide, palladium, fluoride, and β-galactosidase, respectively (Figure 11, D).[272] Later work also included triggers for β-glucosidase, α-mannosidase and phosphatase.[273] Notably, the galactosidase probe was demonstrated to be capable of detecting its target enzyme in galactosidase-expressing *lacZ*+ bacteria, constituting a pioneering approach in designing enzyme-responsive lanthanide luminescent probes for the monitoring of enzymatic activity within live bacterial cells. However, rapid clearance of the activated probe to the extracellular medium was observed, rendering it ineffective for microscopic investigations of probe localization. This behavior was attributed to bacterial efflux systems by the authors.[272]

Although interesting approaches exist for the development of reactivity-based lanthanide luminescent probes, their application for the imaging of enzymatic activity are mostly still restricted to *in vitro* setups. This might to some extent originate from physicochemical limitations such as low brightness and photon efflux, excitation at short wavelengths and hardly predictable cellular permeability.[220,234,236,238,274-275] However, the presented recent developments in conjunction with the inherent optophysical advantages of sensitized lanthanide luminescence show that these probes bear great potential for the real-time imaging of enzymatic activity within biological systems.[236]

2 MOTIVATION AND AIM

2.1 Project I: Development of a DOTAM-Based, Dual Functional Fluorescent Probe for Cancer Cell Imaging

2.1.1 Scientific Background

Cancer is a major burden for our society and the public health system; it is ranked as the second leading cause of death globally, with an estimated ten million deaths and 19 million new cases in 2020.[92,276] The early detection and reliable diagnosis of cancer is considered one of the most important and effective strategies to reduce cancer-associated death rates and increase chances for effective treatment.[277-278] Consequently, there is a strong need for highly sensitive tools that enable the detection of cancer at early stages.

Proteases like cathepsin S are consistently upregulated and aberrantly activated in cancers and are strongly associated with the formation, growth, and invasion of tumors. Consequently, cysteine cathepsins are highly relevant enzymatic targets and biomarkers for the development of imaging probes for cancer (see chapter 1.1.1).[39,47-49,53] An effective strategy for the generation of fluorescent probes for proteases is the utilization of internally quenched fluorescent (IQF) substrates that are specifically cleaved and activated by their target protease. It has been demonstrated that these substrate-based fluorescent probes activatable by cancer-associated proteases constitute a viable strategy for sensitive cancer imaging, namely due to the huge signal amplification as well as the good contrast these probes can provide[279] based on their target-specific activation (see chapter 1.1.2).[59,63,69,280] However, often encountered drawbacks with this type of probes are insufficient permeability and the lack of proper tumor accumulation when administered systemically.[69,281]

Receptor targeting is a widely utilized concept for the site-specific delivery of therapeutic payloads or imaging reporters. Integrins have been shown to play key roles cancer; they are involved in virtually all stages of cancer development and progression, and accordingly are strongly overexpressed in many cancers.[160,163] For this reasons, integrins have become highly useful targeting receptors for cancer imaging and treatment (see chapter 1.2.1).[178,182,282] Yet, targeted imaging probes mostly are “always-on” probes, emitting a signal regardless of receptor interaction and thus suffer from relatively high background signal. Additional time to allow for clearance of nonspecifically bound reporter molecules or washing steps to remove excess and unbound probe are often necessary and complicate reliable detection.[283-285]

In order to overcome the limitations of both principles, namely enzyme-activatable "smart" probes and receptor targeted "always-on" probes, enzyme-activatable probes that additionally incorporate lipids for membrane anchoring[69] or feature conjugation to cell-penetrating peptides[286-287], folic acid[288] and RGD-peptides[192] have been developed and investigated. While these probes were generally successful and exhibited better sensitivity and selectivity as compared to their activatable precursors, this concept has not been explored in detail, conceivably due to difficult synthetic access and the lack of a central strategy to construct such probes.

It has been shown that the DOTA scaffold, mainly known for its ability to form highly stable complexes with a series of metals and in particular lanthanides for PET, MRI or luminescence applications, can serve as biocompatible, water-soluble and multifunctionalizable key template for the generation of fluorescent probes.[209,289] The DOTA scaffold and its amide-derivated analogue DOTAM have been extensively exploited for conjugation to multiple targeting ligands[194,230], and some reports on conjugation to protease-activatable probes have been published[231-232]. However, the exploitation of the DOTA framework combining cellular targeting and enzyme-specific activation has not yet been investigated. Moreover, the DOTA scaffold has not been examined as an inherent structural motif of an IQF substrate, connecting both a dye and a sequence attached to a dark quencher through two different carboxylate functionalities. This strategy would allow for high functional flexibility of the probe, being able to modify the fluorophore and quencher independently.

2.1.2 Conceptualization and Aims

Given the need for highly sensitive diagnostic tools for non-invasive cancer imaging, we envisioned that the DOTA scaffold would constitute an appropriate central multimeric template for the generation of dual functional, targeted, activatable fluorescent probes. To this end, we aimed at functionalizing DOTA with a known and well profiled cathepsin S cleavable IQF substrate, originally generated by reverse design from a covalent cathepsin S inhibitor.[67-69] In order to obtain flexibility with regard to the choice of target protease and FRET pair, the DOTA scaffold should constitute an inherent structural motif of the IQF probe, connecting both a fluorescent dye and the cathepsin S sequence substituted with a suitable quencher *via* two opposing carboxylate arms. The two residual carboxylic acid arms would serve as conjugation sites to cRGDfK peptides for targeting to $\alpha_v\beta_3$ integrin receptors (Scheme 4). In the light of many reports describing beneficial effects of multimeric cRGD conjugates on binding affinity to $\alpha_v\beta_3$ integrins[187,189-191,290], attachment of two cRGD peptides seemed an attractive option for the design of this probe.

Ideally, such targeted activatable probe would combine the following advantageous properties: 1) probe activation by the tumor-associated protease cathepsin S would lead to a highly sensitive and specific detection of cancer cells, 2) the cRGDfK targeting moieties additionally effect an enrichment of the probe in $\alpha_v\beta_3$-integrin expressing cancer cells by binding to and facilitating internalization into cancer cells, further enhancing the probe's selectivity and sensitivity as compared to a monofunctional activatable probe or "always-on" probe, 3) the DOTA core as modular IQF probe template allows for an efficient refunctionalization to effectively adapt the probe to specific requirements.

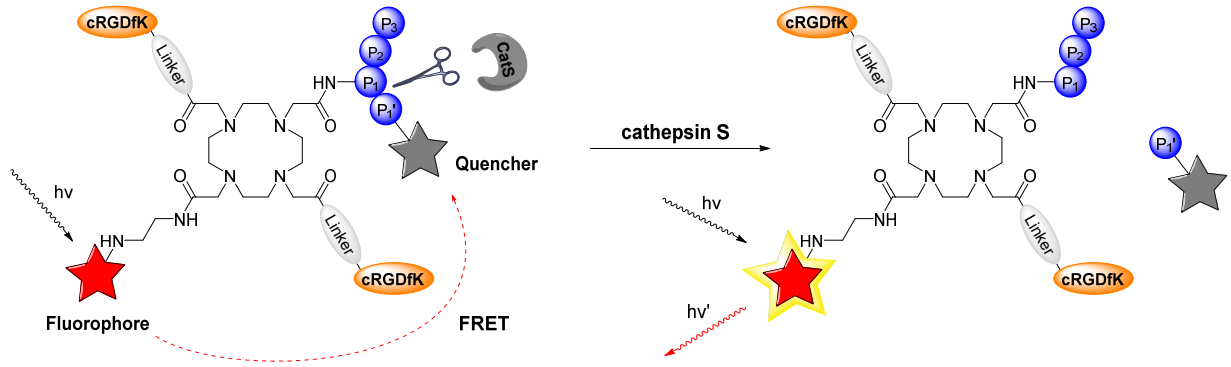

Scheme 4: Schematic representation and mode of action of a cRGDfK targeted cathepsin S activatable fluorescent probe based on the DOTAM template as inherent structural motif of the IQF sequence.

Within the scope of the present project, multiple challenges had to be tackled. The first aim of my thesis was to develop a suitable modular synthetic strategy for the present probe design, that is, a DOTAM construct substituted with three structurally distinct and diverse substituents (fluorophore, cathepsin S-quencher conjugate, and cRGDfK peptides), especially since the vast majority of DOTA- and DOTAM-derived probes are substituted in a 3:1 fashion based on synthetic feasibility. An orthogonal protecting group strategy would have to be used in order to be able to successively conjugate the substituents to the DOTA core in a controlled manner. The second aim of this work was to validate the FRET functionality of the probe and address several questions emerging from the present concept: Is the DOTA core a suitable bridging template for the generation of IQF probes? Will the sequence be recognized by cathepsin S when attached to a complex multifunctionalized DOTAM construct? If yes, will it affect the cleavage efficiency? Finally, the probe should be profiled in a cellular context with the help of collaboration partners in order to validate the potential of the present dual functionality approach with regard to sensitivity and selectivity for cancer cell imaging over presently existing strategies.

2.2 Project II: Development of a Nitroreductase-Responsive Lanthanide Luminescent Probe for Bacterial Imaging

2.2.1 Scientific Background

The alarming rise of antimicrobial multidrug resistance (MDR) is a major health care concern, originating from the overuse and inappropriate prescription of antibiotics. Global deaths due to drug-resistant infections are estimated to increase from 700,000 in 2016 to 10 million in 2050 if no measures are taken.[94] In particular, bacterial pathogens of the ESKAPE panel (*Enterococcus faecium, Staphylococcus aureus, Klebsiella pneumoniae, Acinetobacter baumannii, Pseudomonas aeruginosa,* and *Enterobacter* species) constitute a highly relevant target, being accountable for the majority of nosocomial infections and listed by the World Health Organization (WHO) amongst 12 prioritized bacterial strains that urgently require the development of new antibiotics.[118-120,291] Available diagnostic approaches mainly rely on time-consuming cultivation, molecular techniques (nucleic acid amplification (PCR) and mass spectrometry), and biopsy.[93,98] In particular, they require the collection of clinical samples that may not accurately represent the local biology at the infection site and only capture a single time point. Current nuclear imaging tools used to diagnose bacterial infections employ ^{111}In- or ^{99m}Tc-labeled leukocytes for SPECT imaging and PET imaging with ^{18}F-fluorodeoxyglucose (FDG). These agents are highly sensitive but non-specific and indicate certain physiological changes linked to host response to the infection, but do not allow the detection of the pathogens itself. Furthermore, there use is strongly limited due to the high costs related to the synthesis of radiolabeled tracers, their short half-life, and radiation exposure of the patient.[97] Hence, there is high incentive in developing optical probes as novel molecular tools capable of the non-invasive, selective, and sensitive detection of infection sites in real time.

Nitroreductases are a family of flavin-dependent enzymes that are able to reduce aromatic nitro groups in the presence of NADH or NADPH.[77-78,80] Since these enzymes are almost exclusively present in the bacterial realm, they have become attractive enzymatic targets for bacterial imaging, in particular in the context of bacterial infections, as well as bacterial gene delivery (see chapter 1.1.3).[80,91] Optical, fluorogenic NTR-activatable probes for the imaging of bacterial infections are subject of current research and are extensively investigated (see chapter 1.1.4).[91,113,122]

Lanthanide luminescence is an emerging attractive complementary optical imaging modality for future biosensing and bioimaging applications that has inherent advantages over conventional fluorescence based on organic fluorophores.[234,238,275] Remarkable photophysical properties include long-lived emission that allows for elimination of short-lived background fluorescence through time-gated imaging techniques, a

large shift between absorption and emission thus minimizing self-absorption, fingerprint-like emission bands that are mainly unaffected by the chemical environment of the lanthanide, and high photostability (see chapter 1.3.3.1)[248] While these features have prompted the development of analyte-responsive lanthanide luminescent probes that are able to effectively detect small inorganic molecules, pH changes, and redox activity with high sensitivity and also in live cells[245-246,292-295], their applications for the detection of enzymatic activity are still restricted to assay formats and lack the capability of live-cell *in situ* imaging (see chapter 1.3.3.2).[236,238]

2.2.2 Conceptualization and Aims

In order to contribute to the ongoing efforts in developing sensitive imaging tools for bacterial infections as well as to expand the scope of applications for enzyme-responsive lanthanide luminescent probes to live-cell imaging, we aimed at developing an NTR-responsive probe based on lanthanide luminescence. We were intrigued by the concept of 'analyte-triggered antenna formation' that was introduced by the Borbas group for the design of analyte-responsive lanthanide luminescent probes. The approach relied on the analyte-induced formation of a sensitizing coumarin antenna from a non-sensitizing substituted diethyl benzylidenemalonate precursor.[272-273] The Borbas group demonstrated the utility of this concept for a galactosidase-activatable probe that was capable of monitoring intracellular enzymatic activity in galactosidase overexpressing *E. coli* bacteria, representing a first effort in tracing and imaging intracellular enzymatic activity by lanthanide luminescent probes.[272] However, the probe lacked effective cellular localization. Based on these initial reports and a study on Eu(III) and Tb(III) complexes with differently substituted and attached antennas[296], we conceived the following design for an NTR-activatable lanthanide luminescent probe considering multiple factors: First, it was intended to directly attach the sensitizing antenna to the lanthanide-complexing DOTA cycle, based on findings that close proximity of antenna and lanthanide center is a critical factor for efficient energy transfer.[296] Second, we aimed for a carbostyril antenna in connection with a terbium center, because carbostyrils are known to be effective and superior sensitizers for terbium compared to coumarins.[296-299] We envisioned that a caged 2,4-diaminobenzylidenemalonate precursor should constitute a precursor able to undergo cyclization to the corresponding sensitizing carbostyril antenna (Scheme 5).[300-303] As activation trigger for NTR we planned to introduce a 4-nitrobenzylcarbamate masking the 2-amine, inducing fragmentation of a iminoquinone methide and carbon dioxide upon NTR-mediated reduction of the nitro functionality releasing its parent amine. The 4-amine would serve as a direct attachment point to the DOTA-terbium complex.

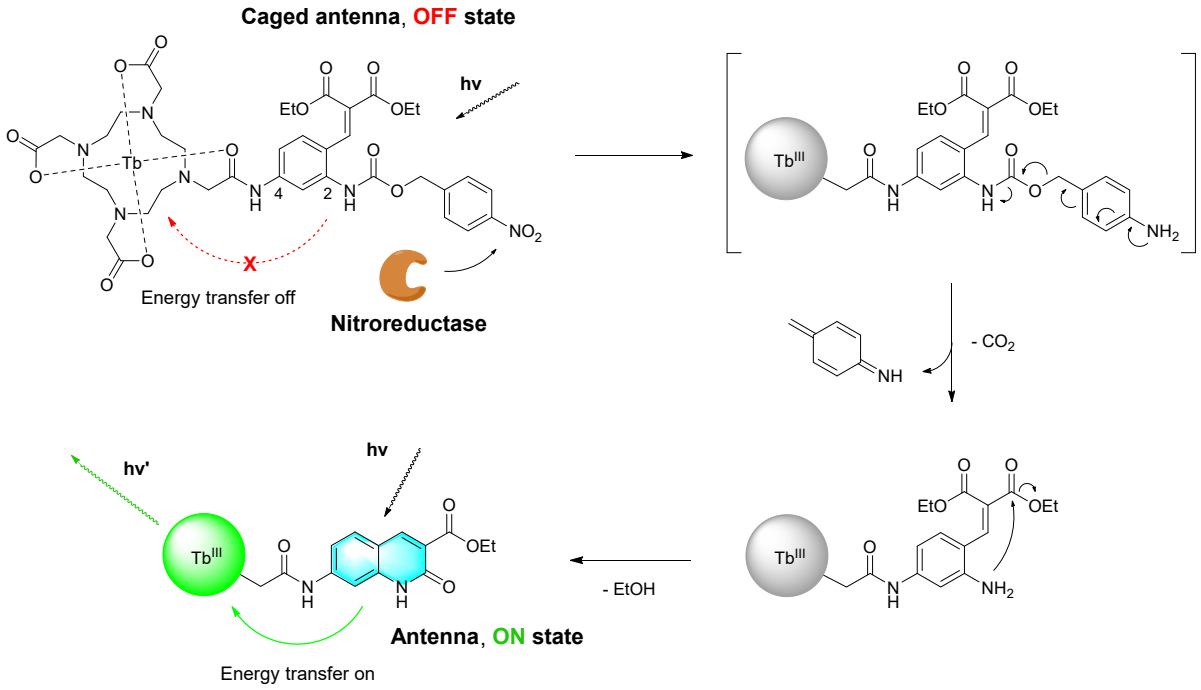

Scheme 5: Design rationale and mode of action of an NTR-responsive luminescent lanthanide probe based on carbostyril antenna formation.

The initial aim of this project was to elaborate the synthesis of the caged antenna precursor and the activated antenna, which would be needed as reference for the activated probe. A caging concept for a carbostyril antenna had not been designed prior to this work, and a well-considered synthetic strategy would be required in order to successfully obtain the densely functionalized caged antenna precursor. In particular, controlled regioselective substitution of the amines at C-2 and C-4 would pose a major challenge.

The second aim was to demonstrate the functionality of the overall probe concept. This would include a verification of the NTR-mediated activation mechanism followed by effective sensitization of the terbium luminescence, and a photophysical profiling of the carbostyril-conjugated activated probe. The final goal of this project was to demonstrate the ability of our probe system to detect and image NTR activity in live bacterial cells of MDR strains with the help of collaboration partners, possibly providing a new approach to bacterial imaging with optical probes.

3 IMPLEMENTATION OF PUBLICATIONS

3.1 DOTAM-Based, Targeted, Activatable Fluorescent Probes for the Highly Sensitive and Selective Detection of Cancer Cells

Benjamin Brennecke[1], Qinghua Wang[1], Wolfgang Haap, Uwe Grether, Hai-Yu Hu*, and Marc Nazaré*

[1]these authors contributed equally

This chapter was published in *Bioconjugate Chem.* **2021**, *32*, 702-712.

https://dx.doi.org/10.1021/acs.bioconjchem.0c00699

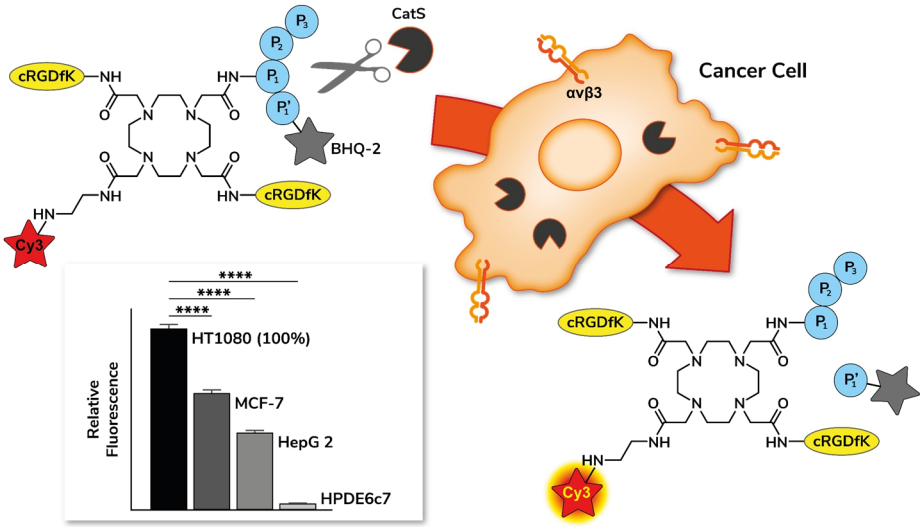

TOC graphics by Barth van Rossum.

Author Contributions

Benjamin Brennecke, Hai-Yu Hu and Marc Nazaré designed the research approach. Benjamin Brennecke carried out all chemical synthesis, performed LC/MS cleavage studies with cathepsin S and enzyme kinetic measurements as well as the *in vitro* inhibition assay, including data analysis, performed the selectivity assay against related cathepsins, and wrote the manuscript draft. Qinghua Wang performed the stability assay against small molecule analytes, cell viability assays, cell imaging studies, co-localization experiments, and FACS analyses. Wolfgang Haap and Uwe Grether provided the selective cathepsin S inhibitor RO5461111.

3.2 An Activatable Lanthanide Luminescent Probe for Time-Gated Detection of Nitroreductase in Live Bacteria

Benjamin Brennecke, Qinghua Wang, Qingyang Zhang, Hai-Yu Hu*, and Marc Nazaré*

This chapter was published in *Angew. Chem. Int. Ed.* **2020**, *59*, 8512-8516.

https://doi.org/10.1002/anie.202002391

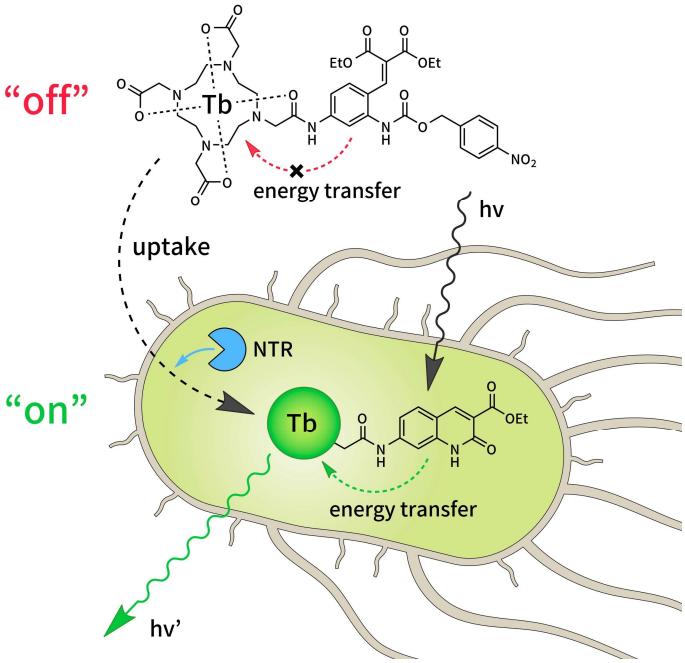

TOC graphics by Barth van Rossum.

Author Contributions

Benjamin Brennecke, Hai-Yu Hu, and Marc Nazaré designed the research approach. Benjamin Brennecke carried out all chemical synthesis, measured absorption and emission spectra, performed the LC/MS cleavage studies with nitroreductase, and wrote the manuscript draft. Qinghua Wang did the kinetic profiling of enzymatic cleavage, inhibitor studies, pH/temperature dependence of the emission, quantum yield measurements, and all bacterial imaging experiments. Qingyang Zhang carried out the lifetime measurements.

How to cite: *Angew. Chem. Int. Ed.* **2020**, *59*, 8512–8516
International Edition: doi.org/10.1002/anie.202002391
German Edition: doi.org/10.1002/ange.202002391

Luminescent Probes | Hot Paper

An Activatable Lanthanide Luminescent Probe for Time-Gated Detection of Nitroreductase in Live Bacteria

Benjamin Brennecke, Qinghua Wang, Qingyang Zhang, Hai-Yu Hu, and Marc Nazaré**

Abstract: *Herein we report the development of a turn-on lanthanide luminescent probe for time-gated detection of nitroreductases (NTRs) in live bacteria. The probe is activated through NTR-induced formation of the sensitizing carbostyril antenna and resulting energy transfer to the lanthanide center. This novel NTR-responsive trigger is virtually non-fluorescent in its inactivated form and features a large signal increase upon activation. We show that the probe is capable of selectively sensing NTR in lysates as well as in live bacteria of the ESKAPE family which are clinically highly relevant multi-resistant pathogens responsible for the majority of hospital infections. The results suggest that our probe could be used to develop diagnostic tools for bacterial infections.*

Optical imaging tools are an indispensable analytical modality for the investigation and understanding of complex biological processes ranging from molecular level to whole organisms. Small-molecule fluorophores are of particular relevance as their properties are readily tuned and modified to incorporate specific functions for monitoring and determining biological activity in situ. In this context, luminescent lanthanide complexes have attracted considerable attention since they have several inherent advantages over conventional organic fluorophores, making them highly promising tools for future medical applications, such as biosensing and bioimaging.[1] These features include a large Stokes shift avoiding spectral cross-talk, long-lived emission allowing for time-gated detection without interfering background fluorescence, high photostability as well as simple tuning of the emission wavelengths from visible to near infrared and lanthanide-dependent fingerprint-like emission bands allowing for ratiometric analyses.[2]

As a result of Laporte-forbidden f–f transitions and the resulting low extinction coefficient, effective excitation of the lanthanide requires a sensitizing antenna in the form of an organic chromophore enabling energy transfer.[2] Elegant examples for responsive lanthanide luminescent probes based on the analyte-induced modulation of the antenna or the chelation properties of the lanthanide have been designed for sensing small inorganic species, such as $^1O_2$, HCO_3^-, and pH changes in cells.[3] However, tracking intracellular enzymatic activity with such probes still poses a major obstacle and, despite recent pioneering efforts,[4] is often hampered by synthetic hurdles and suboptimal physicochemical properties, such as low permeability and weak emission.[5]

As part of our program on DOTA-based fluorescent probes[6] we were in particular interested in investigating activatable lanthanide luminescent probes for the detection of nitroreductase (NTR) in bacteria.[7] NTRs are a family of flavin-containing bacterial enzymes that are able to reduce nitro functional groups and other nitrogen-containing functionalities in the presence of NADH or NADPH.[8] The occurrence of NTRs in bacterial pathogens, such as in members of the ESKAPE family (*Enterococcus faecium*, *Staphylococcus aureus*, *Klebsiella pneumoniae*, *Acinetobacter baumannii*, *Pseudomonas aeruginosa*, and *Enterobacter* species), which are responsible for the majority of hospital infections with multiresistant strains escaping the standard antibiotics treatment, makes this enzyme family a highly relevant diagnostic target for the detection of bacterial infections.[9] Although probes capable of detecting NTRs in bacteria have been developed, the exploitation of NTRs as diagnostic markers for bacterial infections remains scarce.[7b,10] Moreover, probes utilizing the advantageous features of lanthanide luminescence have not been investigated so far.

Herein, we present the development of the first enzyme-triggered lanthanide NTR probe which 1) is based on a novel responsive antenna-forming element, 2) is highly sensitive, selective and stable, 3) gives a fluorescence readout over virtually no background signal and 4) is capable of selectively tracking NTR activity in live bacteria.

The overall concept for the design of our NTR-responsive lanthanide probe was to employ a non-sensitizing caged antenna precursor which, upon interaction with the enzyme, would initiate a self-immolative fragmentation cascade thereby forming the antenna enabling energy transfer to the lanthanide center (Scheme 1).[4,11] Constructing a stably caged, non-sensitizing NTR-responsive antenna precursor as key element for our probe proved to be crucial. Although carbostyril antennas are known to be efficient sensitizers and

[*] B. Brennecke, Dr. M. Nazaré
Medicinal Chemistry
Leibniz-Forschungsinstitut für Molekulare Pharmakologie
13125 Berlin (Germany)
E-mail: nazare@fmp-berlin.de
Q. Wang, Dr. Q. Zhang, Prof. Dr. H.-Y. Hu
State Key Laboratory of Bioactive Substances and Function of Natural Medicine, Institute of Materia Medica, Peking Union Medical College and Chinese Academy of Medical Sciences
Beijing 100050 (China)
E-mail: haiyu.hu@imm.ac.cn
Supporting information and the ORCID identification number(s) for the author(s) of this article can be found under: https://doi.org/10.1002/anie.202002391.

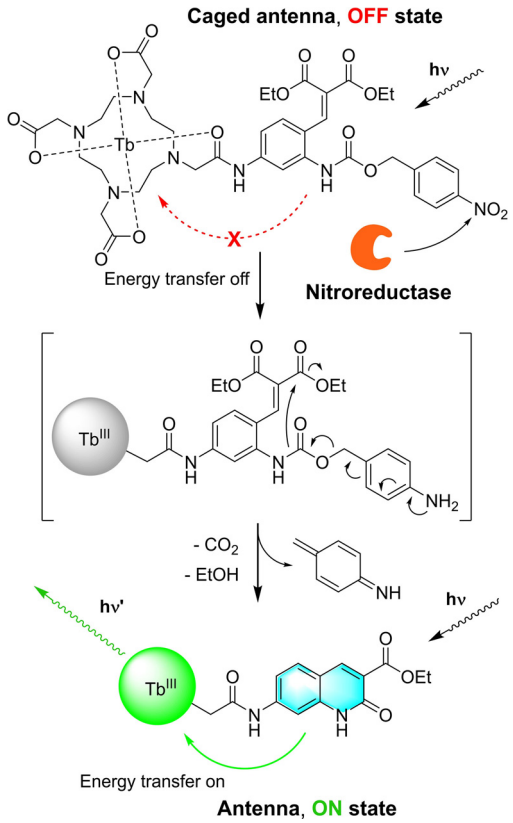

Scheme 1. Design rationale and mode of action of the carbostyril-based NTR activatable luminescent lanthanide probe.

might offer distinct advantages over their corresponding coumarin analogues, such as a more efficient energy transfer and higher quantum yields,[12] a caging strategy for carbostyril precursors has so far not been investigated. We designed our probe in such a way that antenna formation occurs upon NTR-mediated reduction of the nitro group of the *para*-nitro benzylcarbamate to the corresponding aniline, initiating fragmentation to the iminoquinone methide (Scheme 1). Subsequent lactamization through intramolecular attack of the liberated amine at the ester should then yield the corresponding carbostyril as an effective sensitizer of the terbium center. Additionally, by directly attaching the precursor to one carboxylic acid arm of the DOTA scaffold we aimed for a short distance between carbostyril antenna and lanthanide center as it is reported as a critical factor for an effective sensitization of the lanthanide.[12d]

The synthesis of both the antenna **6** as well as the caged antenna precursor **8** started from 2-bromo-4-nitrobenzoic acid (**1**, Scheme 2, left) which was converted into the amino-ester **2**. Reduction to the alcohol and Boc protection of the amine furnished **3**, which was further converted into the corresponding benzaldehyde **4** serving as important intermediate to access both **6** and **8**. For the subsequent Buchwald-Hartwig type coupling with either *tert*-butyl carbamate or 4-nitrobenzyl carbamate, XantPhos Pd G3 was employed as a palladacycle precatalyst.[13] This reaction served as key step in the synthesis of both the carbostyril **6** and the caged antenna precursor **8** and allowed us to selectively introduce and discriminate between the two functionalized amines at C-2 and C-4 in compound **7**. Furthermore, this strategy enables for simple functionalization at C-2 and thus constitutes a robust and general modular approach for the synthesis of similar types of analyte-responsive triggers. Condensation with diethyl malonate[14] and subsequent Boc deprotection yielded the caged antenna **8**, or, in case of **5**, induced cyclization to the carbostyril antenna **6**. Attachment of the caged antenna and the carbostyril to the DOTA scaffold was accomplished by reaction of the amine intermediates **6** and **8** with bromoacetyl bromide and subsequent alkylation of the free amine of *tert*-butyl protected DO3A (Scheme 2, right). Acidic cleavage of the *tert*-butyl groups furnished conjugates **9** and **11**. Terbium(III) complexation was accomplished by reaction with $TbCl_3$ in ethanol at slightly elevated temperatures with small amounts of water to facilitate dissolution. The application of such mild conditions ensured that the ethyl esters of both **10** and **12** remained intact during the course of the reaction.

Figure 1 A shows the absorption, excitation and fluorescence spectra of the carbostyril probe **10** and the fluorescence

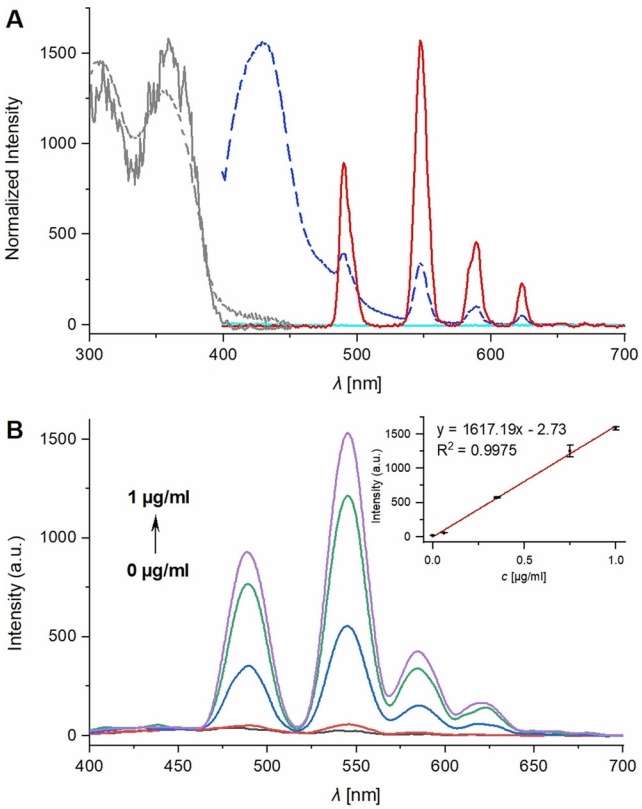

Figure 1. A) Normalized absorption (dotted gray), excitation (monitored at 545 nm, gray) and fluorescence spectra of reference **10** (steady-state, dark blue and with 50 µs delay, red) and fluorescence spectrum of probe **12** (steady-state, light blue), each 20 µM in PBS pH 7.4. B) Gated emission spectra of probe **12** (20 µM) upon titration with different concentrations of NTR (0, 0.0625, 0.35, 0.75 and 1.0 µg mL^{-1}) in TRIS buffer (50 mM, pH 7.4) at 37 °C for 2 h. Inset: Linear correlation between NTR concentration and emission intensity at 550 nm, 50 µs delay, λ_{ex} = 355 nm. Results for (B) representative of two independent experiments.

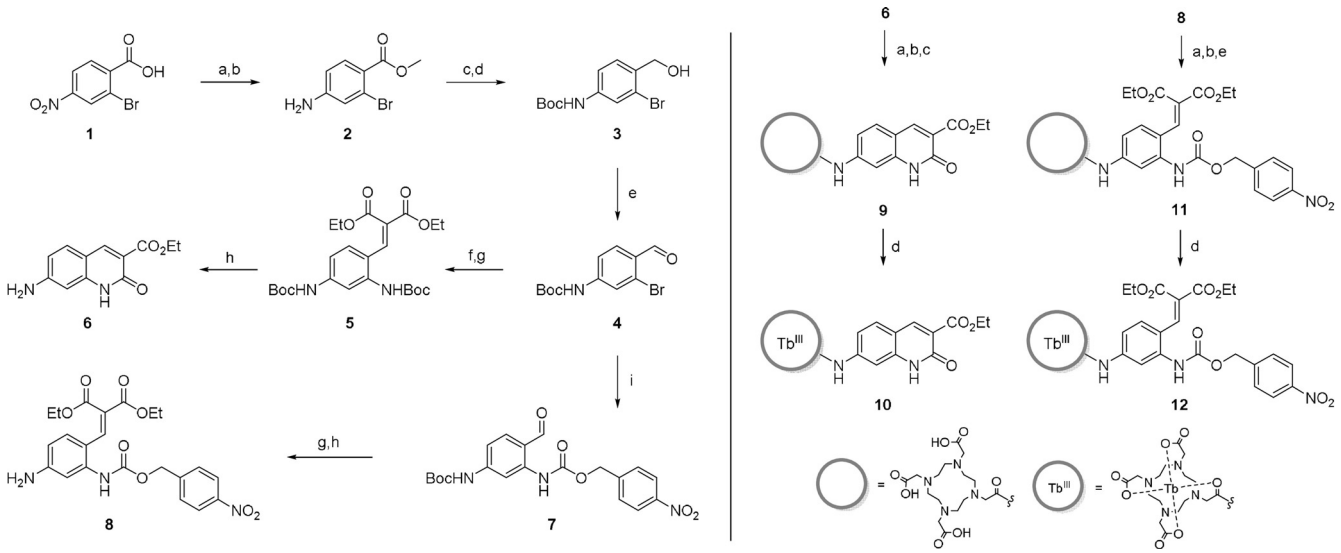

Scheme 2. Left: Synthesis of Antenna **6** and caged antenna **8**. a) $SOCl_2$, MeOH, reflux, 18 h, 92%. b) $SnCl_2$ $2H_2O$, EtOH, reflux, 4 h, 94%. c) $LiAlH_4$, THF, 0°C, 4 h, 67%. d) Boc_2O, DIPEA, THF, RT, 4 days, 82%. e) Dess–Martin-reagent, CH_2Cl_2, RT., 18 h, 76%. f) *tert*-Butyl carbamate, XantPhos Pd G3, Cs_2CO_3, dioxane, 100°C, 18 h, 69%. g) Diethyl malonate, $TiCl_4$, pyridine, THF, 0°C–RT, 18 h, **5**: 32% **8**: 81%. h) TFA/DCM 1:1, RT, 30 min, **6**: quant., **8**: 64%. i) 4-Nitrobenzyl carbamate, XantPhos Pd G3, Cs_2CO_3, dioxane, 100°C, 4 h, 88%. Right: Attachment of **6** and **8** to the DOTA scaffold leading to carbostyril reference probe **10** and NTR probe **12**. a) Bromoacetyl bromide, K_2CO_3, CH_3CN, 0°C, 2 h. b) Tris-(*t*Bu)DO3A, K_2CO_3, CH_3CN, RT, 18 h. c) TFA/DCM 1:1, RT, 18 h, 14% over 3 steps. d) $TbCl_3$, H_2O, EtOH, 45°C, 24 h, 10: 50%, 12: 40%. e) 4 N HCl in dioxane, RT, 18 h, 47% over 3 steps.

spectrum of the caged precursor **12**. As expected, the caged probe **12** does not exhibit any fluorescence at all, also showing that the caged antenna **8** is not able to sensitize the terbium-(III) complex.

While the steady-state emission of reference probe **10**, constituting the probe's activated state, contains the strong antenna fluorescence signal at 435 nm, under time-gated conditions (50 μs delay) only the terbium emission bands are visible. The absorption and excitation spectrum are similar, validating Tb sensitization by the antenna. The total luminescence quantum yield of complex **10** was determined to be 1.67%, which is amongst the best values for turn-on luminescent probes featuring analyte-triggered antenna formation.[4,11] The lifetime of the complex was determined to be 68 μs, which significantly increased to 580 μs upon deoxygenation of the sample solution, indicating energy back transfer from the Tb excited state to the carbostyril triplet state (see Figure S4, Table S1 in the Supporting Information).

Next, we investigated the probe's response to NTR and its ability for sensing NTR in a biochemical setting. Figure 1B shows the gated emission spectra of probe **12** in presence of increasing amounts of NTR. While in absence of the activating enzyme no fluorescence can be detected, the emission intensities gradually increase with rising concentrations of NTR with a 126-fold signal increase at 550 nm at 1 $\mu g\,mL^{-1}$ NTR. A linear correlation was obtained over a broad range of enzyme concentration versus emission intensity at 550 nm. Furthermore, the detection limit ($3\sigma/k$)[15] was calculated to be as low as 4.4 $ng\,mL^{-1}$. The apparent kinetic parameters K_M and v_{max} for the activation of our probe by NTR (18.4 μM and 0.027 $\mu M\,min^{-1}$, respectively, see Figures S4 and S5) are in good agreement with previously reported values for other NTR probes.[10d] LC/MS studies further substantiated the underlying activation mechanism of caged probe **12** by NTR suggested in Scheme 1 by confirming the time-dependent conversion to its activated state **10** as well as revealing the appearance of a carbamic acid intermediate resulting from the fragmentation (see Figure S6). Evidence for the NTR-specificity of our probe emerged from the addition of ascending concentrations of the NTR-inhibitor dicoumarin[16] where we observed a concentration dependent gradual reduction of the luminescence, confirming that activation of our probe arises from the NTR enzyme-catalyzed reduction reaction (see Figures S9, S10).

Subsequently, we determined the specificity and stability of our probe **12** against other commonly present bioanalytes in the bacterial cellular environment, as it is crucial to exclude any interfering factors for an accurate determination of NTR activity when applied in bacteria. As shown in Figure 2A, exclusively NTR triggered a response while the probe remained virtually silent in presence of other species including high concentrations of reductive thiols such as glutathione or dithiothreitol, indicating high specificity for NTR detection.

We then examined the ability of our probe to detect NTR in bacterial lysates. Six bacterial strains of the clinically relevant ESKAPE panel as well as *E. coli* were selected. The bacteria were lysed by sonication and the lysate was incubated with probe **12** with or without dicoumarin inhibitor for 2 h before recording the emission signal at 550 nm. As shown in Figure 2B, our probe was strongly activated in *K. pneumoniae*, *A. baumannii*, *E. cloacae*, and *E. coli* while the activation was less pronounced in the other three strains. Co-incubation with the NTR-inhibitor significantly reduced

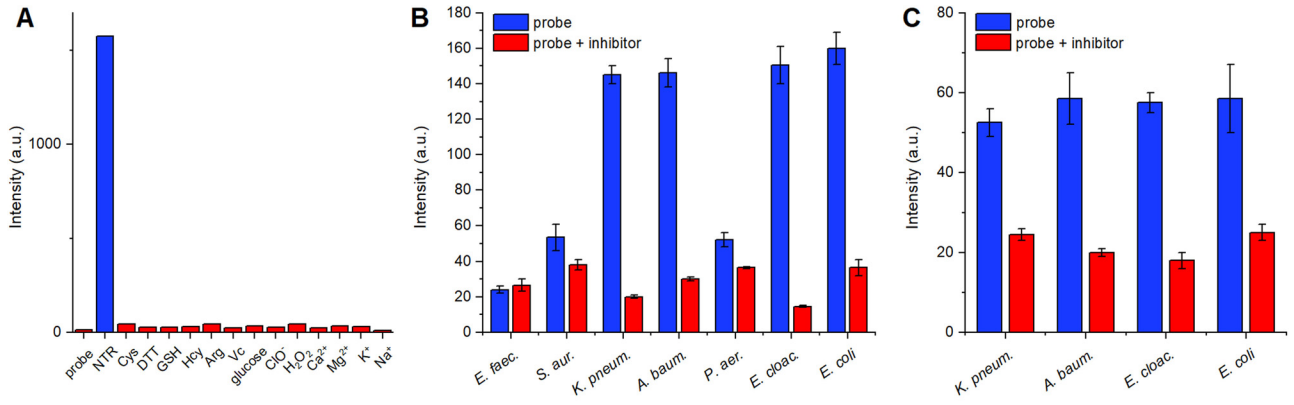

Figure 2. A) Fluorescence responses of probe **12** (20 μM) to various species after 2 h incubation: NTR (1 μg mL^{-1}), Cys (1 mM), DTT (1 mM), GSH (1 mM), Hcy (1 mM), Arg (1 mM), Vc (1 mM), glucose (10 mM), ClO^- (10 mM), H_2O_2 (10 mM), $CaCl_2$ (2.5 mM), $MgCl_2$ (2.5 mM), KCl (10 mM), and NaCl (10 mM). B) Emission intensities of ESKAPE cell lysates incubated with probe **12** (20 μM) in the absence or presence of the NTR inhibitor dicoumarin (0.1 M) for 2 h. C) Fluorescence intensities of live *K. pneumoniae*, *A. baumannii*, *E. cloacae*, and *E. coli* cells incubated with probe **12** (20 μM) in the absence or presence of the NTR inhibitor dicoumarin (0.1 M) for 4 h. All spectra were acquired at 37 °C in 0.05 M Tris buffer (pH 7.4). $\lambda_{ex}/\lambda_{em}$ = 355/550 nm, 50 μs delay. Results representative of two independent experiments.

probe activation in *K. pneumonia, A. baumannii*, *E. cloacae*, and *E. coli*, indicating selective intracellular activation by NTR, while showing little to no effect in the other three. These differences could be attributed to different expression levels as well as species differences of NTR enzymes amongst the bacterial strains, as sequence alignments of those enzymes showed low conservation amongst the bacterial strains as proposed in preceding work.[10d]

We advanced to test whether we could detect NTR in live bacteria. We were pleased to get similar results in *K. pneumoniae*, *A. baumannii*, *E. cloacae*, and *E. coli* to those obtained with the lysates. While probe **12** was highly activated in all four strains, co-incubation with NTR-inhibitor dicoumarin led to a drastic decrease in activation (Figure 2C). The activation of probe **12** was further investigated by fluorescence lifetime imaging (FLIM) in live *E. coli*. Figure 3 shows the long-lived emission fluorescence signals with an average lifetime of 31 μs. These results suggest that probe **12** was readily taken up by the bacterial cells and triggered by intracellular NTRs. To our knowledge, this is the first example of FLIM applied to image enzymatic activity in live bacteria with lanthanide luminescent probes. Interestingly, we observed that in contrast to caged probe **12**, which was readily taken up by bacterial cells, the activated reference **10** was not able to permeate into and label bacterial cells (Figure S11). Moreover, in the FLIM experiments activated probe **10** remained localized in the bacterial intracellular compartments and was not cleared to the extracellular medium, for example, by an efflux mechanism, as observed for a previous enzyme-activatable lanthanide probe.[4] Collectively, these findings suggest a synergistically enhanced localization, detection specificity, and contrast due to intracellular enrichment of the activated probe **10**.

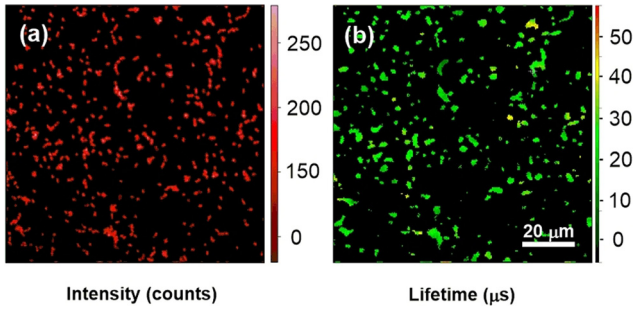

Figure 3. Fluorescence lifetime imaging of live *E. coli* bacteria incubated with probe **12** (20 μM) for 4 h at 37 °C. a) Fluorescence intensity image, b) lifetime map. λ_{ex} = 375 nm, fluorescence intensities and lifetimes were collected through a 641/75 nm long-pass edge filter.

In summary, we have developed the first luminescent turn-on probe for the highly selective and sensitive detection of nitroreductase. Installation of a new type of analyte-responsive carbostyril forming switch was enabled through the key Buchwald–Hartwig type synthetic transformation providing a robust modular approach for the facile access to similar probes. Owing to its effective intracellular enrichment, our probe enables the simple detection and imaging of nitroreductase activity in live bacteria that belong to potentially multiresistant strains of the clinically highly relevant ESKAPE panel. This permitted the first demonstration of fluorescence lifetime imaging (FLIM) to trace enzymatic activity in live bacteria with lanthanide luminescent probes. Taken together these features illustrate that this type of probe concept is an attractive option for future analytical applications in medical diagnostics.

Acknowledgements

We would like to thank Dr. Edgar Specker and the NMR core facility of the FMP for their excellent support on compound characterization and the FMP Screening Unit for access to a plate reader. We thank Dr. Uwe Grether and Dr. Raffael Koller for helpful discussions and Dr. Barth van Rossum for preparing graphical artwork. This work was supported by the Sino-German research project (GZ 1271).

Conflict of interest

The authors declare no conflict of interest.

Keywords: bacterial imaging · enzymes · lanthanides · luminescence · nitroreductase

[1] J.-C. G. Bünzli, *J. Lumin.* **2016**, *170*, 866 – 878.
[2] a) A. Thibon, V. C. Pierre, *Anal. Bioanal. Chem.* **2009**, *394*, 107 – 120; b) M. C. Heffern, L. M. Matosziuk, T. J. Meade, *Chem. Rev.* **2014**, *114*, 4496 – 4539; c) S. H. Hewitt, S. J. Butler, *Chem. Commun.* **2018**, *54*, 6635 – 6647.
[3] a) B. Song, G. Wang, M. Tan, J. Yuan, *J. Am. Chem. Soc.* **2006**, *128*, 13442 – 13450; b) Y. Bretonniere, M. J. Cann, D. Parker, R. Slater, *Org. Biomol. Chem.* **2004**, *2*, 1624 – 1632; c) R. Pal, D. Parker, *Org. Biomol. Chem.* **2008**, *6*, 1020 – 1033.
[4] E. Pershagen, J. Nordholm, K. E. Borbas, *J. Am. Chem. Soc.* **2012**, *134*, 9832 – 9835.
[5] E. J. New, D. Parker, D. G. Smith, J. W. Walton, *Curr. Opin. Chem. Biol.* **2010**, *14*, 238 – 246.
[6] a) H.-Y. Hu, N.-H. Lim, H.-P. Juretschke, D. Ding-Pfennigdorff, P. Florian, M. Kohlmann, A. Kandira, J. Peter von Kries, J. Saas, K. A. Rudolphi, K. U. Wendt, H. Nagase, O. Plettenburg, M. Nazare, C. Schultz, *Chem. Sci.* **2015**, *6*, 6256 – 6261; b) H.-Y. Hu, N.-H. Lim, D. Ding-Pfennigdorff, J. Saas, K. U. Wendt, O. Ritzeler, H. Nagase, O. Plettenburg, C. Schultz, M. Nazare, *Bioconjugate Chem.* **2015**, *26*, 383 – 388.
[7] a) Y. Liu, L. Zhang, M. Nazare, Q. Yao, H.-Y. Hu, *Acta Pharm. Sin. B* **2018**, *8*, 401 – 408; b) L. Zhang, Y. Liu, Q. Zhang, T. Li, M. Yang, Q. Yao, X. Xie, H.-Y. Hu, *Anal. Chem.* **2018**, *90*, 1934 – 1940.
[8] a) D. W. Bryant, D. R. McCalla, M. Leeksma, P. Laneuville, *Can. J. Microbiol.* **1981**, *27*, 81 – 86; b) M. D. Roldán, E. Pérez-Reinado, F. Castillo, C. Moreno-Vivián, *FEMS Microbiol. Rev.* **2008**, *32*, 474 – 500; c) E. Akiva, J. N. Copp, N. Tokuriki, P. C. Babbitt, *Proc. Natl. Acad. Sci. USA* **2017**, *114*, E9549 – E9558.
[9] a) L. B. Rice, *J. Infect. Dis.* **2008**, *197*, 1079 – 1081; b) H. W. Boucher, G. H. Talbot, J. S. Bradley, J. E. Edwards, D. Gilbert, L. B. Rice, M. Scheld, B. Spellberg, J. Bartlett, *Clin. Infect. Dis.* **2009**, *48*, 1 – 12; c) S. E. Cellitti, J. Shaffer, D. H. Jones, T. Mukherjee, M. Gurumurthy, B. Bursulaya, H. I. Boshoff, I. Choi, A. Nayyar, Y. S. Lee, J. Cherian, P. Niyomrattanakit, T. Dick, U. H. Manjunatha, C. E. Barry, G. Spraggon, B. H. Geierstanger, *Structure* **2012**, *20*, 101 – 112.
[10] a) Z. Li, X. Gao, W. Shi, X. Li, H. Ma, *Chem. Commun.* **2013**, *49*, 5859 – 5861; b) S. Michael, C. Michelle, L. Panos, T. Mark, *Curr. Gene Ther.* **2015**, *15*, 277 – 288; c) R. H. F. Wong, T. Kwong, K.-H. Yau, H. Y. Au-Yeung, *Chem. Commun.* **2015**, *51*, 4440 – 4442; d) S. Xu, Q. Wang, Q. Zhang, L. Zhang, L. Zuo, J.-D. Jiang, H.-Y. Hu, *Chem. Commun.* **2017**, *53*, 11177 – 11180; e) Y. Ji, Y. Wang, N. Zhang, S. Xu, L. Zhang, Q. Wang, Q. Zhang, H.-Y. Hu, *J. Org. Chem.* **2019**, *84*, 1299 – 1309.
[11] E. Pershagen, K. E. Borbas, *Angew. Chem. Int. Ed.* **2015**, *54*, 1787 – 1790; *Angew. Chem.* **2015**, *127*, 1807 – 1810.
[12] a) M. Li, P. R. Selvin, *J. Am. Chem. Soc.* **1995**, *117*, 8132 – 8138; b) P. Ge, P. R. Selvin, *Bioconjugate Chem.* **2004**, *15*, 1088 – 1094; c) M. S. Tremblay, M. Halim, D. Sames, *J. Am. Chem. Soc.* **2007**, *129*, 7570 – 7577; d) D. Kovacs, X. Lu, L. S. Mészáros, M. Ott, J. Andres, K. E. Borbas, *J. Am. Chem. Soc.* **2017**, *139*, 5756 – 5767.
[13] K. N. Hearn, T. D. Nalder, R. P. Cox, H. D. Maynard, T. D. M. Bell, F. M. Pfeffer, T. D. Ashton, *Chem. Commun.* **2017**, *53*, 12298 – 12301.
[14] W. Lehnert, *Tetrahedron* **1973**, *29*, 635 – 638.
[15] Y. Chen, C. Zhu, Z. Yang, J. Chen, Y. He, Y. Jiao, W. He, L. Qiu, J. Cen, Z. Guo, *Angew. Chem. Int. Ed.* **2013**, *52*, 1688 – 1691; *Angew. Chem.* **2013**, *125*, 1732 – 1735.
[16] R. L. Koder, A.-F. Miller, *Biochim. Biophys. Acta Protein Struct. Mol. Enzymol.* **1998**, *1387*, 395 – 405.

Manuscript received: February 15, 2020
Accepted manuscript online: March 25, 2020
Version of record online: April 16, 2020

Angewandte Chemie
Eine Zeitschrift der Gesellschaft Deutscher Chemiker

Supporting Information

An Activatable Lanthanide Luminescent Probe for Time-Gated Detection of Nitroreductase in Live Bacteria

Benjamin Brennecke, Qinghua Wang, Qingyang Zhang, Hai-Yu Hu, and Marc Nazaré**

anie_202002391_sm_miscellaneous_information.pdf

SUPPORTING INFORMATION

Table of Contents

SUPPORTING INFORMATION

Experimental Procedures

Preparative Methods

Reactions requiring anhydrous conditions were carried out in dry solvents stored over molecular sieves (THF, DCM, toluene, pyridine, DMF from Sigma Aldrich) which were used as received. These moisture- and air-sensitive reactions were conducted under nitrogen using Schlenk-technique.

Purification of compounds was performed by flash chromatography on silica using a Biotage Isolera One apparatus or by HPLC using a Waters system equipped with a Waters 2489 UV/visible detector, a Waters 2545 Binary Gradient Module and a Nucleodur 100-7 C18ec column from Macherey-Nagel. Water/acetonitrile with 0.1% TFA was used as the solvent system, with one of the following methods. **Method A:** 15-45% CH_3CN 0-18 min, then 45-100% 18-23 min, 100% 23-28 min. **Method B:** 5-35% CH_3CN 0-24 min, 35-100% 24-30 min, 100% 30-34 min. **Method C:** 5-50% CH_3CN 0-35 min, 50-100% 35-40 min, 100% 40-43 min.

Analytical Methods

NMR spectra were acquired on devices from the company Bruker (AV 300, AV 600). All ^{13}C-NMR-spectra were recorded with ^{1}H-broad-band decoupling. Calibration of the chemical shift was conducted using the solvent residual signals. Numbering of the denoted compounds arises from the IUPAC nomenclature. Mass spectra were recorded with an Agilent 1260 liquid chromatography coupled accurate mass time-of-flight 6230 detector. Standard analysis of reaction time courses were conducted with an Agilent 1260 infinity liquid chromatography coupled quadrupole mass spectrometer 6120 detector.

UV-VIS absorption and fluorescence spectra

The concentration of DMSO stock solution of control probe **10** (10 mM) and nitroreductase probe **12** (10 mM) were diluted to 20 µM in the according buffer. The UV-Visible spectra were recorded using a Tecan Spark™ 10M Multimode Microplate Reader, wavelength interval: 5.0 nm. Fluorescence spectroscopic studies were also performed at the excitation wavelength of 355 nm, wavelength interval: 5.0 nm.

Determination of luminescent lifetimes

The luminescence emission decays of the compounds (20 µM in Tris-HCl buffer, pH 7.4) were recorded with an Edinburgh photonics FLS980 with the excitation wavelength set to 355 nm and the emission monitored at 550 nm. The luminescence emission was fitted to a single exponential decay as the most suitable fit according to R^2 and χ^2 to obtain the lifetime constants. Data is representative of a single experiment.

Determination of luminescence quantum yield

The total quantum yield of the complex was determined in aq. PBS pH 7.4 with an integrating sphere using an Edinburgh photonics FLS980. The quantum yield was calculated using the direct excitation method, consecutively exciting a reference sample solution containing aq. PBS and a probe containing sample solution set to an optical density of around 0.1 at the excitation wavelength. All emissions were corrected by the wavelength sensitivity of the spectrometer. The total quantum yield was then calculated according to the equation $\Phi_{tot} = (E_s\text{-}E_r)/(S_r\text{-}S_s)$, where E_s and E_r correspond to the integrated emission peaks of the sample and the reference, and S_s and S_r correspond to the integrated scatter peaks of the sample and the reference, respectively.[1] Data is representative of a single experiment.

Measurements of NTR activity in bacterial lysates and live bacteria

Nitroreductase (≥100 units/mg) from Escherichia coli and reduced nicotinamide adenine dinucleotide (NADH) were purchased from Sigma-Aldrich. The bacterial strains *Escherichia coli* (*E. coli*, ATCC 25922), *Staphylococcus aureus* (*S. aureus*, ATCC 29213), *Klebsiella pneumoniae* (*K. pneumonia*, ATCC 700603), *Pseudomonas aeruginosa* (*P. aeruginosa*, ATCC 27853) were purchased from American Type Culture Collection (ATCC), USA. *Enterococcus faecium* (*E. faecium*, CICC 10840) and *Acinetobacter baumannii* (*A.*

baumannii, CICC 22933) were purchased from China Center of Industrial Culture Collection, CICC®. OD values were recorded in a 10 mm path quartz cell on a Metash UV-5100B spectrometer.

NTR activity in bacterial lysates. The six bacterial strains were cultured for 12 h in Luria-Bertani (LB) medium at 37 °C, then harvested and washed twice with Tris buffer (pH 7.4). The washed cells were resuspended in Tris buffer with an OD600 of 10.0. The cell suspension was then aliquoted and lysed by sonication. The lysates were then treated with 20 μM of nitroreductase probe **12** for 2 h with or without dicoumarin (0.1 mM) and fluorescence of the reaction solutions was measured using a Tecan Spark™ 10M Multimode Microplate Reader. ($\lambda_{ex}/\lambda_{em}$ = 355/550 nm)

NTR activity in live bacteria. The three bacterial strains were cultured for 12 h in Luria-Bertani (LB) medium at 37 °C, and then harvested and washed twice with Tris buffer (pH 7.4). The washed cells were resuspended in Tris buffer with an OD600 of 2.0. The cell suspension was then aliquoted and treated with 20 μM of nitroreductase probe **12** for 4 h and 12 h with or without dicoumarin (0.1 mM). Fluorescence of the bacterial solutions was measured using a Tecan Spark™ 10M Multimode Microplate Reader ($\lambda_{ex}/\lambda_{em}$ = 355/550 nm).

Uptake of probe 12 and reference 10 in live bacteria. *E. coli*, *K. pneumoniae, A. baumannii* and *E. cloacae* cells were cultured for 12 h in Luria-Bertani (LB) medium at 37 °C, and then harvested and washed twice with Tris buffer (pH 7.4). The washed cells were resuspended in Tris buffer with an OD_{600} of 2.0. The cell suspension was then aliquoted and treated with 20 μM of probe **12** and reference **10** for 12 h. The cells were then washed twice with 1× PBS buffer. Fluorescence of the bacterial solutions was measured ($\lambda_{ex}/\lambda_{em}$ = 355/550 nm).

Fluorescence lifetime imaging of live *E. coli*. *E.coli* (ATCC25922) cells cultured overnight in LB medium were harvested and washed twice with PBS buffer solution. The washed cells were resuspended in 50 mM Tris-HCl (pH 7.4) buffer with an OD600 of 0.5 - 0.7. Then 500 μL aliquots were treated with 20 μM of probe **12**. After incubation at 37 °C for 4 h, a drop of the suspension was added into an 8-well chamber followed by covering with agarose pads. Fluorescence lifetime images were acquired by an ISS Q2 confocal laser scanning system coupled to a Nikon TE2000 microscope with the 60×/1.2 NA WI objective lens. The excitation wavelength of the probe **12** was 375 nm (5000 Hz repetition rate), fluorescence emission and lifetime signals were collected through a 641/75 nm long-pass edge filter.

SUPPORTING INFORMATION

Synthetic Procedures

Methyl 2-bromo-4-nitrobenzoate

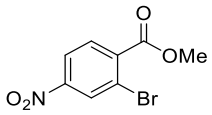

2-Bromo-4-nitrobenzoic acid (**1**, 500 mg, 2.03 mmol) was dissolved in MeOH (10 ml) and thionyl chloride (295 µl, 4.06 mmol) was added. The mixture was stirred at 65°C for 18 h, allowed to cool down to r.t. and neutralized by addition of aq. sat. $NaHCO_3$. The aq. phase was extracted with EtOAc (3x) and the combined org. layers were dried over $MgSO_4$, filtered and the solvent was evaporated to provide 483 mg (92%) as methyl 2-bromo-4-nitrobenzoate as colorless solid.

^{1}H-NMR (300 MHz, $CDCl_3$): δ = 3.99 (s, 3 H, CH_3), 7.92 (d, J = 8.5 Hz, 1 H, 6-H), 8.21 (dd, J = 8.5, 2.2 Hz, 1 H, 5-H), 8.52 (d, J = 2.2 Hz, 1 H, 3-H) ppm. Data matches literature.[2]

Methyl 4-amino-2-bromobenzoate (2)

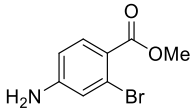

Methyl 2-bromo-4-nitrobenzoate (364 mg, 1.40 mmol) was dissolved in ethanol/ethyl acetate (20+10 ml) and tin chloride dihydrate (1.58 g, 7.00 mmol) was added. The solution was heated to 85°C for 4 h, then was cooled down to r.t. and poured into water (30 ml). Sat. aq. $NaHCO_3$ (10 ml) was added dropwise and the slurry was extracted two times with ethyl acetate. The org. layers were washed with brine, dried over $MgSO_4$, and filtered. Evaporation of the solvents yielded 304 mg (94%) methyl 4-amino-2-bromobenzoate (**2**) as yellow resin.

^{1}H-NMR (300 MHz, $CDCl_3$): δ = 3.86 (s, 3 H, CH_3), 6.56 (dd, J = 8.5, 2.3 Hz, 1 H, 5-H), 6.93 (d, J = 2.3 Hz, 1 H, 3-H), 7.76 (d, J = 8.5 Hz, 1 H, 6-H) ppm. **^{13}C-NMR** (75 MHz, $CDCl_3$): δ = 52.0 (CH_3), 112.9 (C-5), 119.8 (C-1), 119.9 (C-3), 124.3 (C-2), 133.8 (C-6), 150.6 (C-4), 166.1 (CO_2Me) ppm. **HRMS** (pos. ESI-TOF): *m/z* calculated for $C_8H_9BrNO_2$ $[M+H]^+$ 229.9811, found 229.9818.

(4-Amino-2-bromophenyl)methanol

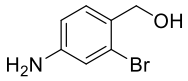

A solution of methyl 4-amino-2-bromobenzoate (**2**, 500 mg, 2.17 mmol) in THF (7 ml) was added dropwise to a solution of lithiumtetrahydroaluminate (3.26 ml, 6.52 mmol, 2 M in THF) in THF (7 ml) at 0°C. The reaction was stirred for 3 h while cooling. Water was added carefully, then 2 M NaOH was added and the mixture was stirred until a fine precipitate had formed. The mixture was filtered over celite, ethyl acetate was added and the org. layer was separated. The aq. phase was extracted with ethyl acetate and the combined org. layers were washed with brine, dried over $MgSO_4$ and filtered. The crude was purified by flash chromatography (SiO_2, cHex/EA 3:1 - 1:1) to provide 299 mg (67%) (4-amino-2-bromophenyl)methanol as colorless crystalline solid.

^{1}H-NMR (300 MHz, CD_3CN): δ = 3.02 (t, J = 5.9 Hz, 1 H, OH), 4.26 (s, 2 H, NH_2), 4.47 (d, J = 5.7, 2 H, CH_2), 6.61 (dd, J = 8.2, 2.3 Hz, 1 H, 5-H), 6.84 (d, J = 2.3 Hz, 1 H, 3-H), 7.16 (d, J = 8.2 Hz, 1 H, 6-H) ppm. **^{13}C-NMR** (75 MHz, CD_3CN): δ = 64.2 (CH_2), 114.5 (C-5), 118.4 (C-3), 123.9 (C-2), 129.5 (C-1), 131.0 (C-6), 149.6 (C-4) ppm. **HRMS** (pos. ESI-TOF): *m/z* calculated for C_7H_9BrNO $[M+H^+]$ 201.9862, found 201.9869.

tert-Butyl (3-bromo-4-(hydroxymethyl)phenyl)carbamate (3)

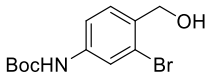

(4-Amino-2-bromophenyl)methanol (45 mg, 0.22 mmol) was dissolved in THF (5 ml) and DIPEA (58 µl, 0.34 mmol) and boc anhydride (97 mg, 0.45 mmol) was added. The reaction was stirred at r.t. for 4 d. It was diluted with water and the solution was extracted with ethyl acetate (2x) dried over $MgSO_4$ and filtered. Purification of the crude by flash chromatography (cHex/EA 3:1) yielded 55 mg (82%) of the title compound (**3**) as colorless oil.

^{1}H-NMR (300 MHz, $CDCl_3$): δ = 1.51 .(s, 9 H, $C(CH_3)_3$), 4.68 (s, 2 H, CH_2OH), 6.52 (s, 1 H, N*H*Boc), 7.21 (dd, *J* = 8.3, 2.2 Hz, 1 H, 6-H), 7.35 (d, *J* = 8.3 Hz, 1 H, 5-H), 7.73 (d, *J* = 2.2 Hz, 1 H, 2-H) ppm. **^{13}C-NMR** (75 MHz, $CDCl_3$): δ = 28.4 ($C(CH_3)_3$), 64.9 (CH_2OH), 81.2 ($C(CH_3)_3$), 117.5 (C-6), 122.3 (C-2), 123.2 (C-3), 129.6 (C-5), 134.2 (C-4), 139.1 (C-1), 152.5 (CONH) ppm. **HRMS** (pos. ESI-TOF): *m/z* calculated for $C_{12}H_{16}BrNO_3Na$ $[M+Na]^+$ 326.0186, found 326.0181.

***tert*-Butyl (3-bromo-4-formylphenyl)carbamate (4)**

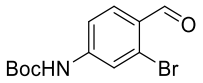

tert-Butyl (3-bromo-4-(hydroxyl-methyl)phenyl)carbamate (**3**, 70 mg, 0.23 mmol) was dissolved in dichloromethane (10 ml) and Dess-Martin periodinane (147 mg, 0.35 mmol) was added. The reaction was stirred at r.t. for 18 h, diluted with ethyl acetate and washed with sat. aq. $NaHCO_3$, water, and brine. The org. layer was dried over $MgSO_4$ and filtered. Purification of the crude by flash chromatography (SiO_2, cHex/EA = 4:1) yielded 52 mg (76%) *tert*-butyl (3-bromo-4-formylphenyl)carbamate (**4**) as colorless solid.

^{1}H-NMR (300 MHz, $CDCl_3$): δ = 1.52 (s, 9 H, $C(CH_3)_3$), 6.94 (s, 1 H, NH), 7.28 (ddd, *J* = 8.5, 2.1, 0.8 Hz, 1 H, 6-H), 7.84 (d, *J* = 8.5 Hz, 1 H, 5-H), 7.92 (d, *J* = 2.1 Hz, 1 H, 2-H), 10.21 (d, *J* = 0.8 Hz, 1 H, CHO) ppm. **^{13}C-NMR** (75 MHz, $CDCl_3$): δ = 28.3 ($C(CH_3)_3$), 82.1 ($C(CH_3)_3$), 117.0 (C-6), 122.0 (C-2), 128.3 (C-4), 128.7 (C-3), 130.8 (C-5), 144.9 (C-1), 151.9 (CONH), 191.0 (CHO) ppm. **HRMS** (pos. ESI-TOF): *m/z* calculated for $C_{12}H_{15}BrNO_3$ $[M+H]^+$ 302.0210, found 302.0215.

Di-*tert*-butyl (4-formyl-1,3-phenylene)dicarbamate

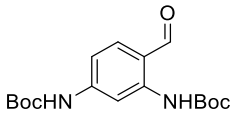

In a screw-cap vial, *tert*-Butyl (3-bromo-4-formylphenyl)carbamate (**4**, 54 mg, 0.18 mmol), caesium carbonate (88 mg, 0.27 mmol) and *tert*-butyl carbamate (28 mg, 0.23 mmol) were dissolved in dioxane and the solvent was deoxygenated by bubbling nitrogen through the solution for 15 min. Xantphos Pd G3 (6 mg, 0.006 mmol) was added and the mixture was heated to 100°C for 18 h. After cooling down to r.t. it was partitioned between DCM and water and the org. layer was separated, dried over $MgSO_4$ and filtered. Flash chromatography (SiO_2, cHex/EA = 95:5) provided 42 mg (69%) of the title compound as colorless crystalline solid.

^{1}H-NMR (300 MHz, $CDCl_3$): δ = 1.48, 1.50 (2 s, 18 H, $C(CH_3)_3$), 6.83 (s, 1 H, NH), 7.53 (s, 2 H, 5,6-H), 8.16 (s, 1 H, 3-H), 9.74 (s, 1 H, CHO), 10.51 (s, 1 H, NH) ppm. **^{13}C-NMR** (75 MHz, $CDCl_3$): δ = 28.4, 28.4 ($C(CH_3)_3$), 81.2, 81.7 ($C(CH_3)_3$), 106.4 (C-3), 110.8 (C-5), 117.0 (C-1), 138.1 (C-6), 143.1 (C-2), 145.7 (C-4), 152.0, 153.1 (NHCO), 193.4 (CHO) ppm. **HRMS** (pos. ESI-TOF): *m/z* calculated for $C_{17}H_{24}N_2O_5Na$ $[M+Na]^+$ 359.1577, found 359.1591.

Diethyl 2-(2,4-bis((tert-butoxycarbonyl)amino)benzylidene)malonate (5)

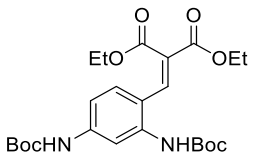

This compound was prepared following a procedure from Lehnert.[3] A solution of titanium tetrachloride (16 µl, 0.14 mmol) in THF (5 ml) was cooled to 0°C. Di-*tert*-butyl (4-formyl-1,3-phenylene)dicarbamate (24 mg, 0.07 mmol) and diethyl malonate (13 µl, 0.09 mmol) in THF (5 ml) were added, then pyridine (23 µl, 0.28 mmol) was added dropwise. The solution was stirred for 4 h while warming up to r.t. Water was added and the mixture was extracted with ethyl acetate (3x). The combined org. layers were dried over $MgSO_4$, filtered and the crude was purified by flash chromatography (cHex/EA = 4:1) to yield 11 mg (32%) of the title compound (**5**) as colorless oil.

^{1}H-NMR (300 MHz, $CDCl_3$): δ = 1.22 (t, J = 7.1 Hz, 3 H, CH_3), 1.33 (t, J = 7.1 Hz, 3 H, CH_3), 1.50 (s, 9 H, $C(CH_3)_3$), 1.51 (s, 9 H, $C(CH_3)_3$), 4.24 (q, J = 7.1 Hz, 2 H, CH_2CH_3), 4.30 (q, J = 7.1 Hz, 2 H, CH_2CH_3), 6.45, 6.66 (2 s, 2 H, NHCO), 7.24-7.33 (m, 2 H, 5-H, 6-H), 7.74 (s, 1 H, CH), 7.78 (m_c, 1 H, 3-H) ppm. **^{13}C-NMR** (75 MHz, $CDCl_3$): δ = 14.1, 14.3 (CH_3), 28.4, 28.4 ($C(CH_3)_3$), 61.8, 61.9 (CH_2CH_3), 81.1, 81.5 ($C(CH_3)_3$), 110.7 (C-3) 113.5 (C-5), 118.6 (C-1), 127.9 (C-2), 129.6 (C-6), 137.7 (CH), 137.9 (*C*-CH), 141.3 (C-4), 152.4, 152.6 (CONH), 164.2, 166.3 (COOEt). **HRMS** (pos. ESI-TOF): *m/z* calculated for $C_{24}H_{35}N_2O_8$ $[M+H]^+$ 479.2388, found 479.2396.

Ethyl 7-amino-2-oxo-1,2-dihydroquinoline-3-carboxylate (6)

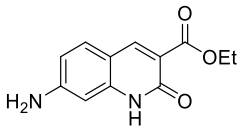

Diethyl 2-(2,4-bis((tert-butoxycarbonyl)amino)benzylidene)malonate (**5**, 9 mg, 0.02 mmol) was dissolved in DCM/TFA (5 ml, 1:1) and the solution was stirred at r.t. for 30 min. The solvent was evaporated and the residue was suspended in H_2O and lyophilized to yield 7 mg (quant.) ethyl 7-amino-2-oxo-1,2-dihydroquinoline-3-carboxylate (**6**) as pale yellow powder.

^{1}H-NMR (300 MHz, CD_3OD): δ = 1.36 (t, J =7.1 Hz, 3 H, CH_3), 4.32 (q, J = 7.1 Hz, 2 H, CH_2), 6.40 (s, 1 H, 8-H), 6.64 (d, J = 8.7 Hz, 1 H, 6-H), 7.43 (d, J = 8.7 Hz, 1 H, 5-H), 8.48 (s, 1 H, 4-H) ppm. **^{13}C-NMR** (75 MHz, CD_3OD): δ = 14.6 (CH_3), 62.0 (CH_2), 96.5 (C-8), 111.9 (C-4-*C*-C-5), 114.4 (C-6), 132.6 (C-5), 144.6 (C-8-*C*-N), 147.7 (C-4), 156.4 (C-7), 163.2 (NHCO), 167.1 (NHCO) ppm. **HRMS** (pos. ESI-TOF): *m/z* calculated for $C_{12}H_{13}N_2O_3$ $[M+H]^+$ 233.0921, found 233.0917.

***tert*-Butyl (4-nitrobenzyl) (4-formyl-1,3-phenylene)dicarbamate (7)**

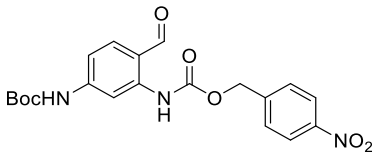

4-Nitrobenzyl carbamate was prepared as described previously.[4]

tert-Butyl (3-bromo-4-formylphenyl)carbamate (**4**, 200 mg, 0.67 mmol), caesium carbonate (326 mg, 1.0 mmol) and 4-nitrobenzyl carbamate (170 mg, 0.87 mmol) were added in a screw-cap vial, dioxane (5 ml) was added and the solution was deoxygenated by bubbling argon through the solution for 15 min. Subsequently, Xantphos Pd G3 (22 mg, 23 µmol) was added and the reaction was heated to 100°C for 5 h. Water and ethyl acetate were added and the org. layer was separated. The aq. phase was extracted once with ethyl acetate and the combined org. layers were dried over Na_2SO_4, filtered and the crude was purified by flash chromatography (Hept/EA = 8:2 - 6:4) to yield 258 mg (88%) *tert*-butyl (4-nitrobenzyl) (4-formyl-1,3-phenylene)dicarbamate (**7**) as colorless solid.

^{1}H-NMR (600 MHz, DMSO-D_6): δ = 1.48 (s, 9 H, $C(CH_3)_3$), 5.35 (s, 2 H, CH_2), 7.29 (dd, J = 8.6, 2.0 Hz, 1 H, 5-H), 7.67-7.73 (m, 2 H, 2',6'-H), 7.75 (d, J = 8.6 Hz, 1 H, 6-H), 8.24-8.29 (m, 2 H, 3',5'-H), 8.51 (d, J = 2.0 Hz, 1 H, 3-H), 9.78 (s, 1 H, NH), 9.99 (s, 1 H, NH), 10.82 (s, 1 H, CHO) ppm. **^{13}C-NMR** (150 MHz, DMSO-D_6): δ = 28.0 ($C(CH_3)_3$), 65.2 (CH_2), 80.1 ($C(CH_3)_3$), 106.4 (C-3), 112.0 (C-5), 116.8 (C-1), 123.7 (C-3',5'), 128.6 (C-2',6'), 136.7 (C-6), 141.4 (C-2), 144.0 (C-1'), 146.6 (C-4), 147.2 (C-4'), 152.3 (NHCO), 152.4 (NHCO), 193.9 (*C*HO) ppm. **HRMS** (neg. ESI-TOF): *m/z* calculated for $C_{20}H_{20}N_3O_7$ $[M-H]^-$ 414.1307, found 414.1323.

Boc-protected caged antenna

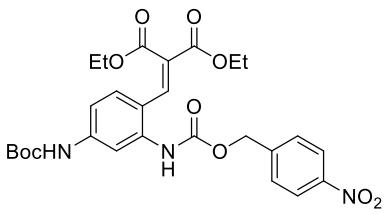

SUPPORTING INFORMATION

A solution of titanium tetrachloride (1.16 ml, 1.16 mmol, 1 M in DCM) in tetrahydrofuran (2 ml) was cooled to 0°C. *tert*-Butyl (4-nitrobenzyl) (4-formyl-1,3-phenylene)dicarbamate (**7**, 240 mg, 0.58 mmol) in tetrahydrofuran (2 ml) and diethyl malonate (106 µl, 0.69 mmol) were added, then pyridine (186 µl, 2.31 mmol) was added dropwise. The solution was allowed to warm up to r.t. and stirred for 18 h. 2 M aq. $KHCO_3$ and ethyl acetate were added and the layers were separated. The aq. phase was extracted once with ethyl acetate and the combined org. phases were washed with brine, dried over Na_2SO_4 and filtered. Purification of the crude by flash chromatography (Hept/EA = 7:3 - 1:1) yielded 261 mg (81%) of the title compound as light yellow solid.

^{1}H-NMR (600 MHz, DMSO-D_6): δ = 1.19 (t, *J* = 7.1 Hz, 3 H, CH_3), 1.22 (t, *J* = 7.1 Hz, 3 H, CH_3), 1.47 (s, 9 H, $C(CH_3)_3$), 4.21 (q, *J* = 7.1 Hz, 2 H, CH_2CH_3), 4.23 (q, *J* = 7.1 Hz, 2 H, CH_2CH_3), 5.30 (s, 2 H, CH_2), 7.21-7.25 (m, 1 H, 6-H), 7.26-7.29 (m, 1 H, 5-H), 7.68 (d, *J* = 8.7 Hz, 2 H, 2',6'-H), 7.71 (d, *J* = 1.4 Hz, 1 H, 3 H), 7.73 (s, 1 H, CH=C), 8.26 (d, *J* = 8.7 Hz, 2 H, 3',5'-H), 9.67, 9.71 (2 s, 2 H, NHCO) ppm. **^{13}C-NMR** (150 MHz, DMSO-D_6): δ = 13.4 (CH_3), 13.9 (CH_3), 28.0 ($C(CH_3)_3$), 61.2 (CH_2CH_3), 61.2 (CH_2CH_3), 64.8 (CH_2Ar), 79.7 ($C(CH_3)_3$), 115.0 (C-5), 120.6 (C-1), 123.6 (C-3',5'), 124.2 (CH=*C*), 128.3 (C-2',6'), 128.4 (C-6), 137.8 (*C*H=C), 138.2 (C-2), 142.4 (C-4), 144.6 (C-1'), 147.0 (C-4'), 152.5 (NHCO), 153.9 (NHCO), 163.8 (CO_2Et), 166.0 (CO_2Et) ppm. **HRMS** (pos. ESI-TOF): *m/z* calculated for $C_{27}H_{32}N_3O_{10}$ $[M+H]^+$ 558.2082, found 558.2080.

Caged antenna (8)

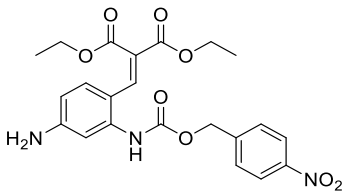

Boc-protected antenna precursor (349 mg, 0.63 mmol) was dissolved in DCM/TFA (10 ml, 1:1) and the solution was stirred for 30 min. The solvents were evaporated and the residue was suspended in water/acetonitrile and lyophilized to obtain 183 mg (64%) of the title compound (**8**) as pale yellow powder which was directly used for the next step without further purification.

DOTA antenna conjugate (9)

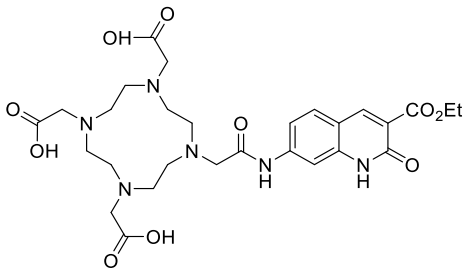

Ethyl 7-aminoquinolin-2-one-3-carboxylate (**6**, 73 mg, 0.16 mmol) was dissolved in DMF (5 ml) and the solution was cooled to 0°C. Bromoacetyl bromide (20 µl, 0.22 mmol) and potassium carbonate (48 mg, 0.34 mmol) were added successively and the reaction was stirred at 0°C for 2 h. The mixture was diluted with dichloromethane (20 ml) and the org. layer was washed with water, dried over $MgSO_4$ and filtered. The solvents were evaporated, the residue was dissolved in DMF (5 ml) and *tri*-tert-butyl 2,2',2''-(1,4,7,10-tetraazacyclododecane-1,4,7-triyl)triacetate (115 mg, 0.22 mmol) and potassium carbonate (48 mg, 0.34 mmol) were added and the mixture was stirred at r.t. for 18 h. The solids were removed by filtration over celite and the solvents were evaporated. The crude was dissolved in TFA/DCM (5 ml, 1:1) and the solution was stirred for 18 h at r.t. Evaporation of the solvents and purification by HPLC (**Method A**) yielded 15 mg (14% over 3 steps) of the title compound (**9**) as colorless powder after lyophilization.

^{1}H-NMR (600 MHz, MeOD): δ = 1.41 (t, *J* = 7.1 Hz, 3 H, CH_3), 3.30-4.35 (m, 24 H, NCH_2CH_2, NCH_2CO), 4.37 (q, *J* = 7.1 Hz, 2 H, CH_2CH_3), 6.89 (bs, 1 H, 6-H), 7.39 (d, *J* = 8.5 Hz, 1 H, 5-H), 7.81 (s, 1 H, 8-H), 8.33 (s, 1 H, 4-H) ppm. **^{13}C-NMR** (150 MHz, MeOD): δ = 14.7 (CH_3), 50.1, 52.4 (NCH_2CH_2), 54.1, 55.8, 56.2 (NCH_2CO), 62.2 (CH_2CH_3), 105.3 (C-8), 115.7 (C-3), 116.1 (C-6), 118.2 (q, *J* = 290 Hz, CF_3COO), 120.1 (C-4-*C*-C-5), 131.1 (C-5), 142.3 (C-8-*C*), 144.3 (C-7), 146.4 (C-4), 161.8 (CONH), 162.8 (q, *J* = 34 Hz, CF_3COO), 165.8 (COOEt), 170.6 (CH_2CONH), 173.9 (COOH) ppm. **HRMS** (pos. ESI-TOF): *m/z* calculated for $C_{28}H_{39}N_6O_{10}$ $[M+H]^+$ 619.2722, found 619.2723.

DOTA caged antenna conjugate (11)

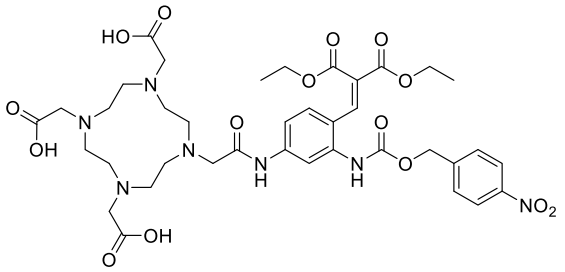

Caged antenna (**8**, 73 mg, 0.16 mmol) was dissolved in acetonitrile (5 ml) and the solution was cooled to 0°C. Potassium carbonate (44 mg, 0.32 mmol) and bromoacetyl bromide (18 µl, 0.21 mmol) were added successively and the reaction was stirred at 0°C for 2 h. The mixture was diluted with dichloromethane (20 ml) and the org. layer was washed with water, dried over $MgSO_4$ and filtered. The solvents were evaporated to furnish 93 mg (quant.) of a yellow oil which was used without further purification. It was dissolved in acetonitrile (5 ml) and *tri*-tert-butyl 2,2',2''-(1,4,7,10-tetraazacyclododecane-1,4,7-triyl)triacetate (91 mg, 0.18 mmol) and potassium carbonate (34 mg, 0.24 mmol) were added and the mixture was stirred at r.t. for 18 h. The solids were removed by filtration over celite and the solvents were evaporated to yield 152 mg of the *tert*-butyl protected DOTA derivative as yellow oil. It was dissolved in 4 N HCl in dioxane (5 ml) and the solution was stirred at r.t. for 18 h. The solvents were evaporated and the residue was purified by HPLC (**Method B**) to yield 64 mg (47% over 3 steps) of the title compound (**11**) as white powder.

^{1}H-NMR (300 MHz, MeOD): δ = 1.24 (t, J = 7.1 Hz, 3 H, CH_3), 1.29 (t, J = 7.1 Hz, 3 H, CH_3), 2.85-3.55 (m, 16 H, NCH_2CH_2), 3.65-4.07 (m, 8 H, NCH_2CO), 4.26 (q, J = 7.1 Hz, 4 H, CH_2CH_3), 5.29 (s, 2 H, CH_2Ar), 7.34 (d, J = 8.5 Hz, 1 H, 5-H), 7.58 (d, J = 8.5 Hz, 1 H, 6-H), 7.63 (d, J = 8.4 Hz, 2 H, 2',6'-H), 7.69 (bs, 1 H, 3-H), 7.77 (s, 1 H, $CH(CO_2Et)_2$), 8.23 (d, J = 8.4 Hz, 2 H, 3',5'-H) ppm. **^{13}C-NMR** (75 MHz, MeOD): δ = 14.3, 14.5 (CH_3), 50.8, 51.5 ($N(CH_2CH_2)$), 55.6, 56.1 (NCH_2CO), 62.8, 62.9 (CH_2CH_3), 66.6 (CH_2Ar), 116.9 (C-3), 117.8 (C-6), 118.2 (q, $^1J_{CF}$ = 293 Hz, CF_3CO_2H), 124.7 (C-3',5'), 127.4 ($C(CO_2Et)_2$), 129.3 (C-2',6'), 130.3 (C-5), 139.1 (C-1), 139.5 ($CHC(CO_2Et)_2$), 142.4 (C-4), 145.7 (C-1'), 148.9 (C-4'), 156.3 ($NHCO_2$), 162.8 (q, $^3J_{CF}$ = 35 Hz, CF_3CO_2H), 165.6, 168.1 (CO_2Et) ppm. CO_2H and CONH are not really visible presumably due to different conformational isomers and the resulting decrease in peak intensity. **HRMS** (pos. ESI-TOF): *m/z* calculated for $C_{38}H_{50}N_7O_{15}$ $[M+H]^+$ 844.3359, found 844.3372.

General procedure for terbium chelation

DOTA conjugate (1 eq.) was dissolved in ethanol (0.01 M) and terbium trichloride (3 eq.) was added. Water was added dropwise until full dissolution of the components, then the solution was heated to 45°C and stirred for 24 h. Water (3 ml) was added, ethanol was evaporated and the aqueous solution was purified by HPLC.

Tb - DOTA antenna conjugate (10)

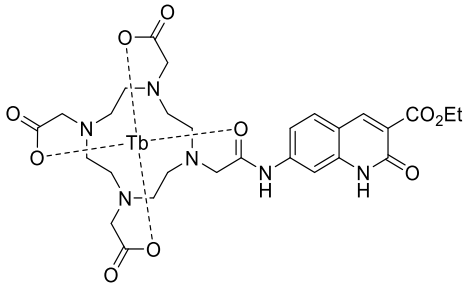

HPLC **Method A**, 8 mg (50%). **HRMS** (pos. ESI-TOF): *m/z* calculated for $C_{28}H_{36}N_6O_{10}Tb$ $[M+H]^+$ 775.1741, found 775.1758.

Tb - DOTA caged antenna conjugate (12)

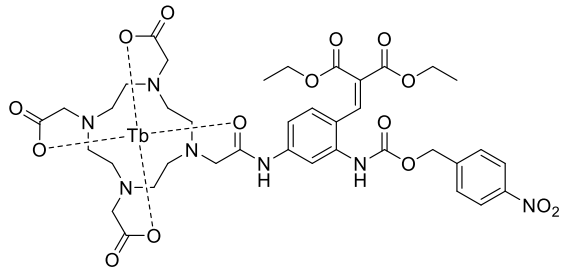

HPLC **Method C**, 24 mg (40%). **HRMS** (pos. ESI-TOF): *m/z* calculated for $C_{38}H_{47}N_7O_{15}Tb$ $[M+H]^+$ 1000.2378, found 1000.2382.

Probe Characterization

Absorption/Excitation/Emission Spectra

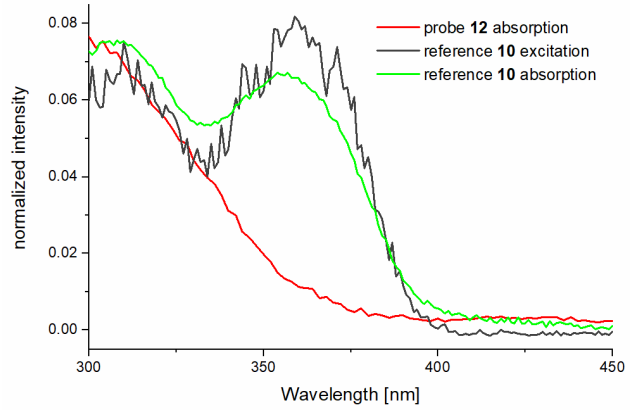

Figure S1. Absorption spectra of reference **10** and probe **12** and excitation spectrum of reference **10** (20 µM) in PBS buffer pH 7.4. Excitation monitored at 545 nm.

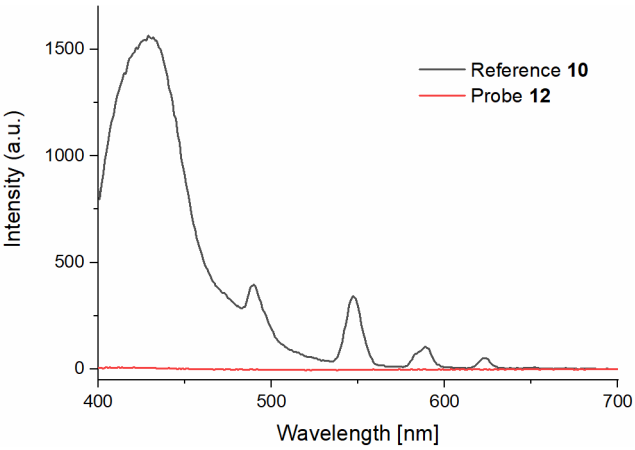

Figure S2. Steady-state fluorescence spectra of reference **10** and probe **12** (20 µM) in PBS pH 7.4, λ_{ex} = 355 nm.

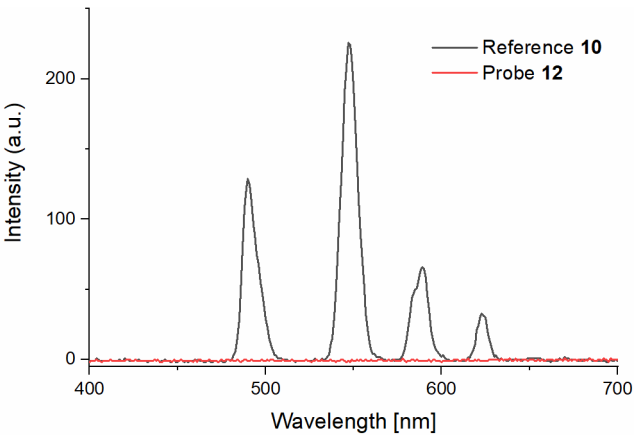

Figure S3. Time-gated fluorescence spectra reference **10** and probe **12** (20 µM) in PBS pH 7.4 (50 µs delay), λ_{ex} = 355 nm.

Lifetime Measurements

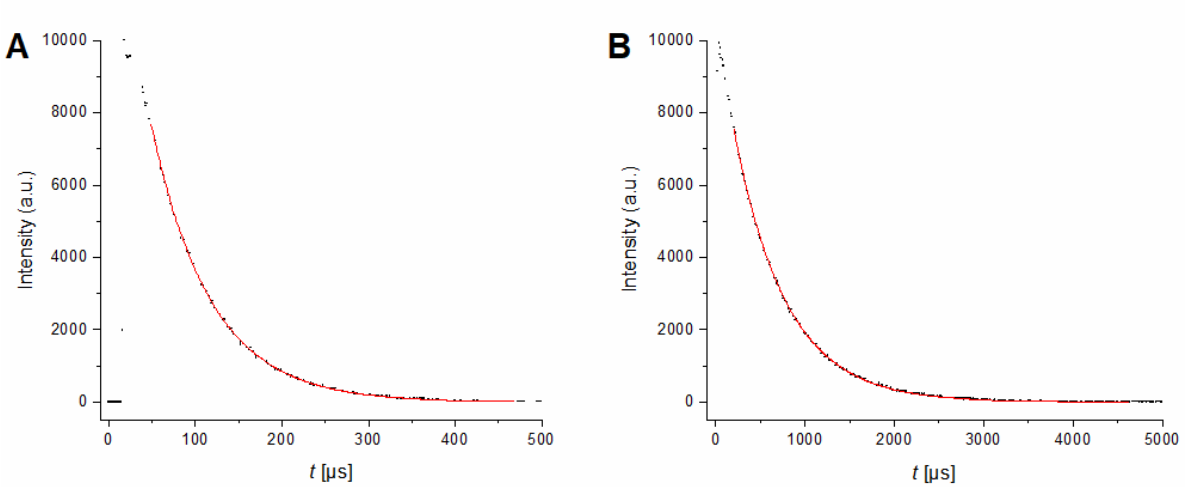

Figure S4: Photoluminescence intensity decays of reference **10**, 20 µM in TRIS-HCl buffer (pH 7.4) at r.t. (black dots) and monoexponential decay fits (red lines, R^2 = 0.9996). **A:** under air environment; **B:** oxygen-free. λ_{ex} = 355 nm, λ_{em} = 550 nm.

Table S1. Luminescent lifetimes of compounds **10** and **12** obtained from single exponential fit of the intensity decays.

	τ [µs][a]	τ [µs][b]
reference **10**	68	580
probe **12**[c]	n.a.	n.a.

[a]Under air environment; [b]oxygen-free; [c]probe **12** is non-fluorescent.

Determination of kinetic parameters

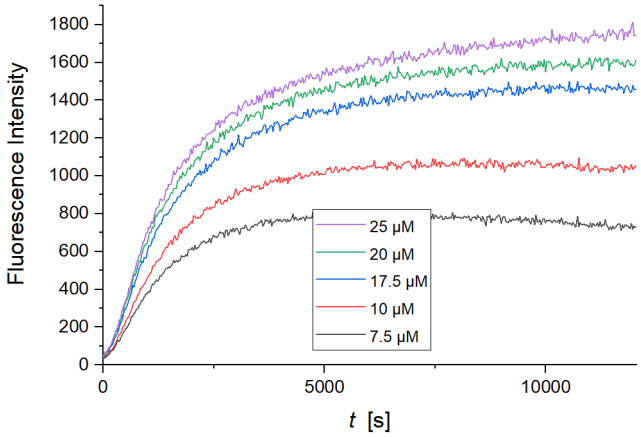

Figure S5. Fluorescence intensity of probe **12** (7.5, 10.0, 15.0, 17.5, 20.0, 25.0 µM) at 550 nm upon incubation with nitroreductase (1 µg/ml). The measurements were performed at 37 °C in 0.05 M Tris buffer (pH 7.4) in the presence of 50 µM NADH. λ_{ex} = 355 nm. Results are representative of two independent experiments.

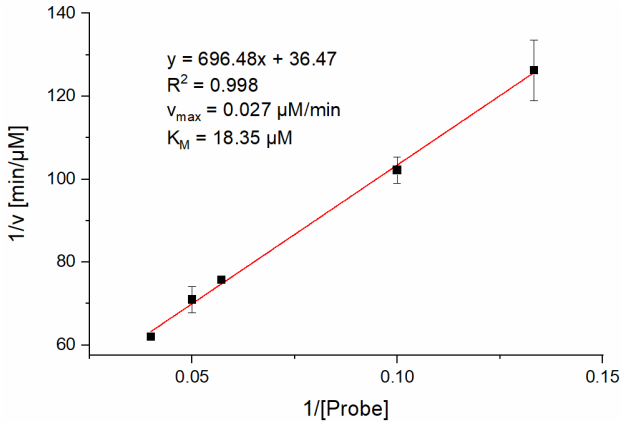

Figure S6. Lineweaver-Burk plot for the nitroreductase-mediated activation of probe **12** derived from the Michaelis-Menten equation. The Michaelis-Menten equation is described as: $v = v_{max}$[probe]/(Km + [probe]), where v is the reaction rate, [Probe] is the probe concentration, and K_M is the Michaelis-Menten constant. Conditions: 1 µg/mL NTR, 50 µM NADH, 7.5-25 µM of the probe, $\lambda_{ex}/\lambda_{em}$ = 355/550 nm. Points are fitted using a linear regression model (correlation coefficient: R^2= 0.998). Results are representative of two independent experiments.

LC/MS activation studies

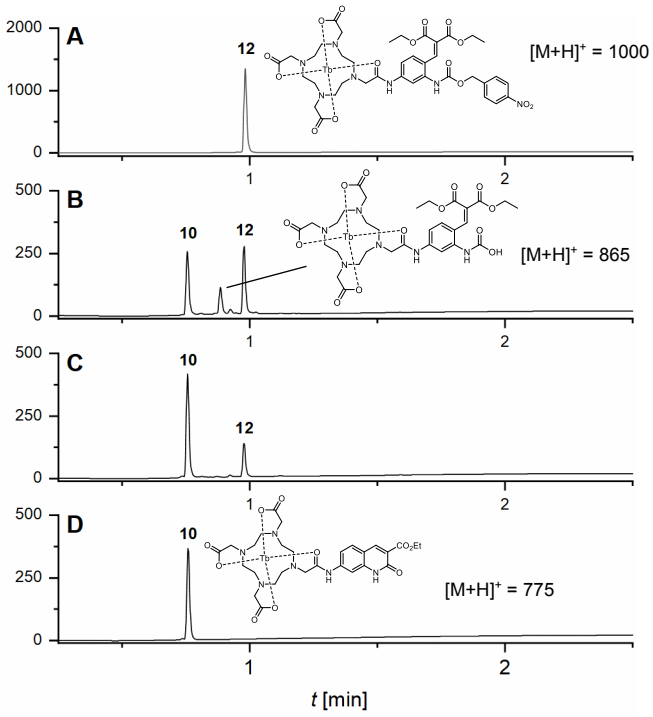

Figure S7. LC/MS activation studies with probe **12 (**100 µM**)** and nitroreductase (30 µg/ml) in presence of NADH (500 µM). **A.** probe **12** + NADH (control); **B.** probe **12** + NADH + nitroreductase (2 h); **C.** probe **12** + NADH + nitroreductase (4.5 h); **D.** reference **10** (control).

Figure 6 shows LC/MS activation studies of probe **12**. **A** and **D** show LC/MS traces of probe **12** and reference **10**, respectively. In presence of nitroreductase and NADH (**B** and **C**, 2 h and 4.5 h incubation, respectively) a time-dependent conversion of probe **12** towards activated probe (reference) **10** is observed. The small peak in **B** corresponds to $[M+H]^+$ = 865, the mass of the carbamic acid fragmentation intermediate.

Effects of pH and temperature

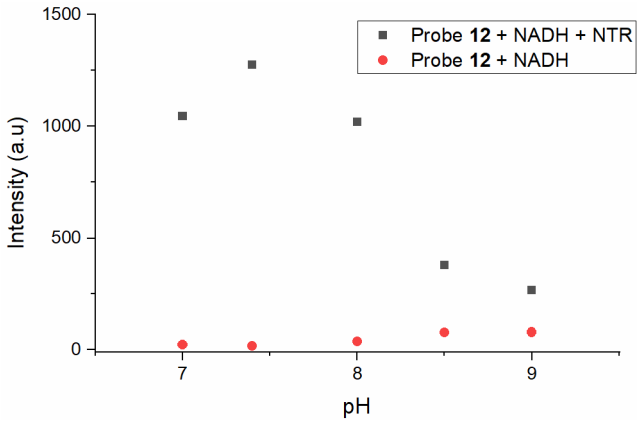

Figure S8. Effect of pH on the fluorescence intensity of probe **12** (20 μM) in absence or presence of nitroreductase (1 μg/mL) and NADH (50 μM) in 0.05 M Tris buffer for 2 h. $\lambda_{ex}/\lambda_{em}$ = 355/550 nm. Results are representative of two independent experiments (error bars not shown when lying within symbol boarders).

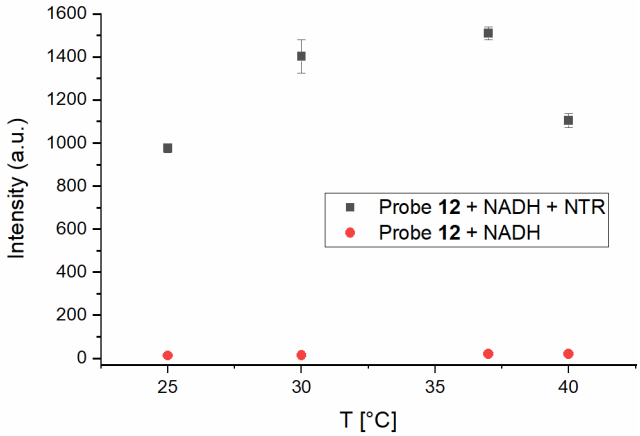

Figure S9. Effect of temperature on the fluorescence intensity of probe **12** (20 μM) in absence or presence of nitroreductase (1 μg/mL) and NADH (50 μM) in 0.05 M Tris buffer for 2 h. $\lambda_{ex}/\lambda_{em}$ = 355/550 nm. Results are representative of two independent experiments (error bars not shown when lying within symbol boarders).

Detection Limit

The detection limit was calculated according to the formula 3σ/k, where σ is the standard deviation of the background noise of 20 μM probe collected at 12 time points and k is the slope of the linear fit obtained from enzyme concentration vs probe emission intensity at 550 nm, 20 μM probe (inset Fig. 1A). With σ = 2.357 and k = 1617 ml/μg, 3σ/k = 4.4 ng/ml.

Inhibition Studies

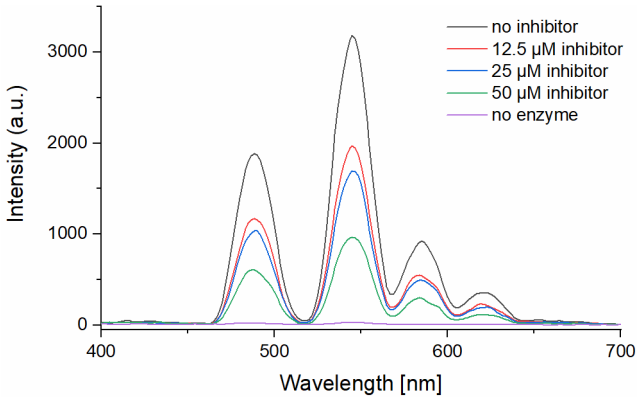

Figure S10. Fluorescence emission spectra of probe **12** (20 µM) with NTR (1 µg/mL) and NADH (50 µM) and with added NTR inhibitor dicoumarin (12.5, 25, 50 µM). *Purple*: probe in pH 7.4 Tris buffer (control). All measurements were carried out after mixing for 2 h at 37 °C. λ_{ex} = 355nm.

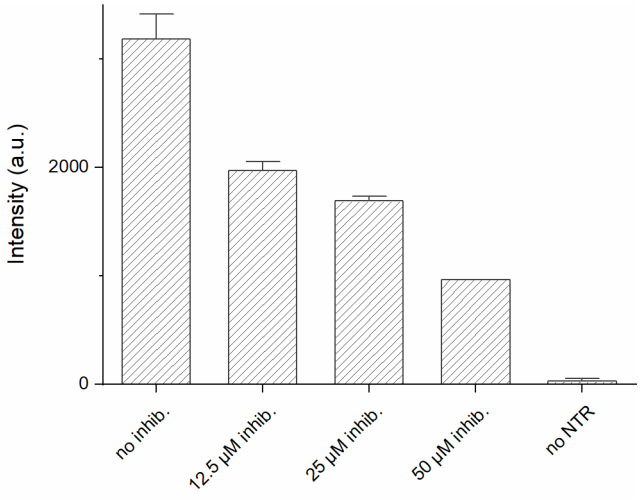

Figure S11. Quantification of emission intensity of probe **12** at 550 nm incubated with NTR and dicoumarin as shown in Figure 9.

Probe and reference uptake in live bacteria

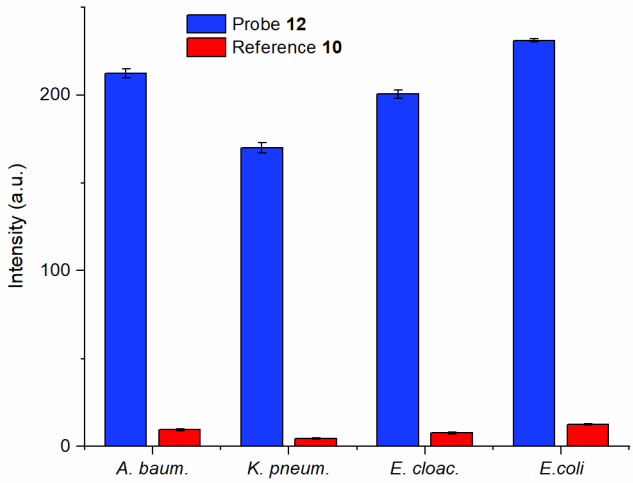

Figure S12. Fluorescence intensities of live *E. coli*, *K. pneumoniae, A. baumannii* and *E. cloacae* cells incubated with 20 µM probe **12** and reference **10** at 37 °C in 0.05 M Tris buffer (pH 7.4) for 12 h. $\lambda_{ex}/\lambda_{em}$ = 355/550 nm, 50 µs delay. Results representative of two independent experiments**.**

Author Contributions

Marc Nazaré and Hai-Yu Hu conceived the research.
Marc Nazaré and Hai-Yu Hu acquired funding for this project.
Benjamin Brennecke, Qinghua Wang, Hai-Yu Hu and Marc Nazaré designed the research approach.
Benjamin Brennecke, Qinghua Wang and Qingyang Zhang performed experiments, analyzed raw data and worked on probe validation.
Benjamin Brennecke, Qinghua Wang, Hai-Yu Hu and Marc Nazaré analyzed all data generated, and wrote the manuscript.

[1] L. Mangolini, D. Jurbergs, E. Rogojina, U. Kortshagen, *J. Lumin.* **2006**, *121*, 327-334.
[2] P. Wu, J. Zhang, Q. Meng, B. Nare, R. T. Jacobs, H. Zhou, *Eur. J. Med. Chem.* **2014**, *81*, 59-75.
[3] W. Lehnert, *Tetrahedron* **1973**, *29*, 635-638.
[4] K. N. Hearn, T. D. Nalder, R. P. Cox, H. D. Maynard, T. D. M. Bell, F. M. Pfeffer, T. D. Ashton, *Chem. Commun.* **2017**, *53*, 12298-12301.

4 SUMMARY AND CONCLUSIONS

In the first project of this work, the development of a cathepsin S activatable, integrin-targeting, DOTAM-based fluorescent probe for the highly selective and sensitive detection of cancer cells is presented. It was demonstrated that by applying an orthogonal protecting group strategy for the DOTA carboxylic acid side chains, highly sophisticated, multifunctionalized probes can be generated through the successive and modular introduction of functional scaffolds. These comprise a fluorescent dye, a cathepsin S cleavable sequence conjugated to an appropriate dark quencher, and cRGDfK peptides for integrin targeting. It could be shown that the DOTA scaffold is a well-suited template for the generation of such dual functionality probes and that it constitutes an appropriate inherent structural motif of a FRET/IQF sequence, retaining excellent activation properties while connecting both a dye and a quencher-conjugated enzyme-cleavable sequence through two opposing carboxylate arms.

The functionality of the presented probe concept was verified by both *in vitro* enzyme-kinetic methods and in various relevant cell lines. Analysis of Michaelis-Menten parameters revealed low values for the Michaelis-Menten constant K_M and high rate constants of product formation from the enzyme-substrate complex, k_{cat}. This resulted in high overall catalytic efficiencies k_{cat}/K_M for activation of the probes by cathepsin S, which were significantly higher as reported for previous probes utilizing the same cleavage sequence. Incubation with cathepsin S led to a very strong increase of fluorescence intensity, i.e. 45- and 70-fold, for activation of targeted probe and non-targeted control probe, respectively. While the cathepsin S mediated cleavage *in vitro* was verified by application of the low-nanomolar covalent reversible inhibitor RO5461111, cleavage site-specificity was substantiated by LC/MS measurements.

The probes remained stable upon exposure to commonly present intracellular bioanalytes, including oxidative and reductive species, and a selectivity profiling revealed predominant activation by cathepsin S, while the family members cathepsin L and V also induced slight activation. These findings indicate a cathepsin-selective activation of the probes.

Evaluation of the probes in cancer cell lines by microscopy and flow-cytometry revealed a significantly higher extent of activation for the cRGDfK-targeted probe in cancer cells compared to the non-targeted control. This was dependent on the extent of $\alpha_v\beta_3$ integrin receptor expression on those different cell lines as reported in the literature. While in fibrosarcoma-derived HT1080 cells a strong difference in activation could be observed, activation of the targeted probe was attenuated in breast cancer-derived MCF-7 and hepatocellular carcinoma-derived HepG2 cells. Furthermore, the extent of probe activation was not only strongly mitigated but even reversed for both probes in healthy human pancreatic duct epithelial cells

(HPDE6-C7). This could be partly explained with the zwitterionic nature of the targeted probe strongly hindering passive diffusion, caused by the under physiological pH positively charged arginine and negatively charged aspartic acid side chains of the targeting peptides. Preferential activation of the targeted probe is likely to occur as a result of enhanced uptake through receptor-mediated endocytosis; application of a blocking concentration of free cRGDfK peptide did significantly impair activation of the targeted probe in HT1080 cells, while activation of the non-targeted control remained unaffected. Intracellular activation of the probes could be verified through coincubation with the cell-permeable covalent broad spectrum cysteine protease inhibitor E-64d that caused a drastic decrease of activation for both probes, whereas the non-permeable variant E-64 had no effect on activation. However, it has to be mentioned that the highly selective cathepsin S inhibitor used for *in vitro* blocking studies, which should be well suited for cellular applications due to extensive pharmacokinetic optimization, did also not significantly affect cellular probe activation (results not shown). This could be a consequence of the probes being activated by related cysteine proteases such as cathepsin L, as the probes were activated highly preferentially, but not exclusively, by cathepsin S *in vitro*. Finally, co-localization experiments with LysoTracker Red revealed a predominantly lysosomal enrichment of the probes. This can be considered as additional beneficial feature of the developed probe system since the activating target protease cathepsin S is likely predominantly localized in lysosomes.

In summary, a highly sensitive and selective dual functional fluorescent probe for cancer cell imaging was developed. Through the synergistic combination of a targeting approach with a substrate-based approach, favorable features of both concepts could be exploited, i.e. cancer cell-selective uptake through integrin receptor mediated endocytosis as well as highly preferential, cathepsin S induced, activation in cancer cells as compared to healthy cells. High integrin expression proved favorable for overall staining efficiency. Yet, low-expressing cell lines also induced a significant activation, underscoring the general applicability of this probe concept for the detection of cancer cells. Furthermore, the modular approach of this strategy is well suited for the generation of similar FRET-quenched probes that can be adapted with regard to enzymatic target, photophysical properties of the FRET system, and cancer cell-receptor specificity. Collectively, our results imply that DOTAM-based dual functional probes represent an attractive design concept for imaging probes which meet the urgent need for novel, highly sensitive tools for the early detection of cancer.

Future investigations will need to focus on the application of NIR probe variants for the imaging of preclinical animal tumor models to be able to evaluate the probe distribution and activation behavior *in vivo* to further corroborate the advantageous properties of dual functional probes for cancer imaging.

The second part of this work describes the development of a nitroreductase-activatable lanthanide luminescent probe for the imaging of bacteria. At first, the development of synthetic routes for accessing a novel carbostyril antenna as well as a new type of caged antenna precursor for carbostyrils is presented. Furthermore, a strategy was elaborated that enables attachment of these functionalities to the DOTA core. Notably, regioselective substitution and differentiation of the amines at C-2 and C-4 of the central benzylidenemalonate building block posed a major conceptual and synthetic hurdle, which was overcome through implementation of a Buchwald-Hartwig type cross coupling. This synthetic step allowed for the selective introduction of the 4-nitrobenzylcarbamate at C-2 as trigger for NTR activation, as well as for the introduction of a *tert*-butyl carbamate residue that subsequently enabled access to the activated antenna structure. Moreover, this coupling step could be utilized for the introduction of other functional triggers containing a terminal amine or carbamate and thus constitutes a robust modular approach for the generation of similar caged carbostyril antenna precursors.

Subsequently, it was demonstrated that the novel caged precursor is capable of undergoing cyclization to form the carbostyril antenna upon activation by NTR, as verified by LC/MS studies. Furthermore, it was shown that the carbostyril moiety serves as efficient antenna for energy transfer to the terbium center, activating the probe's luminescence. In addition, application of a gating window of 50 μs fully suppressed the short-lived fluorescence signal from the antenna itself. Importantly, the caged antenna precursor is not able to sensitize the terbium at the excitation wavelength of 355 nm, rendering the probe non-emissive in absence of its target enzyme.

The probe was found to exhibit excellent, highly sensitive activation properties in response to NTR. It was obtained a linear correlation between a broad range of NTR concentration and emission intensity at 550 nm, and the probe also displayed a strong 126-fold signal increase at 1 μg/ml NTR that could be blocked in a dose-dependent manner by addition of the NTR-inhibitor dicoumarin. The highly sensitive activation resulted in a limit of detection being as low as 4.4 ng/ml. Beyond that, analytes commonly present in a cellular environment such as reductive thiols or strongly oxidative species such as hydrogen peroxide did not induce probe activation at all, which indicates high stability and selectivity of the probe.

Following this extensive profiling, the probe's ability to detect NTR in bacterial lysates of the ESKAPE family was examined. From the seven bacterial strains investigated, four strains (*K. pneumonia*, *A. baumannii*, *E. cloacae*, *E. coli*) induced a strong response which could be blocked to a great extent by dicoumarin, while the other three strains (*E. faecium*, *S. aureus*, *P. aeruginosa*) elicited only a weak response that was only marginally affected by the NTR inhibitor. These results could be attributed to different expression levels and species variety amongst nitroreductase enzymes in the bacterial strains investigated.

Finally, the probe's capability of detecting NTR in live bacteria was investigated in members of the high-response group. Again, all strains induced an activation of our probe that could be strongly blocked by dicoumarin. Moreover, fluorescence lifetime imaging was applied for the detection of activated probe in these bacterial strains, constituting the first example of FLIM for tracing enzymatic activity in live bacteria with lanthanide luminescent probes. Activation of our probe in fully intact bacteria further implies efficient uptake of the caged probe, whereas interestingly, the activated probe could not penetrate bacterial cells. This suggests a synergistic interaction of intracellular enrichment and NTR-mediated activation, resulting in increased overall detection sensitivity.

To conclude, the probe developed within this work allowed for the selective NTR-mediated luminescence imaging of live bacteria that belong to the ESKAPE panel, representing clinically highly relevant targets and major contributors to nosocomial infections. The presented probe concept constitutes a substantial advancement for the detection of enzymatic activity in living systems with lanthanide luminescent probes. Not only did we present a new design paradigm for NTR activatable optical probes, but also the first lanthanide luminescent probe that enabled the detection and imaging of an endogenous bacterial enzyme. Further efforts will have to be put into ligand design and the concomitant choice of the lanthanide ion in order to improve the probe's overall quantum yield and brightness, as well as to redshift the sensitization wavelength. Future directions might cover the application of other antenna-forming mechanisms as well as the incorporation of different activation triggers, such as specific protease sequences.

Collectively, the presented work demonstrates the high relevance and utility of enzymes as markers and targets for the study of biological processes, diseases, and organisms, as well as optical imaging as an efficient and powerful means to interrogate these systems and their underlying mechanisms. Moreover, it showcases the value of the DOTA scaffold in serving as a central, multifunctionalizable and highly flexible template for the generation of new kinds of sensitive and selective optical molecular probes that rely on mechanistically distinct functional bases.

5 REFERENCES

[1] J. Chan, S. C. Dodani, C. J. Chang, *Nat. Chem.* **2012**, *4*, 973-984.
[2] K. Chen, X. Chen, *Curr. Top. Med. Chem.* **2010**, *10*, 1227-1236.
[3] R. Weissleder, *Science* **2006**, *312*, 1168-1171.
[4] E. Lacivita, M. Leopoldo, F. Berardi, N. A. Colabufo, R. Perrone, *Curr. Med. Chem.* **2012**, *19*, 4731-4741.
[5] J. Weber, P. C. Beard, S. E. Bohndiek, *Nat. Methods* **2016**, *13*, 639-650.
[6] Y. Liu, L. Nie, X. Chen, *Trends Biotechnol.* **2016**, *34*, 420-433.
[7] K. Glunde, A. P. Pathak, Z. M. Bhujwalla, *Trends Mol. Med.* **2007**, *13*, 287-297.
[8] R. Weissleder, M. J. Pittet, *Nature* **2008**, *452*, 580-589.
[9] T. Ueno, T. Nagano, *Nat. Methods* **2011**, *8*, 642-645.
[10] L. Yuan, W. Lin, K. Zheng, L. He, W. Huang, *Chem. Soc. Rev.* **2013**, *42*, 622-661.
[11] L. Yuan, W. Lin, K. Zheng, S. Zhu, *Acc. Chem. Res.* **2013**, *46*, 1462-1473.
[12] H. M. Kim, B. R. Cho, *Chem. Rev.* **2015**, *115*, 5014-5055.
[13] W. Sun, S. Guo, C. Hu, J. Fan, X. Peng, *Chem. Rev.* **2016**, *116*, 7768-7817.
[14] M. Garland, Joshua J. Yim, M. Bogyo, *Cell Chem. Biol.* **2016**, *23*, 122-136.
[15] M. Gao, F. Yu, C. Lv, J. Choo, L. Chen, *Chem. Soc. Rev.* **2017**, *46*, 2237-2271.
[16] C. Wang, Z. Wang, T. Zhao, Y. Li, G. Huang, B. D. Sumer, J. Gao, *Biomaterials* **2018**, *157*, 62-75.
[17] H.-W. Liu, L. Chen, C. Xu, Z. Li, H. Zhang, X.-B. Zhang, W. Tan, *Chem. Soc. Rev.* **2018**, *47*, 7140-7180.
[18] Y. Kitagawa, S. Tanaka, Y. Kuriki, K. Yamamoto, A. Ogasawara, T. Nejo, R. Matsuura, T. Koike, T. Hana, S. Takahashi et al., *Front. Oncol.* **2019**, *9:727*.
[19] P. Debie, S. Hernot, *Front. Pharmacol.* **2019**, *10:510*.
[20] G. Weber, G. Banerjee, S. B. Bronstein, *J. Biol. Chem.* **1961**, *236*, 3106-3111.
[21] P. M. Siegel, J. Massagué, *Nat. Rev. Cancer* **2003**, *3*, 807-820.
[22] M. Fahad Ullah, S. H. Bhat, M. Tariq, F. M. Abuduhier. Clinical Significance of Enzymes in Disease and Diagnosis. In: *Biocatalysis.* Q. Husain, M. Ullah, Eds. Springer, Cham: 2019, pp 213-231.
[23] J. Neefjes, N. P. Dantuma, *Nat. Rev. Drug Discov.* **2004**, *3*, 58-69.
[24] H. Zhu, I. Hamachi, *J. Pharm. Anal.* **2020**, *10*, 426-433.
[25] X. Wu, W. Shi, X. Li, H. Ma, *Acc. Chem. Res.* **2019**, *52*, 1892-1904.
[26] H. Singh, K. Tiwari, R. Tiwari, S. K. Pramanik, A. Das, *Chem. Rev.* **2019**, *119*, 11718-11760.
[27] H. Wei, G. Wu, X. Tian, Z. Liu, *Future Med. Chem.* **2018**, *10*, 2729-2744.
[28] W. Chyan, R. T. Raines, *ACS Chem. Biol.* **2018**, *13*, 1810-1823.
[29] G. Blum, S. R. Mullins, K. Keren, M. Fonovic, C. Jedeszko, M. J. Rice, B. F. Sloane, M. Bogyo, *Nat. Chem. Biol.* **2005**, *1*, 203-209.
[30] K. Oresic Bender, L. Ofori, W. A. van der Linden, E. D. Mock, G. K. Datta, S. Chowdhury, H. Li, E. Segal, M. Sanchez Lopez, J. A. Ellman et al., *J. Am. Chem. Soc.* **2015**, *137*, 4771-4777.
[31] Y. Takaoka, Y. Nishikawa, Y. Hashimoto, K. Sasaki, I. Hamachi, *Chem. Sci.* **2015**, *6*, 3217-3224.
[32] T. Tamura, T. Ueda, T. Goto, T. Tsukidate, Y. Shapira, Y. Nishikawa, A. Fujisawa, I. Hamachi, *Nat. Commun.* **2018**, *9:1870*.
[33] T. Tamura, I. Hamachi, *J. Am. Chem. Soc.* **2019**, *141*, 2782-2799.
[34] C. López-Otín, J. S. Bond, *J. Biol. Chem.* **2008**, *283*, 30433-30437.
[35] C. López-Otín, C. M. Overall, *Nat. Rev. Mol. Cell Biol.* **2002**, *3*, 509-519.

[36] O. Katerina, K. H. Kristina, S. Mahmoud, V. Nathalie, T. Illa, P. D. Eleftherios, D. H. Morley, *Biol. Chem.* **2006**, *387*, 677-685.
[37] E. Culp, G. D. Wright, *J. Antibiot.* **2017**, *70*, 366-377.
[38] A. A. Agbowuro, W. M. Huston, A. B. Gamble, J. D. A. Tyndall, *Med. Res. Rev.* **2018**, *38*, 1295-1331.
[39] V. Turk, V. Stoka, O. Vasiljeva, M. Renko, T. Sun, B. Turk, D. Turk, *Biochimica et Biophysica Acta* **2012**, *1824*, 68-88.
[40] L. C. Hsing, A. Y. Rudensky, *Immunol. Rev.* **2005**, *207*, 229-241.
[41] A. Cstorer, R. Ménard, *Methods Enzymol.* **1994**, *244*, 486-500.
[42] I. Schechter, A. Berger, *Biochem. Biophys. Res. Commun.* **1968**, *32*, 898-902.
[43] S. D. Lewis, F. A. Johnson, J. A. Shafer, *Biochemistry* **1981**, *20*, 48-51.
[44] T. Klein, U. Eckhard, A. Dufour, N. Solis, C. M. Overall, *Chem. Rev.* **2018**, *118*, 1137-1168.
[45] H. Wu, Q. Du, Q. Dai, J. Ge, X. Cheng, *J. Atheroscler. Thromb.* **2018**, *25*, 111-123.
[46] N. Ganesan. Cysteine Cathepsins: In Health and Rheumatoid Arthritis. In: *Proteases in Human Diseases.* S. Chakraborti, T. Chakraborti, N. S. Dhalla, Eds. Springer: Singapore, 2017, pp 103-130.
[47] M. M. Mohamed, B. F. Sloane, *Nat. Rev. Cancer* **2006**, *6*, 764-775.
[48] O. C. Olson, J. A. Joyce, *Nat. Rev. Cancer* **2015**, *15*, 712-729.
[49] R. Löser, J. Pietzsch, *Front. Chem.* **2015**, *3:37*.
[50] I. Berdowska, *Clin. Chim. Acta* **2004**, *342*, 41-69.
[51] N. Harbeck, U. Alt, U. Berger, A. Krüger, C. Thomssen, F. Jänicke, H. Höfler, R. E. Kates, M. Schmitt, *Clin. Cancer Res.* **2001**, *7*, 2757-2764.
[52] J. A. Gormley, S. M. Hegarty, A. O'Grady, M. R. Stevenson, R. E. Burden, H. L. Barrett, C. J. Scott, J. A. Johnston, R. H. Wilson, E. W. Kay et al., *Br. J. Cancer* **2011**, *105*, 1487-1494.
[53] R. D. Wilkinson, R. Williams, C. J. Scott, R. E. Burden, *Biol. Chem.* **2015**, *396*, 867-882.
[54] N. A. Thornberry, K. T. Chapman, D. W. Nicholson, *Methods Enzymol.* **2000**, *322*, 100-110.
[55] V. Gurtu, S. R. Kain, G. Zhang, *Anal. Biochem.* **1997**, *251*, 98-102.
[56] R. B. Banati, G. Rothe, G. Valet, G. W. Kreutzberg, *Glia* **1993**, *7*, 183-191.
[57] L. Qian, C.-W. Zhang, Y. Mao, L. Li, N. Gao, K.-L. Lim, Q.-H. Xu, S. Q. Yao, *Sci. Rep.* **2016**, *6*, 26385.
[58] M. Poreba, A. Szalek, W. Rut, P. Kasperkiewicz, I. Rutkowska-Wlodarczyk, S. J. Snipas, Y. Itoh, D. Turk, B. Turk, C. M. Overall et al., *Sci. Rep.* **2017**, *7:43135*.
[59] R. Weissleder, C.-H. Tung, U. Mahmood, A. Bogdanov, *Nat. Biotechnol.* **1999**, *17*, 375-378.
[60] C.-H. Tung, U. Mahmood, S. Bredow, R. Weissleder, *Cancer Res.* **2000**, *60*, 4953-4958.
[61] V. Cortez-Retamozo, F. K. Swirski, P. Waterman, H. Yuan, J. L. Figueiredo, A. P. Newton, R. Upadhyay, C. Vinegoni, R. Kohler, J. Blois et al., *J. Clin. Invest.* **2008**, *118*, 4058-4066.
[62] E. Gounaris, C. H. Tung, C. Restaino, R. Maehr, R. Kohler, J. A. Joyce, H. L. Plough, T. A. Barrett, R. Weissleder, K. Khazaie, *PLoS One* **2008**, *3:e2916*, e2916.
[63] M. J. Whitley, D. M. Cardona, A. L. Lazarides, I. Spasojevic, J. M. Ferrer, J. Cahill, C.-L. Lee, M. Snuderl, D. G. Blazer, E. S. Hwang et al., *Sci. Transl. Med.* **2016**, *8:320ra4*.
[64] ClinicalTrials.gov. Bethesda (MD): National Library of Medicine (US). September 26, 2018; Identifier NCT03686215. Pivotal Study of Intraoperative Detection of Residual Cancer in Breast Cancer Patients. Available from: https://clinicaltrials.gov/ct2/show/NCT03686215 (accessed 17.11.2020).
[65] ClinicalTrials.gov. Bethesda (MD): National Library of Medicine (US). October 22, 2015; Identifier NCT02584244. Feasibility of the LUM Imaging System for Detection of Gastrointestinal Cancers. Available from: https://clinicaltrials.gov/ct2/show/NCT02584244 (accessed 17.11.2020).

[66] ClinicalTrials.gov. Bethesda (MD): National Library of Medicine (US). June 22, 2020; Identifier NCT04440982. Feasibility Study of Intraoperative Detection of Residual Cancer in Breast Cancer Patients Receiving Neoadjuvant Therapy. Available from: https://clinicaltrials.gov/ct2/show/NCT04440982 (accessed 17.11.2020).
[67] A. Watzke, G. Kosec, M. Kindermann, V. Jeske, H.-P. Nestler, V. Turk, B. Turk, K. U. Wendt, *Angew. Chem. Int. Ed.* **2008**, *47*, 406-409.
[68] D. Caglič, A. Globisch, M. Kindermann, N.-H. Lim, V. Jeske, H.-P. Juretschke, E. Bartnik, K. U. Weithmann, H. Nagase, B. Turk et al., *Bioorg. Med. Chem.* **2011**, *19*, 1055-1061.
[69] H.-Y. Hu, D. Vats, M. Vizovisek, L. Kramer, C. Germanier, K. U. Wendt, M. Rudin, B. Turk, O. Plettenburg, C. Schultz, *Angew. Chem. Int. Ed.* **2014**, *53*, 7669-7673.
[70] S. Miah, M. Nilsson, H. Wahling, M. Pelcman, X.-X. Xhou, C. Clissold, A. Rae, M. Tozer, D. Hardick, WO2005/082876, **2005**.
[71] S. Serim, U. Haedke, S. H. L. Verhelst, *ChemMedChem* **2012**, *7*, 1146-1159.
[72] E. Deu, M. Verdoes, M. Bogyo, *Nat. Struct. Mol. Biol.* **2012**, *19*, 9-16.
[73] J. A. Joyce, A. Baruch, K. Chehade, N. Meyer-Morse, E. Giraudo, F.-Y. Tsai, D. C. Greenbaum, J. H. Hager, M. Bogyo, D. Hanahan, *Cancer Cell* **2004**, *5*, 443-453.
[74] L. E. Edgington, A. B. Berger, G. Blum, V. E. Albrow, M. G. Paulick, N. Lineberry, M. Bogyo, *Nat. Med.* **2009**, *15*, 967-973.
[75] M. Verdoes, K. O. Bender, E. Segal, W. A. van der Linden, S. Syed, N. P. Withana, L. E. Sanman, M. Bogyo, *J. Am. Chem. Soc.* **2013**, *135*, 14726-14730.
[76] Laura E. Sanman, Wouter A. van der Linden, M. Verdoes, M. Bogyo, *Cell Chem. Biol.* **2016**.
[77] D. W. Bryant, D. R. McCalla, M. Leeksma, P. Laneuville, *Can. J. Microbiol.* **1981**, *27*, 81-86.
[78] E. Akiva, J. N. Copp, N. Tokuriki, P. C. Babbitt, *Proc. Natl. Acad. Sci. U. S. A.* **2017**, *114*, E9549-E9558.
[79] F. J. Peterson, R. P. Mason, J. Hovsepian, J. L. Holtzman, *J. Biol. Chem.* **1979**, *254*, 4009-4014.
[80] M. D. Roldán, E. Pérez-Reinado, F. Castillo, C. Moreno-Vivián, *FEMS Microbiol. Rev.* **2008**, *32*, 474-500.
[81] S. Zenno, H. Koike, A. N. Kumar, R. Jayaraman, M. Tanokura, K. Saigo, *J. Bacteriol.* **1996**, *178*, 4508-4514.
[82] S. Zenno, H. Koike, M. Tanokura, K. Saigo, *J. Biochem.* **1996**, *120*, 736-744.
[83] J. Zhang, V. Kale, M. Chen, *AAPS J.* **2015**, *17*, 102-110.
[84] G. Chung-Faye, D. Palmer, D. Anderson, J. Clark, M. Downes, J. Baddeley, S. Hussain, P. I. Murray, P. Searle, L. Seymour et al., *Clin. Cancer Res.* **2001**, *7*, 2662-2668.
[85] D. H. Palmer, V. Mautner, D. Mirza, S. Oliff, W. Gerritsen, J. R. M. v. d. Sijp, S. Hubscher, G. Reynolds, S. Bonney, R. Rajaratnam et al., *J. Clin. Oncol.* **2004**, *22*, 1546-1552.
[86] P. Patel, J. G. Young, V. Mautner, D. Ashdown, S. Bonney, R. G. Pineda, S. I. Collins, P. F. Searle, D. Hull, E. Peers et al., *Mol. Ther.* **2009**, *17*, 1292-1299.
[87] Elsie M. Williams, Rory F. Little, Alexandra M. Mowday, Michelle H. Rich, Jasmine V. E. Chan-Hyams, Janine N. Copp, Jeff B. Smaill, Adam V. Patterson, David F. Ackerley, *Biochem. J.* **2015**, *471*, 131-153.
[88] N. A. Helsby, D. M. Ferry, A. V. Patterson, S. M. Pullen, W. R. Wilson, *Br. J. Cancer* **2004**, *90*, 1084-1092.
[89] R. J. Knox, F. Friedlos, T. Marchbank, J. J. Roberts, *Biochem. Pharmacol.* **1991**, *42*, 1691-1697.
[90] Susan E. Cellitti, J. Shaffer, David H. Jones, T. Mukherjee, M. Gurumurthy, B. Bursulaya, Helena I. Boshoff, I. Choi, A. Nayyar, Yong S. Lee et al., *Structure* **2012**, *20*, 101-112.
[91] S. Michael, C. Michelle, L. Panos, T. Mark, *Curr. Gene Ther.* **2015**, *15*, 277-288.
[92] G. A. Roth, *The Lancet* **2018**, *392*, 1736-1788.

[93] A. A. Ordonez, M. A. Sellmyer, G. Gowrishankar, C. A. Ruiz-Bedoya, E. W. Tucker, C. J. Palestro, D. A. Hammoud, S. K. Jain, *Sci. Transl. Med.* **2019**, *11:eaax8251*.
[94] J. O`Neill, *Tackling Drug-Resistant Infections Globally: Final Report and Recommendations* (Report). Review on Antimicrobial Resistance, London, 2016.
[95] M. S. Mulani, E. E. Kamble, S. N. Kumkar, M. S. Tawre, K. R. Pardesi, *Front. Microbiol.* **2019***:10*.
[96] B. Mills, M. Bradley, K. Dhaliwal, *Clin. Transl. Imaging* **2016**, *4*, 163-174.
[97] S. K. Jain, *Mol. Imaging Biol.* **2017**, *19*, 341-347.
[98] S. Bhattacharya, *Virulence* **2013**, *4*, 172-184.
[99] W. Qin, C. Xu, Y. Zhao, C. Yu, S. Shen, L. Li, W. Huang, *Chin. Chem. Lett.* **2018**, *29*, 1451-1455.
[100] Y.-L. Qi, L. Guo, L.-L. Chen, H. Li, Y.-S. Yang, A.-Q. Jiang, H.-L. Zhu, *Coord. Chem. Rev.* **2020**, *421*, 213460.
[101] J. W. Lee, J. Ko, C. Ju, H. K. Eltzschig, *Exp. Mol. Med.* **2019**, *51*, 1-13.
[102] X. Jing, F. Yang, C. Shao, K. Wei, M. Xie, H. Shen, Y. Shu, *Mol. Cancer* **2019**, *18:157*.
[103] J. M. Brown, W. R. Wilson, *Nat. Rev. Cancer* **2004**, *4*, 437-447.
[104] J. E. Friedman, J. A. Watson, D. W.-H. Lam, S. E. Rokita, *J. Biol. Chem.* **2006**, *281*, 2812-2819.
[105] S. E. Rokita, J. M. Adler, P. M. McTamney, J. A. Watson, *Biochimie* **2010**, *92*, 1227-1235.
[106] D. Ross, H. D. Beall, D. Siegel, R. D. Traver, D. L. Gustafson, *Br. J. Cancer Suppl.* **1996**, *27*, S1-S8.
[107] S. Kizaka-Kondoh, H. Konse-Nagasawa, *Cancer Sci.* **2009**, *100*, 1366-1373.
[108] R. T. H. M. Larue, L. Van De Voorde, M. Berbée, W. J. C. van Elmpt, L. J. Dubois, K. M. Panth, S. G. J. A. Peeters, A. Claessens, W. M. J. Schreurs, M. Nap et al., *BMC Cancer* **2016**, *16:644*.
[109] J. P. Laubach, C.-J. Liu, N. S. Raje, A. J. Yee, P. Armand, R. L. Schlossman, J. Rosenblatt, J. Hedlund, M. Martin, C. Reynolds et al., *Clin. Cancer Res.* **2019**, *25*, 478-486.
[110] J. D. Sun, Q. Liu, D. Ahluwalia, W. Li, F. Meng, Y. Wang, D. Bhupathi, A. S. Ruprell, C. P. Hart, *Cancer Biol. Ther.* **2015**, *16*, 438-449.
[111] H. Manoochehri Khoshinani, S. Afshar, R. Najafi, *Cancer Invest.* **2016**, *34*, 536-545.
[112] A. C. Begg, R. J. Hodgkiss, N. J. McNally, R. W. Middleton, M. R. L. Stratford, N. H. A. Terry, *Br. J. Radiol.* **1985**, *58*, 645-654.
[113] M. K. Lee, J. Williams, R. J. Twieg, J. Rao, W. E. Moerner, *Chem. Sci.* **2013**, *4*, 220-225.
[114] K. Maeda, T. Osato, H. Umezawa, *J. Antibiot.* **1953**, *6*, 182.
[115] J. K. Mohindra, A. M. Rauth, *Cancer Res.* **1976**, *36*, 930-936.
[116] J. A. Raleigh, C. J. Koch, *Biochem. Pharmacol.* **1990**, *40*, 2457-2464.
[117] X. Meng, J. Zhang, Z. Sun, L. Zhou, G. Deng, S. Li, W. Li, P. Gong, L. Cai, *Theranostics* **2018**, *8*, 6025-6034.
[118] L. B. Rice, *J. Infect. Dis.* **2008**, *197*, 1079-1081.
[119] H. W. Boucher, G. H. Talbot, J. S. Bradley, J. E. Edwards, D. Gilbert, L. B. Rice, M. Scheld, B. Spellberg, J. Bartlett, *Clin. Infect. Dis.* **2009**, *48*, 1-12.
[120] D. M. P. De Oliveira, B. M. Forde, T. J. Kidd, P. N. A. Harris, M. A. Schembri, S. A. Beatson, D. L. Paterson, M. J. Walker, *Clin. Microbiol. Rev.* **2020**, *33:e00181-19*.
[121] E. McCormack, E. Silden, R. M. West, T. Pavlin, D. R. Micklem, J. B. Lorens, B. E. Haug, M. E. Cooper, B. T. Gjertsen, *Cancer Res.* **2013**, *73*, 1276-1286.
[122] Y. Ji, Y. Wang, N. Zhang, S. Xu, L. Zhang, Q. Wang, Q. Zhang, H.-Y. Hu, *J. Org. Chem.* **2019**, *84*, 1299-1309.
[123] R. H. F. Wong, T. Kwong, K.-H. Yau, H. Y. Au-Yeung, *Chem. Commun.* **2015**, *51*, 4440-4442.
[124] A. G. Vorobyeva, M. Stanton, A. Godinat, K. B. Lund, G. G. Karateev, K. P. Francis, E. Allen, J. G. Gelovani, E. McCormack, M. Tangney et al., *PLoS One* **2015**, *10*, e0131037.
[125] A. Hellebust, R. Richards-Kortum, *Nanomedicine* **2012**, *7*, 429-445.

[126] C. King, M. Kraus, S. Aaronson, *Science* **1985**, *229*, 974-976.
[127] P. Chames, M. Van Regenmortel, E. Weiss, D. Baty, *Br. J. Pharmacol.* **2009**, *157*, 220-233.
[128] R.-M. Lu, Y.-C. Hwang, I. J. Liu, C.-C. Lee, H.-Z. Tsai, H.-J. Li, H.-C. Wu, *J. Biomed. Sci.* **2020**, *27*, 1.
[129] A. Pèlegrin, S. Folli, F. Buchegger, J.-P. Mach, G. Wagnières, H. Van Den Bergh, *Cancer* **1991**, *67*, 2529-2537.
[130] S. Folli, P. Westermann, D. Braichotte, A. Pèlegrin, G. Wagnières, H. van den Bergh, J.-P. Mach, *Cancer Res.* **1994**, *54*, 2643-2649.
[131] B. Ballou, G. W. Fisher, A. S. Waggoner, D. L. Farkas, J. M. Reiland, R. Jaffe, R. B. Mujumdar, S. R. Mujumdar, T. R. Hakala, *Cancer Immunol. Immunother.* **1995**, *41*, 257-263.
[132] K. Imai, A. Takaoka, *Nat. Rev. Cancer* **2006**, *6*, 714-727.
[133] X. Sun, Y. Li, T. Liu, Z. Li, X. Zhang, X. Chen, *Adv. Drug Delivery Rev.* **2017**, *110-111*, 38-51.
[134] C. S. Kue, A. Kamkaew, K. Burgess, L. V. Kiew, L. Y. Chung, H. B. Lee, *Med. Res. Rev.* **2016**, *36*, 494-575.
[135] W. Xin, S. Feng, J. H. Freisheim, L. E. Gentry, M. Ratnam, *Biochem. Pharmacol.* **1992**, *44*, 1898-1901.
[136] B. A. Kamen, A. Capdevila, *Proc. Natl. Acad. Sci. U. S. A.* **1986**, *83*, 5983-5987.
[137] L. B. Bailey, J. F. Gregory, III, *J. Nutr.* **1999**, *129*, 779-782.
[138] L. E. Kelemen, *Int. J. Cancer* **2006**, *119*, 243-250.
[139] W. Xia, P. S. Low, *J. Med. Chem.* **2010**, *53*, 6811-6824.
[140] M. Scaranti, E. Cojocaru, S. Banerjee, U. Banerji, *Nat. Rev. Clin. Oncol.* **2020**, *17*, 349-359.
[141] M. Fernández, F. Javaid, V. Chudasama, *Chem. Sci.* **2018**, *9*, 790-810.
[142] I. Vergote, D. Armstrong, G. Scambia, M. Teneriello, J. Sehouli, C. Schweizer, S. C. Weil, A. Bamias, K. Fujiwara, K. Ochiai et al., *J. Clin. Oncol.* **2016**, *34*, 2271-2278.
[143] R. W. Naumann, R. L. Coleman, R. A. Burger, E. A. Sausville, E. Kutarska, S. A. Ghamande, N. Y. Gabrail, S. E. DePasquale, E. Nowara, L. Gilbert et al., *J. Clin. Oncol.* **2013**, *31*, 4400-4406.
[144] R. T. Morris, R. N. Joyrich, R. W. Naumann, N. P. Shah, A. H. Maurer, H. W. Strauss, J. M. Uszler, J. T. Symanowski, P. R. Ellis, W. A. Harb, *Annal. Onc.* **2014**, *25*, 852-858.
[145] P. P. Peethambaram, L. C. Hartmann, D. J. Jonker, M. de Jonge, E. R. Plummer, L. Martin, J. Konner, J. Marshall, G. D. Goss, V. Teslenko et al., *Invest. New Drugs* **2015**, *33*, 321-331.
[146] C. Wayua, P. S. Low, *Mol. Pharm.* **2014**, *11*, 468-476.
[147] C. Wayua, P. S. Low, *J. Nucl. Med.* **2015**, *56*, 113-119.
[148] S. Chen, X. Zhao, J. Chen, J. Chen, L. Kuznetsova, S. S. Wong, I. Ojima, *Bioconjugate Chem.* **2010**, *21*, 979-987.
[149] S. Maiti, N. Park, J. H. Han, H. M. Jeon, J. H. Lee, S. Bhuniya, C. Kang, J. S. Kim, *J. Am. Chem. Soc.* **2013**, *135*, 4567-4572.
[150] M. Gomes-Porras, J. Cárdenas-Salas, C. Álvarez-Escolá, *Int. J. Mol. Sci.* **2020**, *21*.
[151] S. W. J. Lamberts, A.-J. van der Lely, W. W. de Herder, L. J. Hofland, *N. Engl. J. Med.* **1996**, *334*, 246-254.
[152] L. Anthony, P. U. Freda, *Curr. Med. Res. Opin.* **2009**, *25*, 2989-2999.
[153] S. W. J. Lamberts, W. W. de Herder, L. J. Hofland, *Trends Endocrin. Met.* **2002**, *13*, 451-457.
[154] M. Theodoropoulou, G. K. Stalla, *Front. Neuroendocrin.* **2013**, *34*, 228-252.
[155] J. W. Tamkun, D. W. DeSimone, D. Fonda, R. S. Patel, C. Buck, A. F. Horwitz, R. O. Hynes, *Cell* **1986**, *46*, 271-282.
[156] E. R. Horton, J. D. Humphries, J. James, M. C. Jones, J. A. Askari, M. J. Humphries, *J. Cell Sci.* **2016**, *129*, 4159-4163.

[157] E. R. Horton, A. Byron, J. A. Askari, D. H. J. Ng, A. Millon-Frémillon, J. Robertson, E. J. Koper, N. R. Paul, S. Warwood, D. Knight et al., *Nat. Cell Biol.* **2015**, *17*, 1577-1587.
[158] S. J. Shattil, C. Kim, M. H. Ginsberg, *Nat. Rev. Mol. Cell Biol.* **2010**, *11*, 288-300.
[159] R. O. Hynes, *Cell* **2002**, *110*, 673-687.
[160] H. Hamidi, M. Pietilä, J. Ivaska, *Br. J. Cancer* **2016**, *115*, 1017-1023.
[161] J. D. Humphries, A. Byron, M. J. Humphries, *J. Cell Sci.* **2006**, *119*, 3901-3903.
[162] S. E. Winograd-Katz, R. Fässler, B. Geiger, K. R. Legate, *Nat. Rev. Mol. Cell Biol.* **2014**, *15*, 273-288.
[163] H. Hamidi, J. Ivaska, *Nat. Rev. Cancer* **2018**, *18*, 533-548.
[164] S. M. Weis, D. A. Cheresh, *Cold Spring Harb. Perspect. Med.* **2011**, *1*, a006478.
[165] P. C. Brooks, S. Strömblad, R. Klemke, D. Visscher, F. H. Sarkar, D. A. Cheresh, *J. Clin. Invest.* **1995**, *96*, 1815-1822.
[166] M. Lorger, J. S. Krueger, M. O'Neal, K. Staflin, B. Felding-Habermann, *Proc. Natl. Acad. Sci. U. S. A.* **2009**, *106*, 10666-10671.
[167] I. Saiki, J. Murata, T. Makabe, N. Nishi, S. Tokura, I. Azuma, *Jpn. J. Cancer Res.* **1990**, *81*, 668-675.
[168] R. F. Nicosia, E. Bonanno, *Am. J. Pathol.* **1991**, *138*, 829-833.
[169] P. Brooks, R. Clark, D. Cheresh, *Science* **1994**, *264*, 569-571.
[170] A. M. Montgomery, R. A. Reisfeld, D. A. Cheresh, *Proc. Natl. Acad. Sci. U. S. A.* **1994**, *91*, 8856-8860.
[171] M. Aumailley, M. Gurrath, G. Müller, J. Calvete, R. Timpl, H. Kessler, *FEBS Lett.* **1991**, *291*, 50-54.
[172] R. Haubner, R. Gratias, B. Diefenbach, S. L. Goodman, A. Jonczyk, H. Kessler, *J. Am. Chem. Soc.* **1996**, *118*, 7461-7472.
[173] M. A. Dechantsreiter, E. Planker, B. Mathä, E. Lohof, G. Hölzemann, A. Jonczyk, S. L. Goodman, H. Kessler, *J. Med. Chem.* **1999**, *42*, 3033-3040.
[174] C. Mas-Moruno, F. Rechenmacher, H. Kessler, *Anti-Cancer Agents Med. Chem.* **2010**, *10*, 753-768.
[175] R. Stupp, M. E. Hegi, T. Gorlia, S. C. Erridge, J. Perry, Y.-K. Hong, K. D. Aldape, B. Lhermitte, T. Pietsch, D. Grujicic et al., *Lancet Oncol.* **2014**, *15*, 1100-1108.
[176] R. Haubner, H.-J. Wester, F. Burkhart, R. Senekowitsch-Schmidtke, W. Weber, S. L. Goodman, H. Kessler, M. Schwaiger, *J. Nucl. Med.* **2001**, *42*, 326-336.
[177] R. Haubner, H.-J. Wester, W. A. Weber, C. Mang, S. I. Ziegler, S. L. Goodman, R. Senekowitsch-Schmidtke, H. Kessler, M. Schwaiger, *Cancer Res.* **2001**, *61*, 1781-1785.
[178] C. Rubel, C. Sudipta, D. Ashutosh, *Mini-Rev. Med. Chem.* **2015**, *15*, 1073-1094.
[179] T. Bach-Gansmo, R. Danielsson, A. Saracco, B. Wilczek, T. V. Bogsrud, A. Fangberget, Å. Tangerud, D. Tobin, *J. Nucl. Med.* **2006**, *47*, 1434-1439.
[180] B. Indrevoll, G. M. Kindberg, M. Solbakken, E. Bjurgert, J. H. Johansen, H. Karlsen, M. Mendizabal, A. Cuthbertson, *Bioorg. Med. Chem. Lett.* **2006**, *16*, 6190-6193.
[181] M. K. O'Connor, M. M. B. Morrow, K. N. Hunt, J. C. Boughey, D. L. Wahner-Roedler, A. L. Conners, D. J. Rhodes, C. B. Hruska, *EJNMMI Res.* **2017**, *7:5*.
[182] Y. Ye, X. Chen, *Theranostics* **2011**, *1*, 102-126.
[183] L. Zhiguo, Y. Lun, W. Xiaobo, Z. Xintong, L. Meihui, Z. Wenbin, *Curr. Protein Pept. Sci.* **2016**, *17*, 570-581.
[184] X. Chen, P. S. Conti, R. A. Moats, *Cancer Res.* **2004**, *64*, 8009-8014.
[185] W. Wang, S. Ke, Q. Wu, C. Charnsangavej, M. Gurfinkel, J. G. Gelovani, J. L. Abbruzzese, E. M. Sevick-Muraca, C. Li, *Mol. Imaging* **2004**, *3*, 343-351.
[186] G. Thumshirn, U. Hersel, S. L. Goodman, H. Kessler, *Chem. Eur. J.* **2003**, *9*, 2717-2725.
[187] Z. Cheng, Y. Wu, Z. Xiong, S. S. Gambhir, X. Chen, *Bioconjugate Chem.* **2005**, *16*, 1433-1441.

[188] I. Dijkgraaf, A. Y. Rijnders, A. Soede, A. C. Dechesne, G. W. van Esse, A. J. Brouwer, F. H. M. Corstens, O. C. Boerman, D. T. S. Rijkers, R. M. J. Liskamp, *Org. Biomol. Chem.* **2007**, *5*, 935-944.
[189] X. Zhang, H. Liu, Z. Miao, R. Kimura, F. Fan, Z. Cheng, *Bioorg. Med. Chem. Lett.* **2011**, *21*, 3423-3426.
[190] E. Garanger, D. Boturyn, Z. Jin, P. Dumy, M.-C. Favrot, J.-L. Coll, *Mol. Ther.* **2005**, *12*, 1168-1175.
[191] S. Lucie, G. Elisabeth, F. Stéphanie, S. Guy, H. Amandine, A.-R. Corinne, B. Didier, S. Catherine, G. Alexeï, D. Pascal et al., *Mol. Ther.* **2009**, *17*, 837-843.
[192] L. Zhu, J. Xie, M. Swierczewska, F. Zhang, X. Lin, X. Fang, G. Niu, S. Lee, X. Chen, *Bioconjugate Chem.* **2011**, *22*, 1001-1005.
[193] C. Li, W. Wang, Q. Wu, S. Ke, J. Houston, E. Sevick-Muraca, L. Dong, D. Chow, C. Charnsangavej, J. G. Gelovani, *Nucl. Med. Biol.* **2006**, *33*, 349-358.
[194] W. B. Edwards, W. J. Akers, Y. Ye, P. P. Cheney, S. Bloch, B. Xu, R. Laforest, S. Achilefu, *Mol. Imaging* **2009**, *8*, 7290.2009.00014.
[195] V. Rerat, G. Dive, A. A. Cordi, G. C. Tucker, R. Bareille, J. Amédée, L. Bordenave, J. Marchand-Brynaert, *J. Med. Chem.* **2009**, *52*, 7029-7043.
[196] C. A. Burnett, J. Xie, J. Quijano, Z. Shen, F. Hunter, M. Bur, K. C. P. Li, S. N. Danthi, *Bioorg. Med. Chem.* **2005**, *13*, 3763-3771.
[197] S. Neubauer, F. Rechenmacher, R. Brimioulle, F. S. Di Leva, A. Bochen, T. R. Sobahi, M. Schottelius, E. Novellino, C. Mas-Moruno, L. Marinelli et al., *J. Med. Chem.* **2014**, *57*, 3410-3417.
[198] J. Heroux, A. M. Gharib, N. S. Danthi, S. Cecchini, J. Ohayon, R. I. Pettigrew, *Mol. Imaging Biol.* **2010**, *12*, 2-8.
[199] F. Li, J. Liu, G. S. Jas, J. Zhang, G. Qin, J. Xing, C. Cotes, H. Zhao, X. Wang, L. A. Diaz et al., *Bioconjugate Chem.* **2010**, *21*, 270-278.
[200] F. Danhier, A. L. Breton, V. Préat, *Mol. Pharm.* **2012**, *9*, 2961-2973.
[201] F. Wang, Z. Liu. RGD-Based Molecular Probes for Integrin αvβ3 Imaging. In: *Molecular Imaging: Fundamentals and Applications.* Springer: Berlin, Heidelberg, 2013, pp 513-538.
[202] W. P. Cacheris, S. K. Nickle, A. D. Sherry, *Inorg. Chem.* **1987**, *26*, 958-960.
[203] H. Stetter, W. Frank, *Angew. Chem. Int. Ed.* **1976**, *15*, 686-686.
[204] M. Magerstädt, O. A. Gansow, M. W. Brechbiel, D. Colcher, L. Baltzer, R. H. Knop, M. E. Girton, M. Naegele, *Magn. Reson. Med.* **1986**, *3*, 808-812.
[205] J. Wahsner, E. M. Gale, A. Rodríguez-Rodríguez, P. Caravan, *Chem. Rev.* **2019**, *119*, 957-1057.
[206] L. J. Scott, *Clin. Drug Invest.* **2018**, *38*, 773-784.
[207] C. A. Chang, L. C. Francesconi, M. F. Malley, K. Kumar, J. Z. Gougoutas, M. F. Tweedle, D. W. Lee, L. J. Wilson, *Inorg. Chem.* **1993**, *32*, 3501-3508.
[208] J. A. Peters, K. Djanashvili, C. F. G. C. Geraldes, C. Platas-Iglesias, *Coord. Chem. Rev.* **2020**, *406*, 213146.
[209] G. J. Stasiuk, N. J. Long, *Chem. Commun.* **2013**, *49*, 2732-2746.
[210] E. L. Que, C. J. Chang, *J. Am. Chem. Soc.* **2006**, *128*, 15942-15943.
[211] M. P. Lowe, D. Parker, O. Reany, S. Aime, M. Botta, G. Castellano, E. Gianolio, R. Pagliarin, *J. Am. Chem. Soc.* **2001**, *123*, 7601-7609.
[212] M. M. Ali, M. Woods, P. Caravan, A. C. L. Opina, M. Spiller, J. C. Fettinger, A. D. Sherry, *Chem. Eur. J.* **2008**, *14*, 7250-7258.
[213] S. J. Ratnakar, S. Viswanathan, Z. Kovacs, A. K. Jindal, K. N. Green, A. D. Sherry, *J. Am. Chem. Soc.* **2012**, *134*, 5798-5800.
[214] C. Tu, A. Y. Louie, *NMR Biomed.* **2013**, *26*, 781-787.
[215] J. A. Duimstra, F. J. Femia, T. J. Meade, *J. Am. Chem. Soc.* **2005**, *127*, 12847-12855.

[216] M. Giardiello, M. P. Lowe, M. Botta, *Chem. Commun.* **2007**, 4044-4046.
[217] C.-T. Yang, K. K. Ghosh, P. Padmanabhan, O. Langer, J. Liu, D. N. C. Eng, C. Halldin, B. Gulyás, *Theranostics* **2018**, *8*, 6210-6232.
[218] M. C. Heffern, L. M. Matosziuk, T. J. Meade, *Chem. Rev.* **2014**, *114*, 4496-4539.
[219] S. Shuvaev, M. Starck, D. Parker, *Chem. Eur. J.* **2017**, *23*, 9974-9989.
[220] E. Mathieu, A. Sipos, E. Demeyere, D. Phipps, D. Sakaveli, K. E. Borbas, *Chem. Commun.* **2018**, *54*, 10021-10035.
[221] A. Louie, *Chem Rev* **2010**, *110*, 3146-3195.
[222] *2018 New Drug Therapy Approvals* (Report). U.S. Food and Drug Administration, 2019.
[223] U. Hennrich, M. Benešová, *Pharmaceuticals* **2020**, *13*, 38.
[224] E. Pauwels, F. Cleeren, G. Bormans, C. M. Deroose, *Am. J. Nucl. Med. Mol. Imaging* **2018**, *8*, 311-331.
[225] S. Van Binnebeek, B. Vanbilloen, K. Baete, C. Terwinghe, M. Koole, F. M. Mottaghy, P. M. Clement, L. Mortelmans, K. Bogaerts, K. Haustermans et al., *Eur. Radiol.* **2016**, *26*, 900-909.
[226] Y. Krausz, N. Freedman, R. Rubinstein, E. Lavie, M. Orevi, S. Tshori, A. Salmon, B. Glaser, R. Chisin, E. Mishani et al., *Mol. Imaging Biol.* **2011**, *13*, 583-593.
[227] S. Chakraborty, J. Shi, Y.-S. Kim, Y. Zhou, B. Jia, F. Wang, S. Liu, *Bioconjugate Chem.* **2010**, *21*, 969-978.
[228] K. Ferreira, H.-Y. Hu, V. Fetz, H. Prochnow, B. Rais, P. P. Müller, M. Brönstrup, *Angew. Chem. Int. Ed.* **2017**, *56*, 8272-8276.
[229] H.-Y. Hu, N.-H. Lim, H.-P. Juretschke, D. Ding-Pfennigdorff, P. Florian, M. Kohlmann, A. Kandira, J. P. von Kries, J. Saas, K. A. Rudolphi et al., *Chem. Sci.* **2015**, *6*, 6256-6261.
[230] H.-Y. Hu, N.-H. Lim, D. Ding-Pfennigdorff, J. Saas, K. U. Wendt, O. Ritzeler, H. Nagase, O. Plettenburg, C. Schultz, M. Nazare, *Bioconjugate Chem.* **2015**, *26*, 383-388.
[231] H. Lee, W. Akers, P. Cheney, W. B. Edwards, K. Liang, J. Culver, S. Achilefu, *J. Biomed. Opt.* **2009**, *14:040507*.
[232] C.-W. Huang, Z. Li, P. S. Conti, *Bioconjugate Chem.* **2012**, *23*, 2159-2167.
[233] G. Ren, G. Blum, M. Verdoes, H. Liu, S. Syed, L. E. Edgington, O. Gheysens, Z. Miao, H. Jiang, S. S. Gambhir et al., *PLoS One* **2011**, *6*, 1-9.
[234] J.-C. G. Bünzli, *J. Lumin.* **2016**, *170*, 866-878.
[235] K. Y. Zhang, Q. Yu, H. Wei, S. Liu, Q. Zhao, W. Huang, *Chem. Rev.* **2018**, *118*, 1770-1839.
[236] U. Cho, J. K. Chen, *Cell Chem. Biol.* **2020**, *27*, 921-936.
[237] A. Thibon, V. C. Pierre, *Anal. Bioanal. Chem.* **2009**, *394*, 107-120.
[238] S. H. Hewitt, S. J. Butler, *Chem. Commun.* **2018**, *54*, 6635-6647.
[239] E. Soini, H. Kojola, *Clin. Chem.* **1983**, *29*, 65-68.
[240] I. Hemmilä, S. Dakubu, V.-M. Mukkala, H. Siitari, T. Lövgren, *Anal. Biochem.* **1984**, *137*, 335-343.
[241] E. F. Gudgin Dickson, A. Pollak, E. P. Diamandis, *J. Photochem. Photobiol., B* **1995**, *27*, 3-19.
[242] H. Bazin, E. Trinquet, G. Mathis, *Rev. Mol. Biotechnol.* **2002**, *82*, 233-250.
[243] Y. Jia, C. M. Quinn, A. I. Gagnon, R. Talanian, *Anal. Biochem.* **2006**, *356*, 273-281.
[244] A. K. Hagan, T. Zuchner, *Anal. Bioanal. Chem.* **2011**, *400*, 2847-2864.
[245] M. L. Aulsebrook, B. Graham, M. R. Grace, K. L. Tuck, *Coord. Chem. Rev.* **2018**, *375*, 191-220.
[246] Y. Ning, M. Zhu, J.-L. Zhang, *Coord. Chem. Rev.* **2019**, *399*, 213028.
[247] E. Pazos, M. E. Vázquez, *Biotechnol. J.* **2014**, *9*, 241-252.
[248] J.-C. G. Bünzli, S. V. Eliseeva. Basics of Lanthanide Photophysics. In: *Lanthanide Luminescence: Photophysical, Analytical and Biological Aspects.* P. Hänninen, H. Härmä, Eds. Springer: Berlin, Heidelberg, 2011, pp 1-45.

[249] M. H. V. Werts, *Sci. Prog.* **2005**, *88*, 101-131.
[250] J.-C. G. Bünzli, *Coord. Chem. Rev.* **2015**, *293-294*, 19-47.
[251] B. Brennecke, Q. Wang, Q. Zhang, H.-Y. Hu, M. Nazaré, *Angew. Chem. Int. Ed.* **2020**, *59*, 8512-8516.
[252] M. Kleinerman, *J. Chem. Phys.* **1969**, *51*, 2370-2381.
[253] G. Liu. Electronic Energy Level Structure. In: *Spectroscopic Properties of Rare Earths in Optical Materials.* 1st ed. G. Liu, B. Jacquier, Eds. Springer-Verlag: Berlin Heidelberg, 2005, pp 1-94.
[254] V. L. Ermolaev, E. B. Sveshnikova, *Russ. Chem. Rev.* **1994**, *63*, 905-922.
[255] A. Monguzzi, R. Tubino, F. Meinardi, A. O. Biroli, M. Pizzotti, F. Demartin, F. Quochi, F. Cordella, M. A. Loi, *Chem. Mater.* **2009**, *21*, 128-135.
[256] A. Beeby, D. Parker, J. A. G. Williams, *J. Chem. Soc., Perkin Trans. 2* **1996**, 1565-1579.
[257] E. Deiters, B. Song, A.-S. Chauvin, C. D. B. Vandevyver, F. Gumy, J.-C. G. Bünzli, *Chem. Eur. J.* **2009**, *15*, 885-900.
[258] K. Barthelmes, A. M. Reynolds, E. Peisach, H. R. A. Jonker, N. J. DeNunzio, K. N. Allen, B. Imperiali, H. Schwalbe, *J. Am. Chem. Soc.* **2011**, *133*, 808-819.
[259] J. Vuojola, M. Syrjänpää, U. Lamminmäki, T. Soukka, *Anal. Chem.* **2013**, *85*, 1367-1373.
[260] M. Nitz, M. Sherawat, K. J. Franz, E. Peisach, K. N. Allen, B. Imperiali, *Angew. Chem. Int. Ed.* **2004**, *43*, 3682-3685.
[261] Y. Koshi, E. Nakata, I. Hamachi, *ChemBioChem* **2005**, *6*, 1349-1352.
[262] S. C. Zondlo, F. Gao, N. J. Zondlo, *J. Am. Chem. Soc.* **2010**, *132*, 5619-5621.
[263] J. A. González-Vera, D. Bouzada, C. Bouclier, M. Eugenio Vázquez, M. C. Morris, *Chem. Commun.* **2017**, *53*, 6109-6112.
[264] E. A. Weitz, J. Y. Chang, A. H. Rosenfield, E. A. Morrow, V. C. Pierre, *Chem. Sci.* **2013**, *4*, 4052-4060.
[265] H. Ito, T. Terai, K. Hanaoka, T. Ueno, T. Komatsu, T. Nagano, Y. Urano, *Chem. Commun.* **2015**, *51*, 8319-8322.
[266] R. A. Evangelista, A. Pollak, E. F. Gudgin Templeton, *Anal. Biochem.* **1991**, *197*, 213-224.
[267] C. J. Veiopoulou, E. S. Lianidou, P. C. Ioannou, C. E. Efstathiou, *Anal. Chim. Acta* **1996**, *335*, 177-184.
[268] E. P. Diamandis, *Analyst* **1992**, *117*, 1879-1884.
[269] T. Terai, K. Kikuchi, S.-y. Iwasawa, T. Kawabe, Y. Hirata, Y. Urano, T. Nagano, *J. Am. Chem. Soc.* **2006**, *128*, 6938-6946.
[270] T. Terai, K. Kikuchi, Y. Urano, H. Kojima, T. Nagano, *Chem. Commun.* **2012**, *48*, 2234-2236.
[271] S. Mizukami, K. Tonai, M. Kaneko, K. Kikuchi, *J. Am. Chem. Soc.* **2008**, *130*, 14376-14377.
[272] E. Pershagen, J. Nordholm, K. E. Borbas, *J. Am. Chem. Soc.* **2012**, *134*, 9832-9835.
[273] E. Pershagen, K. E. Borbas, *Angew. Chem. Int. Ed.* **2015**, *54*, 1787-1790.
[274] C. P. Montgomery, B. S. Murray, E. J. New, R. Pal, D. Parker, *Acc. Chem. Res.* **2009**, *42*, 925-937.
[275] J.-C. G. Bünzli, *Chem. Rev.* **2010**, *110*, 2729–2755.
[276] H. Sung, J. Ferlay, R. L. Siegel, M. Laversanne, I. Soerjomataram, A. Jemal, F. Bray, *Global Cancer Observatory: Cancer Today.*, Lyon, France: International Agency for Research on Cancer (IARC), 2020. Available from: https://gco.iarc.fr/today, (accessed 05.01.2020).
[277] R. Etzioni, N. Urban, S. Ramsey, M. McIntosh, S. Schwartz, B. Reid, J. Radich, G. Anderson, L. Hartwell, *Nat. Rev. Cancer* **2003**, *3*, 243-252.
[278] C. P. Wild, E. Weiderpass, B. W. Stewart, Eds., *World Cancer Report: Cancer Research for Cancer Prevention* (Report). International Agency for Research on Cancer, Lyon, France, 2020.

[279] G. Zlokarnik, P. A. Negulescu, T. E. Knapp, L. Mere, N. Burres, L. Feng, M. Whitney, K. Roemer, R. Y. Tsien, *Science* **1998**, *279*, 84-88.
[280] S. A. Esfahani, P. Heidari, M. H. Kucherlapati, J. M. Ferrer, R. S. Kucherlapati, U. Mahmood, *Am. J. Nucl. Med. Mol. Imaging* **2019**, *9*, 230-242.
[281] H.-Y. Hu, S. Gehrig, G. Reither, D. Subramanian, M. A. Mall, O. Plettenburg, C. Schultz, *Biotechnol. J.* **2014**, *9*, 266-281.
[282] S. Raab-Westphal, J. Marshall, S. Goodman, *Cancers* **2017**, *9*, 110.
[283] A. Mochida, F. Ogata, T. Nagaya, P. L. Choyke, H. Kobayashi, *Bioorg. Med. Chem.* **2018**, *26*, 925-930.
[284] H. Kobayashi, P. L. Choyke, *Acc. Chem. Res.* **2011**, *44*, 83-90.
[285] C. Chen, R. Tian, Y. Zeng, C. Chu, G. Liu, *Bioconjugate Chem.* **2020**, *31*, 276-292.
[286] D. Maxwell, Q. Chang, X. Zhang, E. M. Barnett, D. Piwnica-Worms, *Bioconjugate Chem.* **2009**, *20*, 702-709.
[287] Q. T. Nguyen, E. S. Olson, T. A. Aguilera, T. Jiang, M. Scadeng, L. G. Ellies, R. Y. Tsien, *Proc. Natl. Acad. Sci. U. S. A.* **2010**, *107*, 4317-4322.
[288] R. Tian, M. Li, J. Wang, M. Yu, X. Kong, Y. Feng, Z. Chen, Y. Li, W. Huang, W. Wu et al., *Org. Biomol. Chem.* **2014**, *12*, 5365-5374.
[289] P. Lejault, K. Duskova, C. Bernhard, I. E. Valverde, A. Romieu, D. Monchaud, *Eur. J. Org. Chem.* **2019**, *2019*, 6146-6157.
[290] X. Zhang, Z. Xiong, Y. Wu, W. Cai, J. R. Tseng, S. S. Gambhir, X. Chen, *J. Nucl. Med.* **2006**, *47*, 113-121.
[291] E. Tacconelli, E. Carrara, A. Savoldi, S. Harbarth, M. Mendelson, D. L. Monnet, C. Pulcini, G. Kahlmeter, J. Kluytmans, Y. Carmeli et al., *Lancet Infect. Dis.* **2018**, *18*, 318-327.
[292] B. Song, G. Wang, M. Tan, J. Yuan, *J. Am. Chem. Soc.* **2006**, *128*, 13442-13450.
[293] T. Liu, A. Nonat, M. Beyler, M. Regueiro-Figueroa, K. Nchimi Nono, O. Jeannin, F. Camerel, F. Debaene, S. Cianférani-Sanglier, R. Tripier et al., *Angew. Chem. Int. Ed.* **2014**, *53*, 7259-7263.
[294] B. K. McMahon, T. Gunnlaugsson, *J. Am. Chem. Soc.* **2012**, *134*, 10725-10728.
[295] W.-S. Lo, H. Li, G.-L. Law, W.-T. Wong, K.-L. Wong, *J. Lumin.* **2016**, *169*, 549-552.
[296] D. Kovacs, X. Lu, L. S. Mészáros, M. Ott, J. Andres, K. E. Borbas, *J. Am. Chem. Soc.* **2017**, *139*, 5756-5767.
[297] M. Li, P. R. Selvin, *J. Am. Chem. Soc.* **1995**, *117*, 8132-8138.
[298] M. Xiao, P. R. Selvin, *J. Am. Chem. Soc.* **2001**, *123*, 7067-7073.
[299] P. Ge, P. R. Selvin, *Bioconjugate Chem.* **2004**, *15*, 1088-1094.
[300] G. A. Kraus, S. Kesavan, *Tetrahedron Lett.* **2005**, *46*, 1111-1113.
[301] K. Yoshikawa, S. Kobayashi, Y. Nakamoto, N. Haginoya, S. Komoriya, T. Yoshino, T. Nagata, A. Mochizuki, K. Watanabe, M. Suzuki et al., *Bioorg. Med. Chem.* **2009**, *17*, 8221-8233.
[302] N. Draoui, O. Schicke, A. Fernandes, X. Drozak, F. Nahra, A. Dumont, J. Douxfils, E. Hermans, J.-M. Dogné, R. Corbau et al., *Bioorg. Med. Chem.* **2013**, *21*, 7107-7117.
[303] H. Bregman, J. R. Simard, K. L. Andrews, S. Ayube, H. Chen, H. Gunaydin, A. Guzman-Perez, J. Hu, L. Huang, X. Huang et al., *J. Med. Chem.* **2017**, *60*, 1105-1125.

6 APPENDIX

6.1 NMR-Spectra and LCMS Traces of New and Key Compounds

Cathepsin S Sequence (**S1**)

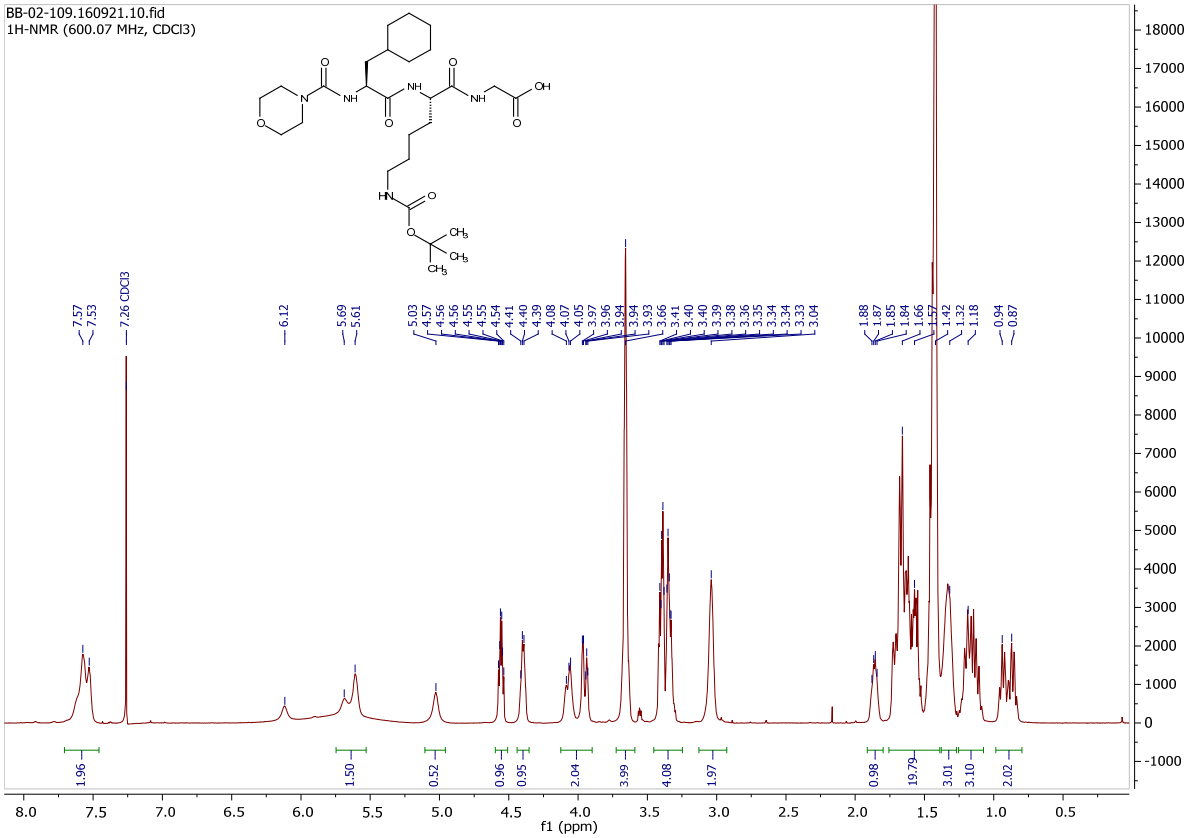

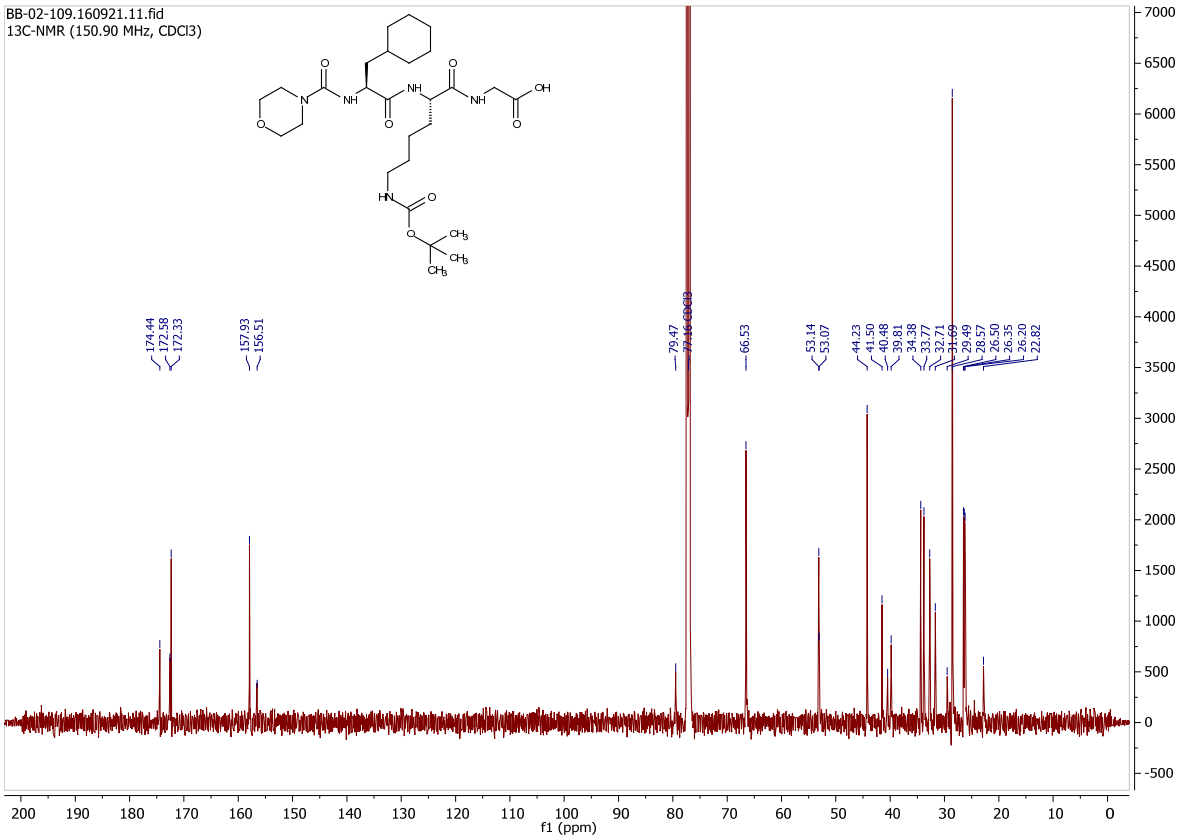

H-D(*t*Bu)-f-K(Cbz)-R(Pbf)-G-OH (**S2**)

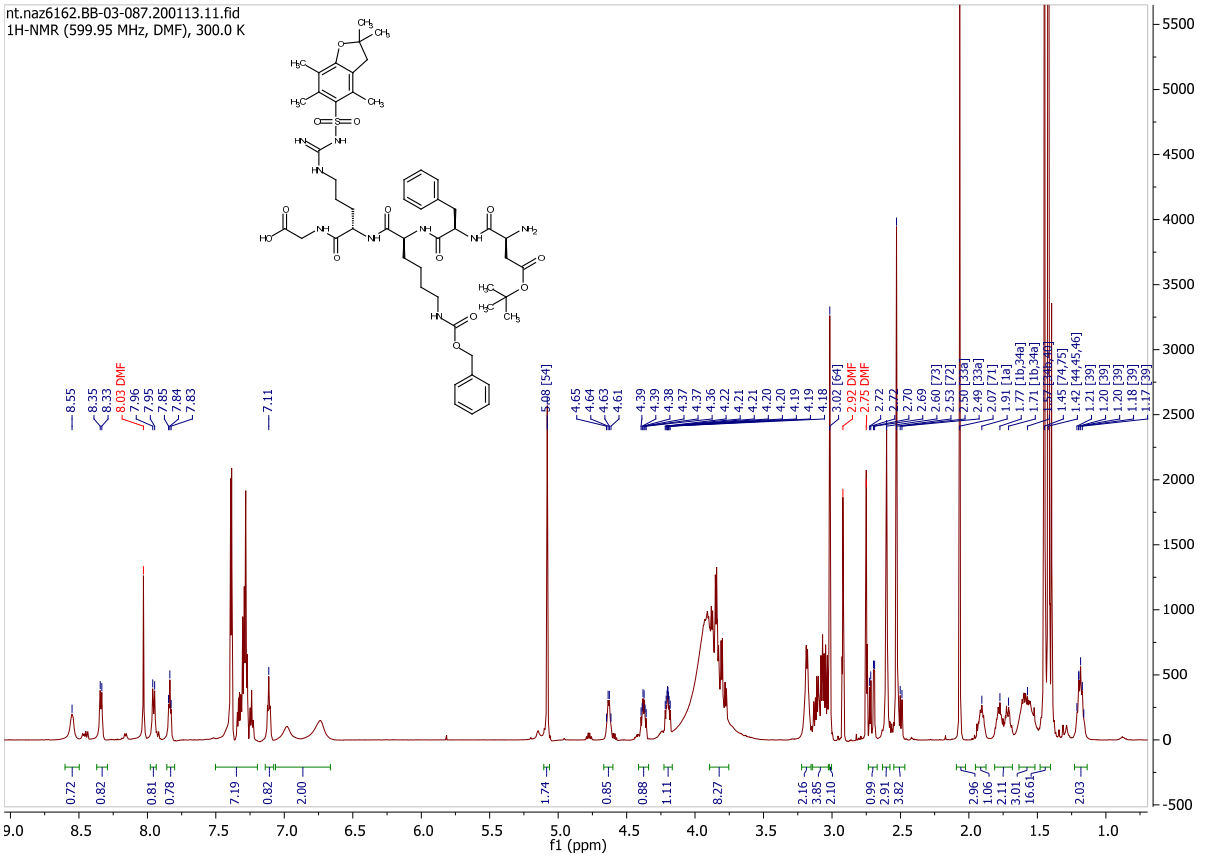

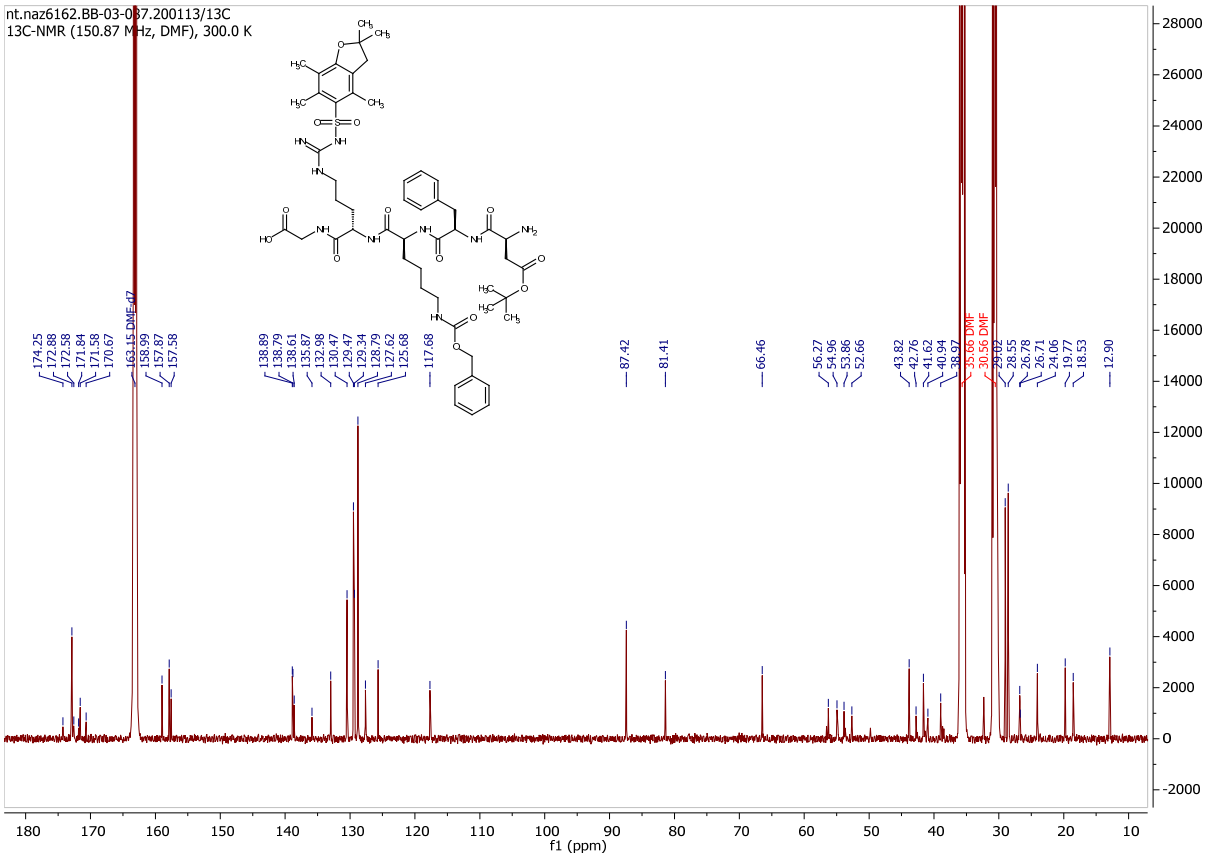

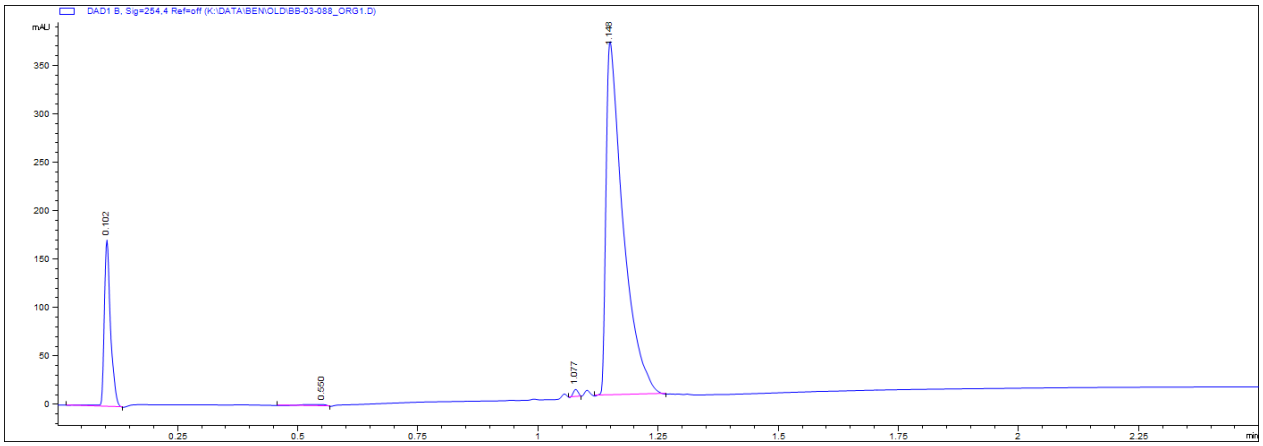
DAD1 B, Sig=254,4 Ref=off (K:\DATA\BEN\OLD\BB-03-088_ORG1.D)
mAU
350
300
250
200
150
100
50
0
0.102
0.550
1.077
1.148
0.25
0.5
0.75
1
1.25
1.5
1.75
2
2.25
min

cR(Pbf)GD(*t*Bu)fK(Cbz) (**S3**)

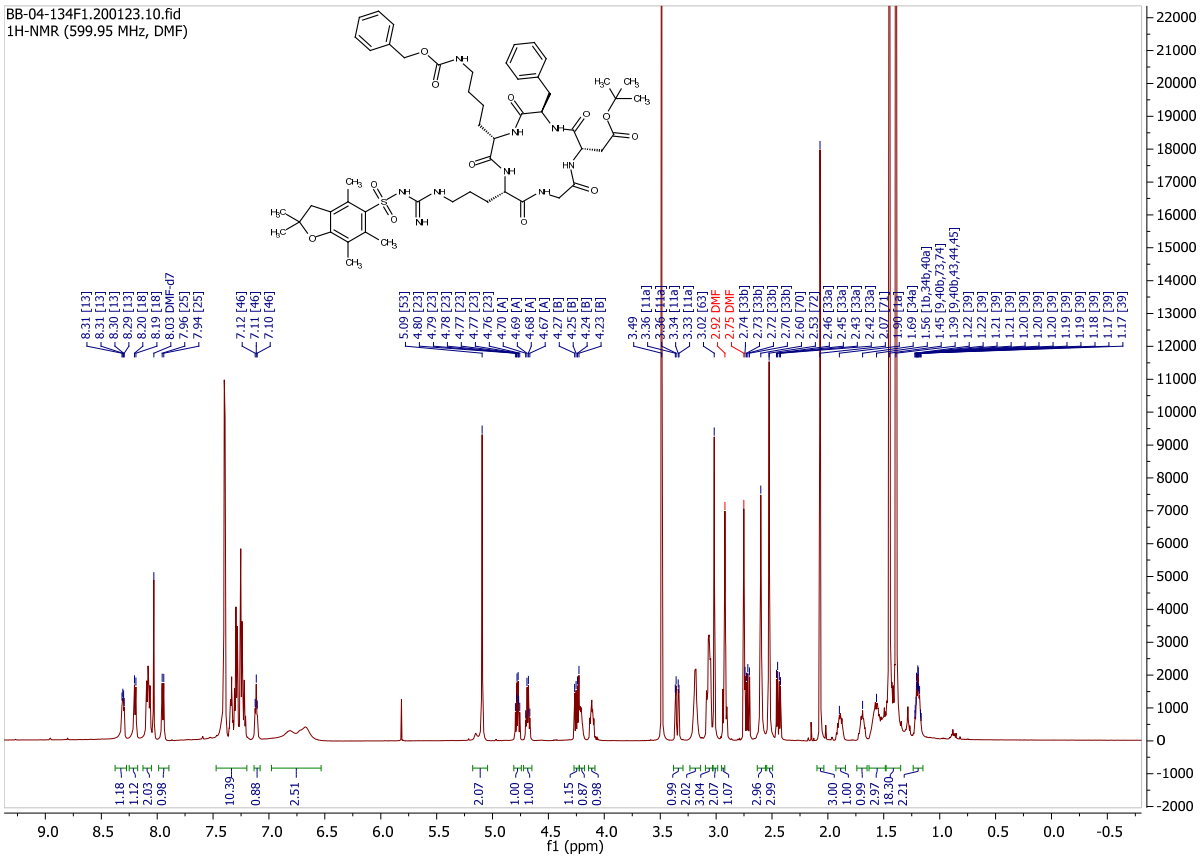

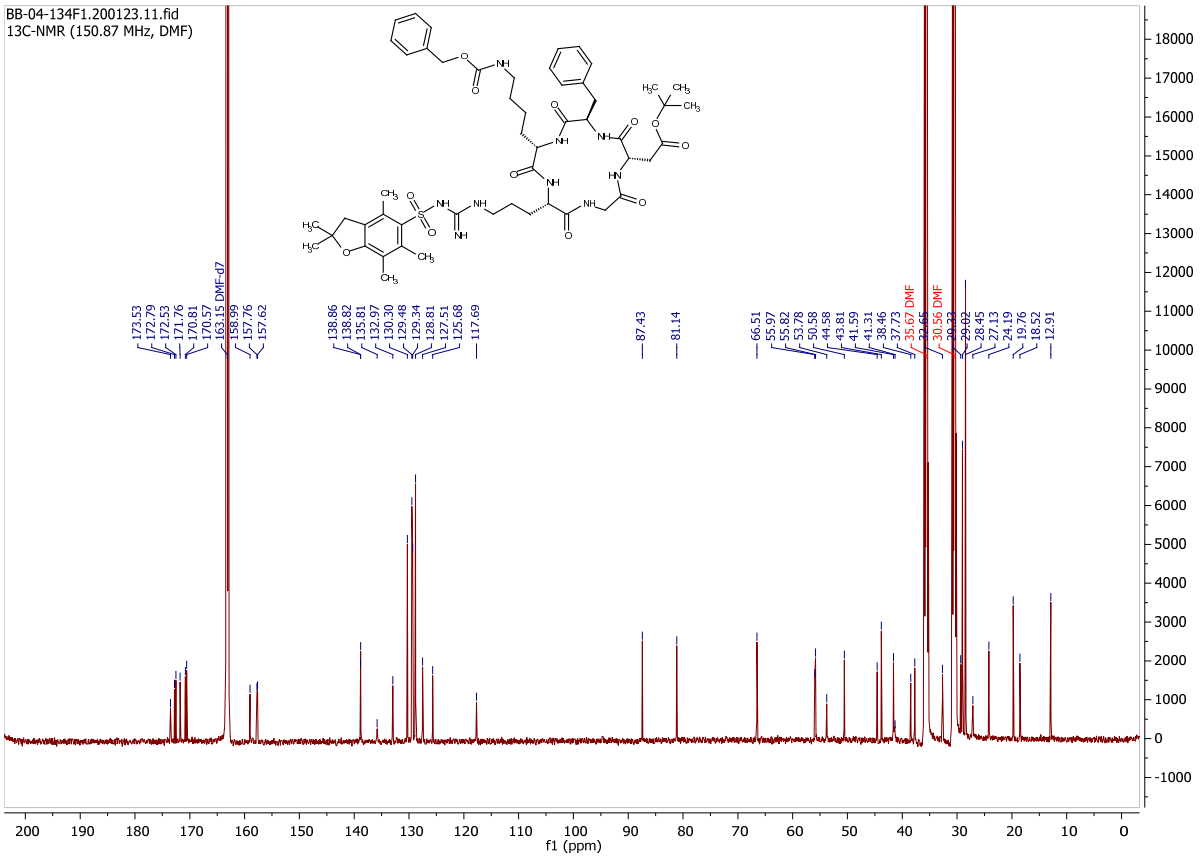

cR(Pbf)GD(*t*Bu)fK (**S4**)

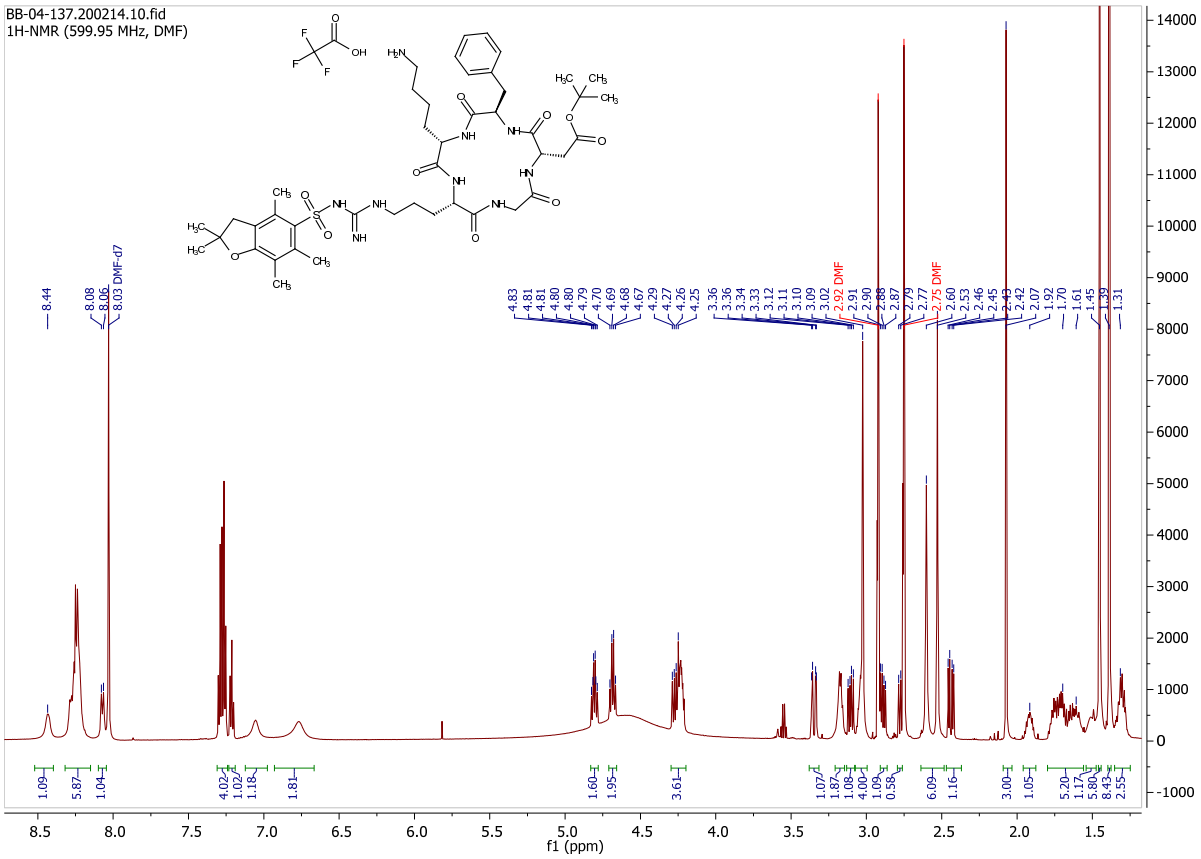

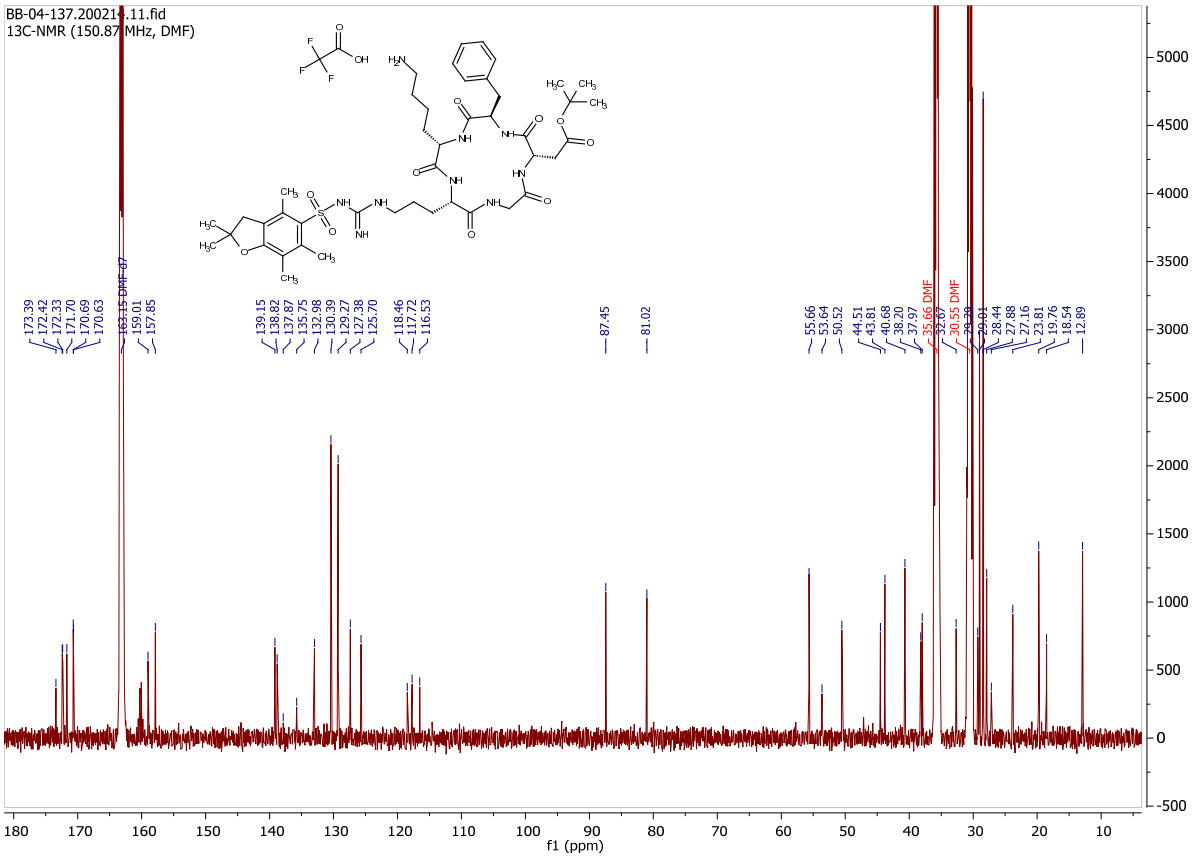

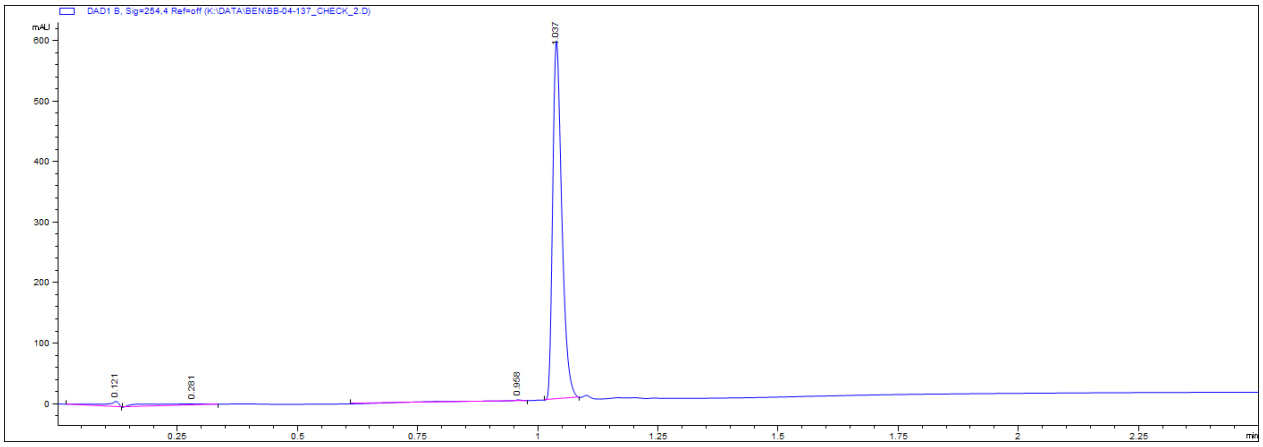
DAD1 B, Sig=254,4 Ref=off (K:\DATA\BEN\BB-04-137_CHECK_2.D)
mAU
600
500
400
300
200
100
0
0.121
0.281
0.968
1.037
0.25
0.5
0.75
1
1.25
1.5
1.75
2
2.25
min

Cy3 (**S7**)

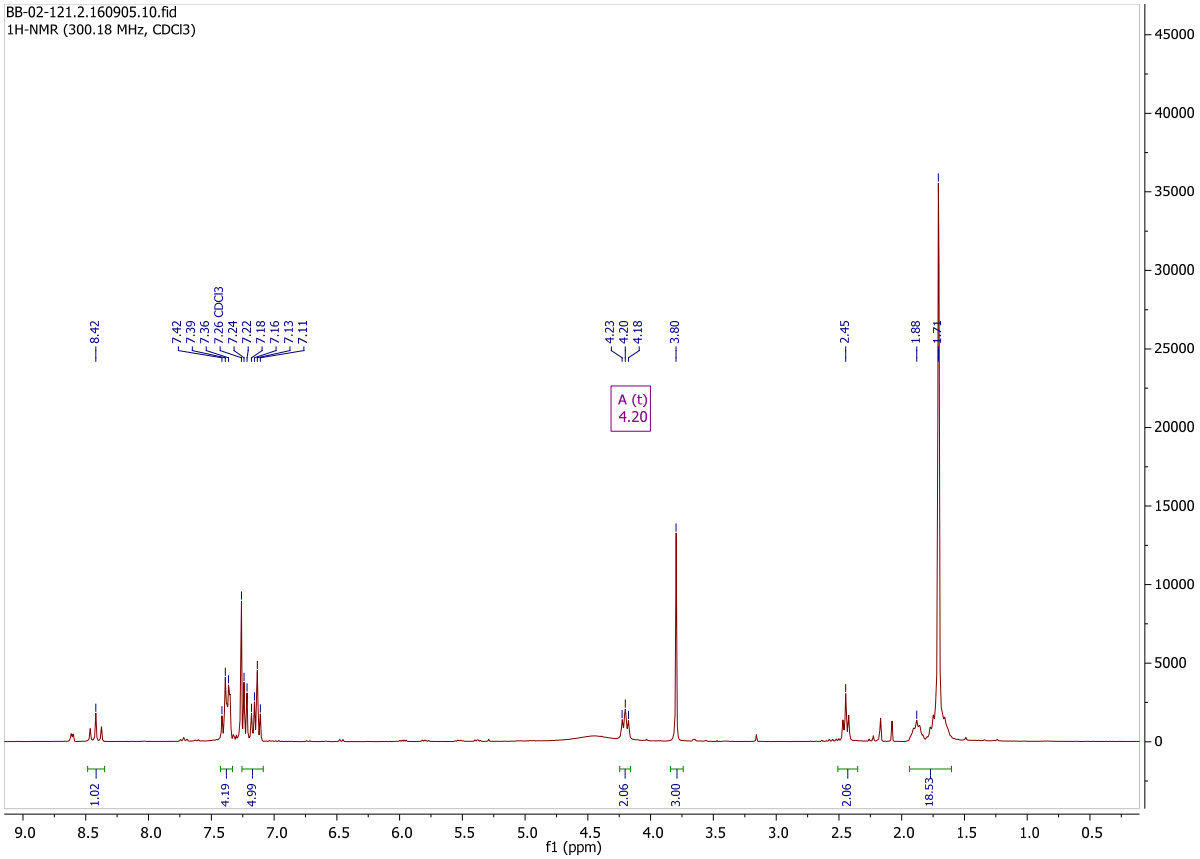
BB-02-121.2.160905.10.fid
1H-NMR (300.18 MHz, CDCl3)
8.42
7.42
7.39
7.36
7.26 CDCl3
7.24
7.22
7.18
7.16
7.13
7.11
4.23
4.20
4.18
3.80
2.45
1.88
1.71
A (t)
4.20
1.02
4.19
4.99
2.06
3.00
2.06
18.53
f1 (ppm)

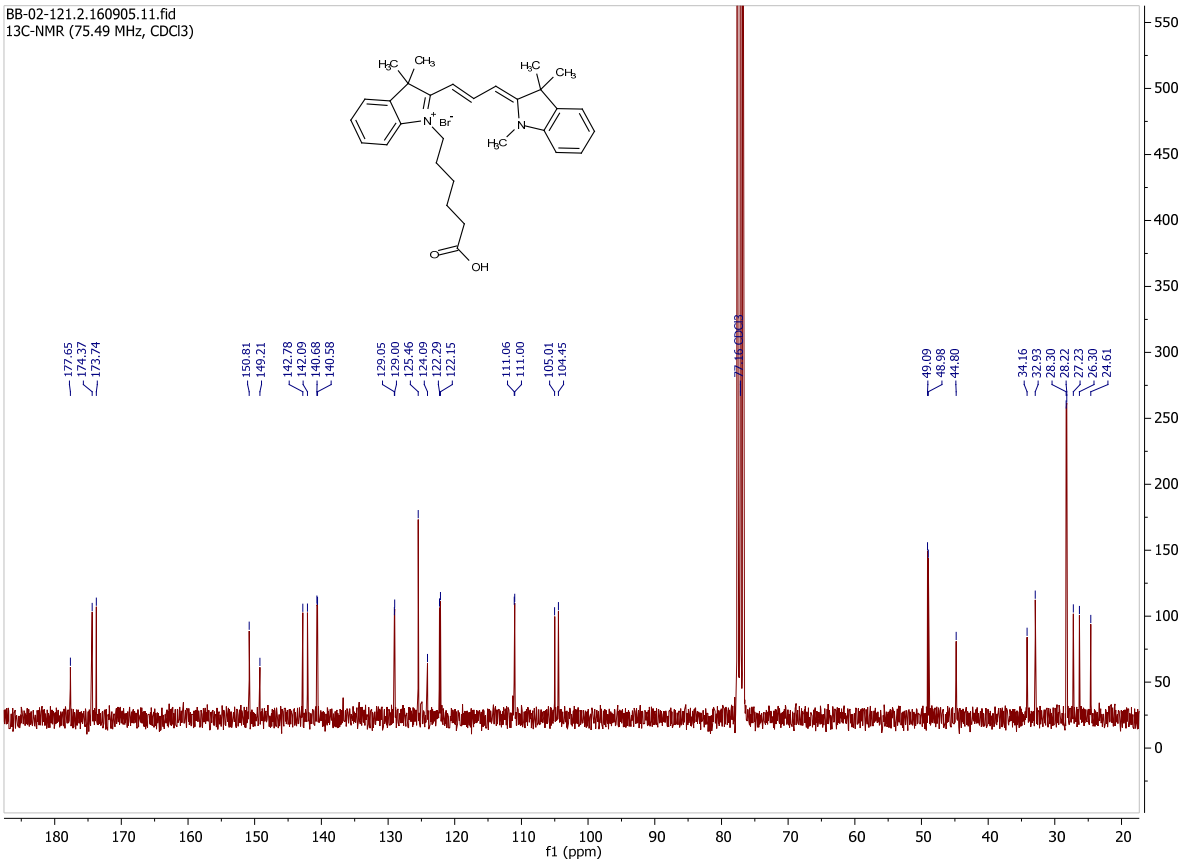
BB-02-121.2.160905.11.fid
13C-NMR (75.49 MHz, CDCl3)
177.65
174.37
173.74
150.81
149.21
142.78
142.09
140.68
140.58
129.05
129.00
125.46
124.09
122.29
122.15
111.06
111.00
105.01
104.45
77.16 CDCl3
49.09
48.98
44.80
34.16
32.93
28.30
28.22
27.23
26.30
24.61
f1 (ppm)

Cy3-EDABoc (**S8a**)

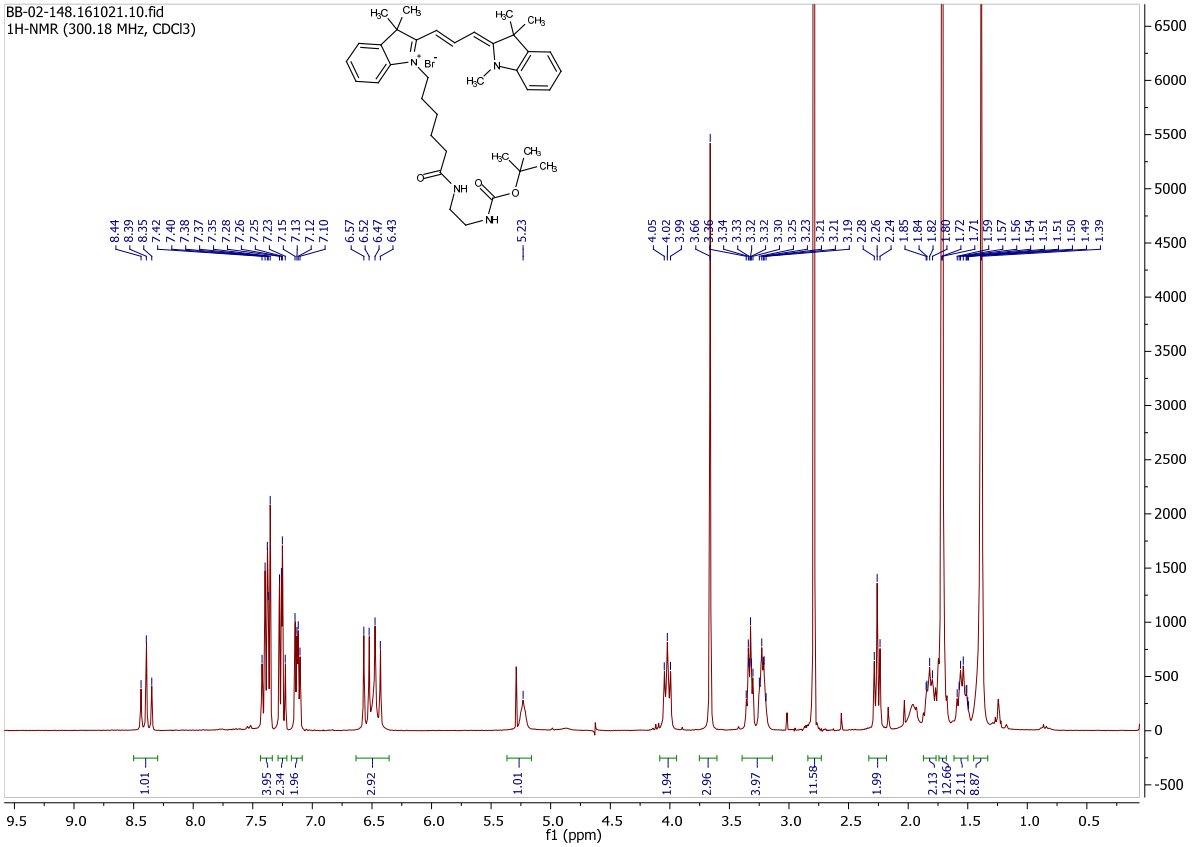

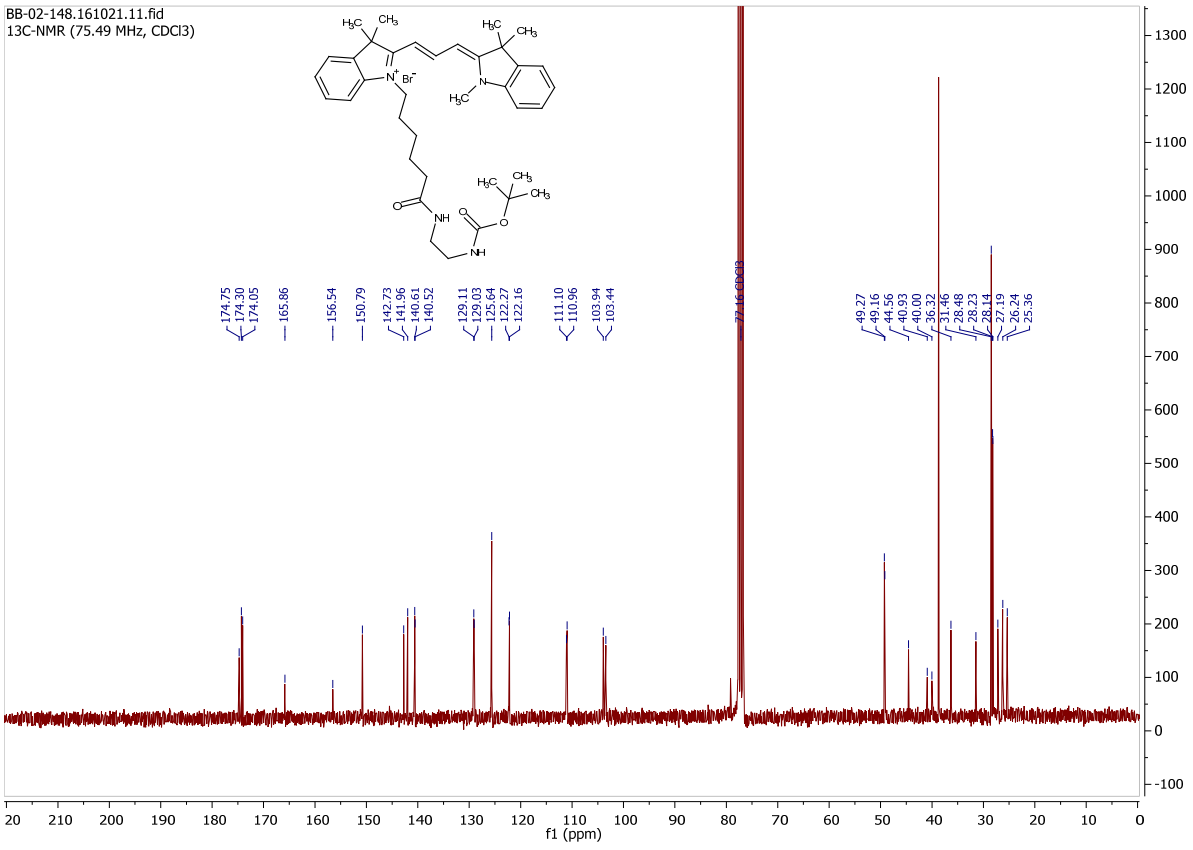

BHQ-2 (**S10**)

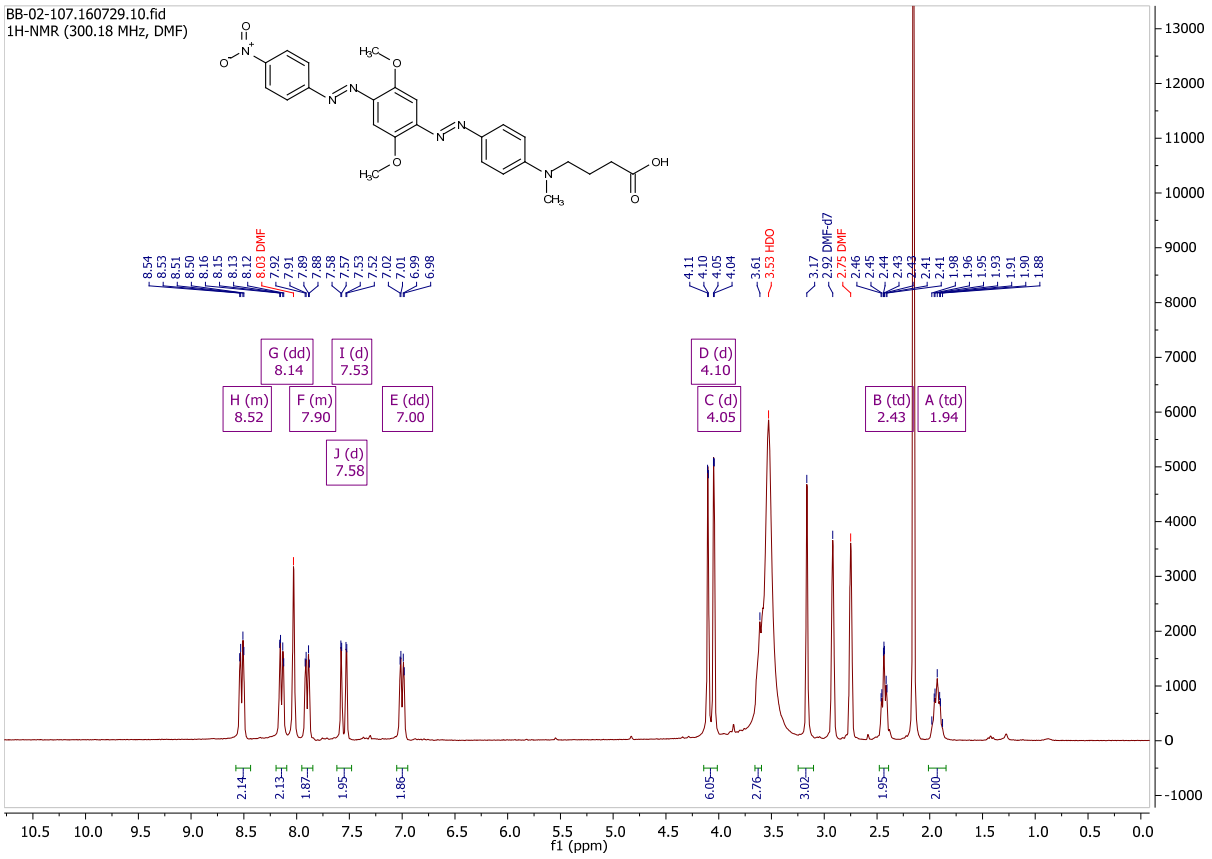
BB-02-107.160729.10.fid
1H-NMR (300.18 MHz, DMF)
G (dd) 8.14
I (d) 7.53
H (m) 8.52
F (m) 7.90
E (dd) 7.00
J (d) 7.58
D (d) 4.10
C (d) 4.05
B (td) 2.43
A (td) 1.94
f1 (ppm)

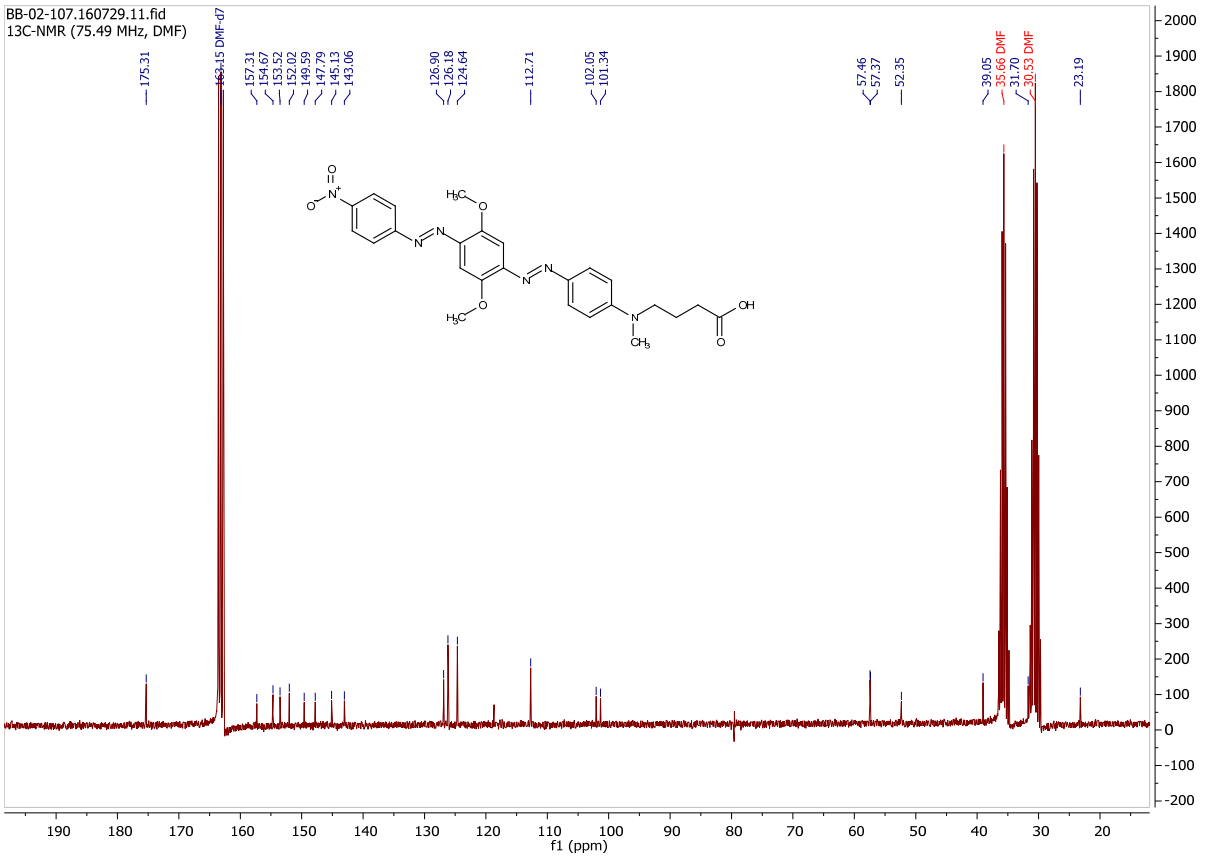
BB-02-107.160729.11.fid
13C-NMR (75.49 MHz, DMF)
f1 (ppm)

BHQ-2-EDABoc (**S11a**)

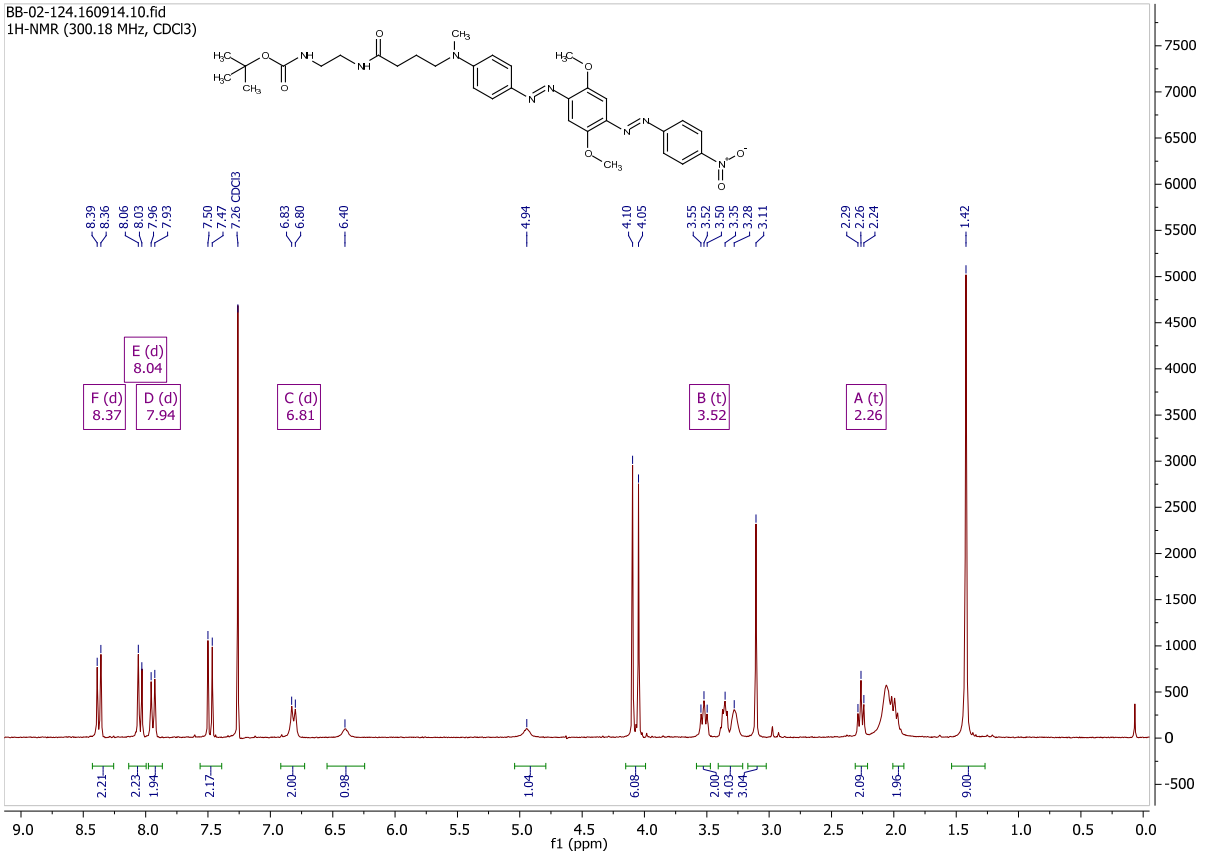

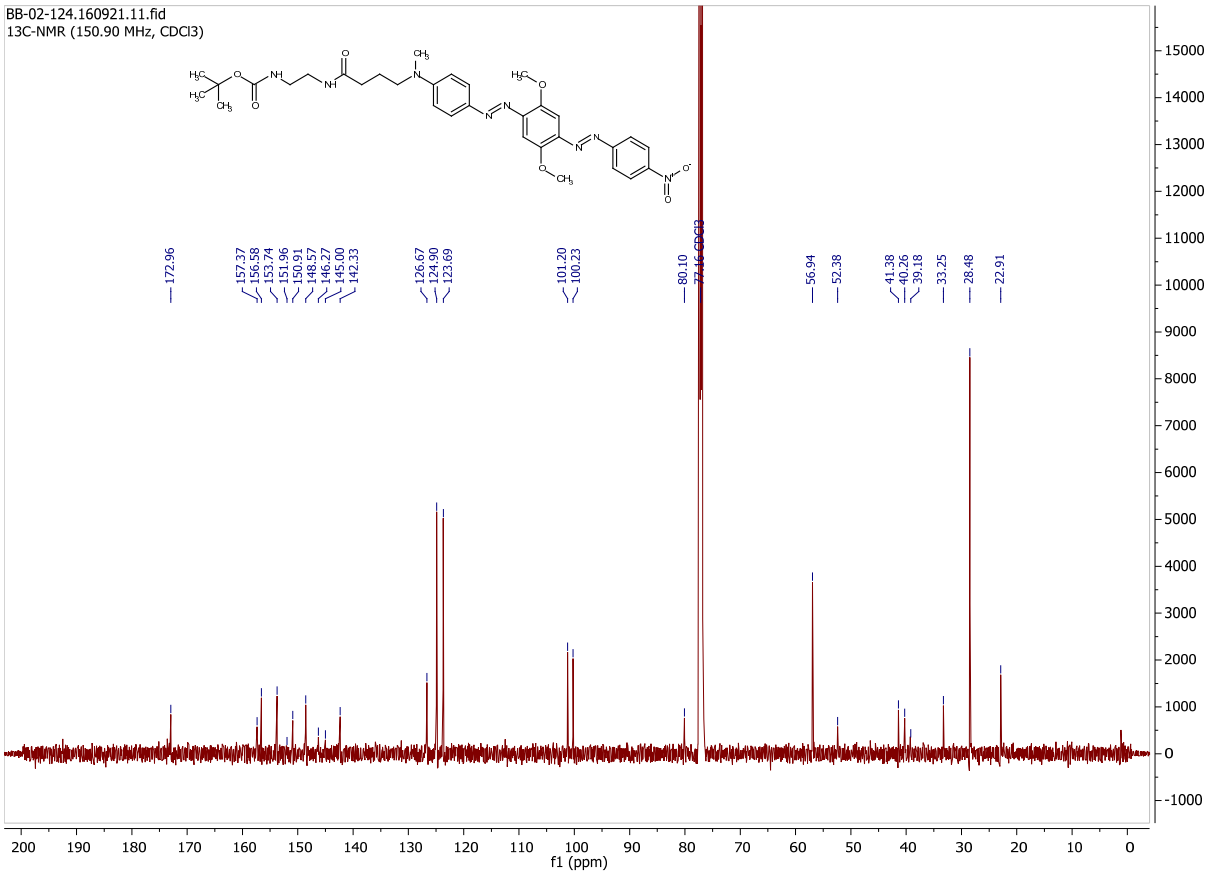

Boc-protected CatS Sequence-BHQ-2 (**S12a**)

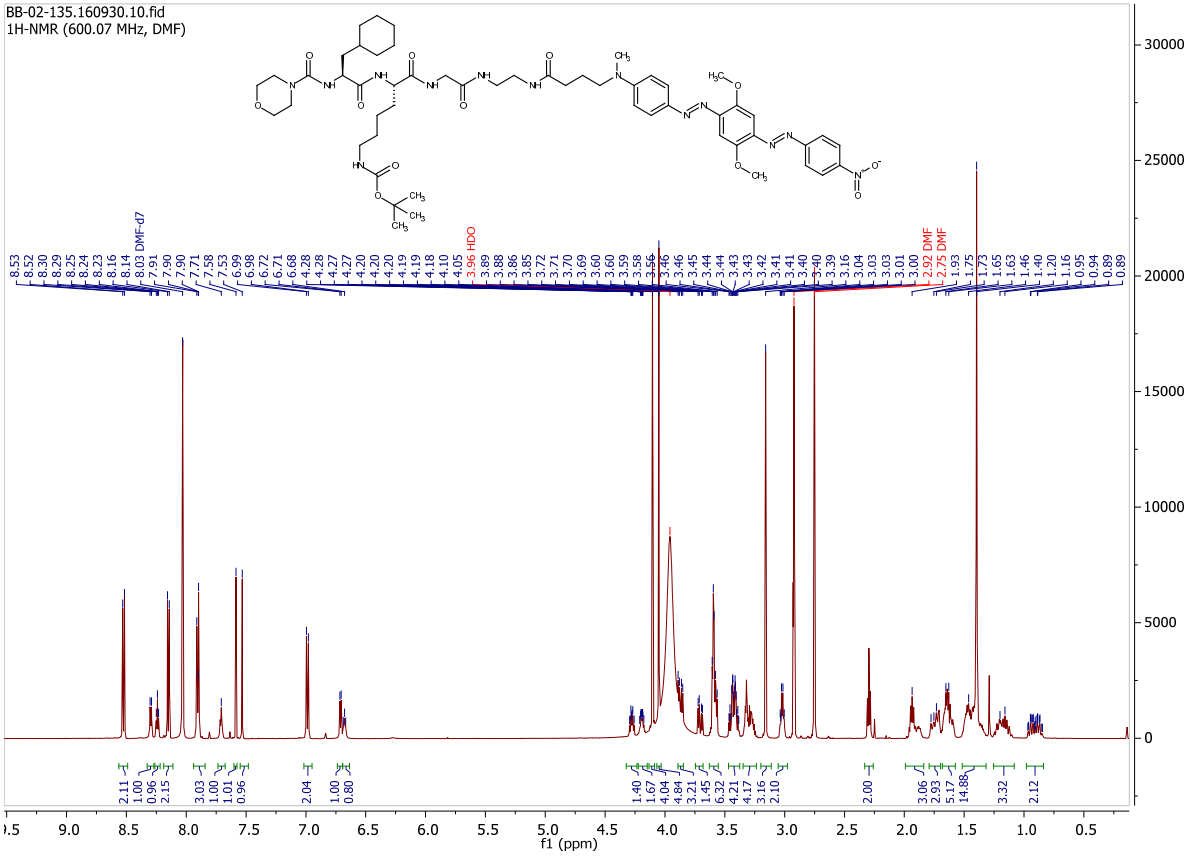

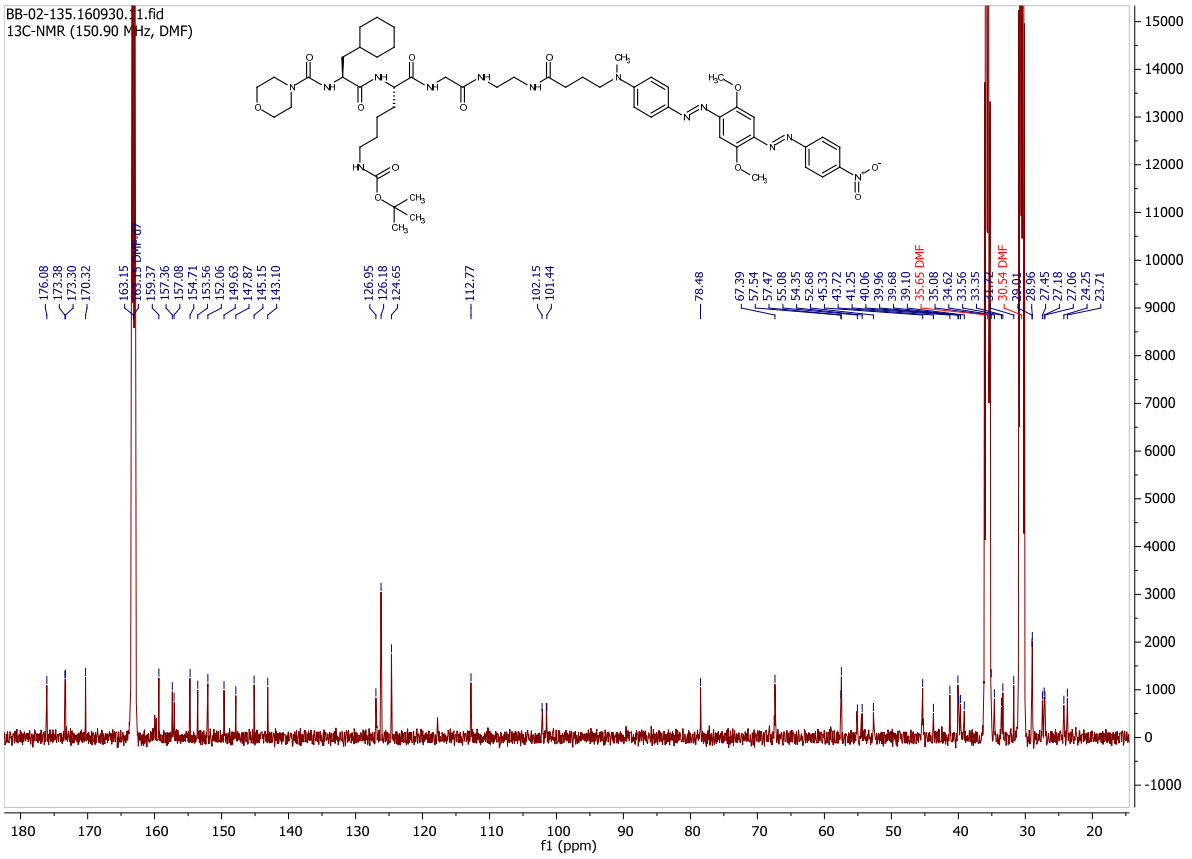

tert-Butyl (17-amino-3,6,9,12,15-pentaoxaheptadecyl)carbamate (**S17**)

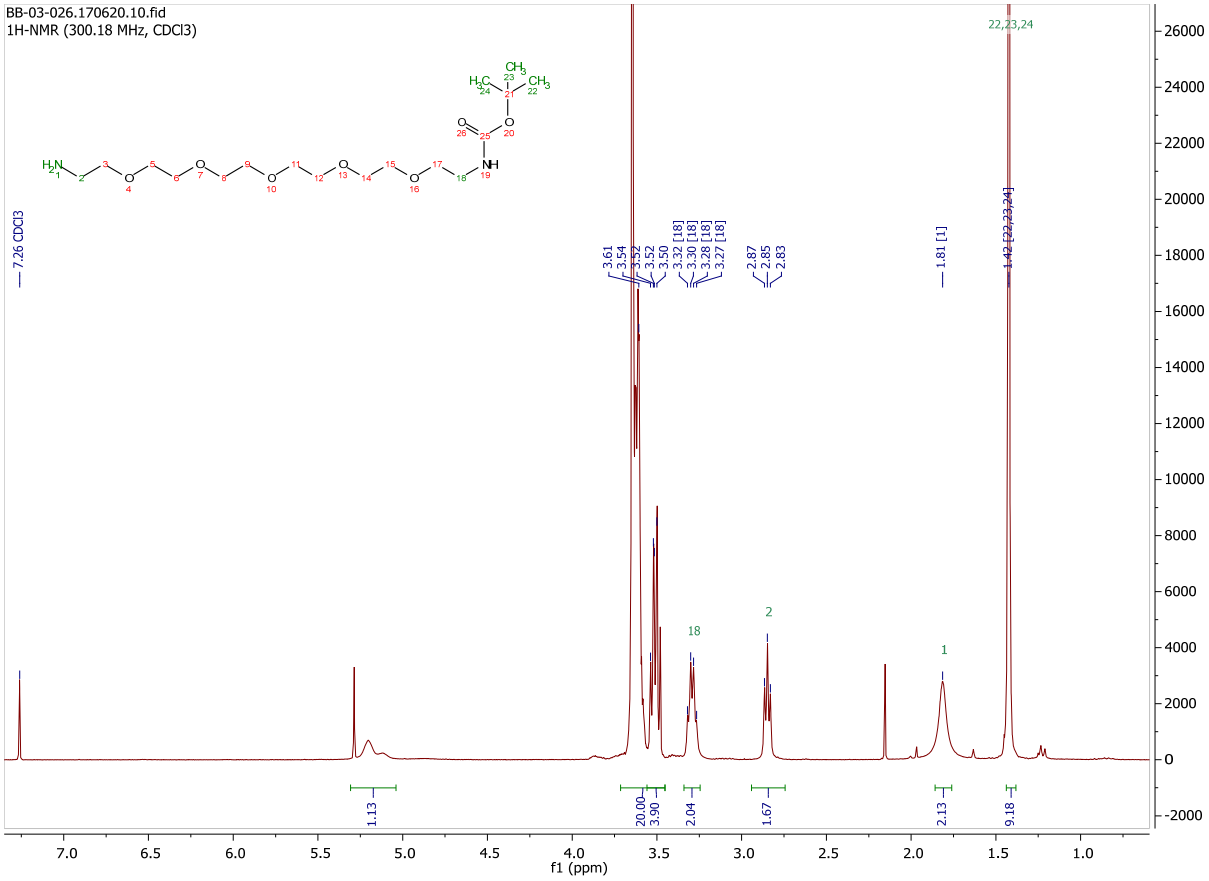

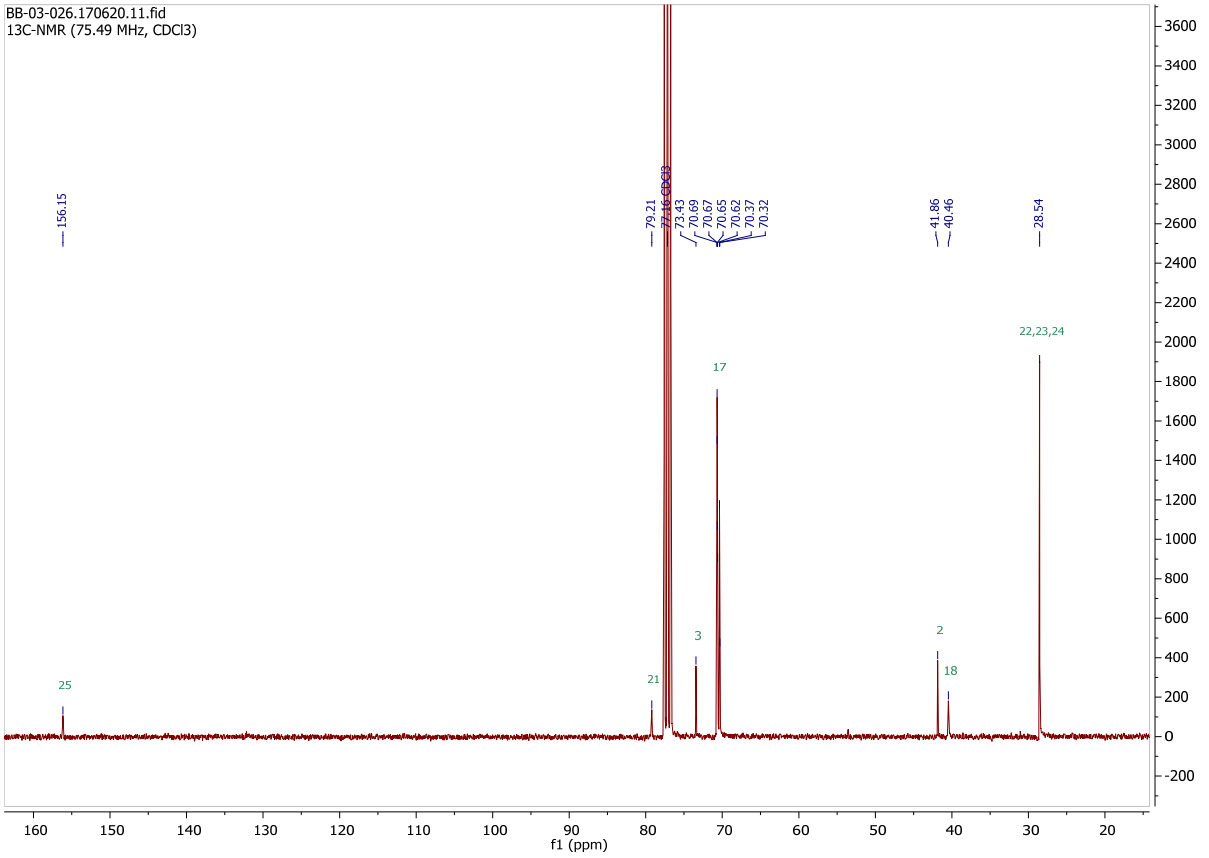

DOTA *N*-1,7-bis(benzyl ester) (**1**)

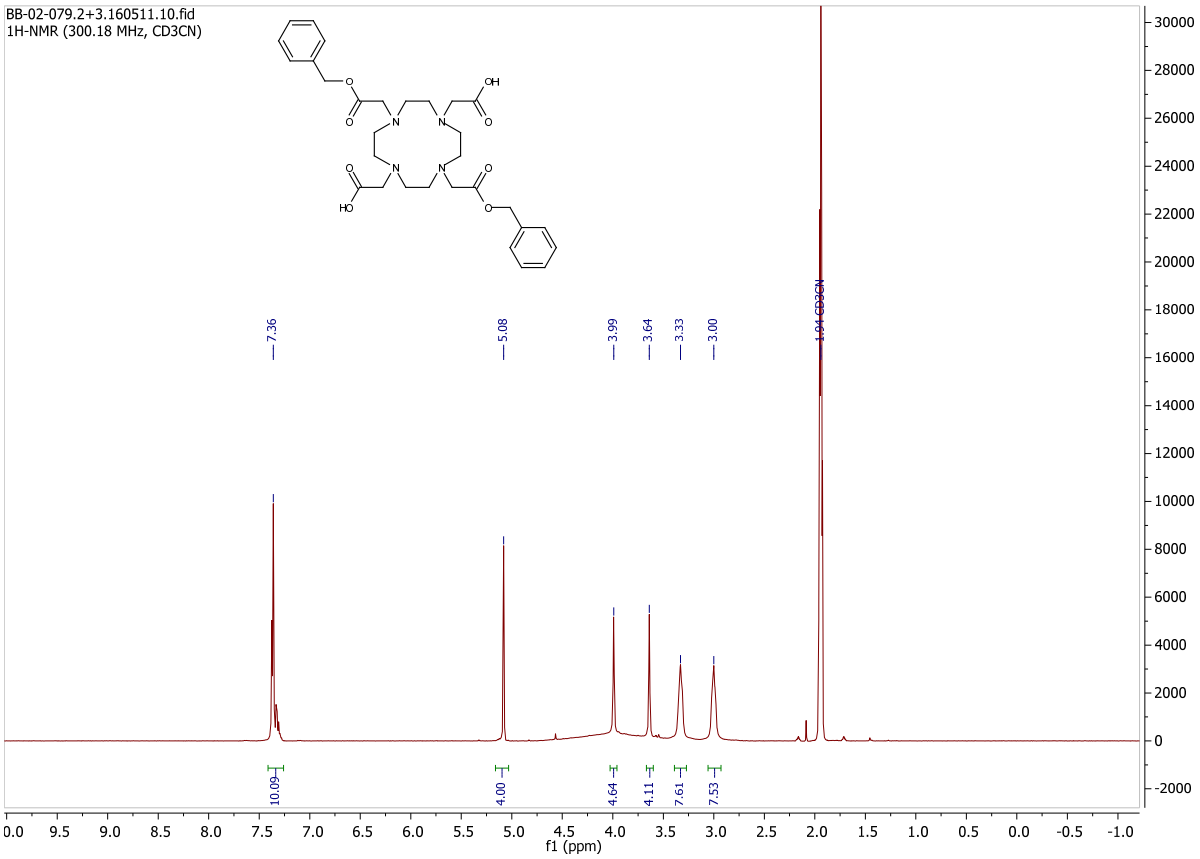

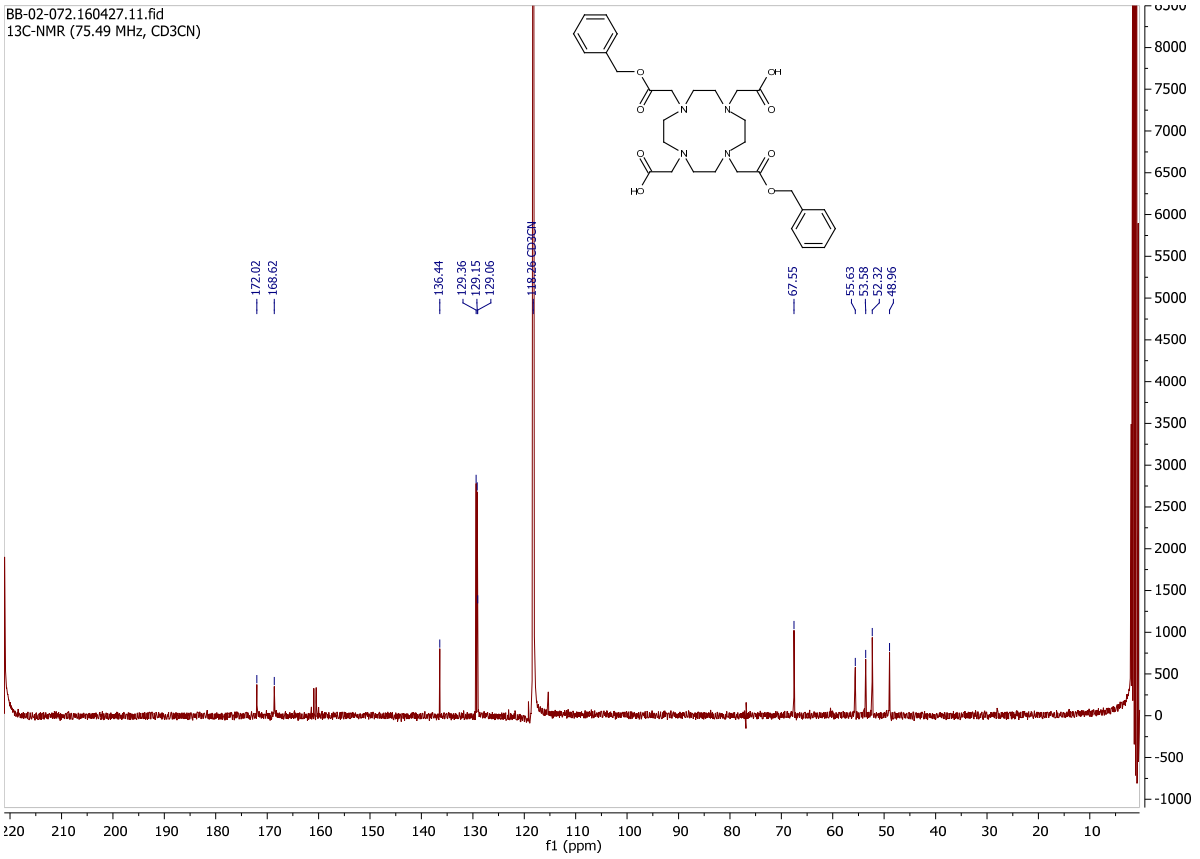

Bis-(PEGNHBoc)-dibenzyl DOTAM (**S21**)

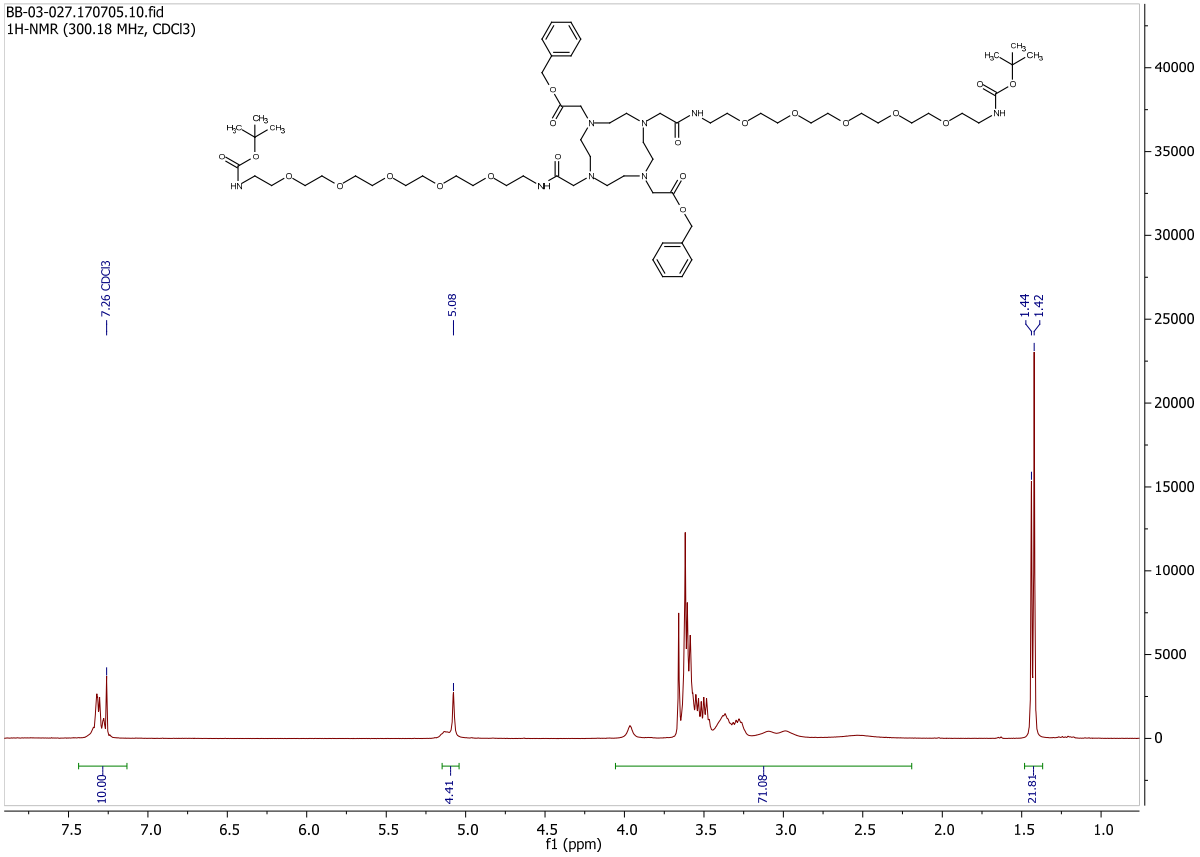

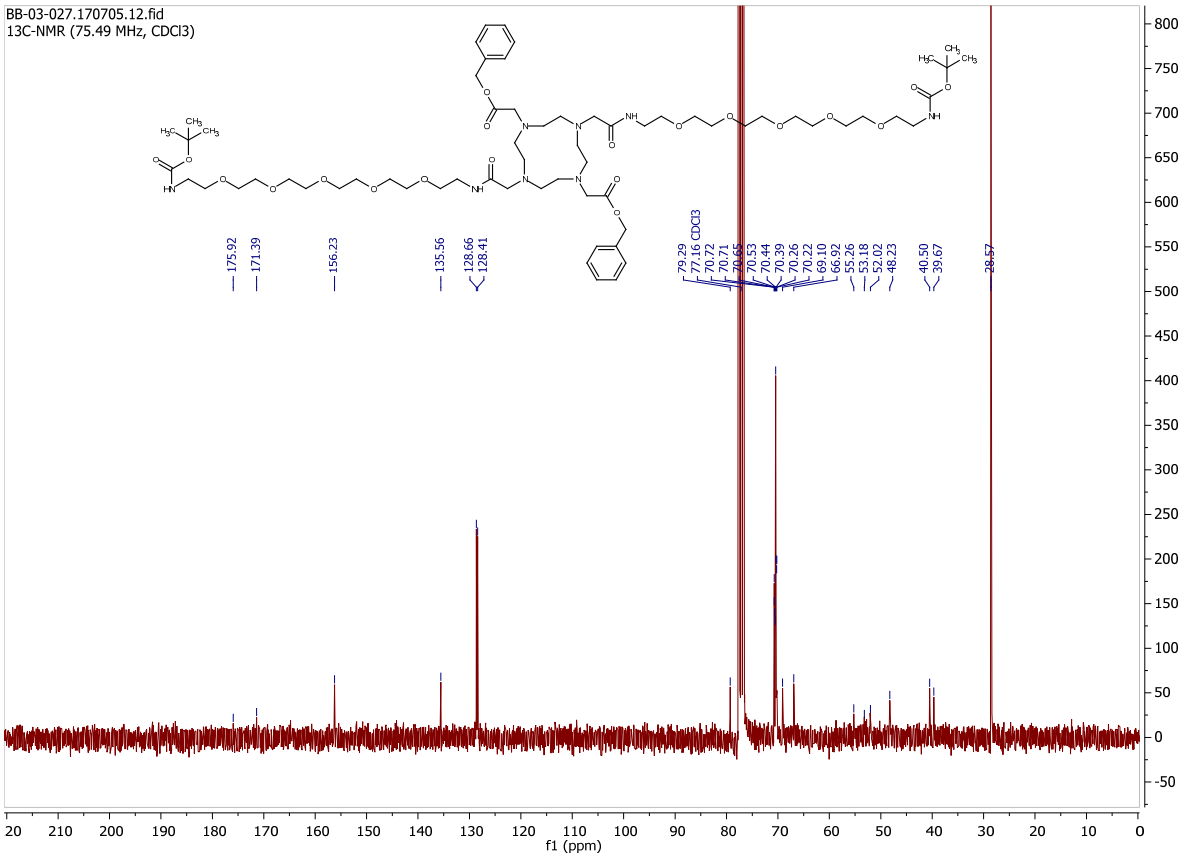

Bis-(PEGNHBoc) DOTAM (**2**)

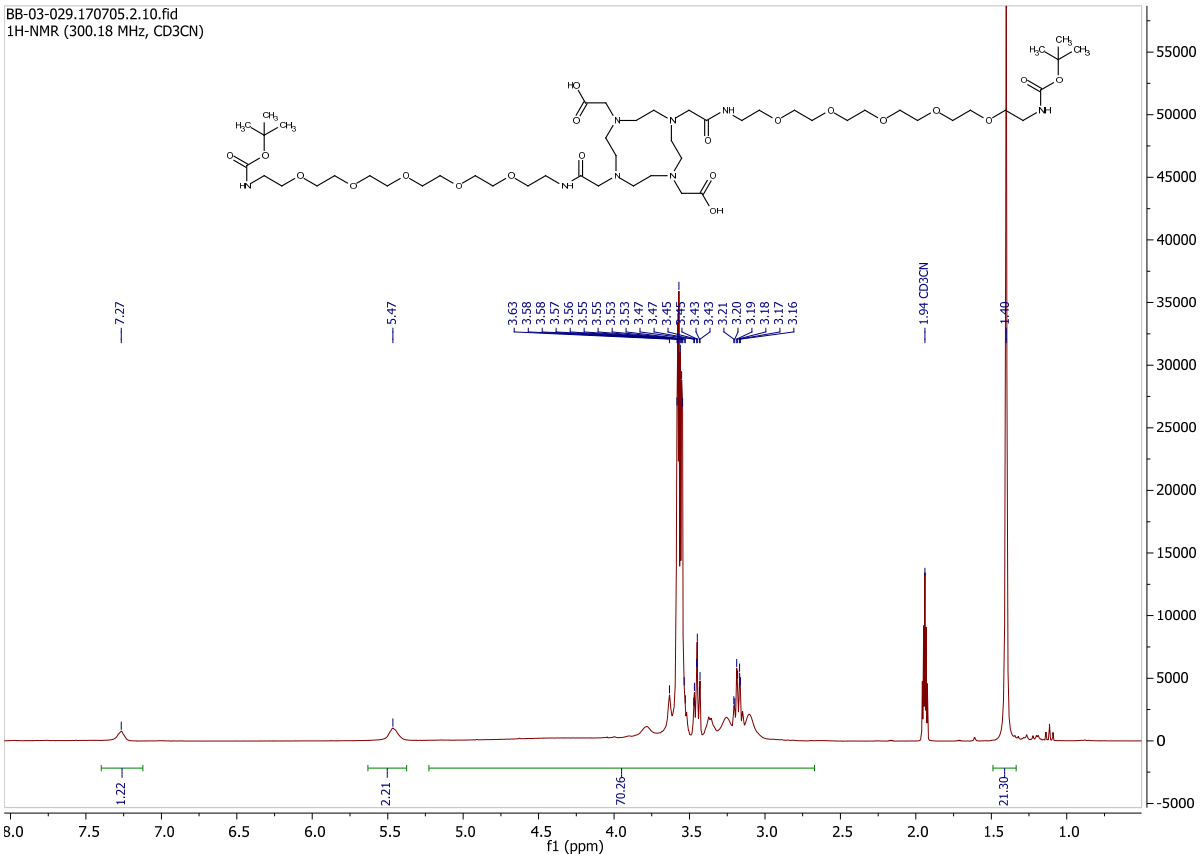

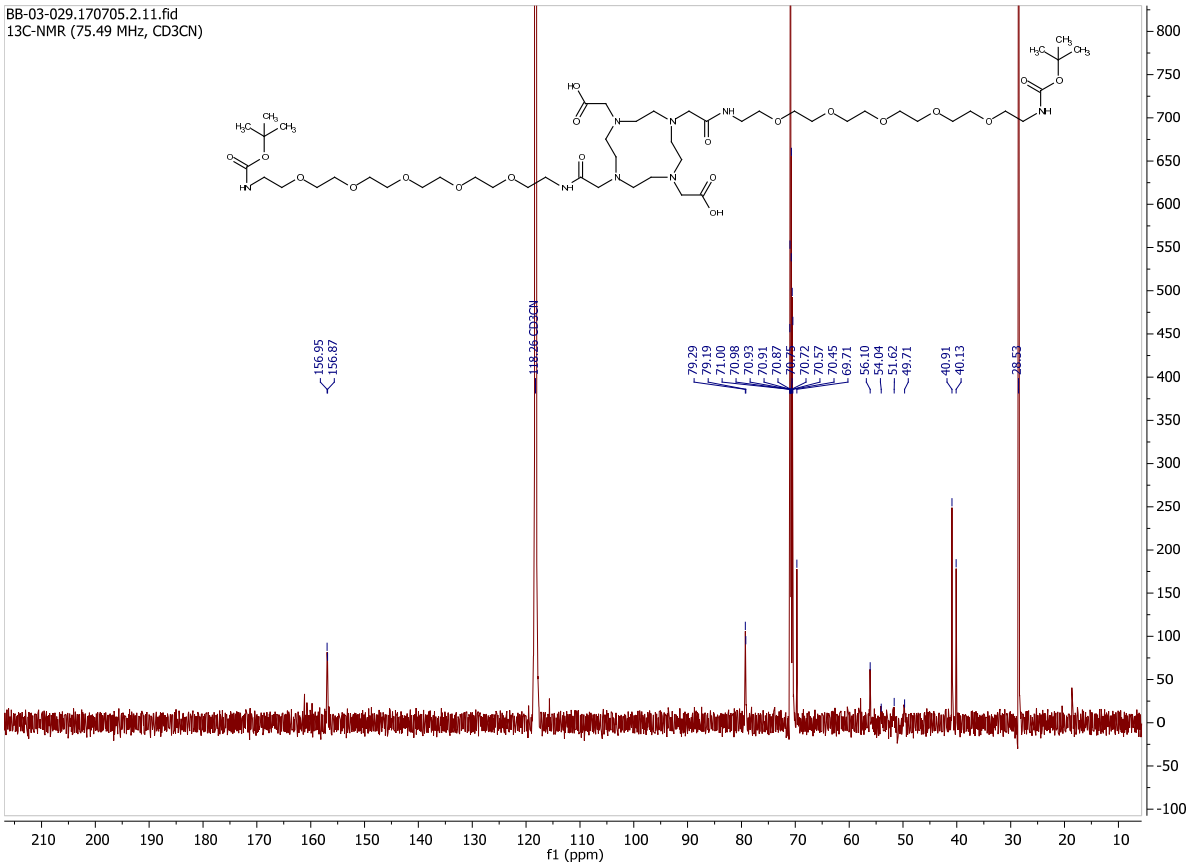

Bis-(PEGNHBoc)-Cy3 DOTAM (**3**)

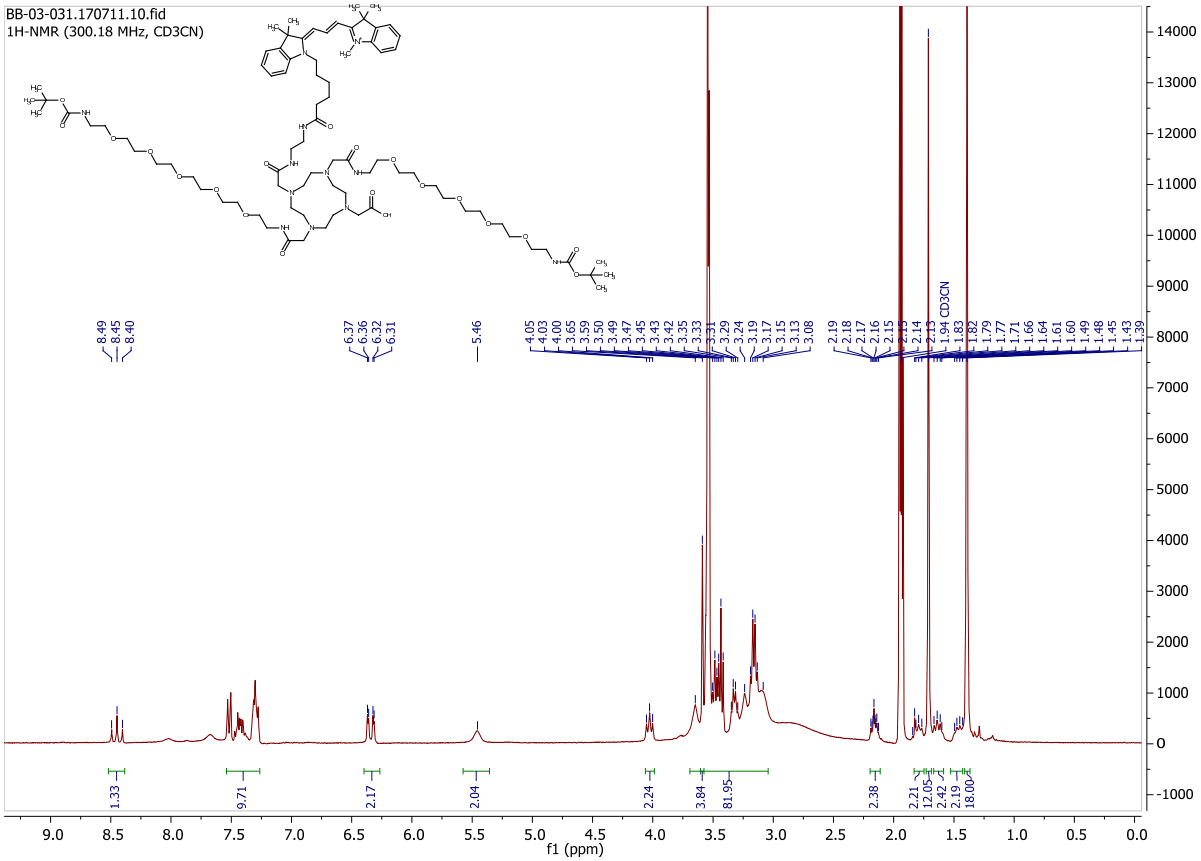

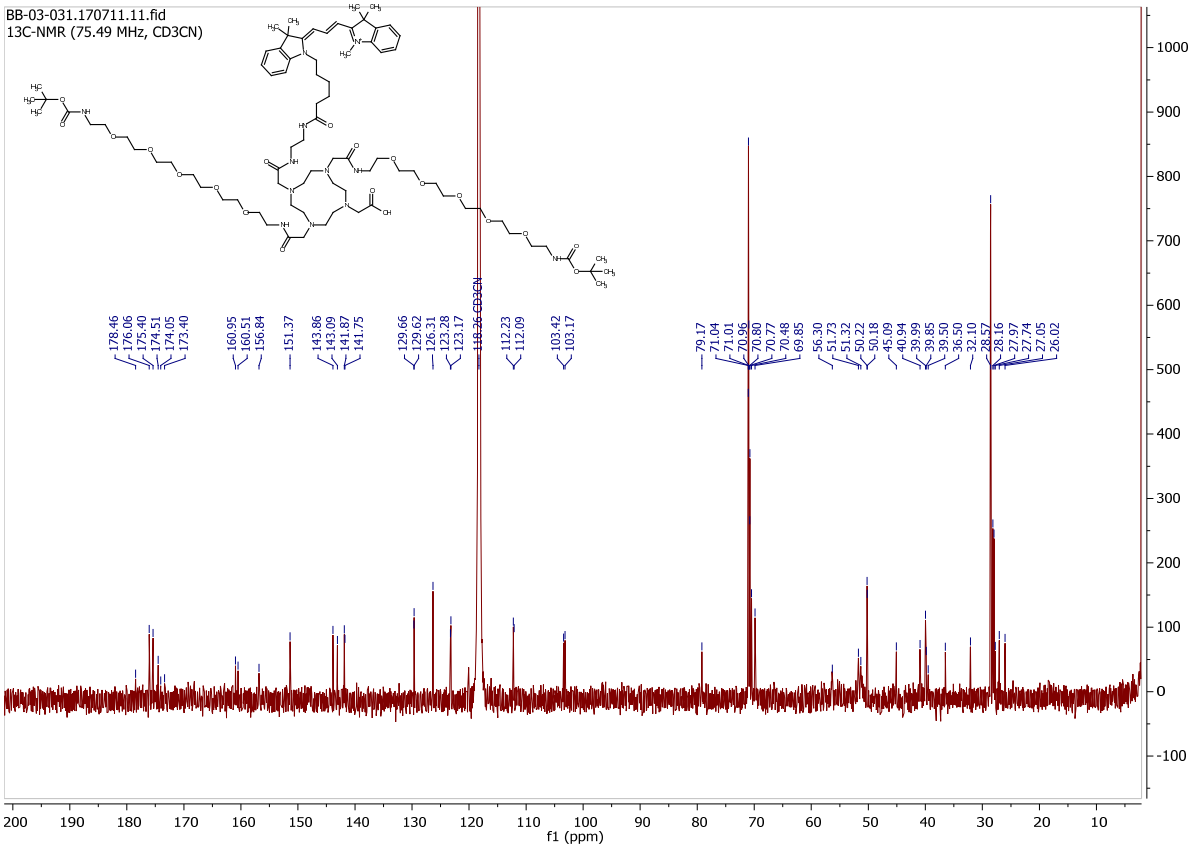

Bis-(PEGNHBoc)-Cy3 DOTAM (**3**)

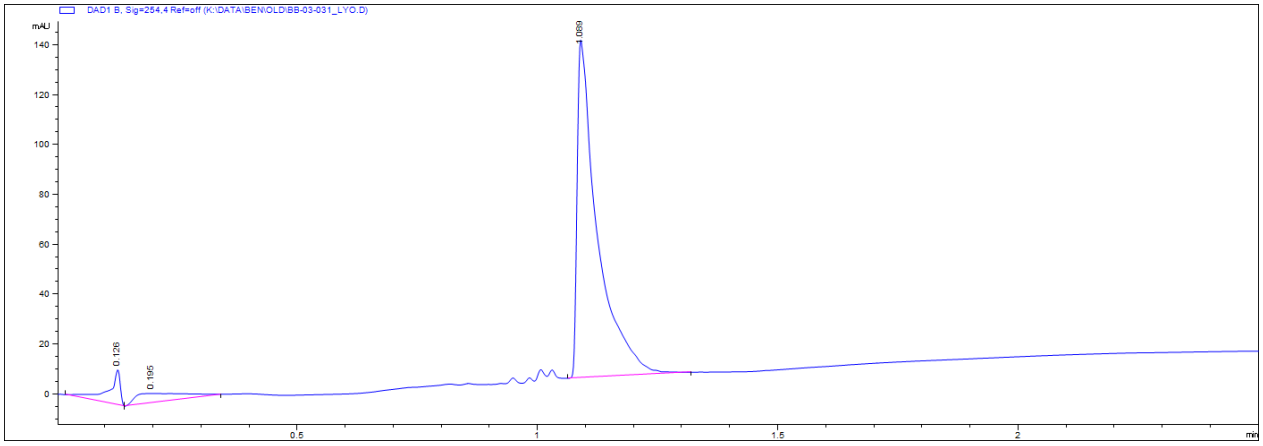

Bis-(PEGNH$_2$)-Cy3-CatSseq-BHQ-2 DOTAM (**4**)

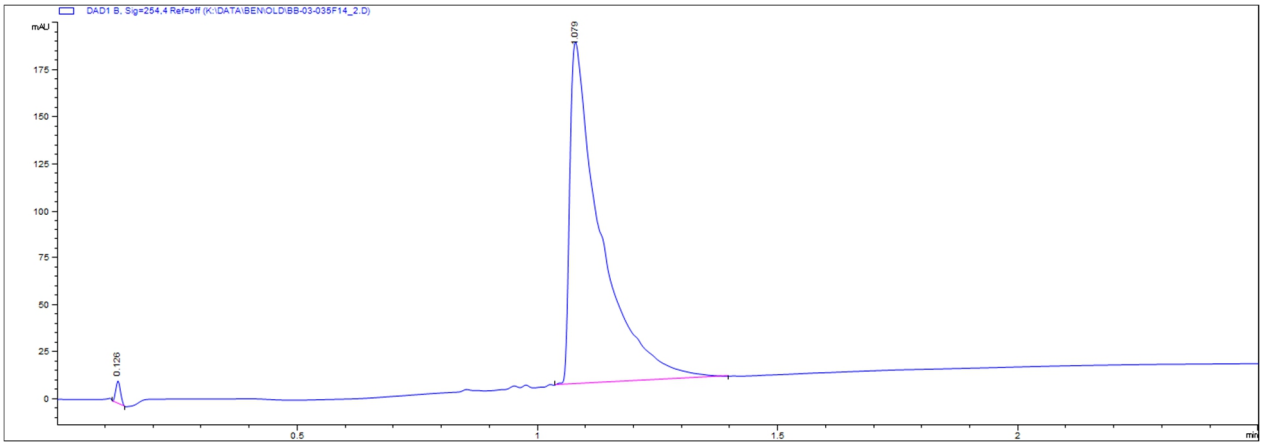

Cy3/BHQ-2 CatS activatable control probe **6**

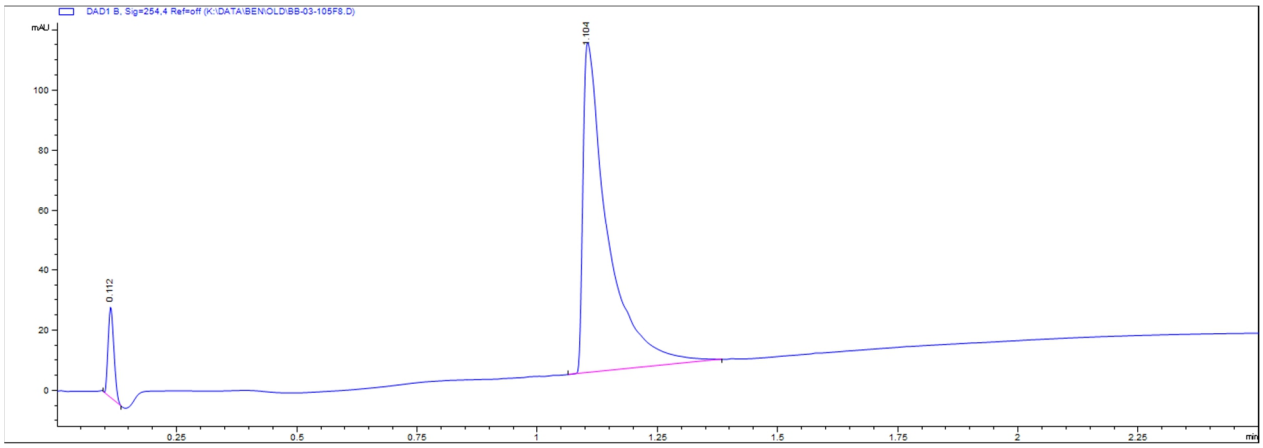

TIC trace with mass peaks at t = 1.14

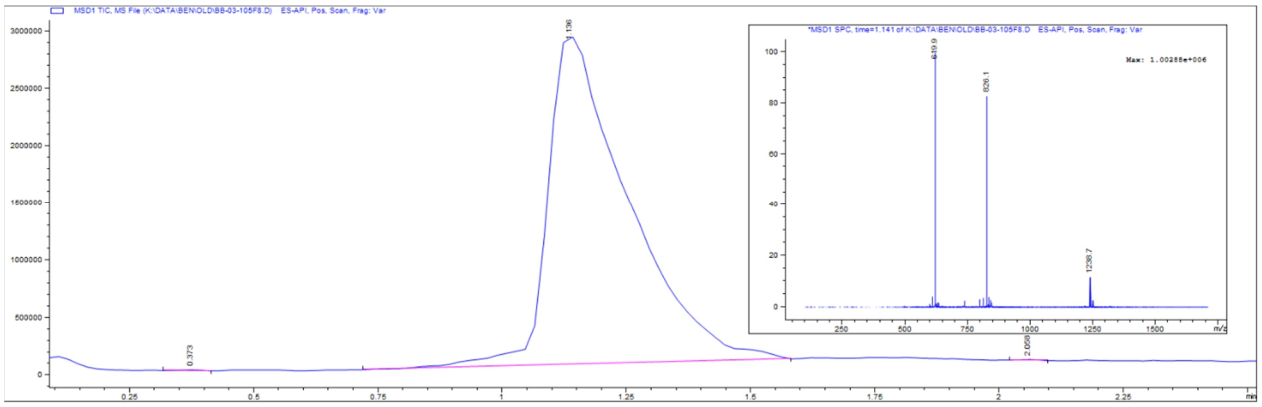

Bis-(PEGNHsucc)-Cy3-CatSseq-BHQ-2 DOTAM (**S22**)

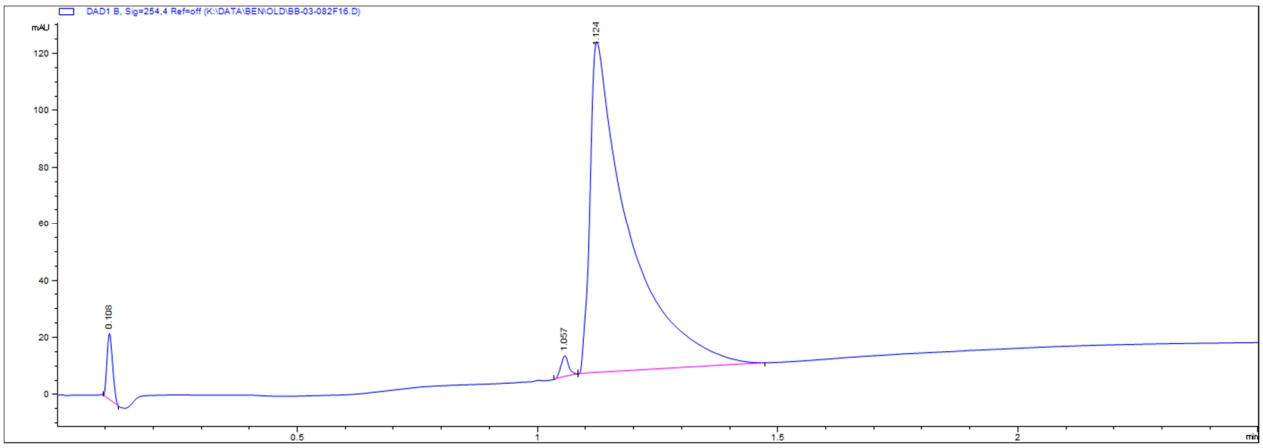

Bis-(cRGDfK)-Cy3/BHQ-2 CatS activatable probe **5**

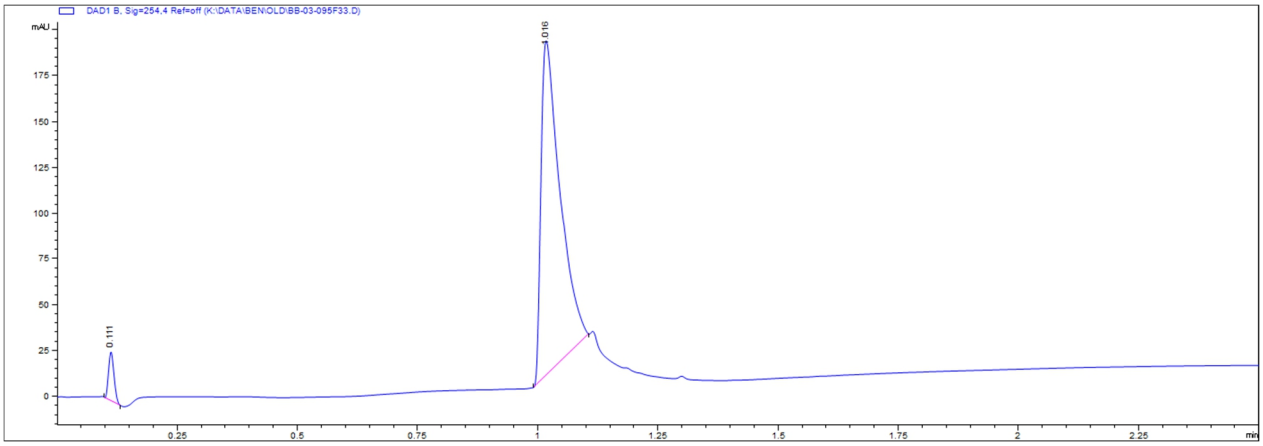

TIC trace with mass peaks at t = 1.08

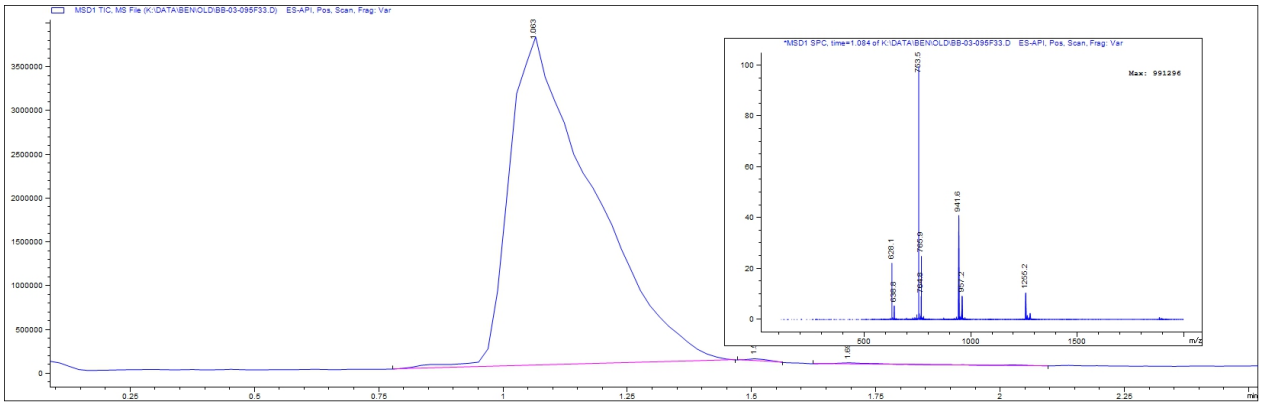

Methyl-2-bromo-4-nitrobenzoate

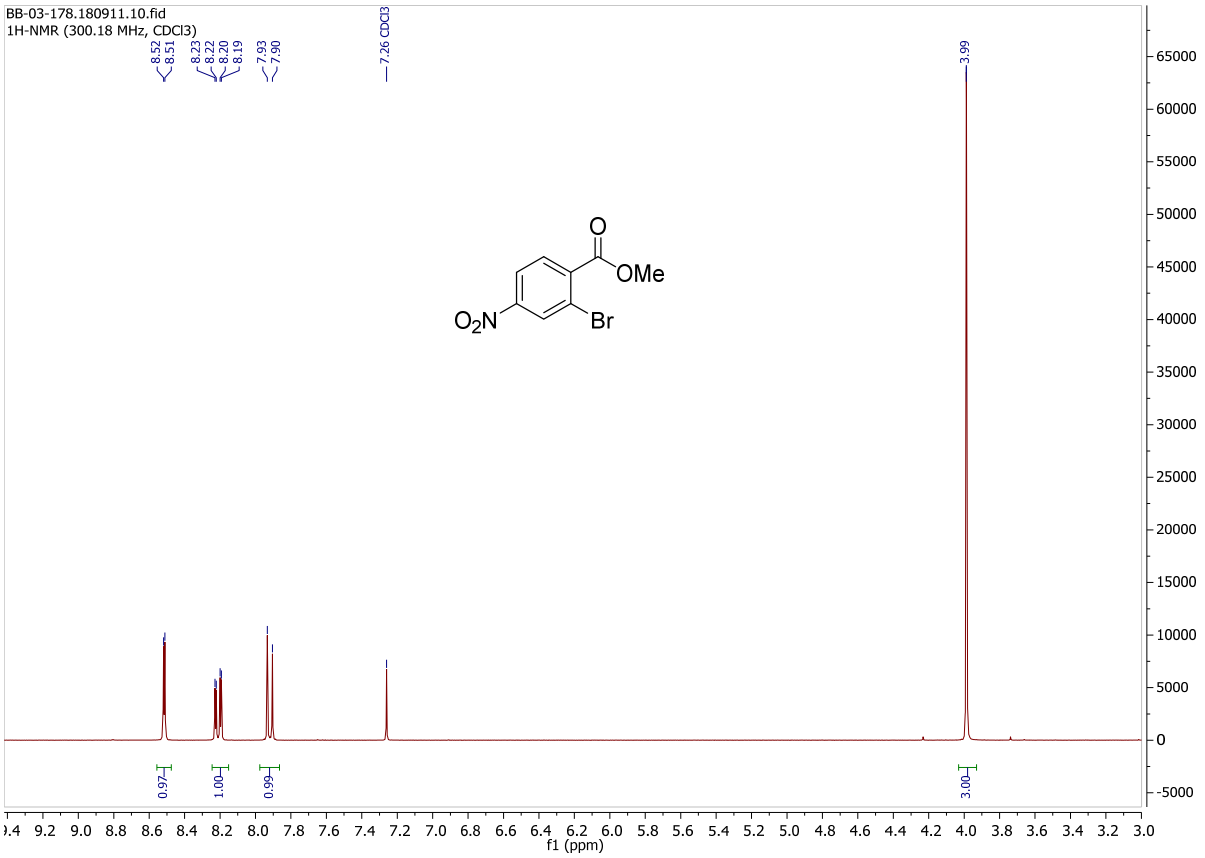

Methyl 4-amino-2-bromobenzoate (**2**)

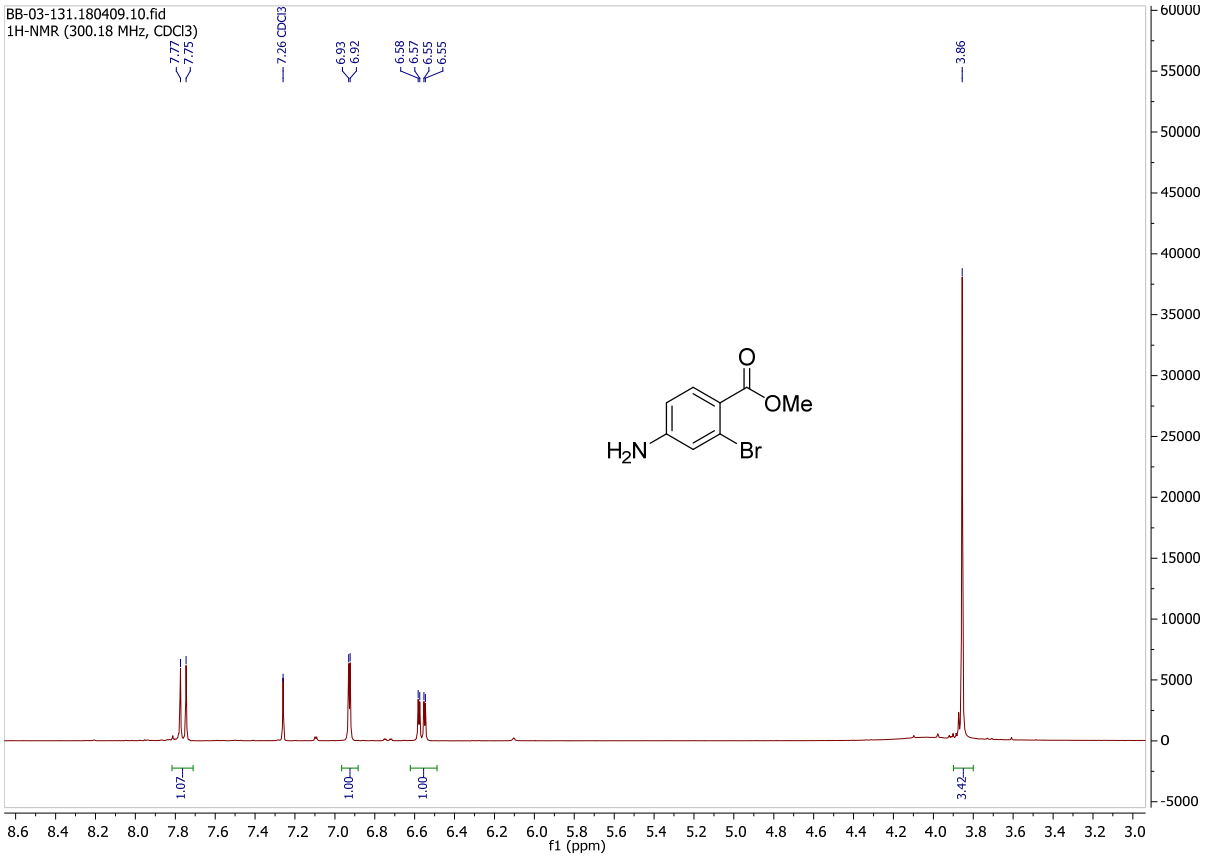

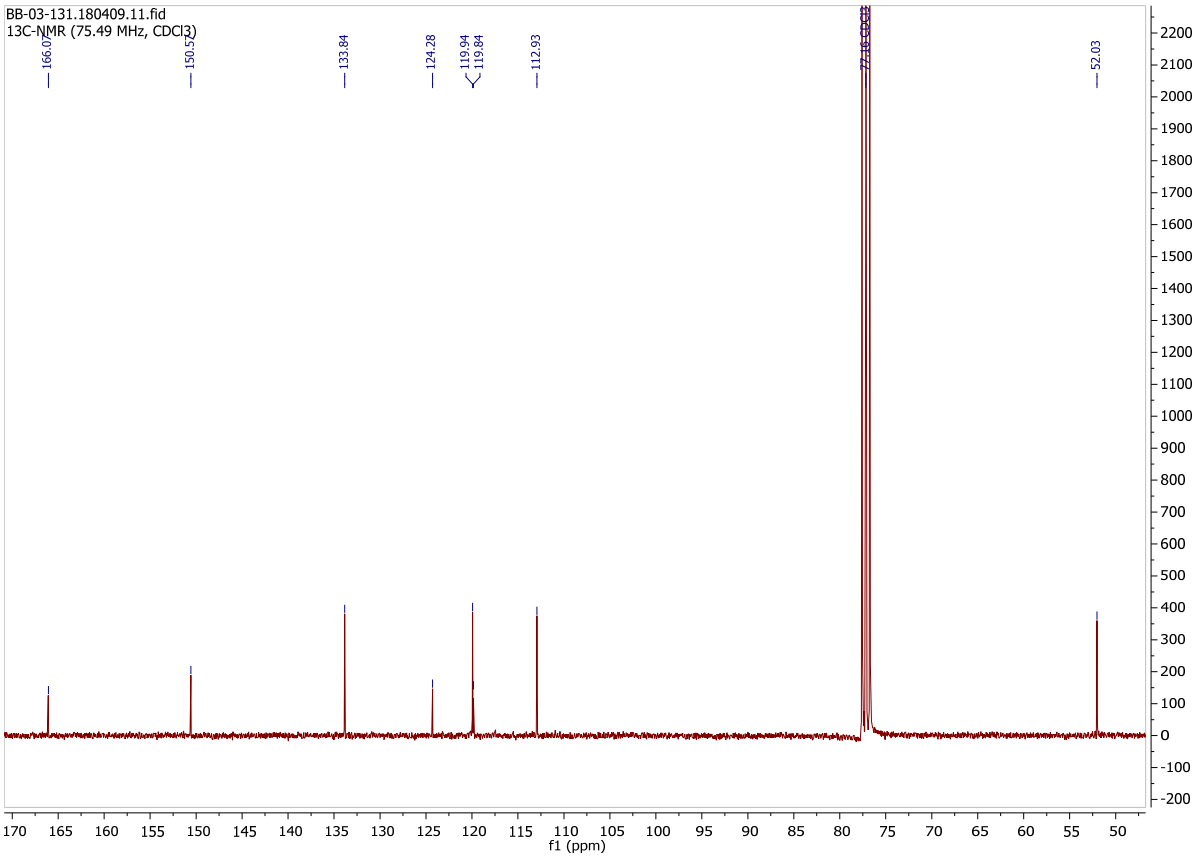

(4-Amino-2-bromophenyl)methanol

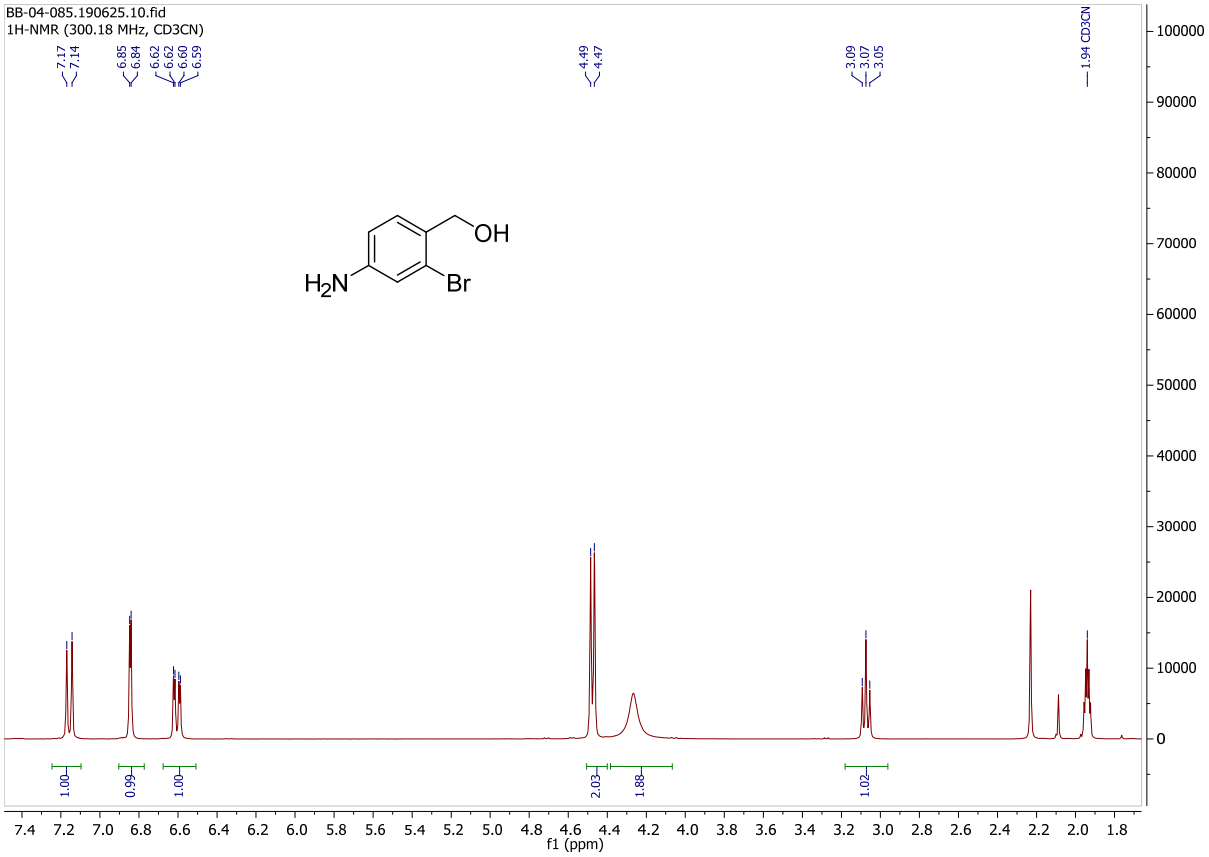

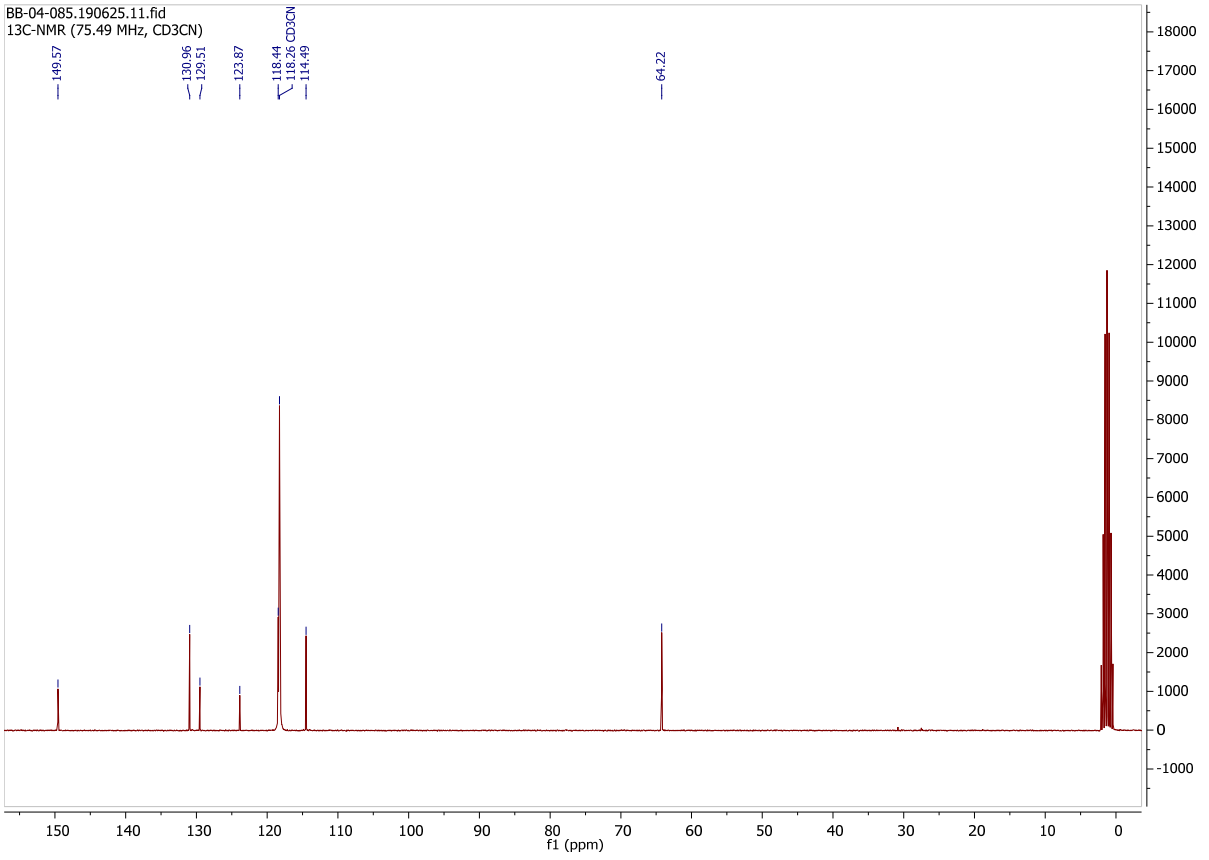

tert-Butyl (3-bromo-4-(hydroxymethyl)phenyl)carbamate (**3**)

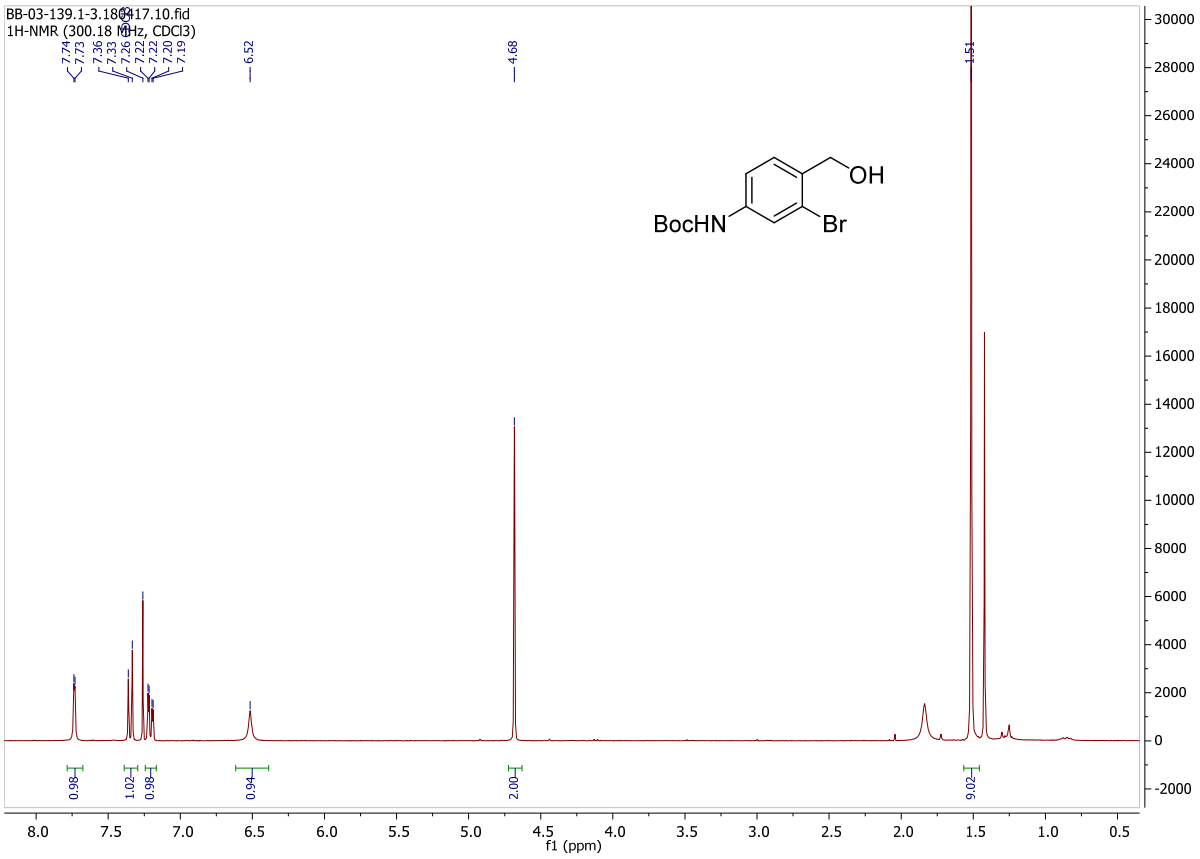

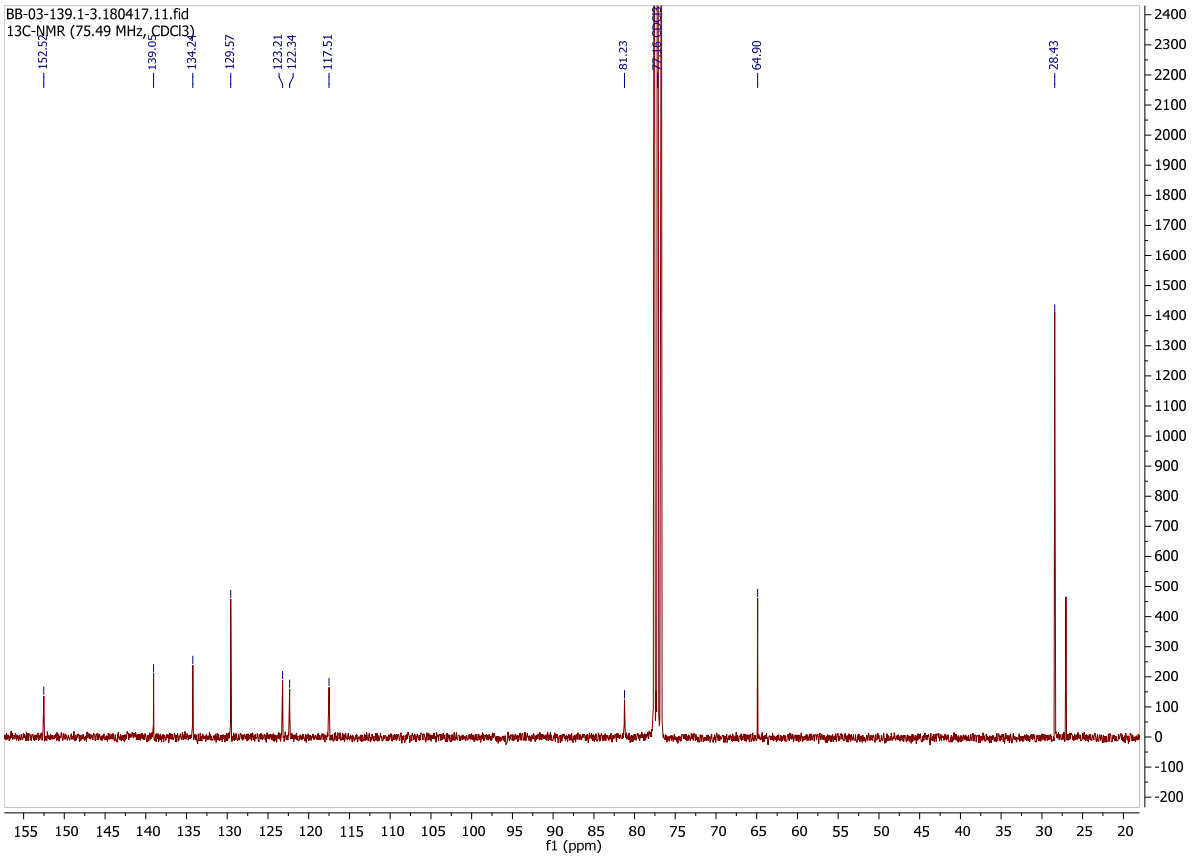

tert-Butyl (3-bromo-4-formylphenyl)carbamate (**4**)

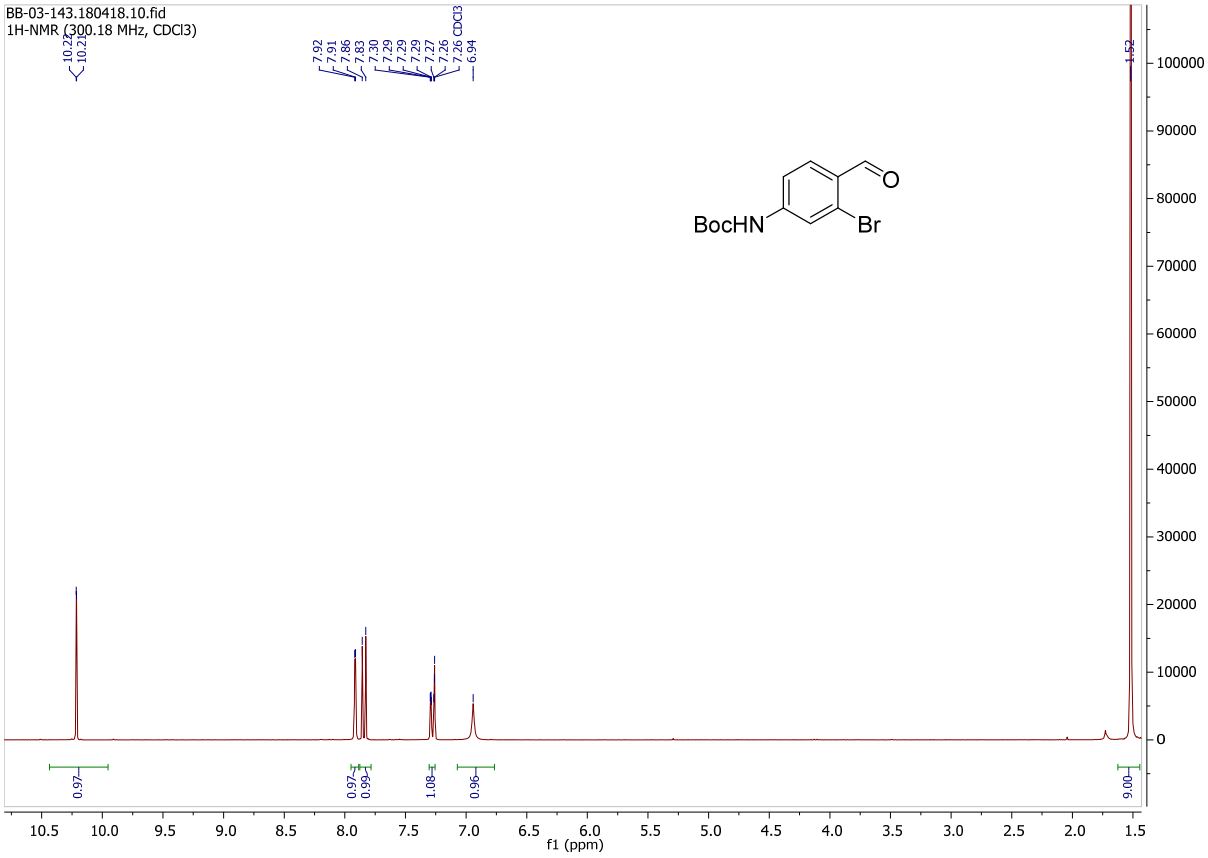

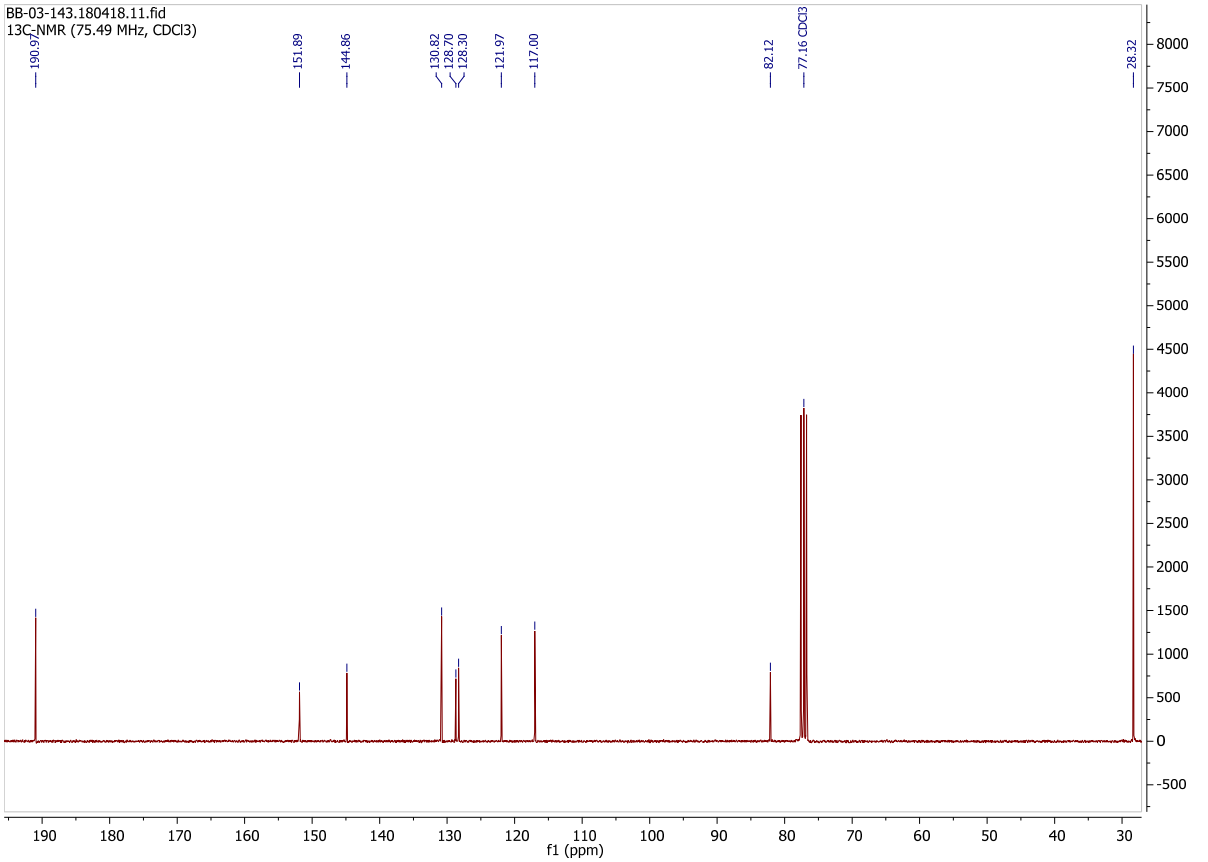

Di-*tert*-butyl (4-formyl-1,3-phenylene)dicarbamate

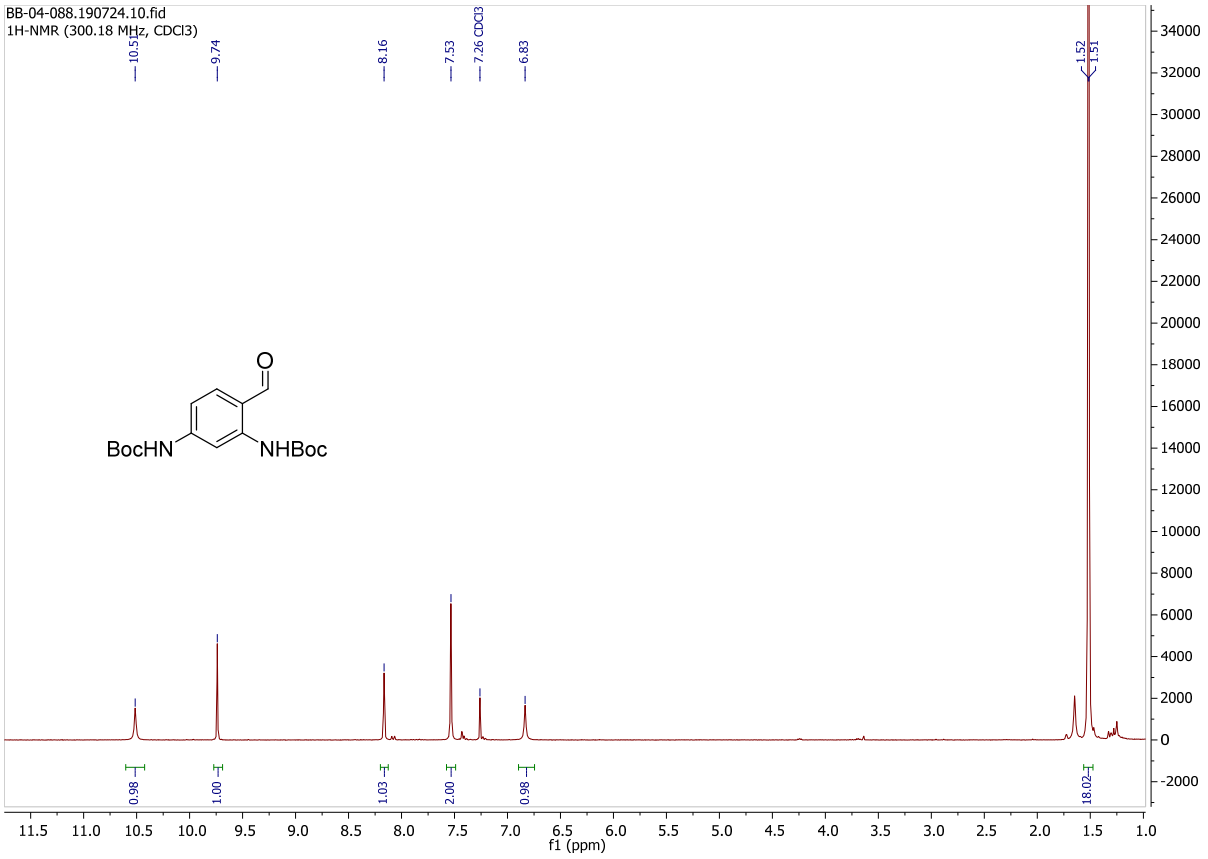

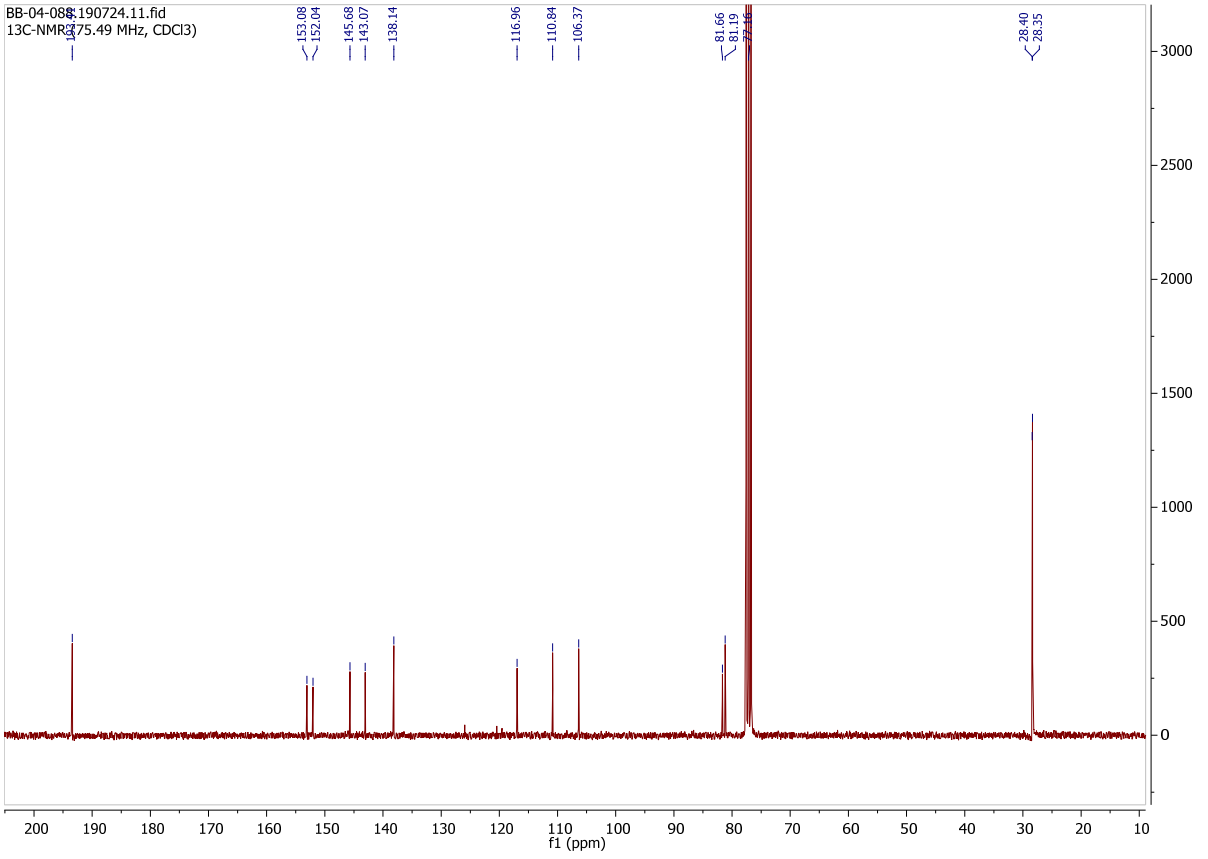

Diethyl 2-(2,4-bis((tert-butoxycarbonyl)amino)benzylidene)malonate (**5**)

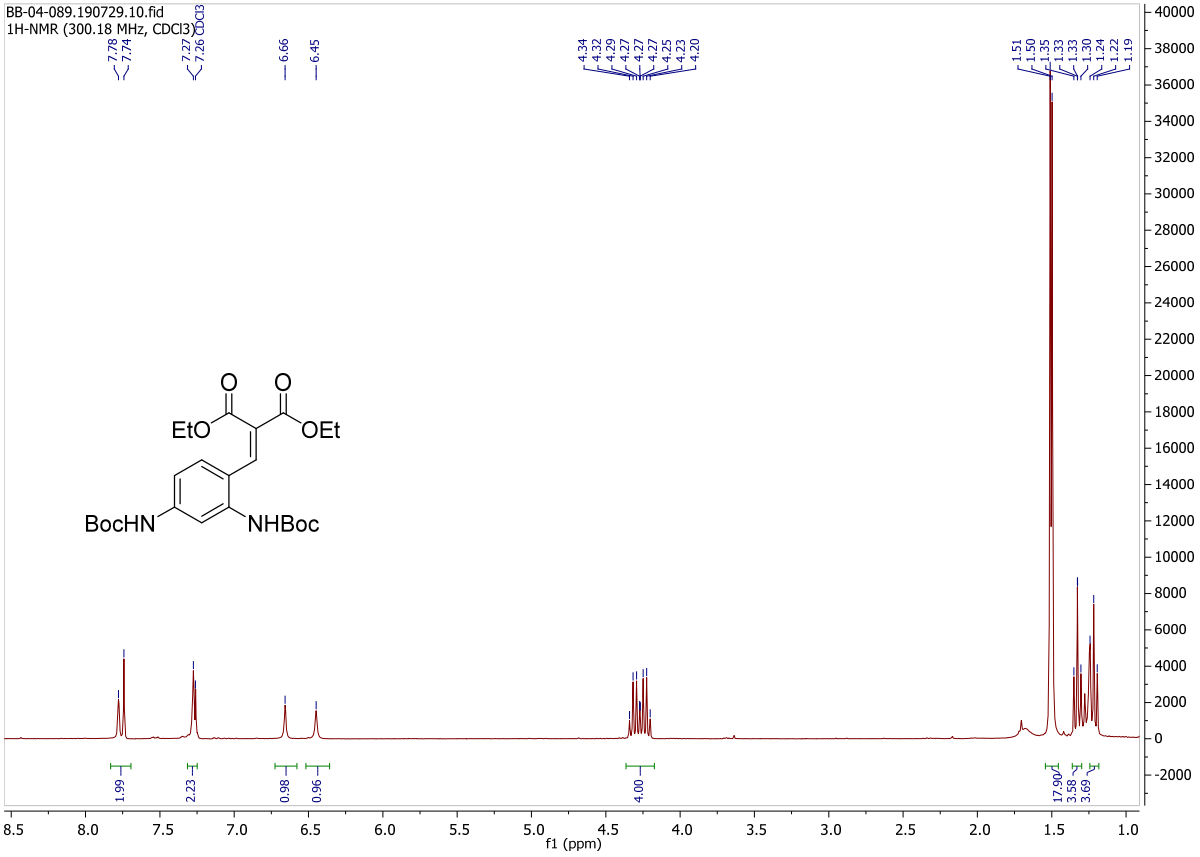

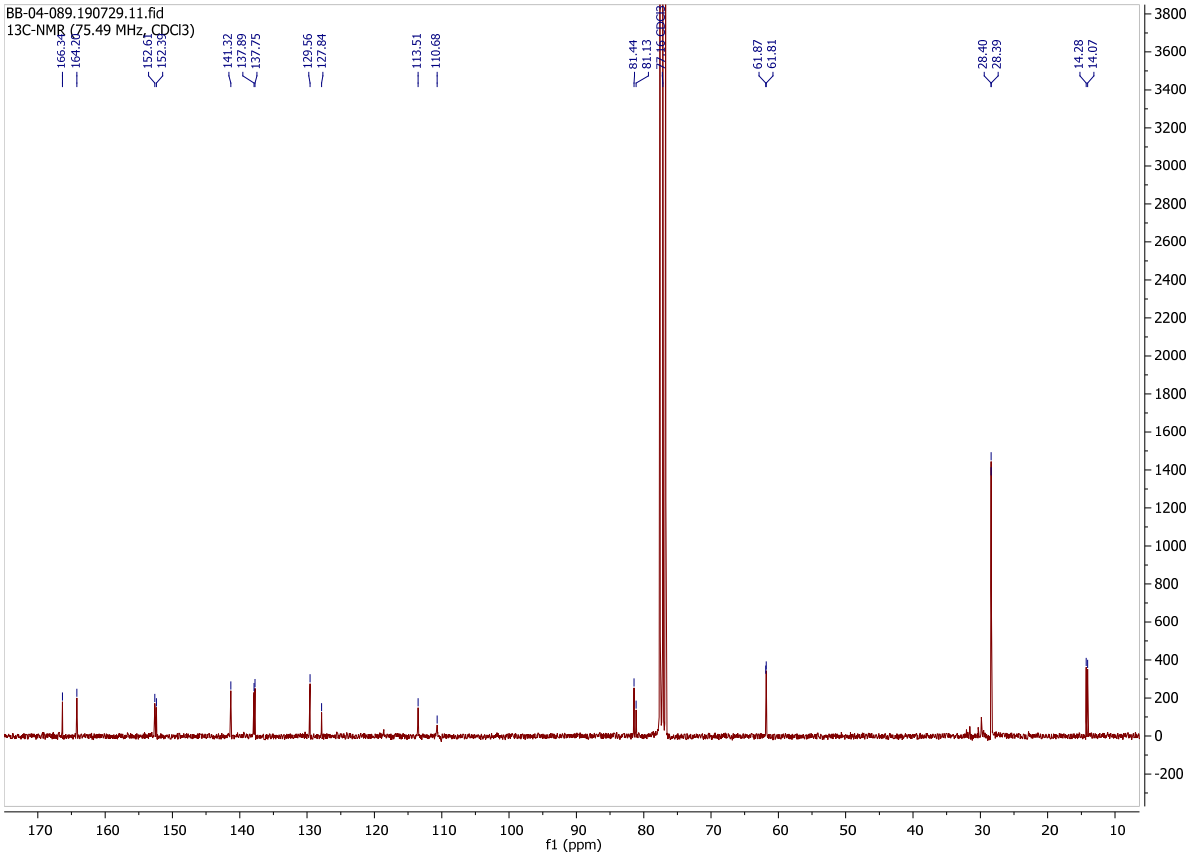

Ethyl 7-amino-2-oxo-1,2-dihydroquinoline-3-carboxylate (**6**)

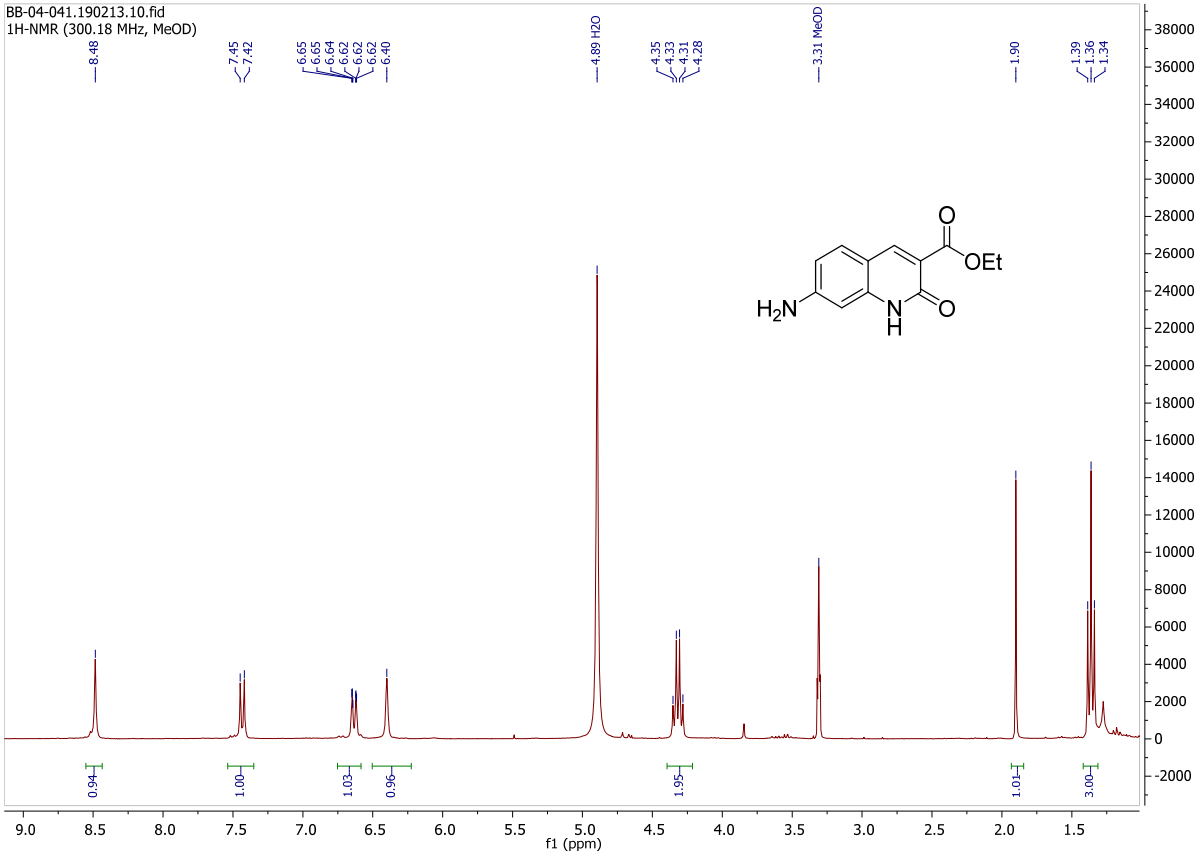

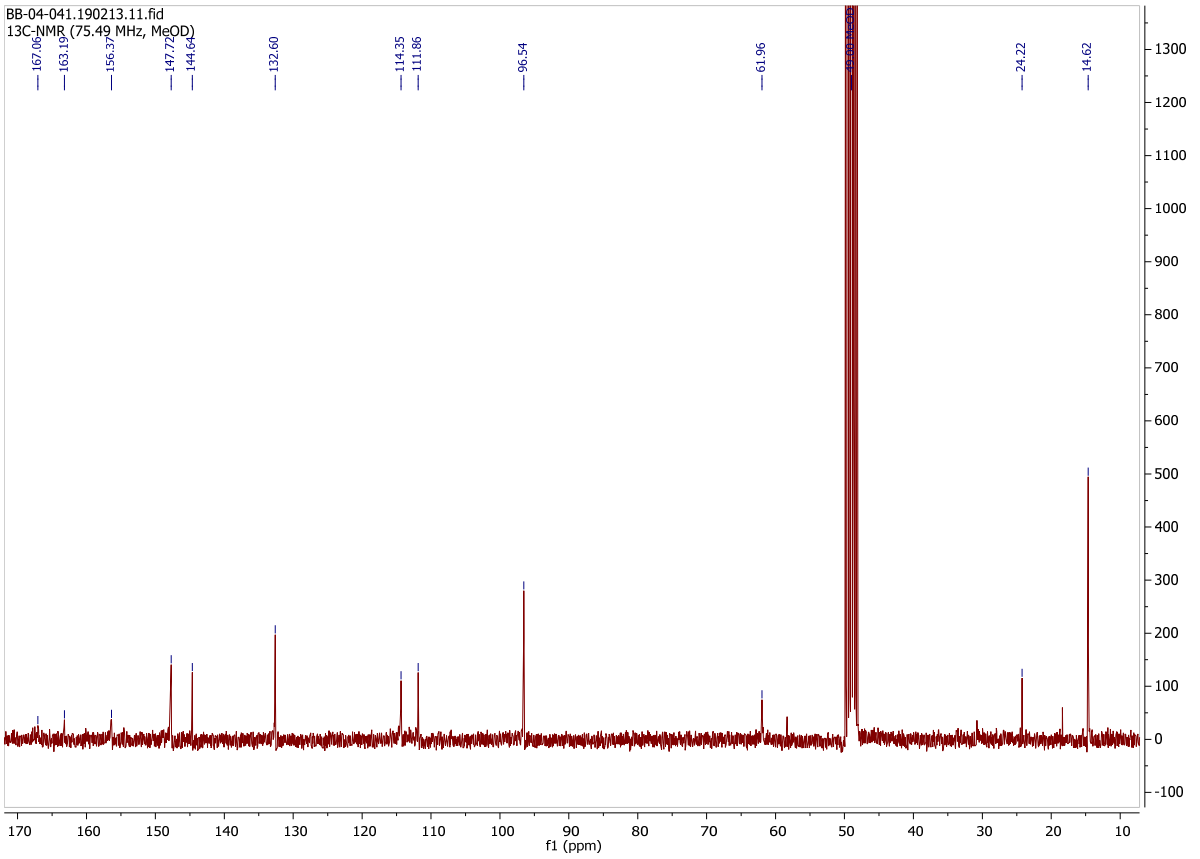

tert-Butyl (4-nitrobenzyl) (4-formyl-1,3-phenylene)dicarbamate (**7**)

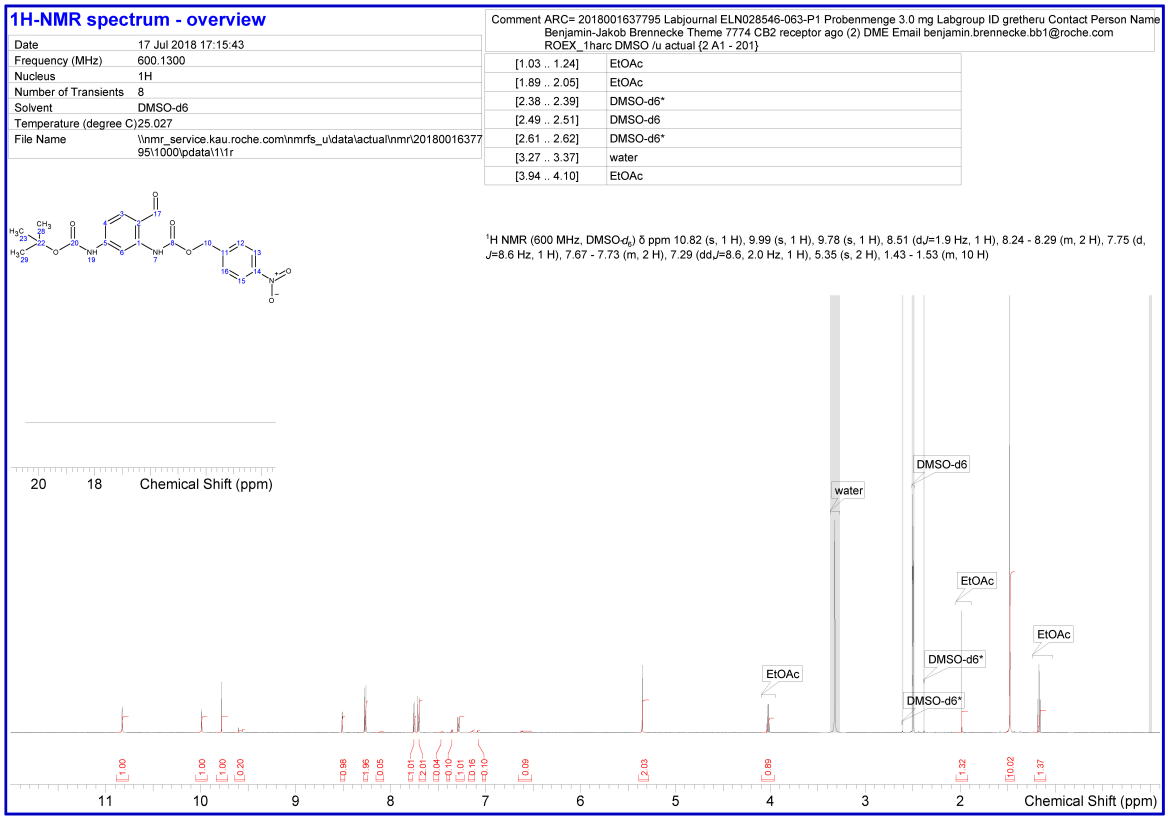

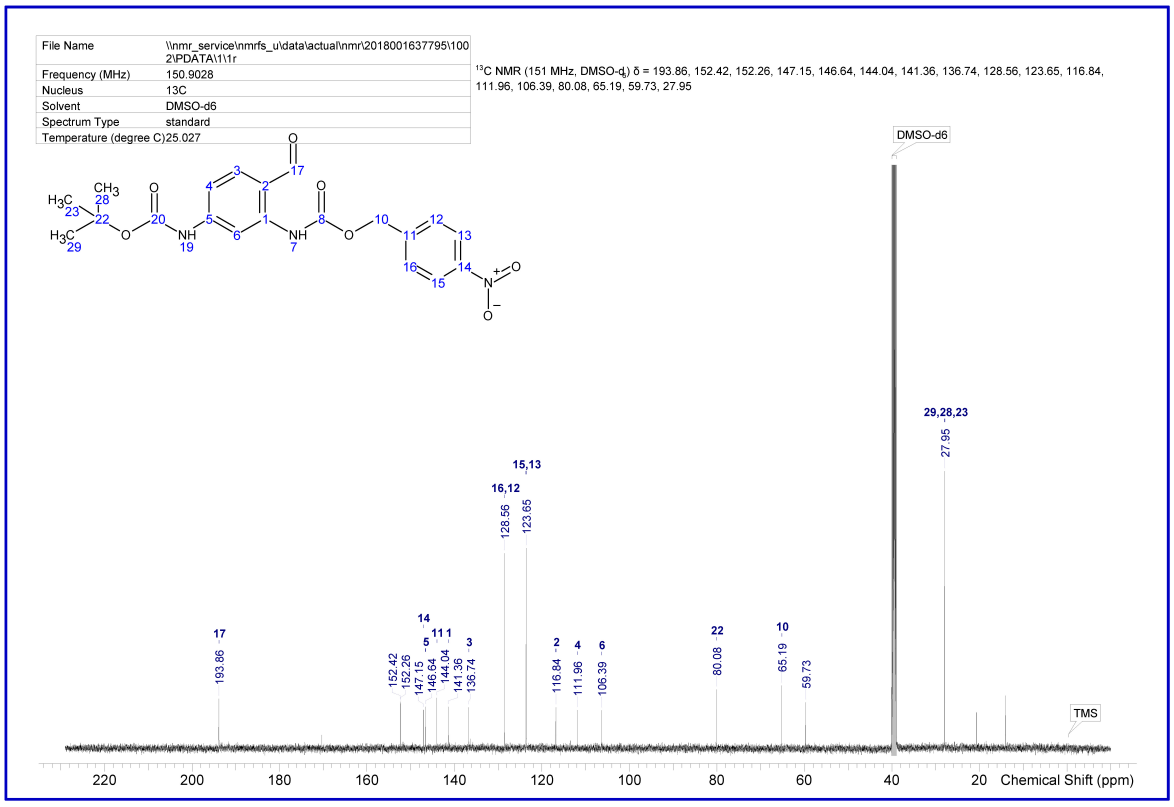

Boc-protected caged antenna

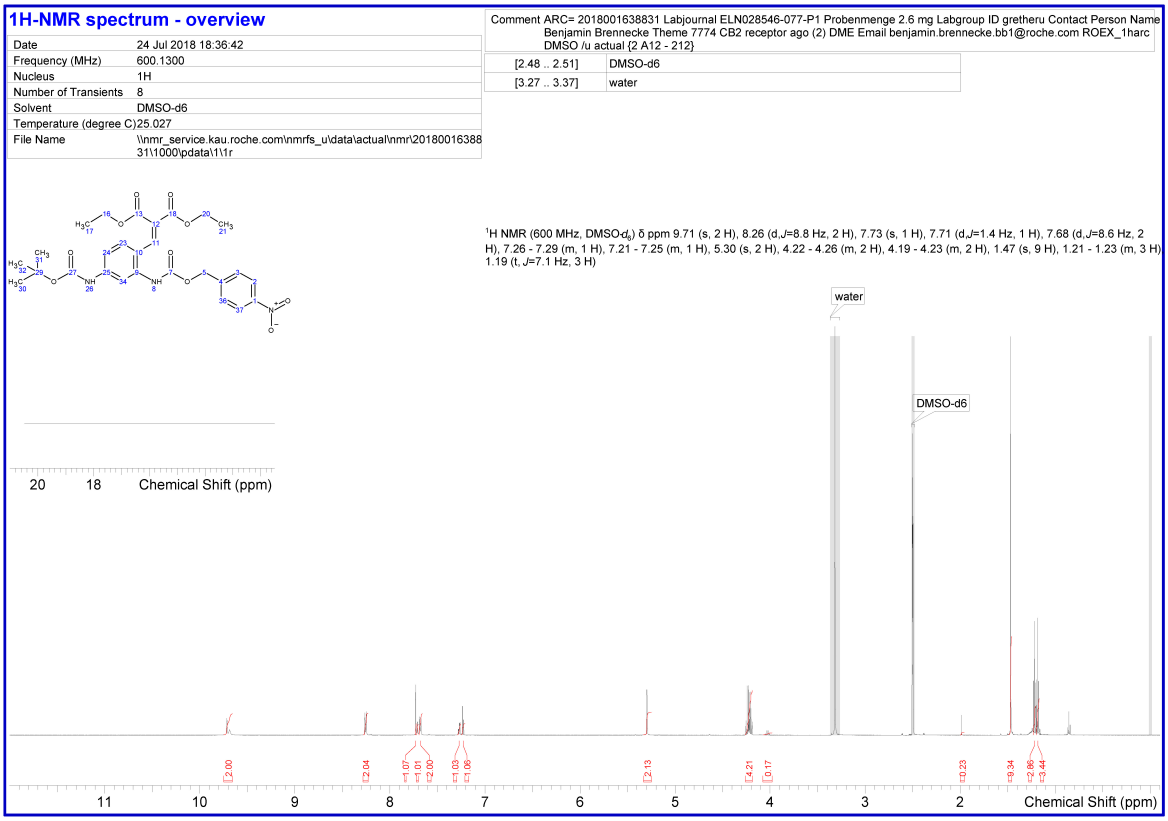

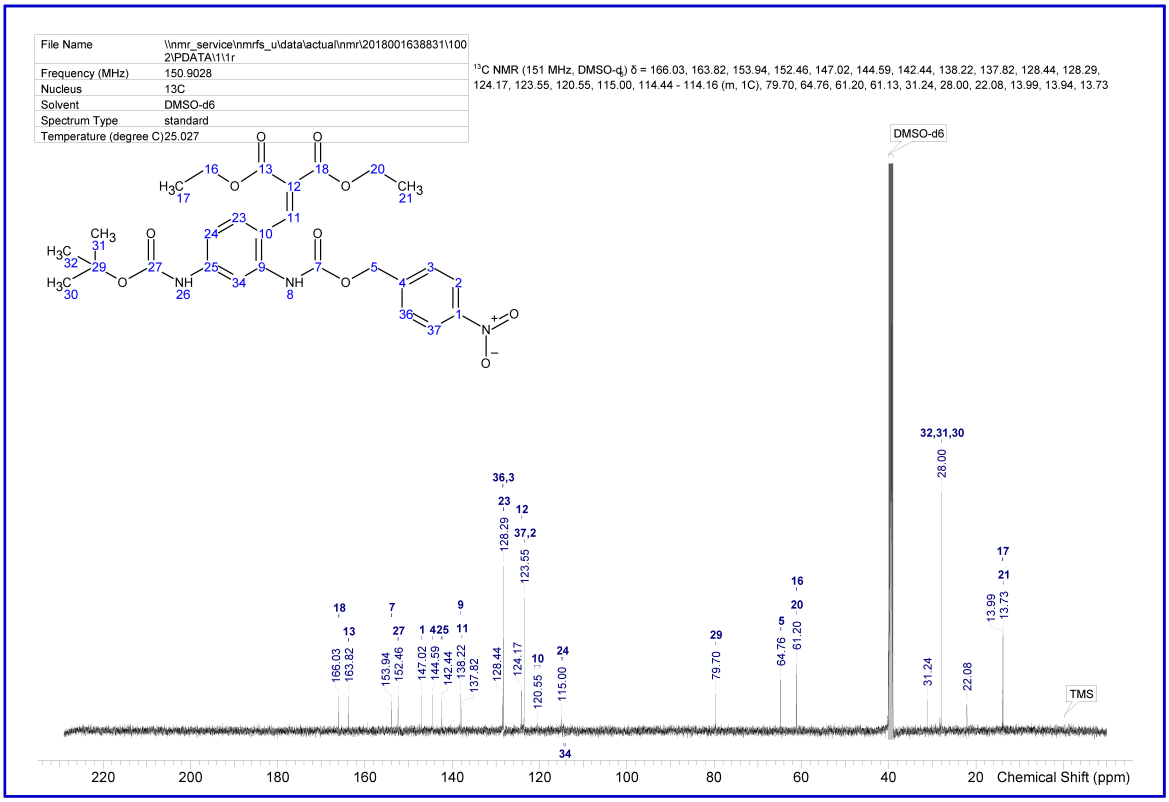

DOTA antenna conjugate (**9**)

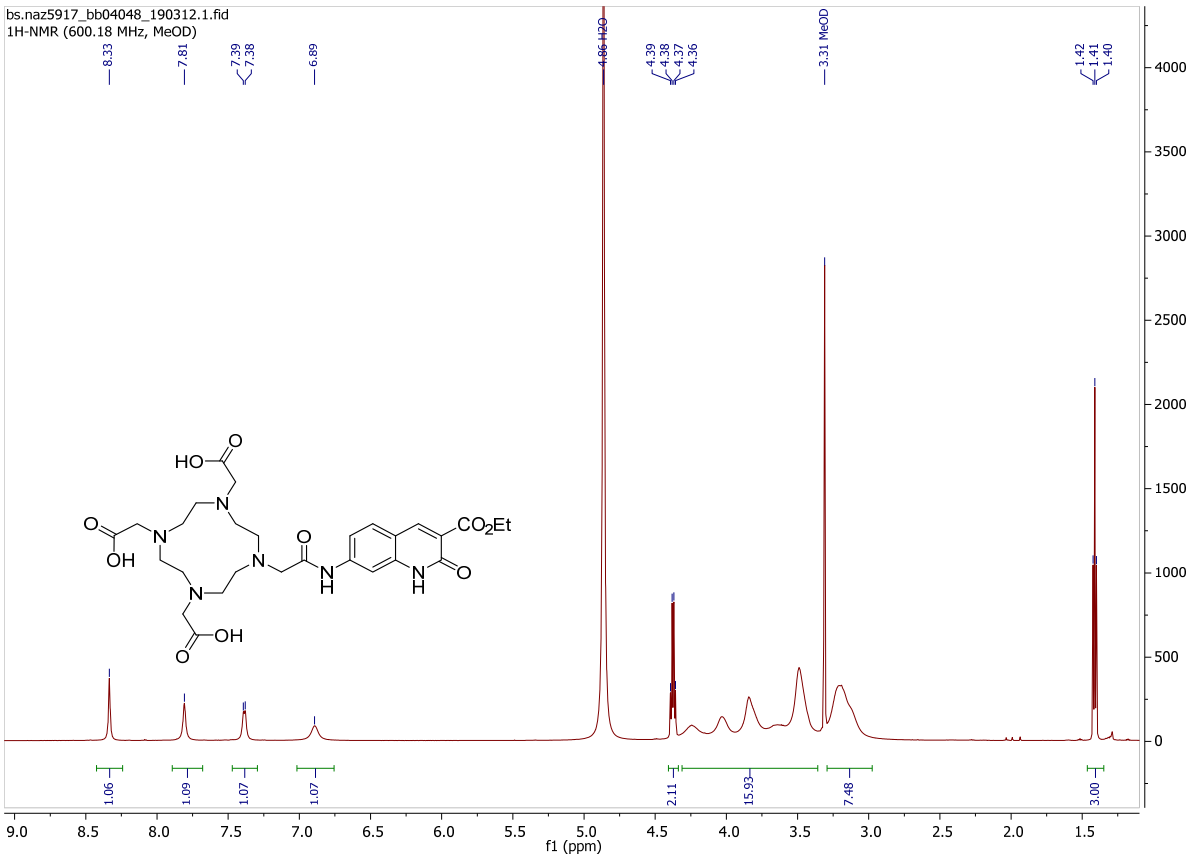

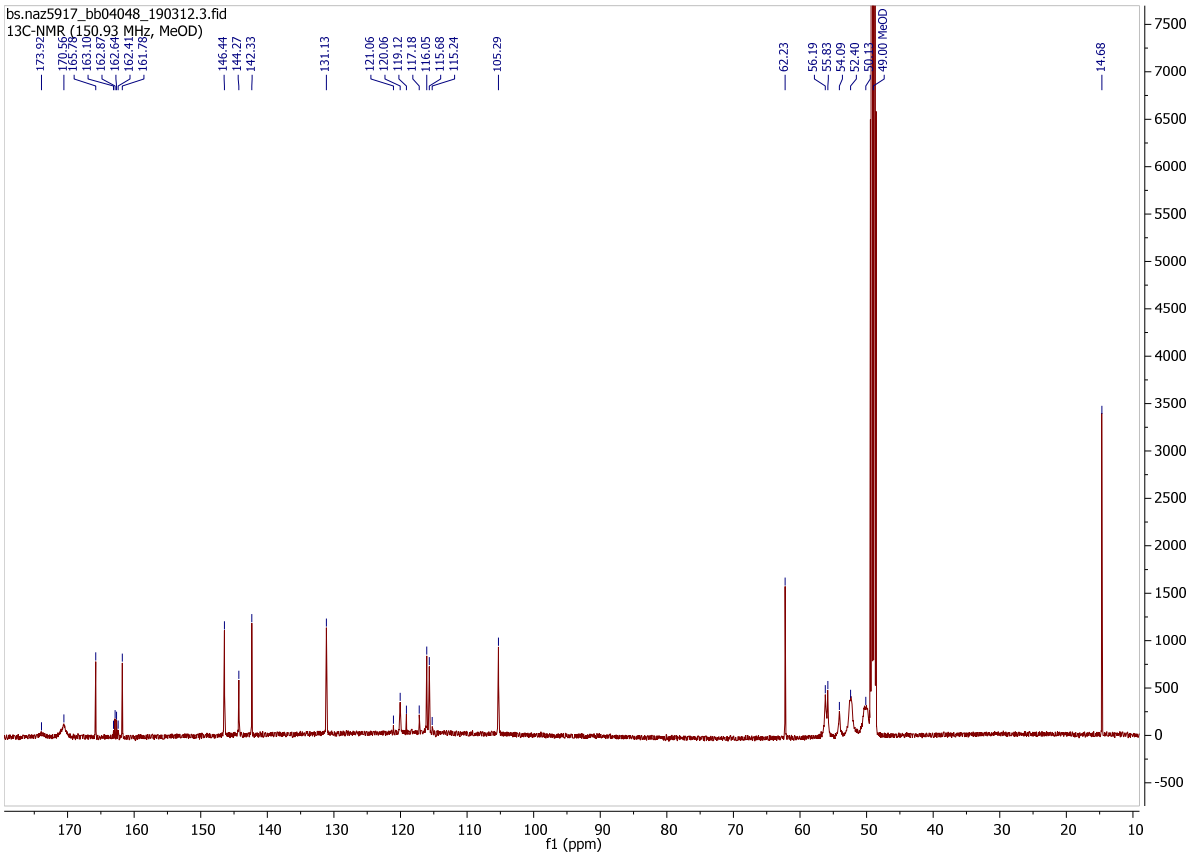

DOTA caged antenna conjugate (**11**)

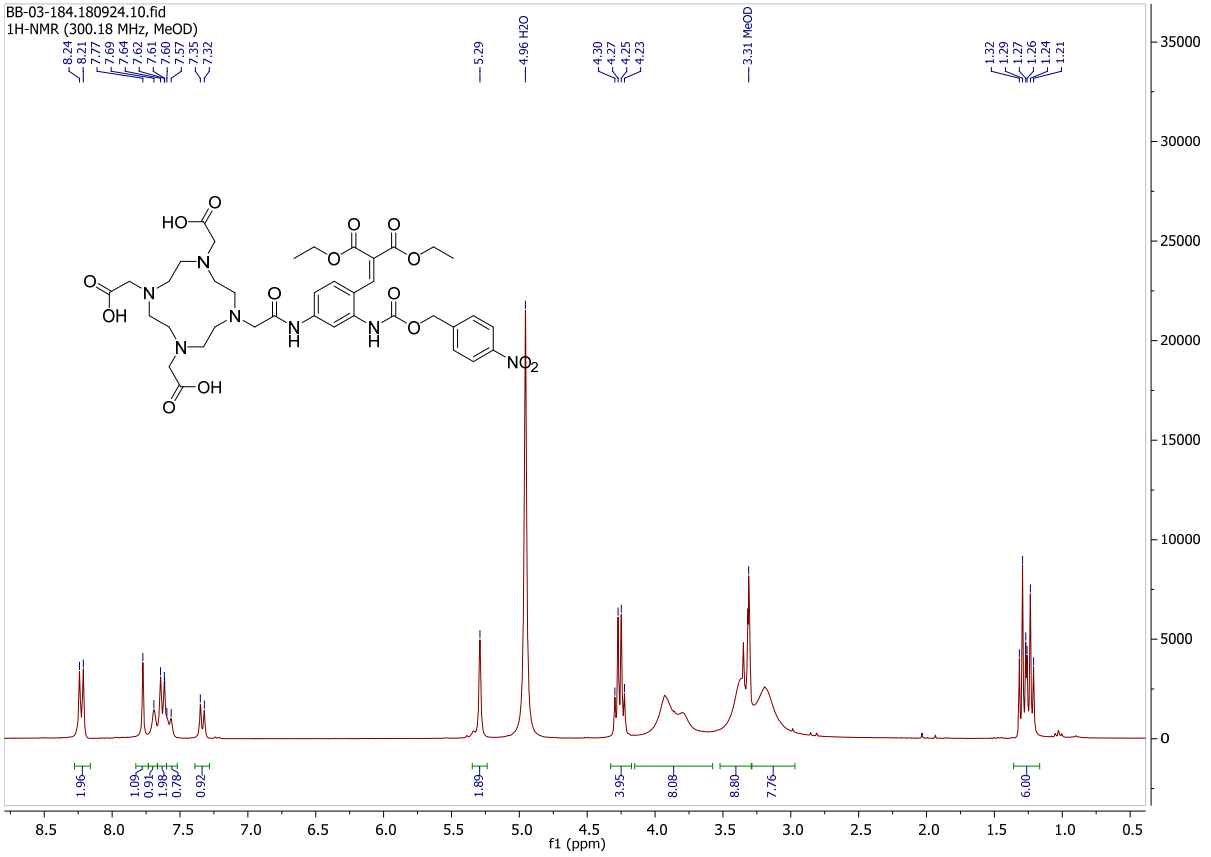

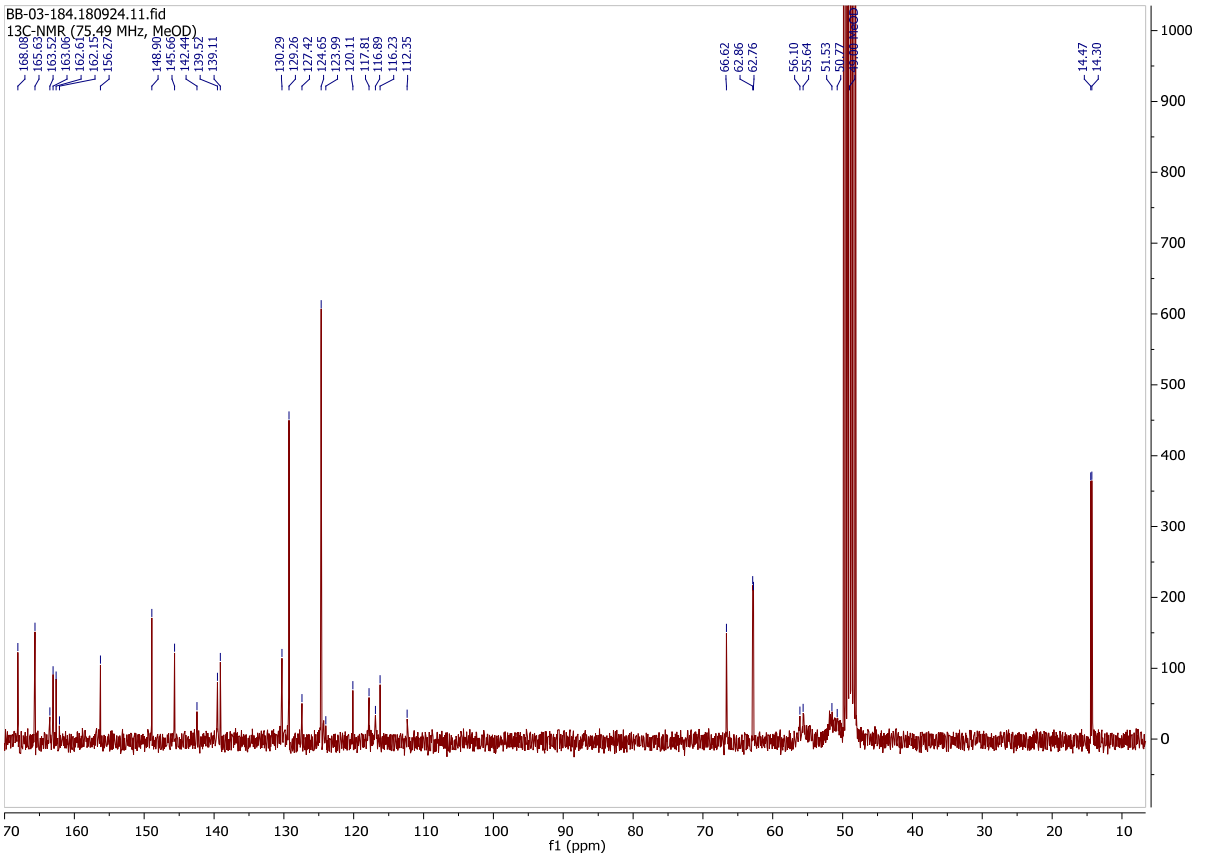

6.2 List of Publications

1. **B. Brennecke**, Q. Wang, W. Haap, U. Grether, H.-Y. Hu, M. Nazaré, **DOTAM-Based, Targeted, Activatable Fluorescent Probes for the Highly Sensitive and Selective Detection of Cancer Cells.** *Bioconjugate Chem.* **2021**, *32*, 702-712. https://doi.org/10.1021/acs.bioconjchem.0c00699.

2. R. C. Sarott, M. V. Westphal, P. Pfaff, C. Korn, D. A. Sykes, T. Gazzi, **B. Brennecke**, K. Atz, M. Weise, Y. Mostinski, P. Hompluem, T. Miljuš, N. J. Roth, H. Asmelash, M. C. Vong, J. Piovesan, W. Guba, A. C. Rufer, E. A. Kusznir, S. Huber, C. Raposo, E. A. Zirwes, A. Osterwald, A. Pavlovic, S. Moes, J. Beck, I. Benito-Cuesta, T. Grande, A. Yeliseev, F. Drawnel, G. Widmer, D. Holzer, T. van der Wel, H. Mandhair, C.-Y. Yuan, W. R. Drobyski, Y. Saroz, N. Grimsey, M. Honer, J. Fingerle, K. Gawrisch, J. Romero, C. J. Hillard, Z. V. Varga, M. van der Stelt, P. Pacher, J. Gertsch, P. J. McCormick, C. Ullmer, S. Oddi, M. Maccarrone, D. B. Veprintsev, M. Nazaré, U. Grether, E. M. Carreira, **Development of High-Specificity Fluorescent Probes to Enable Cannabinoid Type 2 Receptor Studies in Living Cells**. *J. Am. Chem. Soc.* **2020**, *142*, 16953-16954. https://doi.org/10.1021/jacs.0c05587.

3. **B. Brennecke**, Q. Wang, Q. Zhang, H.-Y. Hu, M. Nazaré, **An Activatable Lanthanide Luminescent Probe for Time-Gated Detection of Nitroreductase in Live Bacteria.** *Angew. Chem. Int. Ed.* **2020**, *59*, 8512-8516. https://doi.org/10.1002/anie.202002391. Highlighted as “hot paper” and back cover.

6.3 Curriculum Vitae

The Curriculum Vitae is not published in the online version for reasons of data protection.